Micro-mechanics of weak layers: key role of sediment structure and composition

DISSERTATION

zur Erlangung des Doktorgrades der Naturwissenschaften im Fachbereich Geowissenschaften der Universität Bremen

vorgelegt von

Ricarda Gatter

Bremen, July 2021

Gutachter: Prof. Dr. Katrin Huhn-Frehers

MARUM, Universität Bremen
Leobener Straße 8, MARUM II, 3040
28359 Bremen, Deutschland

Prof. Dr. Sebastian Krastel

Christian-Albrechts-Universität zu Kiel
Otto-Hahn-Platz 1, R. 110
24118 Kiel, Deutschland

Datum des Promotionskolloquiums: 20. September 2021

Versicherung an Eides Statt / *Affirmation in lieu of an oath*

gem. § 5 Abs. 5 der Promotionsordnung vom 18.06.2018 /
according to § 5 (5) of the Doctoral Degree Rules and Regulations of 18 June, 2018

Ich / I, _____
(Vorname / First *Name*, Name / *Name*, Anschrift / *Address*, ggf. Matr.-Nr. / *student ID no., if applicable)*

versichere an Eides Statt durch meine Unterschrift, dass ich die vorliegende Dissertation selbständig und ohne fremde Hilfe angefertigt und alle Stellen, die ich wörtlich dem Sinne nach aus Veröffentlichungen entnommen habe, als solche kenntlich gemacht habe, mich auch keiner anderen als der angegebenen Literatur oder sonstiger Hilfsmittel bedient habe und die zu Prüfungszwecken beigelegte elektronische Version (PDF) der Dissertation mit der abgegebenen gedruckten Version identisch ist. / *With my signature I affirm in lieu of an oath that I prepared the submitted dissertation independently and without illicit assistance from third parties, that I appropriately referenced any text or content from other sources, that I used only literature and resources listed in the dissertation, and that the electronic (PDF) and printed versions of the dissertation are identical.*

Ich versichere an Eides Statt, dass ich die vorgenannten Angaben nach bestem Wissen und Gewissen gemacht habe und dass die Angaben der Wahrheit entsprechen und ich nichts verschwiegen habe*. / I affirm in lieu of an oath that the information provided herein to the best of my knowledge is true and complete.*

Die Strafbarkeit einer falschen eidesstattlichen Versicherung ist mir bekannt, namentlich die Strafandrohung gemäß § 156 StGB bis zu drei Jahren Freiheitsstrafe oder Geldstrafe bei vorsätzlicher Begehung der Tat bzw. gemäß § 161 Abs. 1 StGB bis zu einem Jahr Freiheitsstrafe oder Geldstrafe bei fahrlässiger Begehung. / *I am aware that a false affidavit is a criminal offence which is punishable by law in accordance with § 156 of the German Criminal Code (StGB) with up to three years imprisonment or a fine in case of intention, or in accordance with § 161 (1) of the German Criminal Code with up to one year imprisonment or a fine in case of negligence.*

_____ _____

Ort / *Place*, Datum / *Date* Unterschrift / *Signature*

Summary

Submarine landslides are gravity-driven mass movements that occur in underwater slope settings worldwide. They are one of the volumetrically most important processes for transporting sediments from the continental margin into the deep ocean. Despite the hazard they pose to coastal communities and critical seafloor infrastructure, many aspects of submarine landslides remain poorly understood. Our understanding of submarine landslides is often based on hypotheses that are hard to test, and we tend to infer landslide behaviour rather than understand the reason behind their formation. Sufficient information regarding the internal structure and composition, i.e. from sediment cores and in-situ measurements is often missing. Therefore, some key questions still remain unanswered, which include why some areas fail while adjacent slopes do not, or how submarine landslides can fail on low angle slops (<2°). Many studies proposed that these phenomena and the large areal extend of submarine landslides may be explained by laterally-extensive weak layers within the slope stratigraphy. Our knowledge regarding weak layers, in particular their compositional and structural characteristics, as well as the processes that control and form them, however, is still very limited.

This thesis makes use of a variety of datasets at different scales and resolution in order to both qualitatively and quantitatively investigate the role of sediment structure and composition on weak layer and submarine landslide formation. Furthermore, the role of the environmental setting on the formation of weak layers, and their control on the triggering mechanism are investigated. Establishing such a relation is crucial to identify conditions (i.e. failure mechanism) under which slope failure may occur. Part of this thesis is a comprehensive literature review of published submarine landslide studies that examine the failure planes and apparent weak layers of historic and ancient submarine landslides, to evaluate what types of sediment are capable of forming weak layers and to understand their global distribution. The results show that failure planes usually form in the vicinity of an interface between distinct lithologies that together comprise a weak layer. The review further demonstrates that different types of weak layers show an affinity to specific geographical and physiographical locations. These include contourite or turbidite systems that can create siliciclastic sediment sequences, areas of high productivity or upwelling where biogenic sediments may dominate, or regions that experience repeated ash deposition from proximal or distal volcanic sources.

Weak layers are further investivated by means of two selected case studies, a cohesive submarine landslide that occurred in a low angle sheeted contourite drift (namely the AFEN Slide) and a coastal retrogressive submarine landside that initiated along a regional turbidite event bed (namely the Finneidfjord Slide). The AFEN Slide is investigated using a combination of geophysical, sedimentological, geochemical, and geotechnical data. These data reveal abrupt lithological contrasts

characterised by distinct changes in physical, geochemical and geotechnical properties. The findings indicate that failure likely initiated along this distinct climatically-controlled lithological contrast, which marks the boundary between a sandy contourite and underlying softer mud-rich sediments. Whether climate change played a role in triggering slope failure remains unclear, however, the data demonstrate its role in dictating the location of the failure plane. Furthermore, the results highlight the necessity to integrate high-resolution sediment core analyses and information about the regional setting to identify potential weak layers over the depth range of stratigraphy. The second case study, the Finneidfjord Slide offshore Norway, is investigated by means of high-resolution 3D micro-Computed Tomography imaging. The results reveal clear compositional and structural differences between individual sub-units of the weak layer, as well as the background sediment. The pore space distribution is highly spatially variable. Such high variability may be masked by bulk porosity measurements. Bulk-porosity measurements work on a centimetre-scale, while the observed changes are found on a millimetre-scale. Such differences, however, may be crucial for the formation of weak layers as they appear to dictate the location of the failure plane. These findings have important implications for understanding how weak layers are formed and their influence on failure plane formation. The results further enable a better constraint on the relation between environmental setting and weak layer distribution, as well as triggering and failure mechanisms.

Zusammenfassung

Submarine Hangrutschungen sind schwerkraftgetriebene Massenbewegungen, die weltweit in Unterwasser-Hanglagen auftreten. Sie gehören zu den volumetrisch wichtigsten Prozessen für den Transport von Sediment vom Kontinentalrand in die Tiefsee. Trotz der Gefahr, die sie für Küstengebiete und wichtige Infrastrukturen am Meeresgrund darstellen, sind viele Aspekte submariner Hangrutschungen immer noch unzureichend erforscht. Unser Verständnis submariner Hangrutschungen basiert oft auf Hypothesen die schwer überprüfbar sind, und wir neigen dazu Folgerungen zu deren Verhalten zu ziehen, statt ihre Ursachen zu verstehen. Es fehlt oft an ausreichenden Informationen über die interne Struktur und Zusammensetzung, d.h. basierend auf Sedimentkernen oder In-situ-Messungen. Aus diesem Grund sind einige Fragen noch ungeklärt, unter anderem warum einige Bereiche rutschen, während benachbarte Hänge stabil bleiben, oder wie submarine Rutschungen an Hängen mit geringem Neigungswinkel (<2°) entstehen können. Viele Studien bauen darauf auf, dass diese Phänomene und die große flächenmäßige Ausdehnung submariner Hangrutschungen durch lateral weitläufige „schwache Schichten“ (*Weak Layer*) innerhalb der Hangstratigraphie erklärt werden können. Unser Wissen über solche Schichten, insbesondere über ihre Zusammensetzung und strukturelle Eigenschaften, sowie über die Prozesse die sie beeinflussen und formen, ist jedoch noch immer sehr begrenzt.

Diese Dissertation nutzt eine Vielzahl von Datensätzen verschiedener Größenordnungen und Auflösungen, um sowohl qualitativ als auch quantitativ die Rolle der Struktur und Zusammensetzung des Sediments bei der Bildung von *Weak Layern* und submarinen Hangrutschungen zu untersuchen. Darüber hinaus, wird die Rolle von Umweltbedingungen bei der Bildung von *Weak Layern* und deren Einfluss auf mögliche „Auslösemechanismen“ untersucht. Diese Zusammenhänge zu verstehen ist wesentlich um zu bestimmen, unter welchen Bedingungen (d.h. „Versagensmechanismen“) eine Rutschung auftreten kann. Teil dieser Arbeit ist eine umfassende Literaturrecherche veröffentlichter Studien über submarine Hangrutschungen, welche die „Versagensflächen“ und scheinbare *Weak Layer* historischer submariner Hangrutschungen untersuchen, um herauszufinden, welche Sedimenttypen in der Lage sind *Weak Layer* zu bilden, sowie um deren globale Verteilung zu verstehen. Die Ergebnisse zeigen, dass sich „Versagensflächen“ normalerweise in der Nähe einer Grenzfläche zwischen verschiedenen Lithologien bilden, die zusammen einen *Weak Layer* darstellen. Die Literaturrecherche zeigt außerdem, wie verschiedene Arten von *Weak Layern* eine Affinität zu bestimmten geographischen und physiographischen Standorten aufweisen. Dazu gehören Contourite- oder Turbidit-Systeme, die siliziklastische Sedimentsequenzen erzeugen können, Gebiete mit hoher Produktivität oder Upwelling, in denen biogene Sedimente dominieren können, oder Regionen, die wiederholten Ascheablagerungen aus proximalen oder distalen vulkanischen Quellen ausgesetzt sind.

Weiters werden *Weak Layer* anhand zweier ausgewählter Fallstudien untersucht: eine kohäsive, submarine Rutschung, die in einem „Contourite Drift“ mit geringem Neigungswinkel auftrat (die AFEN-Rutschung) und eine küstennahe, retrograde, submarine Rutschung, die entlang einer regionalen Turbiditlage entstand (die Finneidfjord-Rutschung). Die AFEN-Rutschung wird anhand einer Kombination aus geophysikalischen, sedimentologischen, geochemischen und geotechnischen Daten untersucht. Diese Daten zeigen abrupte lithologische Kontraste, die durch deutliche Veränderungen der physikalischen, geochemischen und geotechnischen Sedimenteigenschaften gekennzeichnet sind. Die Ergebnisse deuten darauf hin, dass die Rutschung wahrscheinlich entlang dieses ausgeprägten, klimatisch gesteuerten, lithologischen Kontrasts begann, der die Grenze zwischen einem sandigen Contourite und den darunter liegenden weicheren, schlammreichen Sediment markiert. Ob der Klimawandel bei der Auslösung der Hangrutschung eine Rolle gespielt hat, bleibt ungeklärt; die Daten zeigen jedoch seine Rolle bei der Lokalisierung der „Versagensfläche“. Darüber hinaus zeigen die Ergebnisse die Notwendigkeit, hochauflösende Sedimentkernanalysen und Informationen über die regionalen Gegebenheiten mit einzubeziehen, um potenzielle *Weak Layer* zu identifizieren. Die zweite Fallstudie, die Finneidfjord-Rutschung vor der Küste Norwegens, wird mittels hochauflösender 3D-Mikro-Computertomographie-Bildgebung untersucht. Die Ergebnisse zeigen deutliche Unterschiede in der Zusammensetzung und Struktur einzelner Untereinheiten des *Weak Layers,* sowie dem Hintergrundsediment. Die Porenraumverteilung ist räumlich sehr variabel. Eine solch hohe Variabilität kann mit „Bulk“-Porositätsmessungen nicht nachgewiesen werden. Diese „Bulk“-Porositätsmessungen operieren auf einer Zentimeter-Skala, während die beobachteten Veränderungen auf einer Millimeter-Skala zu finden sind. Solche Unterschiede können jedoch entscheidend für die Bildung von *Weak Layern* sein, da sie die Lage der „Versagensebene“ zu bestimmen scheinen. Die Ergebnisse haben maßgeblichen Einfluss auf das Verständnis, wie *Weak Layer* gebildet werden, sowie deren Einfluss auf die Bildung von „Versagensflächen“. Des Weiteren ermöglichen die Ergebnisse eine bessere Einschätzung des Zusammenhanges zwischen Umweltbedingungen und der Verteilung von W*eak Layern*, sowie der „Auslöse“- und „Versagensmechanismen“.

Preface

This PhD project was funded by the European Union's Horizon 2020 research and innovation programme under the Marie Skłodowska-Curie grant agreement No 721403, as part of the project SLATE (Submarine Landslides and Their impact on European continental margins). The cumulative doctoral thesis is part of Work Package 1 (WP1) 'Submarine landslides: understanding pre-failure processes, long-term trends in slope evolution and failure mechanisms', and aims to contribute to our understanding of weak layer formation and their control on submarine landslide inception.

Table of contents

List of figures

List of tables

Nomenclature

Roman symbols

F	Factor of safety
N_c	Number of individual cluster per phase
N_v	Number of voxel per phase
c	Cohesion
c_v	Coefficient of compression
k	Permeability
n	Porosity
n_i	Number of voxel per phase cluster i
s	Shear strength
s_u	Undrained shear strength
t_0	Time 0, pre-failure
t_1	Time 1, during failure
u	Pore pressure
Δu	Pore pressure change

Greek symbols

Φ	Angle of internal friction
γ'	Effective unit weight
σ_n	Normal stress
σ_n'	Effective normal stress
σ'_{v0}	Effective vertical overburden stress
τ	Shear strength
τ_{max}	Maximum shear strength

Abbreviations

AFEN	Atlantic Frontier Environmental Network
AIW	Arctic Intermediate Water
APC	Advanced Piston Corer

AUV	Autonomous Underwater Vessel
BOSCORF	British Ocean Sediment Core Research Facility
BP	Before Present
CCD	Charge-Coupled Device
CPTu	Cone Penetration Testing with pore pressure response
DDL	Diffuse Double Layer
DS	Direct Shear test
FF-CPTu	Free-Fall Cone Penetration Testing with pore pressure response
FSCBW	Faroe-Shetland Channel Bottom Water
GC	Gravity Corer
GEBCO	General Bathymetric Chart of the Ocean
GEOMAR	Geomar Helmholtz Centre for Ocean Research Kiel or '*Geomar Helmholtz-Zentrum for Ozeanforschung Kiel*'
GOST	MARUM Geotechnical Offshore Seabed Tool
IFREMER	French Research Institute for Exploitation of the Sea or '*Institut Français de Recherche pour L'Exporation de la Mer*'
IN	Sediment cores/in-situ measurements sampling the basal surface inside the slide area were available
IODP	International Ocean Discovery Program
ITRAX	High-resolution XRF analysis of sediment cores
LGM	Last Glacial Maximum
LL	Liquid Limit
MARUM	Center for Marine Environmental Sciences or '*Zentrum für Marine Umweltwissenschaften der Universität Bremen*'
MeBo	Seafloor drill rig or '*Meeresboden Bohrgerät'*
micro-CT	X-ray micro-Computed Tomography
MNAW	Modified North Atlantic Water
MSCL	Multi-Sensor Core Logger
MSCL-CIS	Core Imaging System
MSCL-S	Standard Multi-Sensor Core Logger
N/A	Not applicable / no information
NAW	North Atlantic Water

NO	Sediment cores/in-situ measurements are available, but did not sample the failure or glide plane
NSAIW	Norwegian Sea Arctic Intermediate Water
ODP	Ocean Drilling Program
OUT	Sediment cores/in-situ measurements sampling the failure plane equivalent sediments outside the slide area are available
PC	Piston Corer
PL	Plastic Limit
PSD	Particle Size Distribution
RV	Research Vessel
SEM	Scanning Electron Microscopy
SLATE	Submarine LAndslides And Their impact on European continental margins
SLS	Swiss Light Source
TOMCAT	A beamline for TOmograpic Microscopy and Coherent rAdiology experimenTs
UiB	University of Bergen
UTM	Universal Transverse Mercator
XCB	Extended Core Barrel
XRF	X-ray Fluorescence
ZIB	Zuse Institut Berlin

1. Introduction

1.1. Submarine landslides

Submarine landslides are 'downward and outward movements of slope-forming materials, wherein shear failure occurs along one or several surfaces' (Hampton et al., 1996). Such events have been recognised in underwater slope settings worldwide (e.g. Hühnerbach et al., 2004, Lee et al., 2007; Chaytor et al., 2009; Urgeles and Camerlenghi, 2013). They can be exceptionally large, orders of magnitudes larger than their terrestrial counterparts (e.g. Hühnerbach et al., 2004; Korup et al., 2007) and are one of the volumetrically most important processes for transporting large amounts of sediment across the continental shelf and slope into the deep ocean (Masson et al., 2006). Moreover, submarine landslides have also been identified on remarkably low angle slopes (<2°) that are almost always stable on land (e.g. Hampton et al., 1996; Evans et al., 2005; Krastel et al., 2019).

The socio-economic consequences of submarine landslides can be severe. They can damage critical offshore infrastructure such as equipment needed for the hydrocarbon industry or telecommunication cables on the seafloor (Piper et al., 1999; Fine et al., 2005; Thomas et al., 2010; Carter et al., 2014; Pope et al., 2017). A famous example is the 1929 Grand Banks (Newfoundland) earthquake-triggered slump that generated a turbidity current, which systematically broke all seafloor cables within 500 km distance of the failure (Heezen and Ewing, 1952). Today, more than 95 % of the global telecommunication transfer use a network of seafloor telecommunication cables (Urlaub et al., 2013; Carter et al., 2014; Clare et al., 2017), and it is thus important to know which sites are suitable for their deployment.

Submarine landslides may also generate devastating and deadly tsunamis (Tappin et al., 2001; ten Brink et al., 2009; Harbitz et al., 2014), and even small landslides can be very hazardous, if occurring in near coastal environments. A notable example is the 1979 Nice Airport Slide offshore Nice, France that caused fatalities, partial destruction of harbour constructions (Assier-Rzadkiewicz et al., 2000) and generated a 2-3 m high tsunami (Gennesseaux et al., 1980). Another example is found offshore Finneidfjord, Norway where a submarine landslide that retrogressed onshore destroyed parts of the highway and caused fatalities (Longva et al., 2003). Many coastal areas are densely populated, with about 1.2 billion people living within 100 km of the shoreline and many buildings and infrastructure close to the sea (Small and Nicholls, 2003).

Their large-scale and the fact that they occur on nearly horizontal slopes, along with the inability to observe them directly, makes submarine landslides more difficult to analyse than many other geohazards. Consequently, they are as of yet poorly understood and hazard assessments are problematic, or involve large uncertainties.

1.1.1. Mechanics of submarine landslides

Submarine landslides will occur if the downwards driving forces (shear stress) exceed the resisting forces (shear strength) of the slope material. This causes slope failure and subsequent slide movement along one or more *glide planes* (e.g. Hampton et al., 1996; Lee et al., 2007). In this thesis, I refer to large features resulting from slope failure collectively as *landslide* (or *slide*) in that they have relatively well-defined boundaries with distinct headwalls and basal surfaces (Mulder and Cochonat, 1996). I refer to *failure plane* as the surface along which failure initiates and define *glide plane* as the surface along which movement occurs. Submarine landslides can feature complex failure mechanisms that can act at the same time, and in which repeated failure along different failure planes can occur (e.g. Kvalstad et al., 2005; Georgiopoulou et al., 2010; Kuhlmann et al, 2017; Gatter et al., 2020).

In general, a submarine landslide is the result of slope failure, which is initiated when the factor of safety (F) drops below one (Morgenstern and Price, 1965):

$$F = s/\tau \tag{1.1}$$

where the shear strength (s) is defined as the maximum shear stress (τ_{max}) the sediment can withstand and τ is the shear stress acting on the slope. The shear strength of a sediment can further be expressed by the Mohr-Coulomb constitutive law (Handin, 1969) and is a function of its cohesion (c), the effective stress acting normal to the failure plane (σ_n'), the angle of internal friction (Φ):

$$s = \tau_{max} = c + \sigma_n' \tan\Phi \tag{1.2}$$

In undrained loading conditions, transient pore pressure change (Δu) decreases the effective normal stress (σ_n') as it acts against the applied normal stress (σ_n) according to (Terzaghi, 1943):

$$\sigma_n' = \sigma_n - u \tag{1.3}$$

As a result, the undrained shear strength (s_u) is lower than the drained shear strength of sediments for drained loading conditions.

1.1.2. Pre-conditioning factors and triggering mechanisms

Submarine landslides occur by either an increase in the applied shear stress, a decrease in shear strength of the slope material, or a combination of both (see Eq. 1.1). Many hypotheses have been put forward concerning factors that control the initiation of submarine landslides (e.g. Hampton et al., 1996; Locat and Lee, 2002; Masson et al., 2006; Lee et al., 2007; Leynaud et al., 2009). These factors can be categorised into long-term pre-conditioning factors (e.g. Lee et al., 2007) that usually act on timescales

of hundreds to thousands of years, and short-term triggering mechanisms that operate on a timescale of hours to days (e.g. Fine et al., 2005).

The most efficient way to decrease the shear strength of a slope material is a transient increase in pore pressure, which causes a decrease in the effective normal stress (see Eq. 1.3). Factors that increase pore pressure include rapid sedimentation, tectonic loading, cyclic loading (i.e. liquefaction related to earthquakes, and tidal or storm waves), gas charging (migration or decay of organic material) and gas hydrate dissociation, fluid flow, and dissolution processes (e.g. Hampton et al., 1996; Lee et al., 2007; Dugan and Sheahan, 2012). Factors that may increase the applied shear stress include static (sedimentary, glacial and tectonic overloading) and cyclic (seismic and storm wave) loading, slope over-steepening (due to tectonic uplift, basal erosion on a submarine slope or diapirism), and volcanic activity (e.g. Hampton et al., 1996; Masson et al., 2006; Lee et al., 2007).

A number of these factors can act as both pre-conditioning factor and ultimate trigger of slope failure. In addition, it has to be noted that the relative importance of individual factors and the interplay between them is still not well understood. For example, in some environments a certain triggering mechanism will dominate, while in other regions entirely different triggers may be found (e.g. Hampton et al., 1996; Sultan et al., 2004; Lee et al., 2007; Urgeles and Camerlenghi, 2013).

1.1.3. The role of weak layers in the inception of submarine landslides

Many studies have invoked that the presence of so-called *weak layers* within the slope stratigraphy plays a key role in the formation of submarine landslides, especially for those of large extent, taking place on nearly horizontal slopes (e.g. Locat and Lee 2002; Lee et al., 2007; Masson et al., 2010; Locat et al., 2014).

Weak layers are inferred to be relatively weaker prior or during failure, thereby enabling focused shearing to take place. That is to say that the shear strength of the layer is reduced or the shear stress acting on the slope is increased to a degree where the driving forces exceed the resisting forces, i.e. the factor of safety drops below one (Eq. 1.1). According to Eq. 1.2 and 1.3, the formation of a weak layer can be achieved by either a modification in cohesion, normal stress, pore pressure, angle of internal friction, or a combination of all.

Various types of sediment and several failure mechanisms have been deemed relevant for the formation of weak layers. Weak layer forming sediments include (a detailed review of weak layers is presented in Chapter 2): soft and sensitive clays (e.g. Kvalstad et al., 2005; L'Heureux et al., 2012), loose sand (e.g. Wilson et al., 2004), porous ash (e.g. Kuhlmann et al., 2016) or diatom ooze (e.g. Urlaub et al., 2018). Such sediments could fail, for example, by strain softening of clays (e.g. L'Heureux et al., 2012), or due

to liquefaction and transient pore pressure generation of sandy sediments (e.g. Wilson et al., 2004). Porous ashes and diatom oozes are thought to fail due to particle crushing, i.e. the loss of sediment structure, under cyclic loading which may also enable the generation of transient pore pressures (e.g. Harders et al., 2010; Urlaub et al., 2018). For pore pressure to accumulate, however, a low-permeability sealing layer is needed to inhibit the vertical dissipation of pore fluids (e.g. Dugan and Sheahan, 2012). Thus, it appears that stratigraphic sequencing plays a key role in the formation of weak layers.

Different types of sediments form weak layers under different conditions, e.g. clay will rather fail by strain softening behaviour, while sand will more likely fail due to liquefaction. It therefore stands to reason that in order to identify the acting failure mechanism we first need to identify the type of weak layer (i.e. the type of sediment). This relationship, however, is not sufficiently established yet, mainly because of the lack of a comprehensive dataset of weak layers and their related failure mechanisms. The identification of the failure mechanism is crucial for submarine landslide hazard and risk assessments.

1.2. Motivation and research hypotheses

Weak layers play a critical role in the inception of submarine landslides as they appear to control the location of failure plane formation. The previous chapter (1.2) has shown that various sediment types and failure mechanisms can involve weak layers; however, to this date very little is known about their actual structure and composition, and the processes that control and form weak layers are still poorly understood. The overarching aim of this doctoral thesis is to qualitatively and quantitatively investigate the role of sediment structure and composition (i.e. different sediment types) on weak layer and submarine landslide formation. To reach this aim, I conducted a thorough literature review, assessing the current state-of-the-art of weak layer research, followed by a detailed analysis of two selected case studies, the AFEN Slide offshore the UK (Fig. 1.1) and the Finneidfjord Slide offshore Norway (Fig. 1.2). To this end, I made use of a variety of datasets at different scales and resolutions. These datasets range from large-scale geophysical mapping data to centimetre-scale sediment core-logging and geotechnical data, and sub-millimetre, high-resolution X-ray micro-Computed Tomography (CT) data. Based on the integration of these datasets, I test the following overarching hypotheses:

(1) Weak layers coincide with prominent sediment horizons within the slope stratigraphy, but distinct lithological contrasts control the formation of weak layers and dictate where failure planes form (Chapter 2).

Nowadays, the concept of weak layers playing a key role in dictating the location and depth of submarine landslides is widely accepted. Most conceptual models of submarine landslides assume that slope failure initiates along weak layers embedded with the slope stratigraphy; however, the exact definition of weak layers is still subject to debate. While many studies have referred to weak layers as mechanically weaker

sediments with intrinsic lower shear strength, other studies have pointed towards the importance of sediment sequencing, especially those of contrasting permeability, in dictating where failure planes form. To this date, the processes that control and form weak layers are still not well understood.

(2) Weak layers are formed as a result of various processes, but the type and distribution of weak layers is controlled by the environmental setting (Chapter 3 and 4).

One of the outstanding challenges in submarine landslide research is the recognition of the ultimate cause of failure. Although many factors have been proposed that may cause slope failure by either increasing the shear stress or decreasing the shear strength, the relative contribution of, and interaction between, individual factors remains unclear. Most of the time, it appears that a combination of different factors (including pre-conditioning and triggering mechanisms) is necessary. Knowing about the type of weak layer, in combination with information regarding the regional setting may help us unravelling this issue, as it allows us to constrain potential failure and triggering mechanisms.

(3) For the identification and characterisation of failure planes and weak layers integration of various datasets is critical, but especially high-resolution (sub-millimetre-scale) datasets are needed to assess their structure (Chapter 4).

Several studies have pointed towards the significance of an inter-disciplinary investigation of submarine landslides and their controlling factors (e.g. Vanneste et al., 2014; Madhusudhan et al., 2017). Although the integration of datasets at different scales and resolution is critical, it has become apparent that questions remain unanswered, even in the case of some of the best studied submarine landslides (e.g. Storegga Slide, Finneidfjord Slide). High-resolution imaging techniques, such as micro-Computed Tomography, may allow to overcome this problem as they enable the visualisation of structures (and processes) that cannot be resolved with conventional sedimentological or geotechnical analyses.

1.3. Selected case studies

The research hypotheses are investigated by means of two case studies: A cohesive submarine landslide, which occurred within a low angle (<2.5°) sheeted contourite drift on the continental slope offshore the UK, and a coastal retrogressive submarine landslide that initiated along a regional event bed (i.e. a turbidite deposit) offshore Finneidfjord, Norway. These submarine landslides were selected for the following reasons:

(1) Owing to their relatively small-scale, these landslides are accessible and therefore, sediment cores that sampled the pre-slide sedimentary sequences, including sediments that correlate stratigraphically with the failure planes, are available.

(2) The type of weak layer (i.e. lithology) associated with these landslides is the same, but the slides are located in different environments. This enables a comparison of failure mechanisms and potential triggers that can be associated with such weak layers.

1.3.1. The AFEN Slide

The AFEN Slide, which is dated to about 16 – 2.8 ka BP, is a four-stage retrogressive submarine landslide that occurred on a low angle (<2.5°) slope, NW of the Shetland Islands (UK) (Fig. 1.1; Wilson et al., 2003, 2004). The landslide mobilised about 200 x 10^6 m^3 of sediment (Wilson et al., 2004).

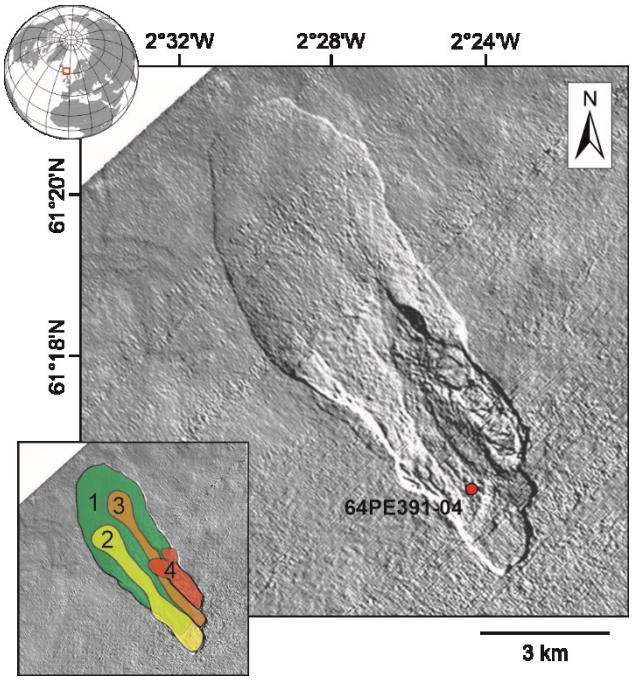

Figure 1.1. Outline of the AFEN Slide (seabed image produced from 3D seismic data). Piston core 64PE391-04 is shown as red dot. Inset image shows the four stages of failure (after Wilson et al., 2004; Gatter et al., 2020).

Several failure mechanisms have been proposed. Initial studies inferred that the landside initiated along a well-sorted sandy contourite layer. Such a layer may liquefy during an earthquake, thereby causing failure (Wilson et al., 2004; Jackson et al., 2004). Madhusudhan et al. (2017), on the other hand, suggested progressive failure of a sensitive clay or liquefaction of silt layers. None of these studies, however, were based on sediment cores that sampled undisturbed sediments that correspond stratigraphically to the failure plane.

1.3.2. The Finneidfjord Slide

The 1996 Finneidfjord Slide initiated offshore before developing in a retrogressive manner, back-stepping 100 – 150 m onshore, thereby claiming four human lives and destroying parts of the main north-south highway (Fig. 1.2; Longva et al., 2003). The landslide mobilised about 1 x 10^6 m^3 of sediment (Longva et al., 2003) and is one of the best studied submarine landslides to date.

Numerous studies have suggested several factors that may have contributed to failure. These include the generation of excess pore pressure as a result of climatic and anthropogenic factors (e.g. Longva et al., 2003), the accumulation of free gas (Best et al., 2003; Morgan et al., 2012), or an increase in overburden stress due to dumping of material along the shoreline (e.g. Vanneste et al., 2011). Failure along a low-permeability regional event bed (i.e. weak layer) combined with periods of heavy rainfall may have enabled the formation of artesian groundwater pressure and caused failure (e.g. L'Heureux et al., 2012).

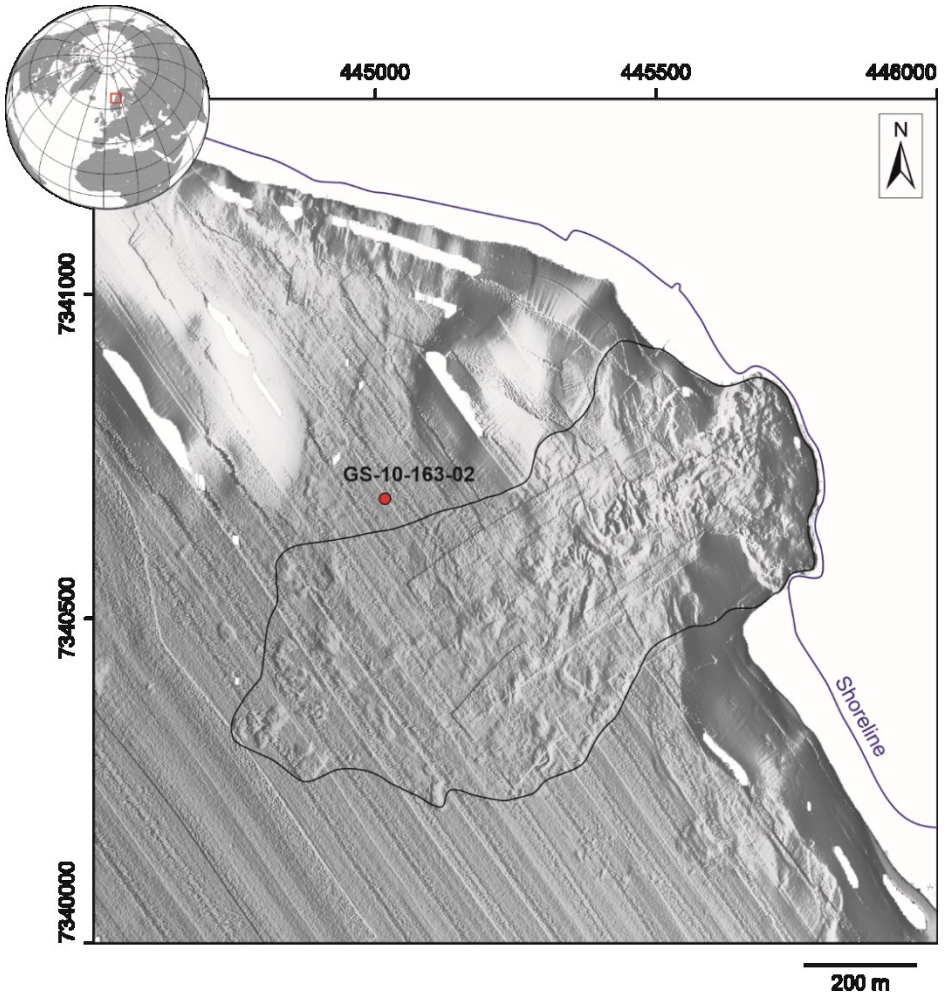

Figure 1.2. Outline of the 1996 Finneidfjord Slide (projection in UTM Zone 33N coordinate system). Calypso piston core GS-10-163-02 is shown as red dot. Data courtesy of SEABED project with the Norwegian Deepwater Program.

1.4. Analysis methods

1.4.1. Conventional methods

Bulk sediment properties can be analysed using laboratory-based methods, such as non-destructive core-logging analyses, e.g. multi-sensor core logging and X-ray fluorescence, or geotechnical tests (explanation of each method used in respective Chapters). Especially geotechnical tests, however, require relatively large amounts of undisturbed sediment from sediment cores, which is often not readily available. In addition, because the test samples are relatively large, small-scale changes will not be resolved as the tests will show a result averaged over the whole sample. In order to resolve small-scale changes, which are thought to control weak layer formation and dictate failure plane location, these tests are not sufficient.

1.4.2. New approach: Micro-Computed Tomography (CT)

To resolve small-(grain)-scale changes within the sediment sequence, high-resolution imaging techniques are necessary. A relatively wide used method is Scanning Electron Microscopy (SEM). Although this method allows the visualisation of sediments down to a micro-scale, it does not enable a structural analysis, which requires a 3D imaging technique. We therefore deploy high-resolution micro-Computed Tomography (CT) to analyse the Finneidfjord weak layer (Chapter 4). This technique enables the 3D visualisation of the internal structure of the scanned material, which allows the detection of small-scale changes.

1.5. Thesis outline

The main hypotheses of this thesis (see 1.2) were addressed within three individual papers that have been published in, are currently under review or in preparation for submission to peer-reviewed international journals and special publications. The main results of these studies in response to the research hypotheses, as well as a detailed description of my contributions towards each manuscript are provided in the following thesis outline:

Chapter 1 outlines the motivation behind the research of submarine landslides in general and this thesis in particular. It introduces the general mechanics of slope failure, discusses causal factors and highlights the socio-economic impacts of submarine landslides. The chapter concludes by outlining the main objectives and hypotheses of this thesis, and the rationale behind choosing selected case studies and micro-Computed Tomography as a special method for weak layer investigation.

In **Chapter 2**,

Characterisation of weak layers, physical controls on their global distribution and their role in submarine landslide formation

Gatter, R., Clare, M.A., Kuhlmann, J., Huhn, K.

Submitted to *Earth-Science Reviews* on 20. April 2021

Under revision with major revisions required since 05. June 2021

a detailed literature review of failure planes and weak layers of submarine landslides is presented that summarises the current state-of-the-art and outlines some of the outstanding challenges in weak layer research. The main aim of the study is to review the current understanding regarding weak layers and their influence on submarine landslide formation (Hypothesis 1), by means of a new global submarine landslide catalogue that comprises 60 case studies. It addresses the following research questions:

- What types of sediments are capable of forming weak layers and how diverse is the nature of weak layers worldwide?
- What are the physical controls on where different types of weak layers form?
- What are the outstanding challenges in identifying and characterising weak layers and how can future studies extend our understanding?

The results of the literature review show that failure planes of submarine landslides usually form in the vicinity of interfaces between distinct lithologies that together comprise a weak layer. These interfaces are the result of contrasting permeability and/or strength parameters within sediment sequences, which appear to be key to the formation of weak layers. Different types of weak layers (which are linked to sediment lithology) can be correlated to specific geographical and physiographic locations, including contourite or turbidite systems that can create siliciclastic sediment sequences. The review concludes by highlighting the importance of an integrated approach towards weak layer investigation, combining geophysical surveys with detailed geotechnical and sedimentological analyses including high-resolution grain-scale observations (e.g. micro-Computed Tomography).

R. Gatter conceptualised the paper, conducted the literature review, and analysed the data with key inputs from supervisors K. Huhn and M.A. Clare. The original manuscript was written by R. Gatter, with various comments from all co-authors. The main author, R. Gatter, would like to acknowledge the constructive discussions and invaluable input from all co-authors.

Chapter 3,

A multi-disciplinary investigation of the AFEN Slide: the relationship between contourites and submarine landslides

Gatter, R., Clare, M.A., Hunt, J.E., Watts, M., Madhusudhan, B.N., Talling, P.J., Huhn, K.

Published in *Geological Society, London, Special Publications*

presents a detailed characterisation of the AFEN Slide, which occurred within a low angle (<2.5°) laterally extensive sheeted contourite drift offshore the UK. The manuscript integrates detailed (physical, sedimentological, geochemical and geotechnical) datasets from a sediment core that sampled the pre-landslide sediment sequence, and includes sediments that correlate stratigraphically with the failure plane located further upslope. Based on this integration, the study sets out to investigate the environmental influence on weak layer properties (Hypothesis 2) and to evaluate the potential of data integration for weak layer research in order to answer the following research questions:

- What is the nature of the undisturbed sediment sequence and do material heterogeneities explain the location of the failure plane?
- What causes the observed heterogeneities within the slope stratigraphy?

The integration of various datasets allows to resolve small-scale material changes within the slope stratigraphy. The results indicate that the AFEN Slide initiated along a distinct lithological interface, which correlates with the base of a sandy contourite overlying a thick, relatively homogeneous silty clay unit. In addition, the data show that this interface may relate to a switch in depositional regime from cold and uniform to warm and more variable depositional conditions. The study concludes that such distinct lithological interfaces may be common in contouritic sediments near ocean gateways where climate change may directly affect thermohaline circulation and bottom current intensity, thereby controlling the depositional regime and location of submarine landslide inception.

R. Gatter gratefully used the data collected by co-authors, analysed the MSCL, XRF and particle size data, and conducted additional geotechnical tests. Conceptualisation of the paper, and analysis of the data was carried out by R. Gatter, with key inputs from supervisor M.A. Clare, J.E. Hunt, and B.N. Madhusudhan. The original manuscript was written by R. Gatter, with constructive comments from all co-authors. The particle size analysis was carried out by J.E. Hunt and permeability measurements from oedometer tests were provided by B.N. Madhusudhan. R. Gatter thanks all co-authors for relentless discussions and their patience during the writing and revision process.

In **Chapter 4**,

Pore structure of weak layers: Micro-CT imaging of the Finneidfjord Slide

Gatter, R., Clare, M.A., Madhusudhan, B.N., Vardy, M., Huhn, K.

In preparation for *Frontiers in Earth Sciences*

The study tests the potential of high-resolution micro-CT imaging for weak layer research based on the analysis of undisturbed sediments that correlate stratigraphically with the previously identified weak layer of the 1996 Finneidfjord Slide offshore Norway. The study aims to investigate whether micro-structural properties, especially pore structure, play a role in weak layer and failure plane formation (Hypothesis 3). The pore structure and potential changes in pore structure throughout the weak layer are visualised and quantified at a sub-micrometre resolution to address the following questions:

- How does pore structure change throughout the weak layer and background sediment?
- What are the factors controlling pore structure?
- What are the outstanding challenges in the application of micro-CT imaging for weak layer research and future directions?

The results show that pore structure not only changes throughout the weak layer, but also shows considerable changes within individual sediment units of the weak layer. Most noticeable are the changes within the sand layer. The recognition of such small-scale changes is crucial, as they may govern failure plane formation.

R. Gatter gratefully used and analysed the micro-CT data collected by B.N. Madhusudhan. Conceptualisation of the paper was done by R. Gatter, with key inputs from supervisors K. Huhn and M.A. Clare, and M. Vardy. The original manuscript was written by R. Gatter, with various comments from all co-authors. The main author, R. Gatter, would like to acknowledge the fruitful discussion and invaluable input from all co-authors.

Chapter 5 summarises the results and main conclusions of the previous chapters, discusses their implications for future weak layer research, and sets out to outline future directions of weak layer investigation.

References

Assier-Rzadkiewicz, S., Heinrich, P., Sabatier, P.C., Savoye, B., Bourillet, J.F., 2000. Numerical Modelling of Landslide-generated Tsunami: The 1979 Nice Event. Pure and Applied Geophysics, 157, 1707-1727.

Best, A.I., Clayton, C.R.I., Longva, O., Szuman, M., 2003. The role of free gas in the activation of submarine slides in Finneidfjord. In: Locat, J., Mienert, J. (Eds) Submarine Mass Movements and Their Consequences, Advances in Natural and Technological Hazards Research, 19, 491–498. Springer, Dordrecht.

Carter, L., Gavey, R., Talling, P.J., Liu, J.T., 2014. Insights into submarine geohazards from breaks in subsea telecommunication cables. Oceanography, 27(2), 58–67, http://dx.doi.org/10.5670/oceanog.2014.40

Chaytor, J.D., ten Brink, U.S., Solow, A.R., Andrews, B.D., 2009. Size distribution of submarine landslides along the U.S. Atlantic margin. Marine Geology, 264(1-2), 16-27, https://doi.org/10.1016/j.margeo.2008.08.007

Clare, M.A., Vardy, M.E., Cartigny, M.J.B., Talling, P.J., Himsworth, M.D., Dix, J.K., Harris, J.M., Whitehouse, R.J.S., Belal, M., 2017. Direct monitoring of active geohazards: emerging geophysical tools for deep-water assessments. Near Surface Geophysics, 15, 427-444, https://doi.org/10.3997/1873-0604.2017033

Dugan, B., Sheahan, T.C., 2012. Offshore sediment overpressures of passive margins: mechanisms, measurement, and models. Review in Geophysics, 50, RG3001, https://doi.org/10.1029/2011RG000379

Evans, D., Harrison, Z., Shannon, P.M., Laberg, J.S., Nielsen, T., Ayers, S., Holmes, R., Hoult, R.J., Lindberg, B., Haflidason, H., Long, D., Kuijpers, A., Andersen, E.S., Bryn, P., 2005. Palaeoslides and other mass failures of Pliocene to Pleistocene age along the Atlantic continental margin of NW Europe. Marine and Petroleum Geology, 22, 1131-1148, https://doi.org/10.1016/j.marpetgeo.2005.01.010

Fine, I.V., Rabinovich, A.B., Bornhold, B.D., Thomson, R.E., Kulikov, E.A., 2005. The Grand Banks landslide-generated tsunami of November 18, 1929: preliminary analysis and numerical modeling. Marine Geology, 215, 45-57, https://doi.org/10.1016/j.margeo.2004.11.007

Gatter, R., Clare, M.A., Hunt, J.E., Watts, M., Madhusudhan, B.N., Talling, P.J., Huhn, K., 2020. A multi-disciplinary investigation of the AFEN Slide: The relationship between contourites and submarine landslides. Geological Society, London, Special Publications, 500: 173-193, https://doi.org/10.1144/SP500-2019-184

Gennesseaux, M., Mauffret, A., Pautot, G., 1980. Les glissements sous-marins de la pente continentale niçoise et la rupture de câbles en mer Ligure (Méditerranee occidentale). Comptes Rendus de l'Académie des Sciences de Paris (Académie des Sciences de Paris), 290(14), 959-962.

Georgiopoulou, A., Masson, D.G., Wynn, R.B., Krastel, S., 2010. Sahara Slide: Age, initiation, and processes of a giant submarine slide. Geochemistry, Geophysics, Geosystems, 11(7), Q07014, https://doi.org/10.1029/2010GC003066

Hampton, M.A., Lee, H.J., Locat, J., 1996. Submarine Landslides. Reviews of Geophysics, 34, 35-59.

Handin, J., 1969. On the Coulomb-Mohr failure criterion. Journal of Geophysical Research, 74(22), 5343-5348, https://doi.org/10.1029/JB074i022p05343

Harbitz, C.B., Løvholt, F., Bungum, H., 2014. Submarine landslide tsunamis: how extreme and how likely?. Natural Hazards, 72, 1341-1374.

Harders, R., Kutterolf, S., Hensen, C., Moerz, T., Brueckmann, W., 2010. Tephra layers: A controlling factor on submarine translational sliding?. Geochemistry, Geophysics, Geosystems, 11(5), Q05S23, https://doi.org/10.1029/2009GC002844

Heezen, B.C., Ewing, M., 1952. Turbidity currents and submarine slumps, and the 1929 Grand Banks Earthquake. American Journal of Science, 250, 849-873, https://doi.org/10.2475/ajs.250.12.849

Hühnerbach, V., Masson, D.G., partners oft he COSTA-Project, 2004. Landslides in the North Atlantic and its adjacent seas: an analysis of their morphology, setting and behaviour. Marine Geology, 213, 343-362, https://doi.org/10.1016/j.margeo.2004.10.013

Jackson, P.D., Gunn, D.A., Long, D., 2004. Predicting variability in the stability of slope sediments due to earthquake ground motion in the AFEN area of the western UK continental shelf. Marine Geology, 213, 363-278. Doi: 10.106/j.margeo.2004.10.014

Korup, O., Clague, J.J., Hermanns, R.L., Hewitt, K., Strom, A.L., Weidinger, J.T., 2007. Giant landslides, topography, and erosion. Earth and Planetary Science Letters, 261, 578-589, https://doi.org/10.1016/j.epsl.2007.07.025

Krastel, S., Urlaub, M., Georgiopoulou, A., Wynn, R.B., Schwenk, T., Stevenson, C., Feldens, P., 2019. Mass wasting along the NW African continental margin. In: Lintern, D.G., Mosher, D.C., Moscardelli, L.G., Bobrowsky, P.T., Campbell, C., Chaytor, J.D., Clague, J.J., Georgiopoulou, A., Lajeunesse, P., Normandeau, A., Piper, D.J.W., Scherwath, M., Stacey, C., Turmel, D. (Eds) Subaqueous Mass Movements. Geological Society, London, Special Publications, 477, 151-167, https://doi.org/10.1144/SP477.36

Kuhlmann, J., Huhn, K., Ikari, M., 2016. Do Embedded Volcanoclastic Layers Serve as Potential Glide Planes: An Integrated Analysis from the Gela Basin Offshore Southern Sicily. In: Lamarche, G., Mountjoy, J., Bull, S., Hubble, T., Krastel, S., Lane, E., Micallef, A., Moscardelli, L., Mueller, C., Pecher, I., Woelz, S. (Eds) Submarine Mass Movements and Their Consequences, Advances in Natural and Technological Hazards Research, 41, 273-280. Springer, Cham.

Kuhlmann, J., Asioli, A., Trincardi, F., Klügel, A., Huhn, K., 2017. Landslide Frequency and Failure Mechanisms at NE Gela Basin (Strait of Sicily). Journal of Geophysical Research: Earth Surface, 122, 2223-2243, https://doi.org/10.1002/2017JF004251

Kvalstad, T.J., Andresen, L., Forsberg, C.F., Berg, K., Bryn, P., Wangen, M., 2005. The Storegga slide: evaluation of triggering sources and slide mechanics. Marine and Petroleum Geology, 22, 245-256, https://doi.org/10.1016/j.marpetgeo.2004.10.019

L'Heureux, JS., Longva, O., Steiner, A., Hansen, L., Vardy, M.E., Vanneste, M., Haflidason, H., Brendryen, J., Kvalstad, T.J., Forsberg, C.F., Chand, S., Kopf, A., 2012. Identification of Weak Layers and Their Role for the Stability of Slopes at Finneidfjord, Northern Norway. In: Yamada, Y., Kawamura, K., Ikehara, K., Ogawa, Y., Urgeles, R., Mosher, D., Chaytor, J., Strasser, M. (Eds) Submarine Mass Movements and Their Consequences, Advances in Natural and Technological Hazards Research, 31, 321-330. Springer, Dordrecht.

Lee, H.J., Locat, J., Desgagnés, P., Parsons, J.D., McAdoo, B.G., Orange, D.L., Puig, P., Wong, F.L., Dartnell, P., Boulanger, E., 2007. Submarine mass movements on continental margins. In: Nittouer, C.A., Austin, J.A., Field, M.E., Kravitz, J.H., Syvitski, J.P.M., Wiberg, P.L. (Eds) Continental Margin Sedimentation: From Sediment Transport to Sequence Stratigraphy, 213-274. Blackwell Publishing Ltd, Oxford, UK, https://doi.org/10.1002/9781444304398.ch5

Leynaud, D., Mienert, J., Vanneste, M., 2009. Submarine mass movements on glaciated and non-glaciated European continental margins: A review of triggering mechanisms and preconditions to failure. Marine and Petroleum Geology, 26, 618-632, https://doi.org/10.1016/j.marpetgeo.2008.02.008

Locat, J., Lee, H.J., 2002. Submarine landslides: advances and challenges. Canadian Geotechnical Journal, 39, 193-212, https://doi.org/10.1139/t01-089

Locat, J., Leroueil, S., Locat, A., Lee, H., 2014. Weak Layers: Their Definition and Classification from a Geotechnical Perspective. In: Krastel, S., Behrmann, JH., Völker, D., Stipp, M., Berndt, C., Urgeles, R., Chaytor, J., Huhn, K., Strasser, M., Harbitz, C.B. (Eds) Submarine Mass Movements and Their Consequences, Advances in Natural and Technological Hazards Research, 37, 3-12. Springer, Cham.

Longva, O., Janbu, N., Blikra, L.H., Bøe, R., 2003. The 1996 Finneidfjord Slide; Seafloor Failure and Slide Dynamics. In: Locat, J., Mienert, J. (Eds) Submarine Mass Movements and Their Consequences, Advances in Natural and Technological Hazards Research, 19, 531-538. Springer, Dordrecht.

Madhusudhan, B.N., Clare, M.A., Clayton, C.R.I., Hunt, J.E., 2017. Geotechnical profiling of deep-ocean sediments at the AFEN submarine slide complex. Quaterly Journal of Engineering Geology and Hydrogeology, 50, 148-157, https://doi.org/10.1144/qjegh2016-057

Masson, D.G., Harbitz, C.B., Wynn, R.B., Pedersen, G., Løvholt, F., 2006. Submarine landslides: processes, triggers and hazard prediction. Philosophical Transactions of The Royal Society, 364, 2009-2039, https://doi.org/10.1098/rsta.2006.1810

Masson, D.G., Wynn, R.B., Talling, P.J., 2010. Large Landslides on Passive Continental Margins: Processes, Hypotheses and Outstanding Questions. In: Mosher, D.C., Shipp, R.C., Moscardelli, L., Chaytor, J.D., Baxter, C.D.P., Lee, H.J., Urgeles, R. (Eds) Submarine Mass Movements and Their Consequences, Advances in Natural and Technological Hazards Research, 28, 153-166. Springer Dordrecht.

Morgan, E.C., Vanneste, M., Lecomte, I., Baise, L.G., Longva, O., McAdoo, B., 2012. Estimation of free gas saturation from seismic reflection surveys by the genetic algorithm inversion of a P-wave attenution model. Geophysics, 77(4), R175-R187, https://doi.org/10.1190/geo2011-0291.1

Morgenstern, N., Price, V. E., 1965. The analysis of the stability of general slip surfaces. Géotechnique, 15, 79-93, https://doi.org/10.1680/geot.1965.15.1.79

Mulder, T., Cochonat, P., 1996. Classification of offshore mass movements. Journal of Sedimentary Research, 66, 43-57, https://doi.org/10.1306/D42682AC-2B26-11D7-8648000102C1865D

Piper, D.J.W., Cochonat, P., Morrison, M.L., 1999. The sequence of events around the epicentre of the 1929 Grand Banks earthquake: initiation of debris flows and turbidity current inferred from sidescan sonar. Sedimentology, 46, 79-97, https://doi.org/10.1046/j.1365-3091.1999.00204.x

Pope, E.L., Talling, P.J., Carter, L., 2017. Which earthquakes trigger damaging submarine mass movements: Insights from a global record of submarine cable breaks?. Marine Geology, 384(1), 131-146, https://doi.org/10.1016/j.margeo.2016.01.009

Small, C., Nicholls, R.J., 2003. A Global Analysis of Human Settlement in Coastal Zones. Journal of Coastal Research, 19(3), 584-599.

Sultan, N., Cochonat, P., Canals, M., Cattaneo, A., Dennielou, B., Haflidason, H., Laberg, J.S., Long, D., Mienert, J., Trincardi, F., Urgeles, R., Vorren, T.O., Wilson, C., 2004. Triggering mechanisms of slope instability processes and sediment failures on continental margins: a geotechnical approach. Marine Geology, 213, 291-321, https://doi.org/10.1016/j.margeo.2004.10.011

Tappin, D.R., Watts, P., McMurtry, G.M., Lafoy, Y., Matsumoto, T., 2001. The Sissano, Papua New Guinea tsunami of July 1998 – offshore evidence on the source mechanism. Marine Geology, 175(1-4), 1-23, https://doi.org/10.1016/S0025-3227(01)00131-1

ten Brink, U.S., Lee, H.J., Geist, E.L., Twitchell, D., 2009. Assessment of tsunami hazard to the U.S. East Coast using relationships between submarine landslides and earthquakes. Marine Geology, 264(1-2), 65-73, https://doi.org/10.1016/j.margeo.2008.05.011

Terzaghi, K., 1943. Theoretical soil mechanics. John Wiley & Sons, New York, 510 pp.

Thomas, S., Hooper, J., Clare, M., 2010. Constraining Geohazards to the Past: Impact Assessment of Submarine Mass Movements on Seabed Developments. In: Mosher, D.C., Shipp, C., Moscardelli, L., Chaytor, J., Baxter, C., Lee, H., Urgeles, R. (Eds) Submarine Mass Movements and Their Consequences, Advances in Natural and Technological Hazards Research, 28, 387-398. Springer Dordrecht.

Urgeles, R., Camerlenghi, A., 2013. Submarine landslides of the Mediterranean Sea: Trigger mechanisms, dynamics, and frequency-magnitude distribution. Journal of Geophysical Research: Earth Surface, 118(4), 2600-2618, https://doi.org/10.1002/2013JF002720

Urlaub, M., Geersen, J., Krastel., S., Schwenk, T., 2018. Diatom ooze: Crucial for the generation of submarine mega-slides?. Geology, 46(4), 331-334, https://doi.org/10.1130/G39892.1

Urlaub, M., Talling, P.J., Masson, D.G., 2013. Timing and frequency of large submarine landslides: implications for understanding triggers and future geohazard. Quaternary Science Reviews, 72, 63-82, https://doi.org/10.1016/j.quascirev.2013.04.020

Vanneste, M., Forsberg, C.F., Kvalstad, T.J., L'Heureux, JS., Longva, O., Chand, S., Rise, L., Vardy, M.E., Brendryen, J., Haflidason, H., Lecomte, I., 2011. C-Dog: Coastal and Deepwater Offshore Geohazards. Report to NDP/SEABED, 20100125-1, 66 pp.

Vanneste, M., Sultan, N., Garziglia, S., Forsberg, C.F., L'Heureux, JS., 2014. Seafloor instabilities and sediment deformation processes: The need for integrated, multi-disciplinary investigations. Marine Geology, 352, 183-214, https://doi.org/10.1016/j.margeo.2014.01.005

Vardy, M.E, L'Heureux, JS., Vanneste, M., Longva, O., Steiner, A., Forsberg, C.F., Haflidason, H., Brendryen, J., 2012. Multidisciplinary investigation of a shallow near-shore landslide, Finneidfjord, Norway. Near Surface Geophysics, 10, 267-277, https://doi.org/10.3997/1873-2012022

Wilson, C.K., Long, D., Bulat, J., 2003. The Afen Slide - A Multistaged Slope Failure in the Faroe-Shetland Channel. In: Locat, J., Mienert, J. (Eds) Submarine Mass Movements and Their Consequences, Advances in Natural and Technological Hazards Research, 19, 317-324. Springer, Dordrecht.

Wilson, C.K., Long, D., Bulat, J., 2004. The morphology, setting and processes of the Afen Slide. Marine Geology, 213, 149-167, https://doi.org/10.1016/j.margeo.2004.10.005

2. Manuscript I

Characterisation of weak layers, physical controls on their global distribution and their role in submarine landslide formation

R. Gatter, M.A. Clare, J. Kuhlmann, K. Huhn

Submitted to *Earth-Science Reviews* on 20. April 2021
Under revision with major revisions required since 05. June 2021
Revised version will be re-submitted soon

Abstract

Submarine landslides pose a hazard to coastal communities as they can generate powerful tsunamis, and threaten critical offshore infrastructure such as seafloor cable networks that underpin global communications. Such events can be orders of magnitude larger than their onshore equivalents, yet despite the hazard they pose, many aspects of submarine landslides remain poorly understood, such as why they fail on low angle (<2°) slopes. Many studies have proposed that this, and the large areal extent of submarine landslides, may be controlled by the presence of laterally-extensive weak layers embedded within the slope stratigraphy, which precondition slopes to failure. Little remains known, however, about the characteristics and the processes that control and form weak layers. We conducted a comprehensive review of published submarine landslide studies that examine the failure planes and apparent weak layers associated with historical and ancient submarine landslides. Based on a new global landslide catalogue that comprises 60 case studies, we aim to investigate what types of sediment can form weak layers and to understand the controls on their global variability. Existing classification schemes are based on mechanical process(es), and do not readily enable a diagnosis of weak layers from unfailed sediments. Here, we introduce a new classification of weak layers based on lithology. This classification enables weak layer recognition from sediment cores (including those sampling unfailed sediments), and allows us to attribute failure mechanisms to different environmental settings where distinct types of weak layers are more likely. Our results show that failure planes usually form in the vicinity of an interface between distinct lithologies that together comprise a weak layer. The weak layers of 21 of our 60 case studies were related to characteristic sediment sequences within the slope stratigraphy, of which 18 were classified based on direct measurements: 15 weak layers were classified as siliciclastic, four as volcaniclastic, and two as fossiliferous sediment sequences. Only three submarine landsides were related to clay-dominated weak layers. In addition, failure along lithological contrasts was inferred for six case studies. We use global depositional models to infer the likely locations of these different types of weak layers. These include oceanic gateways where long-term circulation can create distinct permeability interfaces within siliciclastic sequences, areas of high productivity where biogenic sediments may dominate, and regions that experience widespread ash fall from volcanic eruptions. We highlight how many submarine landslide studies have historically not collected sediment cores that characterise weak layers within intact sedimentary sequences and instead have focused on characterising the slope failure itself. As weak layers can collapse or become heavily modified during failure, there is a widespread omission of key information required for geotechnical analysis to determine where and why certain slopes are predisposed to failure (especially measurements of permeability and undrained shear strength). We conclude by highlighting the need to combine detailed geotechnical measurements with sedimentological and geophysical analyses including grain-scale observations (e.g. micro-Computed

Tomography high-resolution 3D imagery), and emphasise the importance of a uniform workflow that will allow a better comparison between individual studies.

2.1. Introduction

Submarine landslides are gravity-driven mass movements that occur in a variety of underwater slope settings worldwide (e.g. Lee et al., 2007). They can be many orders of magnitude larger than their terrestrial counterparts (Hühnerbach et al., 2004; Korup et al., 2007), involving up to thousands of cubic kilometres of sediment (e.g. Watts and Masson, 1995; Haflidason et al., 2004; Winkelmann et al., 2008). Submarine landslides and their resulting sediment density flows are thus one of the most important processes for transporting large amounts of sediment from the continental slope to the deep ocean (e.g. Talling et al., 2007; Korup, 2012; Talling, 2014). The socio-economic consequences of submarine landslides can be severe, ranging from damage to important seafloor infrastructure such as telecommunication cables and gas and oil production equipment (Piper et al., 1999; Fine et al., 2005; Thomas et al., 2010; Carter et al., 2014; Pope et al., 2017) to the generation of devastating and deadly tsunamis (Tappin et al., 2001; ten Brink et al., 2009; Harbitz et al., 2014). Continued growth in coastal populations and development (i.e. cities and harbours), and increased reliance on subsea energy and communication transfer (e.g. Carter et al., 2014) has led to a growth in research of submarine landslides over the past decades.

Some of the largest submarine landslides have been identified on extremely low angle slopes (<2°) along continental margins (such as offshore Norway, e.g. Evans et al., 2005; or offshore NW Africa, e.g. Krastel et al., 2019). According to standard slope stability concepts, such slopes should be stable (e.g. Leynaud et al., 2007). This contrast between theoretical predictions and observed reality highlights the need to identify additional factors that contribute towards slope failure in the subaqueous realm. Many hypotheses have been put forward concerning factors that control the initiation of submarine landslides (e.g. Hampton et al., 1996; Locat and Lee, 2002; Masson et al., 2006; Lee et al., 2007; Leynaud et al., 2009). Seismic shaking and slope over-steepening were initially inferred to be the dominant triggers for submarine landslides since the early work of Morgenstern (1967); however, more recent studies have shown that in addition to such short-term triggering mechanisms, longer term pre-conditioning factors play a crucial role in the formation of submarine landslides. In particular, the occurrence of so-called *weak layers* embedded within the slope stratigraphy appear to control the localisation of submarine landslides and their failure planes (e.g. Masson et al., 2006; Locat et al., 2014).

Movement of submarine landslides seems to initiate along distinct sediment horizons. These horizons are somehow predisposed to failure, and have been termed as ‘weak layers’ (e.g. Masson et al., 2006,

2010; Locat et al., 2014). Slides have often been observed to follow failure planes at different stratigraphic levels, forming a stepped, staircase-like profile (e.g. AFEN Slide, Wilson et al., 2004; Gatter et al., 2020; Grand Banks, Mosher et al., 2007; Schulten et al., 2019b; Sahara Slide, Georgiopoulou et al., 2010; Li et al., 2017). This phenomenon has been related to weak layers at different stratigraphic depths that become active under different strength thresholds (O'Leary, 1991).

2.1.1. The weak layer concept

The concept of weak layers that control the location and depth of submarine landslides is widely established (e.g. Lewis, 1971; O'Leary, 1991; Masson et al., 2006; L'Heureux et al., 2012; Locat et al., 2014; Rodríguez-Ochoa et al., 2015). The concept suggests that specific sediment layers have intrinsically lower shear strength than the surrounding strata and therefore serve as preferential failure planes of submarine landslides (e.g. Masson et al., 2006, 2010). That is to say that shearing, and thereby failure, is focused along weak layers as their shear strength is transiently reduced and/or the acting shear stress exceeds the shear strength of the layer.

Although a growing number of studies have pointed towards the significance of such weak layers in the inception of submarine landslides, very little is known about their characteristics, nature and global variability (e.g. Lewis, 1971; O'Leary, 1991; Masson et al., 2010; Locat et al., 2014; Huhn et al., 2020). A first attempt to define and classify weak layers from a geotechnical perspective was carried out by Locat et al. (2014). They defined a weak layer as *"a layer (or band) consisting of sediment or rock that has strength potentially or actually sufficiently lower than that of adjacent units (strength contrast) to provide a potential focus for the development of a surface of rupture"*. Based on this definition and their observations, they proposed a classification in which weak layers are categorised into: *inherited* and *induced* weak layers. This clarified, that in addition to weak layers with inherently lower shear strength (i.e. sensitive clay layers), weak layers could also originate from strength reduction e.g. due to changes in pore pressure or as a result of other sedimentological, geochemical or geomechanical processes, which in turn may also influence pore pressure conditions (Fig. 2.1). In particular, the layering of sediments with different physical and geotechnical properties (especially permeability and shear strength) was identified to enable focused shearing and the formation of weak layers (e.g. L'Heureux et al., 2012; Locat et al., 2014). Notably, this layering is not limited to 'traditional' siliciclastic clay-sand sequences, but was also recognised in volcaniclastic and fossiliferous sediments that are common in many marine settings (e.g. Harders et al., 2010; Urlaub et al., 2018).

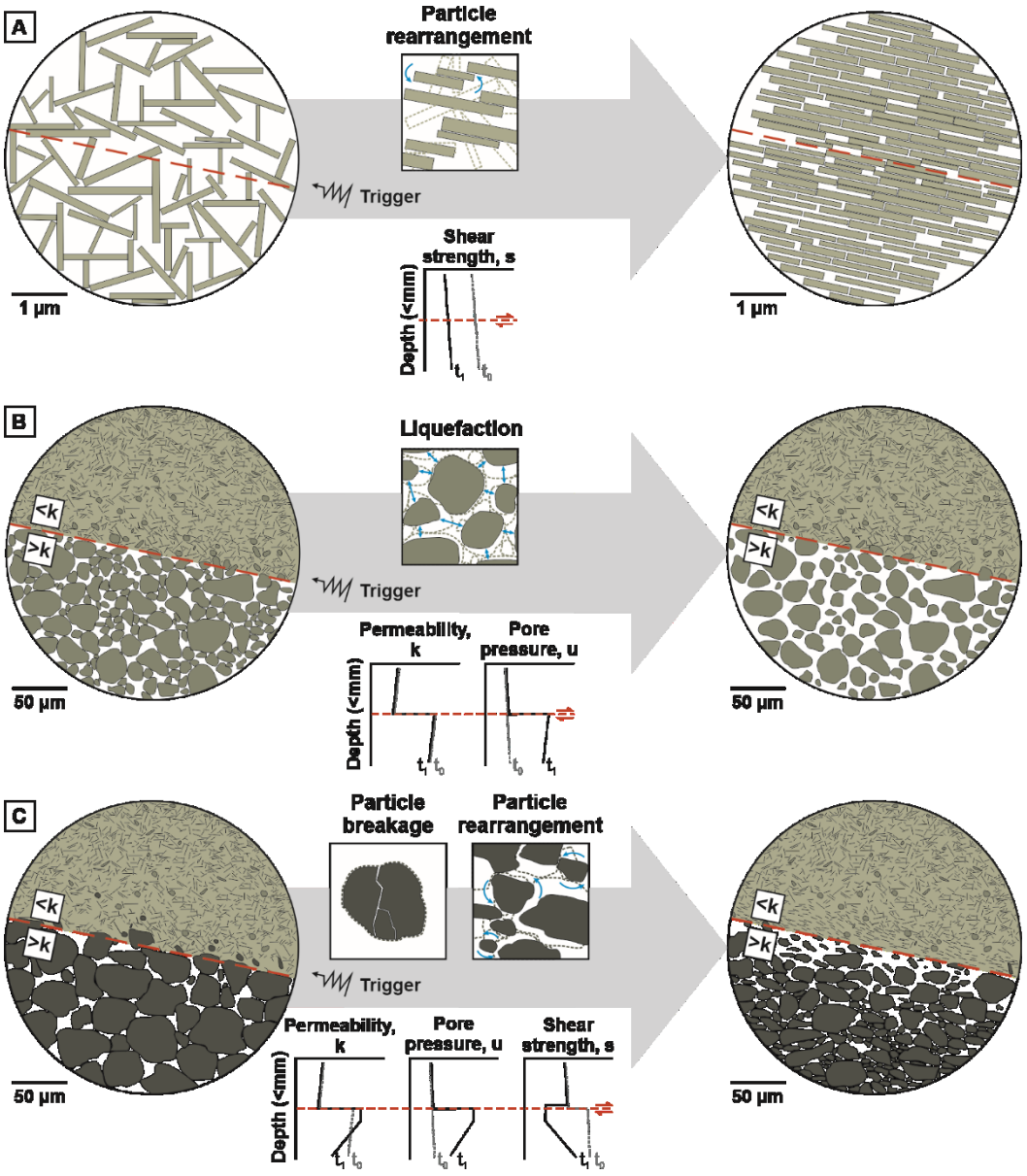

Figure 2.1. Schematic weak layer classification based on the prevailing failure mode; failure due to (**A**) strain softening, (**B**) excess pore pressure generation, (**C**) excess pore pressure generation and strain softening. Shown on the left side are zoom-ins to schematic undisturbed sediment horizons. On the right side, the same sediments are shown in their disturbed form after an external trigger e.g. earthquake acted on the sediment. Potential failure mechanisms are illustrated on top of the arrow, strength reduction caused by excess pore pressure generation due to liquefaction or by particle rearrangement and breakage. X-Y plots illustrate expected permeability (k), pore pressure (u) and shear strength (s) changes before, t_0 (dashed, grey line) and during failure, t_1 (black line), above and below a potential failure plane (dashed, red line). Note: Clay particles (small black lines) in B and C not to scale. Please refer to online version for colours.

The processes that control and form weak layers, as well as their role in the formation of submarine landslides, however, are still subject to debate (e.g. Locat and Lee, 2002; Lastras et al., 2004; Leynaud et al., 2009; Harders et al., 2010; Masson et al., 2010; Wiemer et al., 2015; Madhusudhan et al., 2017; Cukur et al., 2020). In light of the increasing focus on and seeming importance of weak layers (e.g. Talling et al., 2014; Huhn et al., 2020), it is timely to review the current state of knowledge and their controls on submarine landslide formation.

2.1.2. Objectives

Here, we present a global catalogue of case studies that examine the basal surface and potential weak layers of submarine landslides. Based on this compilation, we address three main questions:

- What types of sediment are capable of forming weak layers and how diverse is the nature of weak layers worldwide? We explore which types of sediment and associated physical and geotechnical properties may create weak layers through an analysis of a new global landslide catalogue, which includes submarine slope failures that have been linked to weak layers. We present a new classification system for weak layers, attributing specific properties of different sediment types to their implications for slope failure.
- What are the physical controls on where different types of weak layers form? We provide a general model to explain how and why different types of weak layers dominate in different environmental settings.
- What are the outstanding challenges in identifying and characterising weak layers and how can future studies extend our understanding? Several studies have pointed towards the importance of a multi-disciplinary investigation of submarine landslides in order to identify and understand the processes that control slope failure (e.g. Vanneste et al., 2014). We investigate whether multi-disciplinary investigations are common practice for the identification and characterisation of failure planes and weak layers.

2.2. New global landslide catalogue

This review investigates failure planes and weak layers of submarine landslides by means of a new global catalogue of case studies (Fig. 2.2). Slope failure is initiated when the downward driving forces (shear stress) exceed the resisting forces (shear strength) of the slope material. This causes slope failure and subsequent slide movement along one or more *glide planes* (e.g. Hampton et al, 1996; Lee et al., 2007). We refer to large features resulting from slope failure collectively as *landslide* (or *slide*) in that they have boundaries that are relatively well defined with distinct headwalls and basal surfaces (Mulder

and Cochonat, 1996). We further define *failure plane* as the surface along which failure initiates, and *glide plane* as the surface along which movement occurs. Consequently, failure planes and glide planes are identical surfaces when movement first initiates, but may differ, especially in cases of substantial basal erosion. For more terms and definitions used herein, please refer to the Glossary. Submarine landslides can feature complex failure mechanisms that can act at the same time, and in which repeated failure along different failure planes can occur (e.g. Kvalstad et al., 2005; Georgiopoulou et al., 2010; Kuhlmann et al., 2017).

Our catalogue only includes case studies that satisfied specific requirements. First, the selected landslides had to include information about their source area, i.e. the headwall had to be identified. Second, the basal surface (i.e. failure or glide planes) of the selected submarine landslides had to be identifiable. In total, 60 case studies, equivalent to 174 published studies, satisfied the requirements for this catalogue and have been summarised in Tab. 2.1 (see Appendix 2.A for all details). These case studies cover submarine landslides, or landslide complexes from various environmental settings worldwide. The selected references include mainly peer-reviewed papers as well as technical reports and conference proceedings. The catalogue shows an evident increase in literature on submarine landslide studies in general over the years, with a particular growth in the recognition of glide and failure planes and weak layers (Fig. 2.2). The increase can be attributed to both, the recognition of submarine landslides as a relevant geohazard that requires more attention as well as advances in seafloor surveying techniques, sampling and in-situ measurement equipment and analytical methods. In the following we summarise the information of the case studies in terms of (1) the methods and analyses applied to investigate the selected submarine landslides, in particular their failure planes and weak layers, and (2) the observations and inferences made regarding failure planes and weak layers.

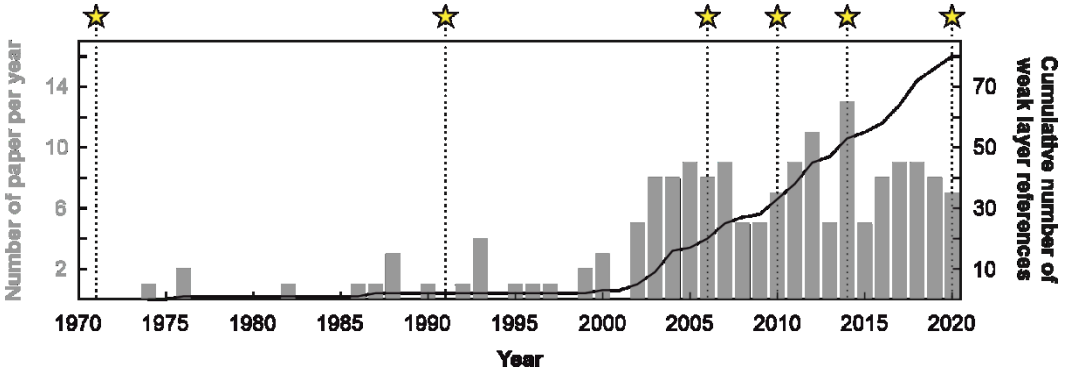

Figure 2.2. Literature on submarine landslides with information about their glide or failure planes and weak layers increased over the years. In total, 174 references that describe 60 individual case studies were selected for this review. Review papers that initiated key discussion on the presence and importance of weak layers are represented as stars (Lewis, 1971; O'Leary, 1991; Masson et al., 2006, 2010; Locat et al., 2014; Huhn et al., 2020).

Table 2.1. Summary of selected case studies, the deployed methods, and information about the failure plane, weak layer and failure mechanism. Based on the available data, we classify the case studies according to Locat et al. (2014). Please refer to Appendix 2.A for all details.

	Slide name	Location	Available data		Classification				Selected references
			Sediment cores	In-situ	Inferred failure plane lithology	Weak layer lithology	Potential failure mechanism	Weak layer type* (after Locat et al., 2014)	
1	AFEN Slide	Offshore northern UK, Faroe-Shetland Channel	IN	N/A	Sand-clay interface	Sand-clay sequence; contourite (?)	Strain softening of a sensitive clay layer, or liquefaction (transient pore pressure generation) along a widespread sandy layer	Induced*	Madhusudhan et al. (2017); Gatter et al. (2020)
2	Agadir Slide	Offshore NW Africa, Atlantic Ocean	NO	N/A	Cannot be classified based on available data	Cannot be classified based on available data	No information	Cannot be deduced from available data	Krastel et al. (2016); Li et al. (2018)
3	Ana Slide (Eivissa Channel Slides)	Offshore Balearic Islands, Eivissa Channel	NO	IN, OUT	Coarse-fine-grained sediment interface	Coarse-fine-grained sediment sequence	Excess pore pressure generation at coarse-fine-grained sediment interface due to methane gas charging and liquefaction	Inherited or induced*	Berndt et al. (2012); Lafuerza et al. (2012)

4	Andøya Slide	Offshore Norway, Norwegian Sea	NO	N/A	Cannot be classified based on available data	Cannot be classified based on available data	No information	Cannot be deduced from available data	Laberg et al. (2000)
5	Baiyun Slide	Offshore China, Pearl River Mouth Basin, northern South China Sea	NO	N/A	Coarse-fine-grained sediment interface* (?)	Coarse-fine-grained sediment sequence (?); turbidite (?)	Excess pore pressure generation due to free gas charging	Inherited or induced*	Li et al. (2014a, b); Sun et al. (2017, 2018)
6	Baraza Slide	Offshore Spain, NW Alboran Sea	N/A	N/A	Cannot be classified based on available data	Cannot be classified based on available data	Excess pore pressure (?)	Cannot be deduced from available data	Casas et al. (2011)
7	Betsiamites (-Colombier) Slides	Offshore Betsiamites River, Canada, Lower St. Lawrence Estuary	NO	OUT	Silty layer	Silt-clay sequence*	Excess pore pressure generation along silt-clay interface due to rapid sedimentation and liquefaction	Induced*	Cauchon-Voyer et al. (2008, 2011, 2012)
8	BIG'95 Slide	Offshore Columbretes Islands, Balearic Sea	NO	N/A	Cannot be classified based on available data	Cannot be classified based on available data	Excess pore pressure (?)	Cannot be deduced from available data	Urgeles et al. (2003, 2006); Lastras et al. (2004, 2007)
9	Bjørnøyrenna (Bear Island Fan) Slide	Offshore Norway, Barents Sea	N/A	N/A	Cannot be classified based on available data	Cannot be classified based on available data	No information	Cannot be deduced from available data	Laberg and Vorren (1993)

10	Bowl Slide	Offshore eastern Australia, Great Barrier Reef, Coral Sea	NO	N/A	Cannot be classified based on available data	Cannot be classified based on available data	No information	Cannot be deduced from available data	Clark et al. (2016); Puga-Bernabéu et al. (2019)
11	Brattøra Slide	Offshore Norway, Trondheimsfjorden	IN	OUT	Clay layer; turbidite	Clay layer; sand-clay sequence*; turbidite	Excess pore pressure generation due to groundwater flow and strain softening behaviour of weak, sensitive clays	Induced*	L'Heureux et al. (2010, 2011)
12	Brunei Slide	Offshore Brunei, South China Sea	N/A	N/A	Cannot be classified based on available data	Cannot be classified based on available data	Excess pore pressure (?)	Cannot be deduced from available data	Gee et al. (2007)
13	Byron Slide	Offshore Byron Bay, eastern Australia, South Pacific Ocean	NO	N/A	Cannot be classified based on available data	Cannot be classified based on available data	No information	Cannot be deduced from available data	Clarke et al. (2016); Mollison et al. (2020)
14	Cap Blanc Slide	Offshore NW Africa, Atlantic Ocean	IN	N/A	Diatom ooze; diatom ooze-clay interface	Diatom ooze-clay sequence	Excess pore pressure generation and further strength reduction due to particle breakage	Induced*	Urlaub et al. (2018, 2020)
15	Cape Fear Slide	Offshore eastern US, Atlantic Ocean	NO	N/A	Cannot be classified	Cannot be classified	Excess pore pressure generation due to	Cannot be deduced from available data	Schmuck et al. (1993); Paull et al. (1996)

					based on available data	based on available data	gas escape from gas hydrates		
16	Crete Slide	Offshore Crete, Cretan Sea	NO	NO	Cannot be classified based on available data	Cannot be classified based on available data	No information	Cannot be deduced from available data	Strozyk et al. (2010a, b)
17	Cudgen Slide	Offshore eastern Australia, South Pacific Ocean	NO	N/A	Cannot be classified based on available data	Cannot be classified based on available data	No information	Cannot be deduced from available data	Clarke et al. (2016)
18	Currituck Slide	Offshore eastern US, Atlantic Ocean	NO	N/A	Cannot be classified based on available data	Cannot be classified based on available data	Excess pore pressure (?)	Cannot be deduced from available data	Prior et al. (1986); Hill et al. (2017)
19	Dakar Slide	Offshore NW Africa, Atlantic Ocean	N/A	N/A	Cannot be classified based on available data	Cannot be classified based on available data	No information	Cannot be deduced from available data	Meyer et al. (2012); Krastel et al. (2019)
20	East Sea Slides I	Offshore Korea, Ulleung Basin, East Sea	NO	N/A	Cannot be classified based on available data	Cannot be classified based on available data	No information	Cannot be deduced from available data	Cukur et al. (2016); Horozal et al. (2019)
21	East Sea Slides II	Offshore Korea, Ulleung Basin, East Sea	IN	N/A	Sand layer* (?)	Sand layer (?); sand-clay sequence* (?)	No information	Cannot be deduced from available data	Horozal et al. (2019); Cukur et al. (2020)

22	Finneidfjord Slide	Offshore Norway, Finneidfjord	IN, OUT	IN, OUT	Clay layer; turbidite	Sand-clay sequence; turbidite	Excess pore pressure generation due to fluid flow and/or liquefaction and/or strain softening of sensitive clay	Induced*	L'Heureux et al. (2012); Steiner et al. (2012); Vardy et al. (2012); Vanneste et al. (2013, 2014, 2015)
23	Fram Slide	Offshore NW Svalbard, Fram Strait	NO	N/A	Cannot be classified based on available data	Cannot be classified based on available data	No information	Cannot be deduced from available data	Elger et al. (2015, 2017); Osti et al. (2017)
24	Gaviota Slide	Offshore California, Santa Barbara Basin	NO	N/A	Cannot be classified based on available data	Cannot be classified based on available data	No information	Cannot be deduced from available data	Edwards et al. (1995); Kluesner et al. (2020)
25	Gebra Slide	Offshore Trinity Peninsula, Antarctica, Bransfield Basin	NO	N/A	Cannot be classified based on available data	Cannot be classified based on available data	No information	Cannot be deduced from available data	Canals et al. (2004)
26	Gloria Knolls Slide	Offshore NW Australia, Great Barrier Reef, Coral Sea	N/A	N/A	Cannot be classified based on available data	Lithological contrast (?)	No information	Cannot be deduced from available data	Puga-Bernabéu et al. (2017, 2019)
27	Goleta Slide	Offshore California Basin, Santa Barbara Basin	NO	N/A	Cannot be classified based on available data	Cannot be classified based on available data	No information	Cannot be deduced from available data	Fisher et al. (2005); Greene et al. (2006); Kluesner et al. (2020)

28	Gondola Slide	Offshore SW Italy, Adriatic Sea	NO	N/A	Cannot be classified based on available data	Clay layer* (?); contourite (?)	Excess pore pressure (?)	Cannot be deduced from available data	Minisini et al. (2006); Verdicchio and Trincardi (2008); Dalla Valle et al. (2015)
29	Grand Banks Slide (surficial failures)	Offshore Newfoundland, Canada, Laurentian Fan	NO	N/A	Cannot be classified based on available data	Cannot be classified based on available data	No information	Cannot be deduced from available data	Piper et al. (1988); Mosher et al. (2007); Schulten et al. (2019a)
30	Great Bahama Bank Failures	Offshore Bahamas, NW Great Bahama Bank	NO	N/A	Cannot be classified based on available data	Cannot be classified based on available data	No information	Cannot be deduced from available data	Principaud et al. (2015, 2018)
31	Hermosa Slide	Offshore Nicaragua, Pacific Ocean	IN	N/A	Ash layer	Ash-clay sequence	Excess pore pressure generation and strength reduction due to particle rearrangement/ breakage	Induced*	Harders et al. (2010)
32	Hinlopen (Yermak) Slide	Offshore northern Svalbard, Arctic Ocean	OUT	N/A	Contourite	Lithological contrast*; contourite* (?)	No information	Cannot be deduced from available data	Vanneste et al. (2006); Winkelmann et al. (2006, 2008); Winkelmann and Stein (2007)
33	Humboldt Slide	Offshore western US, Pacific Ocean	N/A	N/A	Cannot be classified	Cannot be classified	No information	Cannot be deduced from available data	Gardner et al. (1999)

					based on available data	based on available data			
34	Jan Mayen Slide	Offshore SW Jan Mayen Island, Norwegian-Greenland Sea	OUT	N/A	Ash layer (?)	Ash-clay sequence*	No information	Induced* (?)	Laberg et al. (2014)
35	Kitimat Slide	Offshore western Canada, Kitimat Delta	IN, OUT	N/A	Sand layer (?)	Sand layer (?) sand-clay sequence* (?)	No information	Cannot be deduced from available data	Stacey et al. (2018)
36	Licosa Slide	Offshore NW Italy, eastern Tyrrhenian Sea	IN, OUT	N/A	Ash layer	Ash layer; ash-clay sequence*	Excess pore pressure generation	Induced*	Trincardi et al. (2003); Sammartini et al. (2019)
37	Little Bahama Bank Failures	Offshore Bahamas, NW Little Bahama Bank	N/A	N/A	Cannot be classified based on available data	Cannot be classified based on available data	No information	Cannot be deduced from available data	Tournadour et al. (2015)
38	Lofoten Slides	Offshore Norway, Lofoten Basin, Norwegian Sea	IN, OUT	N/A	Silt-clay interface; contourite	Silt-clay sequence; contourite	Strain softening	Induced* (?)	Vanneste et al. (2012); Baeten et al. (2013, 2014)
39	Mauritania Slide	Offshore Mauritania, NW Africa, Atlantic Ocean	IN	N/A	Clay layer	Clay layer; contourite (?)	Excess pore pressure generation due to rapid sedimentation changes	Inherited* (?)	Antobreh and Krastel (2007); Henrich et al. (2008); Förster et al. (2010)
40	Molly Hole Slide	Offshore Svalbard, Fram Strait	N/A	N/A	Cannot be classified	Cannot be classified	No information	Cannot be deduced from available data	Freire et al. (2014)

					based on available data	based on available data			
41	Munson-Nygren-Retriever Slide	Offshore eastern US, Georges Bank, Atlantic Ocean	N/A	N/A	Cannot be classified based on available data	Cannot be classified based on available data	No information	Cannot be deduced from available data	Chaytor et al. (2012)
42	Nice Airport Slide	Offshore Nice, southern France, Ligurian Sea	IN	IN	Clay layer	Clay layer; sand-clay sequence*	Excess pore pressure generation due to seepage from aquifer and further strength reduction due to strain softening	Induced*	Dan et al. (2007); Stegmann et al. (2011); Vanneste et al. (2014); Kopf et al. (2016)
43	North Aegean Slide	Offshore Greece, North Aegean Trough, North Aegean Sea	NO	N/A	Clay layer; sand-clay interface (?)	Sand-clay sequence (?)	No information	Cannot be deduced from available data	Lykousis et al. (2002)
44	Nyk Slide	Offshore Norway, Norwegian Sea	NO	N/A	Contourite (?)	Lithological contrast* (?); contourite* (?)	Excess pore pressure (?)	Cannot be deduced from available data	Lindberg et al. (2004)
45	Orkdalsfjorden Slide	Offshore Norway, Orkdalsfjorden	IN	N/A	Clay layer; sand-clay interface	Sand-clay sequence; turbidite (?)	Excess pore pressure generation due to groundwater pressure and strain softening behaviour of clays	Induced*	L'Heureux et al. (2014)

46	Pianosa Slump	Offshore western Italy, Corsica Trough, Northern Tyrrhenian Sea	OUT	N/A	Clay layer	Clay layer	Strength reduction due to strain softening	Induced*	Miramontes et al. (2018)
47	Ranger Slide	Offshore Baja California, Mexico, northern Sebastian Vizcaino Bay	N/A	N/A	Cannot be classified based on available data	Cannot be classified based on available data	No information	Cannot be deduced from available data	Normark (1974, 1990)
48	Sahara Slide	Offshore NW Africa, Atlantic Ocean	NO	N/A	Cannot be classified based on available data	Lithological contrast* (?)	Excess pore pressure	Induced* (?)	Georgiopoulou et al. (2010); Li et al. (2017)
49	Sklinnadjupet Slide	Offshore Norway, Norwegian Sea	NO	N/A	Clay layer (?)	Diatom-ooze-clay sequence* (?)	Excess pore pressure	Induced* (?)	Rise et al. (2006, 2010)
50	Spitzbergen Fracture Zone Slide	Offshore NW Svalbard, Fram Strait	NO	N/A	Cannot be classified based on available data	Cannot be classified based on available data	No information	Cannot be deduced from available data	Osti et al. (2017)
51	Storegga Slide	Offshore Norway, Norwegian Sea	OUT	N/A	Clay layer; contourite	Clay layer (?); clay-clay sequence* (?); contourite (?)	Excess pore pressure generation due to rapid sedimentation and strain softening behaviour of clays	Inherited* (?)	Bugge et al. (1988); Haflidason et al. (2003, 2004, 2005); Canals et al. (2004); Bryn et al. (2005a); Kvalstad et al. (2005); Solheim et al. (2005)

52	Trænadjupet Slide	Offshore Norway, Lofoten Basin, Norwegian Sea	OUT	N/A	Clay layer; contourite	Clay layer; clay-clay sequence*; contourite	Excess pore pressure generation due to rapid sedimentation	Inherited* (?)	Laberg and Vorren (2000); Laberg et al. (2002, 2003)
53	Tuaheni Slide	Offshore Poverty Bay, eastern New Zealand's North Island, South Pacific Ocean	IN	N/A	Cannot be classified based on available data	Lithological contrast* (?)	Excess pore pressure related to gas hydrates	Inherited*	Kuhlmann et al. (2019); Luo et al. (2020)
54	Twin Slides	Offshore SW Italy, Gela Basin, Sicily Channel	IN	N/A	Ash-clay interface	Ash-clay sequence	Excess pore pressure and further strength reduction due to particle rearrangement	Induced*	Kuhlmann et al. (2014, 2016, 2017)
55	Uruguay Slides	Offshore Uruguay, Atlantic Ocean	NO	N/A	Cannot be classified based on available data	Lithological contrast* (?); contourite	No information	Cannot be deduced from available data	Krastel et al. (2011); Henkel et al. (2011); Ai et al. (2014)
56	Vesterålen Slides	Offshore Norway, Norwegian Sea	OUT	IN, OUT	Clay layer	Sand-clay sequence* (?)	Excess pore pressure generation and strain softening	Induced*	Vanneste et al. (2012, 2014); L'Heureux et al. (2013); Vanneste et al. (2014); Stegmann et al. (2016)
57	Vieste Slide	Offshore eastern Italy, Adriatic Sea	NO	N/A	Cannot be classified	Cannot be classified	No information	Cannot be deduced from available data	Dalla Valle et al. (2015);

					based on available data	based on available data			Gamberi et al. (2019)
58	Villafranca Slide	Offshore Italy, Gioia Basin, Tyrrhenian Sea	NO	N/A	Cannot be classified based on available data	Cannot be classified based on available data	No information	Cannot be deduced from available data	Gamberi et al. (2011); Rovere et al. (2014)
59	Viper Slide	Offshore Australia, Great Barrier Reef, Coral Sea	N/A	N/A	Cannot be classified based on available data	Cannot be classified based on available data	No information	Cannot be deduced from available data	Webster et al. (2016); Puga-Bernabéu et al. (2019)
60	Yamba Slides	Offshore Yamba, eastern Australia, South Pacific Ocean	IN	N/A	Cannot be classified based on available data	Cannot be classified based on available data	No information	Cannot be deduced from available data	Hubble et al. (2019)

Hydroacoustic and geophysical data were available for all selected case studies.
IN = sediment cores/in-situ measurements sampling the basal surface inside the slide area were available
NO = sediment cores/in-situ measurements are available, but did not sample the failure or glide plane
OUT = sediment cores/in-situ measurements sampling the failure plane equivalent sediments outside the slide area are available
(N/A) = no data available
(*) = inferred by authors of this review

2.2.1. Applied methods and analyses

All 60 selected case studies included identification of submarine landslides from hydroacoustic (multi-beam and side-scan sonar) data. Basal surfaces of submarine landslides were further delineated using geophysical data, which included 2D and 3D seismic, and sub-bottom profiler data. Hydroacoustic and geophysical datasets enable the collection of basic morphometric features of the landslides (e.g. area, volume, slope angle), including the identification of the basal surface (see Appendix 2.A). As legacy seafloor data from 30+ years ago is generally of lower resolution than from more recent studies, they typically only provided limited information about basal surfaces. Therefore, if more than one reference was available for a case study, preference was given to that with higher resolution data and information obtained from advanced analytical techniques.

In addition to hydroacoustic and geophysical data, 49 of the 60 case studies also recovered sediment cores (Fig. 2.3A, Tab. 2.1). Different coring devices were used for the recovery of cores, including gravity, piston, MeBo (*Meeresboden Bohrgerät* or seafloor drill rig; Freudenthal and Wefer, 2007, 2013), and cores from deep ocean drilling programmes (IODP – *International Ocean Discovery Program* and ODP – *Ocean Drilling Program*). Not all cores, however, sampled sediment layers relevant to the study of potential weak layers, i.e. ideally failure plane equivalent sediments outside the slide area or the basal surface of the landslide inside the slide area. Of the 49 case studies with sediment cores, the relevant sediments were sampled in only 21 cases.

A detailed investigation of these 21 case studies, which cored and sampled the basal surface or failure plane equivalent sediments, revealed that 20 were subject to further analyses (Fig. 2.3C). MSCL (multi-sensor core logging) measurements were available for cores of four case studies. Data from MSCL and geotechnical analyses (i.e. water content, fall-cone/vane shear tests, PSD (particle size distribution), Atterberg limits, oedometer tests, direct shear tests and/or triaxial tests) were available for three studies. Seven case studies reported MSCL, geotechnical analyses and XRF (X-ray fluorescence) data, while the remaining six studies reported only geotechnical data.

In general, data from MSCL as well as standard geotechnical analyses (water content, fall-cone/vane shear tests and PSD analyses) become readily available, but advanced geotechnical tests are rare (Fig. 2.4). Of the 49 case studies with sediment cores, water content measurements were available for 26 case studies, MSCL and PSD measurements for 24 and undrained shear strength information from fall cone and vane shear tests for 20 case studies. Atterberg limits and oedometer tests, on the other hand, were available for cores of 12 and 13 case studies, respectively. Direct shear and triaxial tests were only performed on sediment cores of 10 case studies.

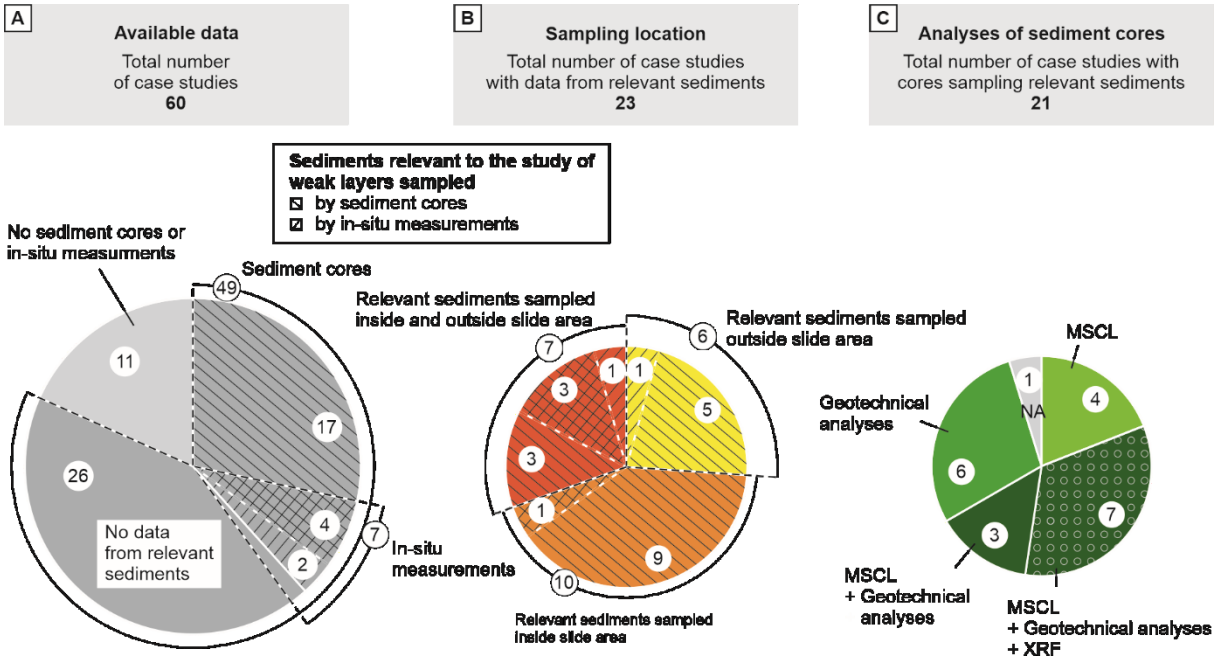

Figure 2.3. Pie charts counting case studies **A.** without data from sediment cores or in-situ measurements – light grey, and with data from sediment cores and in-situ measurements – dark grey: no data from relevant sediments (i.e. basal surface of landslide, or failure plane equivalent sediments) – no pattern, cores sampling relevant sediments – left-tilted lines, in-situ measurements sampling relevant sediments – right-tilted lines; **B.** with sediment cores and in-situ measurements from relevant sediments: inside and outside the slide area – dark orange, inside the slide area – orange, outside the slide area – yellow; and **C.** with analyses on sediment cores that sampled relevant sediments: no information – grey, MSCL (multi-sensor core logging) – light green, geotechnical analyses (water content, undrained (fall cone and vane) shear strength tests, particle size distribution, Atterberg limits, oedometer, direct shear and/or triaxial tests) – green, MSCL and geotechnical analyses – dark green, MSCL, geotechnical analyses and XRF (X-ray fluorescence) – dark green with circles. Please refer to Appendix 2.A for all details. Please refer to online version for colours.

Furthermore, of the 60 case studies, seven used in-situ measurements to characterise landslide materials (Fig. 2.3A; Tab. 2.1). Free-fall and pushed cone penetration testing with pore pressure response (FF-CPTu and CPTu) were the primary geotechnical tools used for offshore in-situ measurements. In total, in-situ measurements were available for seven case studies, of which six included measurements of the relevant sediment layers.

Combining data from both, sediment cores and in-situ measurements, 23 of the 60 case studies obtained information from the basal surface of the landslide or failure plane equivalent sediments outside the slide area. In four cases, information was obtained from in-situ measurements and sediment cores. Two case studies had only in-situ measurements, and the remaining 17 studies only sediment cores that sampled the relevant sediments (Fig. 2.3A, Tab. 2.1). A detailed investigation of these 23 case studies

revealed that six obtained data from outside the slide area (i.e. the undisturbed sediments equivalent to the failure plane), ten from within the slide area (i.e. the basal surface of the landslide), and seven from inside and outside the slide area (Fig. 2.3B, Tab. 2.1). Therefore, these 23 case studies may allow for a deeper insight and analysis of weak layers.

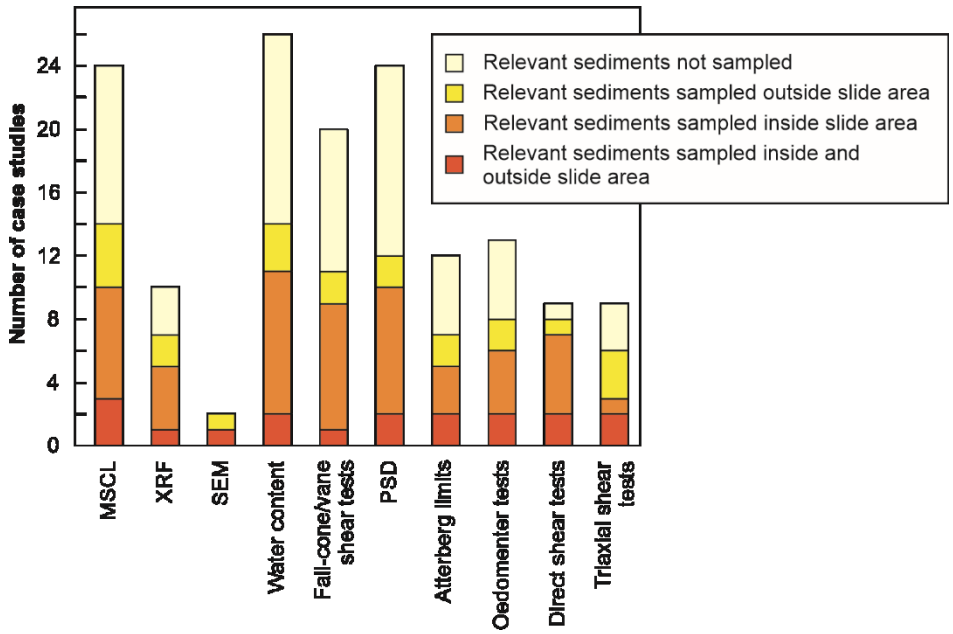

Figure 2.4. Number of case studies that carried out further analyses on available sediment cores (for all details please refer to Appendix 2.A). Colour scale illustrates the coring location: not sampling the relevant sediments – light yellow, sampling failure plane equivalent sediments outside – light orange, the basal surface inside – orange, or both, the basal surface inside and the failure plane equivalent sediments outside the slide area – dark orange. MSCL – multi-sensor core logging, XRF – X-ray fluorescence, SEM – scanning electron microscopy, PSD – particle size distribution. Please refer to online version for colours.

2.2.2. Observations and inferences regarding failure planes and weak layers

The data we have synthesised on submarine landslides and their weak layers (Tab. 2.1) show that various sediment types and failure mechanisms have been inferred to control the formation of weak layers and the generation of submarine landslides.

The main failure mechanisms invoked to form weak layers and promote failure relate to excess pore pressure generation and strain softening (Tab. 2.1); however, failure mechanisms were often deduced from geophysical data alone rather than from direct sampling. Although only 23 of the 60 selected case studies collected data from relevant sediment layers by means of in-situ measurements and sediment coring, 28 discussed potential failure mechanisms (Tab. 2.1).

We have also noticed that the classification of weak layers following Locat et al. (2014) into *inherited* and *induced* weak layers is not applicable for various case studies. The classification considers the processes that may cause excess pore pressure generation or strength reduction, which in turn may result in the formation of weak layers; however, it does not yet enable an identification of potential weak layers within the slope stratigraphy pre-failure. Rather than investigating whether weak layers are inherited or induced, it is crucial to analyse the sediment sequences forming potential weak layers.

Here, we introduce a new classification scheme, for the diagnosis of potential weak layers, and assessment of the conditions (e.g. failure mechanisms) under which they may fail. In order to identify the processes that control and form weak layers, we attempt to classify them in terms of their lithology (see Section 2.3 below). Potential failure mechanisms may then be deduced from those lithologies (Tab. 2.1). The classification further allows us to relate specific weak layer types to different environments and assess their global distribution (Section 2.3).

2.3. Weak layer classification

The pre-requisite for a robust lithological classification of weak layers is data from sediment cores and in-situ measurements that sampled the glide and/or failure planes of the submarine landslide. As discussed earlier (Section 2.2.1), such data was available for 23 of the 60 case studies; nevertheless, a total of 30 case studies discussed the nature of weak layers (Tab. 2.1). Therefore, weak layers are often characterised by relying on information of the study area, and geophysical data and short cores interpolated to the depth of interest, rather than direct measurements.

2.3.1. A lithological approach

Here, we present a classification of weak layers based on their lithology (Tab. 2.2) that includes: (1) Siliciclastic, (2) volcaniclastic and (3) fossiliferous sediments. In siliciclastic sediments, weak layers can form in strain softening sediments, usually sensitive clay layers, or along sediment sequences, where permeability and/or strength contrasts promote failure. Volcaniclastic and fossiliferous weak layers are related to sediment sequences (e.g. ash-clay or diatom-clay) that may fail either due to strain softening of their weathered products or due to strength reduction and excess pore pressure generation as a result of liquefaction and particle breakage.

Table 2.2. Lithological classification of weak layers in submarine landslide studies.

Type	Description	Example	Selected references
Siliciclastic sediments			
Clay layers	Clay layers may have inherently lower shear strength (e.g. montmorillonite) or can face sudden shear strength reduction (e.g. sensitive clays) due to strain softening (i.e. particle re-arrangement)	e.g. Pianosa Slump, offshore western Italy, Northern Tyrrhenian Sea	Miramontes et al. (2018)
Sand-clay sequence	High-permeability sediments (i.e. sand or sandy layers) overlain by low-permeability sediments (i.e. clay layers) may favour the accumulation of excess pore pressure at the material interface, which may also cause strain softening behaviour of the clays	e.g. Finneidfjord Slide, coast Norway, Norwegian Sea	L'Heureux et al. (2012)
Clay-clay sequence	High-water content clay (e.g. contourites) overlain by low-permeability sediments (i.e. clay) may promote excess pore pressure accumulation	e.g. Trænadjupet Slide, offshore Norway, Norwegian Sea	Laberg and Vorren (2000)
Volcaniclastic sediments			
Ash-clay sequence	Permeability interface between highly permeable ash layer versus overlying low-permeability clay layers may promote excess pore pressure generation; strength contrast may also cause strain softening within the overlying clay	e.g. Licosa Slide; offshore NW Italy, eastern Tyrrhenian Sea	Sammartini et al. (2019)

Fossiliferous sediments			
Diatom-clay sequence	Permeability interface between diatom ooze and overlying low-permeability clay layers may cause excess pore pressure generation along the diatom ooze layer or at the material interface; strain softening may occur in the overlying clay	e.g. Cap Blanc Slide, offshore NW Africa, Atlantic Ocean	Urlaub et al. (2018)

2.3.1.1. Siliciclastic sediments

Clay layers

Clay layers have been invoked as weak layers because they can be prone to high compressibility and/or sensitivity (e.g. Locat et al., 2003; L'Heureux et al., 2012), and were identified in three case studies (Tab. 2.1; Förster et al., 2010; Dalla Valle et al., 2015; Miramontes et al., 2018). Clays have unique mechanical and physio-chemical properties that can cause them to be mechanically weaker than other siliciclastic sediments. These unique properties can be explained by the negative charge of clay minerals and their preferential attraction of positively charged ions (diffuse double layer (DDL) theory by Gouy-Chapman; Bolt, 1956). Reducing the ionic concentration or ionic valence will increase the spacing of the DDL and hence the sediment's porosity and volume (Bolt, 1956). Therefore, not only the type of clay minerals (e.g. kaolinite versus montmorillonite), but also the dominant type and concentration of exchangeable cations, and pore water salt concentrations have great influence on the mechanical behaviour of clays (e.g. Moore, 1991).

Miramontes et al. (2018) suggested that failure of the Pianosa Slump, on the eastern margin of the Corsica Trough, initiated along a zeolitic clay layer. Zeolites are known for their cation exchange capabilities (Mumpton, 1999), and could attract more cations than the clay particles. Over time, this results in a decrease of cation concentration around the clays and a weak sediment layer develops, due to the repulsive forces of the clay minerals (Miramontes et al., 2018).

Another process that may lead to a decrease in cation concentration within weak layers is leaching. This process causes the leaching of salt by fresh groundwater and is usually associated with sensitive clays found in Canada and Scandinavia (e.g. Rosenqvist, 1966; Torrance, 1974). Examples can be found offshore Finneidfjord and Trondheimsfjorden (e.g. L'Heureux et al., 2011, 2012; Vardy et al., 2012). Although failure likely initiated along the sensitive clay, the weak layers of these case studies have been

classified as ‘siliciclastic sediment sequence’, as lateral fluid flow along permeable sand layers likely promoted strength reduction in the overlying clay layer (e.g. L’Heureux et al., 2012).

Siliciclastic sediment sequences

Siliciclastic sediment sequences have been inferred as weak layers in 15 case studies. Failure along lithological contrasts was hypothesised for another six case studies, albeit without any validation from sediment cores or in-situ geotechnical testing; hence the precise nature of these contrasts is unknown (Tab. 2.1). Such sediment sequences can be the result of various sedimentation regimes:

Contourites have often been inferred as potential weak layers of submarine landslides due to their inherent compositional and geotechnical properties (e.g. Lindberg et al., 2004; Bryn et al., 2005b). They usually consist of well sorted muddy or sandy sediments that are characterised by high water content and compressibility, which may favour the generation of excess pore pressure (Laberg and Camerlenghi, 2008). In total, four case studies have been related to contouritic sediment sequences (Tab. 2.1). The weak layers of both, the Trænadjupet Slide and the Storegga Slide offshore Norway, are characterised by siliciclastic sediment sequences that resulted from variations in climate-controlled oceanographic conditions (e.g. Laberg et al., 2002; Berg et al., 2005). Rapid deposition of low-permeability glacio-marine sediments above high-water content, fine-grained hemipelagic and/or contouritic sediments likely caused the development of excess pore pressure, thereby increasing the failure potential along this layer (e.g. Laberg and Vorren, 2000; Laberg et al., 2002; Berg et al., 2005; Bryn et al., 2005b; Kvalstad et al., 2005; Solheim et al., 2005). In addition to such permeability contrasts, strength contrasts between contouritic and surrounding sediments can influence the formation of failure planes and promote failure (e.g. Lofoten Slides, offshore Norway, Baeten et al., 2013, 2014; AFEN Slide, offshore northern UK, Wilson et al., 2004; Gatter et al., 2020). Although another five case studies, namely the Hinlopen and Nyk Slide offshore Norway, the Gondola Slide offshore Italy, the Mauritania Slide offshore NW Africa, and the Uruguay Slides offshore Uruguay discussed contourites as potential weak layers, a verification was not possible due to lack of data (Tab. 2.1; Lindberg et al., 2004; Vanneste et al., 2006; Antobreh and Krastel, 2007; Winkelmann and Stein, 2007; Krastel et al., 2011; Dalla Valle et al., 2015).

Turbidites have been identified as weak layers in four case studies (Tab. 2.1). Slope failure of the Baiyun Slide, in the Pearl River Mouth Basin offshore China, was related to the migration of free gas from deeper strata into a permeable turbidite layer. This likely caused the development of excess pore pressure along the interface between the higher-permeable and overlying low-permeable sediments (Li et al., 2014b; Sun et al., 2018). In Norway, turbidite deposits, which likely sourced from quick clay slides on land, have been identified as weak layers of several fjord slides (e.g. Brattøra Slide, L’Heureux et al.,

2011; Finneidfjord Slide, L'Heureux et al., 2012; Orkdalsfjorden Slide, L'Heureux et al., 2014). The contrasting permeability between sand and clay sediments within the turbidite deposits may have enabled sub-lateral fluid migration along the sand layers and the formation of artesian groundwater pressure. Excess pore pressure and strain softening of the weaker, sensitive clay likely caused failure along the clay layer (e.g. L'Heureux et al., 2012; Vardy et al., 2012).

Particular attention should be paid to sequences of coarse- and fine-grained sediments, particularly at river deltas. These sequences can form permeability contrasts and may create vertically confined aquifers that can host artesian groundwater pressures that extend offshore (e.g. Micallef et al., 2021). This has been observed in fjords, but was also suggested to have caused the Nice Airport Slide in 1979. A sandy gravel alluvial aquifer overlain by fine-grained sediments was identified as weak layer for the Nice Airport Slide. Failure likely initiated within the sensitive clay layer which was further weakened by leaching due to fluid flow in the underlying sand (e.g. Dan et al., 2007).

Lastly, weak layers may form due to shear strength degradation by gas exsolution. Excess pore pressure may develop along the interface between methane-charged higher-permeability and overlying fine-grained, low-permeability sediments, and cause slope failure (e.g. Ana Slide, Eivissa Channel, Berndt et al., 2012; Lafuerza et al., 2012).

2.3.1.2. Volcaniclastic sediment sequences

Ash layers have been suggested or identified as weak layers, affecting the formation of failure planes in four case studies (Tab. 2.1; Harders et al., 2010; Laberg et al., 2014; Kuhlmann et al., 2017; Sammartini et al., 2019). Based on their work on submarine landslides offshore Nicaragua, in particular on the Hermosa Slide, Harders et al. (2010) proposed that ash layers overlain by impermeable clay can act as weak layers. They proposed that the rearrangement and breakage of ash particles, e.g. due to seismic shaking, may cause a sudden volume reduction. This would promote compaction within the ash layer and a rapid accumulation of pore fluid along the interface between the ash and the overlying clay. The transient pore pressure increase would thereby cause an abrupt reduction in shear strength at the interface, and focused shearing along the 'compacted' ash layer or within the overlying clay (Harders et al., 2010). Wiemer and Kopf (2017b) noted that hard-grained ash sands (low crushability) may actually increase the shear strength of the slope material due to the particles' roughness and angularity (Riley et al., 2003), favouring seismic strengthening (Fig. 2.5). Soft-grained pumice, however, may be weak due to its high crushability and favour pore pressure build-up (Wiemer and Kopf, 2017b). A coarse-grained ash layer, composed of sub-angular pumice and glass shards, overlain by clayey sediments, has been identified as potential failure plane of the Licosa Slide, offshore south-western Italy. The permeable ash likely enabled lateral fluid flow along the layer. Lateral fluid flow and/or seismic shaking could have

caused excess pore pressure to develop, and together with particle breakage and rearrangement supposedly caused failure in the upper part of the ash layer or along the ash-clay interface (Sammartini et al., 2019). The same mechanism was suggested for the Twin Slides, offshore Sicily (Kuhlmann et al., 2016, 2017).

Another mechanism proposed to form weak layers within volcaniclastic sediments is strain softening of weathered ash, which constitutes mechanically weaker clay. This hypothesis was confirmed by shear experiments on ash samples at different alteration stages, which demonstrated a marked decrease in shear strength with increasing alteration (Wiemer and Kopf, 2015). It was noted, however, that this alteration is usually found below 800 m b.s.f., while submarine landslides are concentrated in the upper 400 m b.s.f. (McAdoo et al., 2000; Hühnerbach et al., 2004). This could explain the lack of matching case studies.

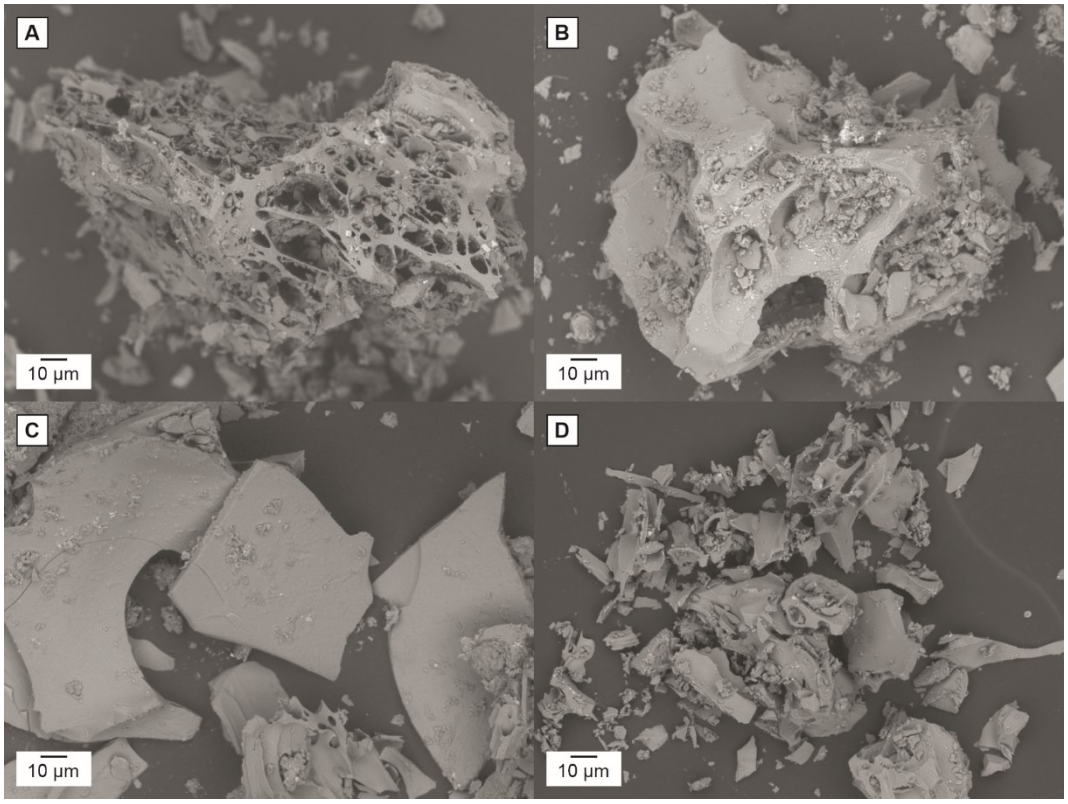

Figure 2.5. Examples of (**A**) porous and (**B**) elongated, dense pumice, (**C**) mafic ash, and (**D**) cuspate-dominated ash from the Hikurangi margin, New Zealand obtained from Scanning Electron Microscopy (SEM).

2.3.1.3. Fossiliferous sediment sequences

Fossiliferous sediments have been proposed to affect submarine slope stability (e.g. Tanaka and Locat, 1999) and have been invoked as potential weak layers (e.g. foraminifera-rich layers; Sawyer and Hodelka, 2016, diatom-rich layers; Volpi et al., 2003; Urlaub et al., 2018). Urlaub et al. (2018) postulated that diatomaceous sediments overlain by impermeable clay layers likely acted as weak layer and promoted failure of the Cap Blanc Slide, offshore NW Africa. From a geotechnical point of view, even minor amounts of diatoms (about 10 %) were found to fundamentally alter key physical properties, often in a complex manner (e.g. Tanaka and Locat, 1999; Shiwakoti et al., 2002; Volpi et al., 2003). Diatomaceous sediments have higher water content, porosity, permeability and compressibility; however, they also exhibit higher shear strength which may make them more resistant to static and cyclic loading compared to sediments that lack diatoms (Shiwakoti et al., 2002; Tanaka et al., 2003; Díaz-Rodríguez, 2011; Wiemer and Kopf, 2017a). It has to be noted though that geotechnical studies on diatoms have been performed mainly on disc-shaped diatom frustules (cells), and that the shear strength of diatomaceous sediments is strongly dependent on the shape of the diatom frustules (Fig. 2.6). High shear strength is attributed to disc-shaped frustules, while tube-shapes exhibit higher compressibility and therefore, have a lower comparative shear strength (Rack et al., 1993).

Another important aspect of diatomaceous sediments is that their presence is also crucial as a source of pore fluid. Similar to ash particles, the crushing of diatoms and subsequent loss of sediment fabric can cause an increase in pore pressure and a significant loss of strength (Urlaub et al., 2015). The pre-requisite for this mechanism to apply is the occurrence of a sealing layer, i.e. clay that prevents the pore fluid to dissipate (e.g. Urlaub et al., 2018). The most likely scenario for slope failure along a diatom-clay weak layer is probably particle breakage due to loading or liquefaction (e.g. seismic shaking), which causes both excess pore pressure generation and strain softening (Rodríguez-Ochoa et al., 2015).

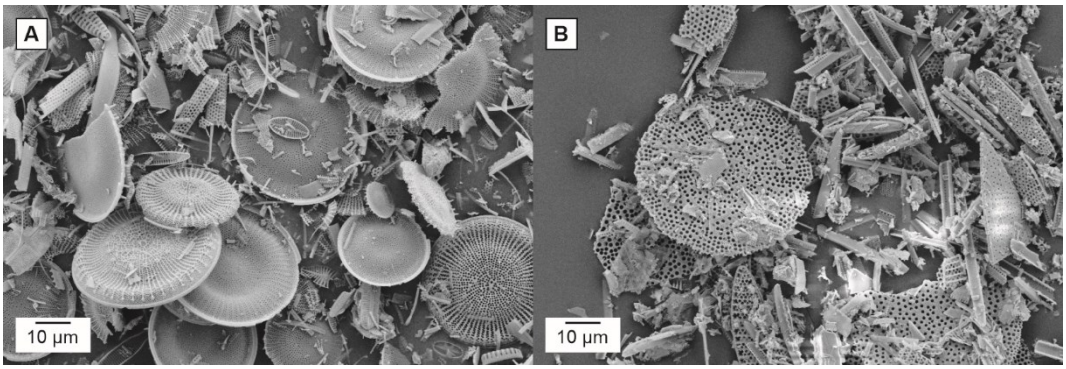

Figure 2.6. Examples of (**A**) mainly centric diatoms from the Lower Saxony, Germany and (**B**) mainly pennate diatoms from the South Sandwich Trench, South Atlantic Ocean, obtained from Scanning Electron Microscopy (SEM; modified from Dziadek, 2014).

2.3.2. Environments and global distribution

As sediment type varies according to different depositional environments (e.g. Dutkiewitcz et al., 2015), it stands to reason that the different types of weak layers (which are linked to sediment lithology) will show an affinity to different geographic and physiographic regions. For example, weak layers attributed to contourites will be more common in higher latitudes, or at oceanic gateways, where thermohaline circulation is pronounced (Rebesco et al., 2014). Weak layers related to sand layers will be more prone where episodic high energy sediment transport occurs, such as offshore from bedload-dominated river deltas or in areas affected by recurrent turbidity currents. We now discuss some of the spatial controls on sediment lithology with a view to provide some general guidance on the environments and regions in which different weak layers may be anticipated; and hence where landslides that are linked to weak layers may be more likely.

Weak layers related to siliciclastic sediment sequences are the most common and are found in various environmental settings worldwide (Fig. 2.7E, F). Although their primary lithology is the same, based on the environmental setting (and therefore, the prevailing sedimentation regime), the physical and geotechnical properties of these weak layers can vary greatly. In addition, depending on the geographic and physiographic regimes, different failure mechanisms may prevail and cause the formation of weak layers.

Figure 2.7. (*next page*) Overview maps of the case studies used in this review (**A**, **C**, **E**). Subsets represent zoom-ins to case studies in the NE Atlantic (X) and the western Mediterranean (Y). Each point represents one submarine landslide or submarine landslide complex (exceptions are the Eastern Sea I and II, Lofoten and Vesterålen Slides for which several smaller, related slides are represented by only one point). Different symbols illustrate the data available for each landslide: **A.** orange cross – sediment cores/in-situ measurements sampling relevant sediments inside slide area, orange circle – sediment cores/in-situ measurements sampling relevant sediments outside slide area, dark orange circle with cross – sediment cores/in-situ measurements sampling relevant sediments inside and outside slide area, and black circle – no sediment cores/in-situ measurements sampling relevant sediment are available. **C.** Symbols illustrate the inferred main failure mode of individual slides: blue cross – failure due to strain softening, blue square – failure due to excess pore pressure generation, blue square with cross – failure due to excess pore pressure generation and strain softening, and black circle – no information available. **E.** Weak layer types, classified by means of their lithology: light brown rectangle – clay layers, brown diamonds – siliciclastic sediment sequence, dark green triangle – volcaniclastic sediment sequence, green ellipse – fossiliferous sediment sequence, and black circle – no information available. Pie charts counting case studies (**B**) with different datasets, (**D**) for each failure mode, and (**F**) for each type of weak layer. Please refer to online version for colours.

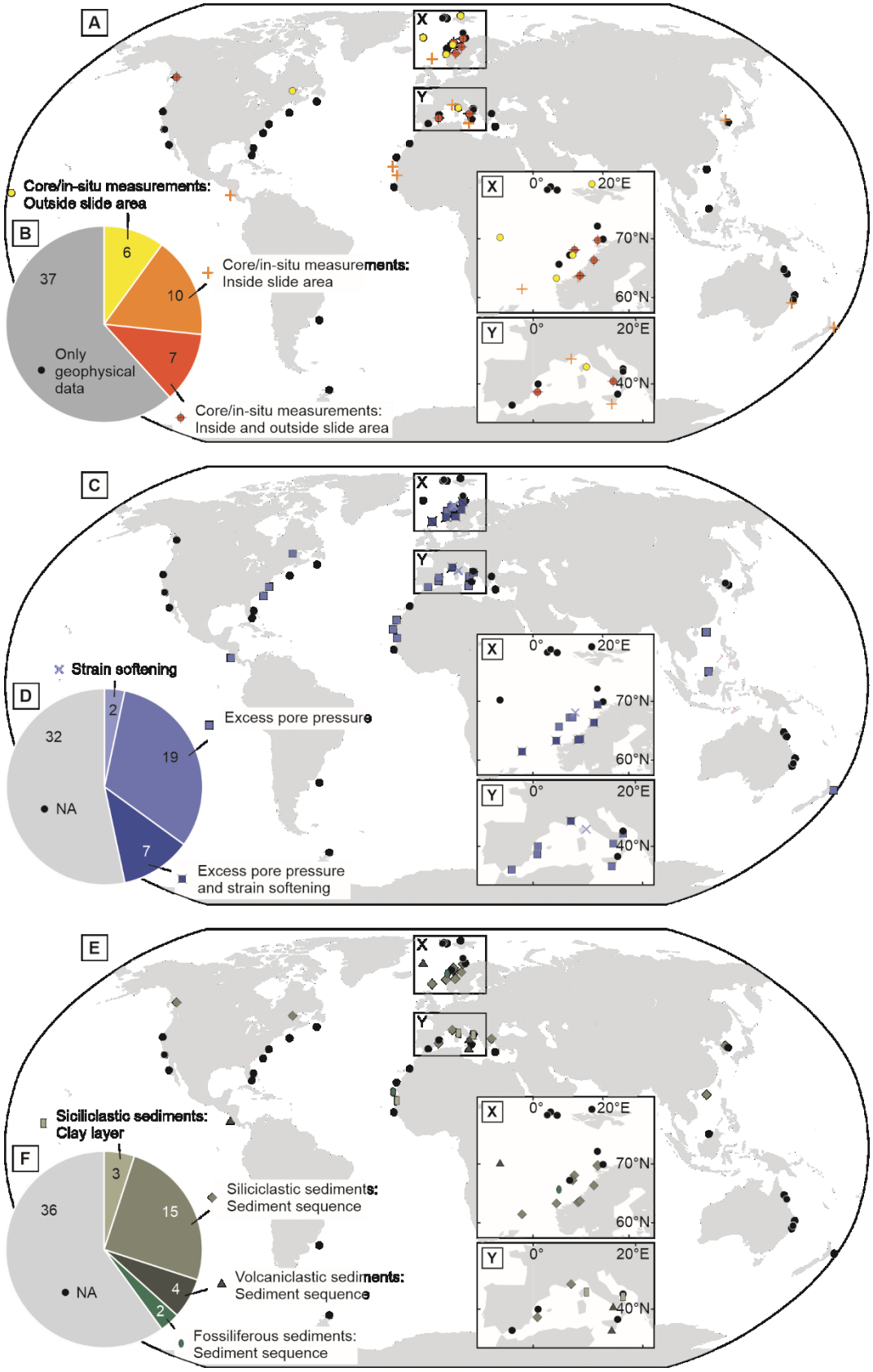
A
X
Y
0°
20°E
70°N
60°N
40°N
Core/in-situ measurements:
Outside slide area
B
6
10
7
37
Only
geophysical
data
Core/in-situ measurements:
Inside slide area
Core/in-situ measurements:
Inside and outside slide area
C
Strain softening
D
2
19
7
32
NA
Excess pore pressure
Excess pore pressure
and strain softening
E
Siciliclastic sediments:
Clay layer
F
3
15
4
2
36
NA
Siliciclastic sediments:
Sediment sequence
Volcaniclastic sediments:
Sediment sequence
Fossiliferous sediments:
Sediment sequence

Coarse-grained (i.e. sand) layers are mainly considered as potential weak layers because of their mechanical behaviour under cyclic loading (e.g. earthquake shaking). Such high-permeability, often under-consolidated layers may collapse under cyclic loading, as the effective stress between grains is lost, resulting in liquefaction (e.g. Sultan et al., 2004). Sandwiched between low-permeability (clay or silt) layers, the sealing-capacity of these sediments may hinder the vertical dissipation of pore fluids and cause transient pore pressure accumulation within the sand layer. Weak layers of such nature are typically associated with contourites (e.g. Wilson et al., 2004; Baeten et al., 2014; Gatter et al., 2020). Contourites are sediment deposits that are characterised by well-sorted, under-consolidated muddy or sandy sediments with high water contents and relatively low shear strength (Laberg and Camerlenghi, 2008). They are typically found on continental slopes, where they may be subject to rapid burial under low-permeability glacio-marine clays. This may enable liquefaction of sandy contourites and the generation of transient pore pressures if subject to seismic shaking (e.g. Wilson et al., 2004). In addition to permeability contrasts, strength contrasts between contouritic and surrounding sediments may also promote failure along their interface (e.g. Baeten et al., 2014). The lateral extend of most contourites could lead to nearly instantaneous failure of large volumes of sediment. Moreover, submarine landslides within contourites are often characterised by repeated failure (e.g. AFEN Slide, Wilson et al., 2003; Storegga Slide, Haflidason et al., 2004; Bryn et al., 2005a). Contourites, and their respective type of weak layers, are typically associated with northern high-latitudes, but they are also found in mid- and low-latitudes (Fig. 2.8A).

Our data show that sand layers have another important function in the formation of submarine landslides. That is, they act as aquifers in near coastal environments (e.g. fjords – Brattøra, Finneidfjord and Orkdalsfjorden Slides, L'Heureux et al., 2011, 2012, 2014; or continental slope – Nice Airport Slide, Dan et al., 2007). Alternating layers of low- and high-permeability sediments can affect the groundwater flow and cause excess pore pressure generation, thereby promoting failure. Failure is typically associated with artesian groundwater pressure along the sand-clay interface and strain softening of the often inherently weaker, sensitive clays (e.g. Dan et al., 2007; L'Heureux et al., 2011, 2012, 2014). Such sensitive clays (often related to quick clay slide activity) are common in uplifted fjord valleys of Scandinavia, Canada and to a lesser extent in Alaska (e.g. Torrance, 1983). These sediments, with similar origin as those found in this study (e.g. Finneidfjord, L'Heureux et al., 2012; Steiner et al., 2012) could play a crucial role in the formation of submarine landslides in near-coastal areas. Although the landslide volumes in fjords are limited by the morphology of these environmental settings (e.g. Syvitski et al., 1987; Prandle, 2009), they can have major social-economic impact due to their near coastal location.

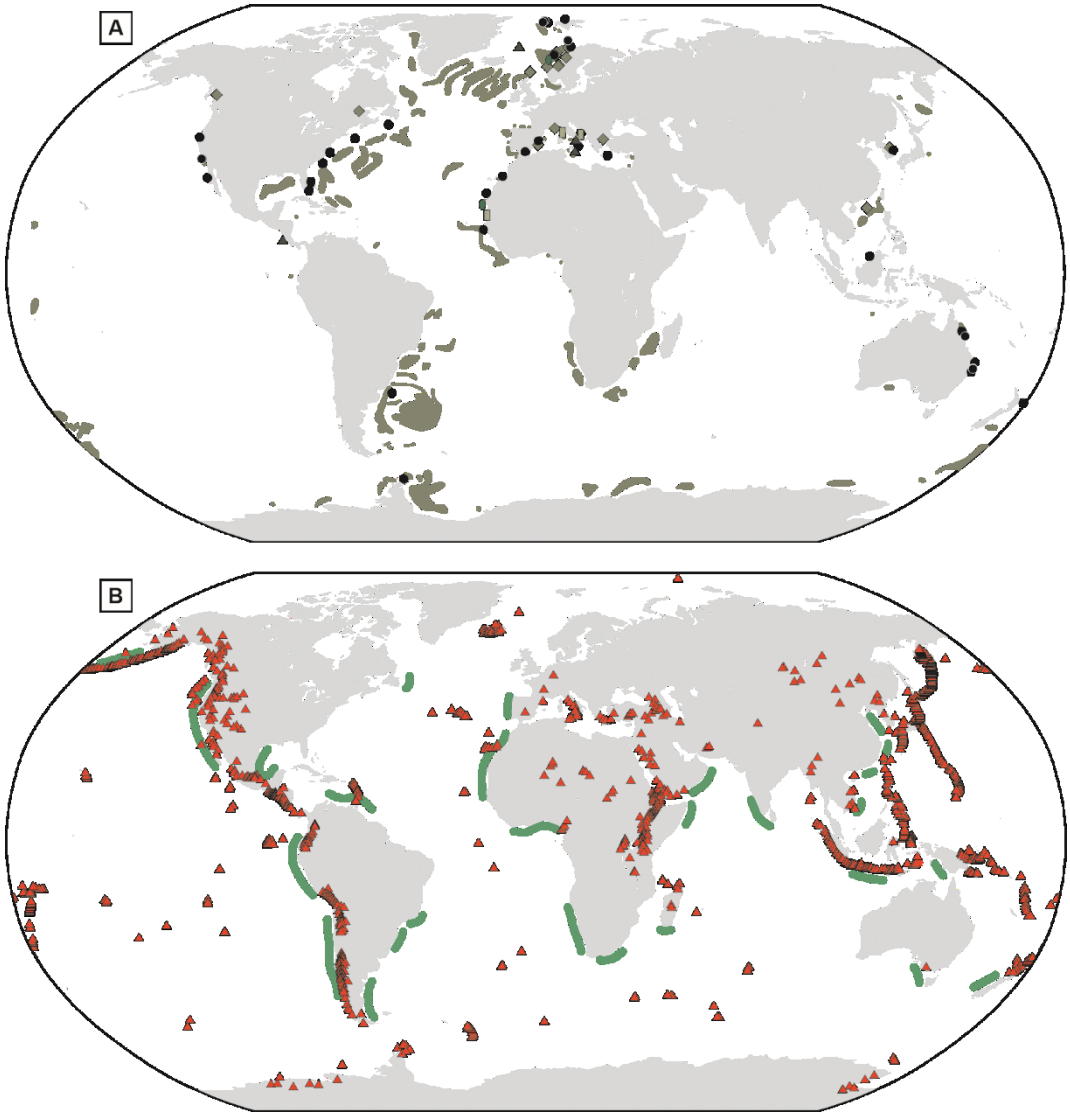

Figure 2.8. World distribution of **(A)** contourites (modified from Rebesco et al., 2014; Thran et al., 2018) and **(B)** volcanoes (red triangles; Global Volcanism Program, 2013) and upwelling regions (green; modified from Kämpf and Chapman, 2016). Please refer to online version for colours.

The main mechanisms proposed to cause failure along volcaniclastic weak layers are particle rearrangement and breakage, and transient pore pressure generation (e.g. Harders et al., 2010). Pore pressure, however, will only accumulate if a sealing layer (i.e. low-permeability layer) prohibits pore pressure dissipation. Therefore, volcaniclastic weak layers have only been identified in the form of sediment sequences (e.g. Hermosa Slide, Harders et al., 2010; Licosa Slide, Sammartini et al., 2019).

The recognition of volcaniclastic sediments as weak layers, has potentially broad implications on submarine landslide hazard since many regions around the world contain abundant volcaniclastic material that may fail under certain conditions (e.g. Miramontes et al., 2018; Fig. 2.8B). Volcanic ash,

in particular, can be transported over large areas, tens to hundreds of kilometres from their source (e.g. Riley et al., 2003), enabling the formation of laterally extensive weak layers. Such weak layers may promote large-scale or repeated slope failures in proximal or distal areas of the volcanic source. Notice that although not included in this review, landslides on volcanic island slopes are common (e.g. Moore et al., 1989; Le Friant et al., 2019), and have to be carefully investigated due to their tsunamigenic potential (e.g. Silver et al., 2009; Watt et al., 2012; Le Friant et al., 2019). In most cases, however, slope failures on volcanic islands include subaerial parts with their headwalls extending onshore (e.g. Hunt et al., 2011; Watt et al., 2012; León et al., 2020), which did not meet our criteria to be included in this landslide catalogue.

Similar to volcaniclastic sediments, particle rearrangement and breakage, and transient pore pressure generation are the main failure mechanisms related to fossiliferous weak layers (e.g. Urlaub et al., 2015). Urlaub et al. (2018) highlighted how diatom ooze layers overlain by clay likely acted as weak layers for the Cap Blanc Slide, offshore NW Africa, while diatom ooze layers overlain by coarser sediments did not show such a correlation. This shows that, although high shear strength of diatom ooze would suggest a strengthening effect, their high compressibility may lead to a drastic volume reduction and transient pore pressure generation during burial.

Such fossiliferous weak layers may precondition large submarine landslides. For example, periodical upwelling of diatom ooze offshore NW Africa, enables the formation of laterally extensive weak layers on the otherwise sediment-starved continental slope, promoting large-scale submarine landslides (e.g. Cap Blanc Slide; Urlaub et al., 2018). Such upwelling regions are found all over the world (Fig. 2.8B) and should be investigated with great care.

We demonstrated the advantage of a lithology-based classification by highlighting the correlation between the type of weak layer and specific geographical and physiographic locations. Depending on the environmental setting and the dominant sedimentation regimes, we can infer the likely location of different weak layers and further related them to individual failure mechanisms (Fig. 2.7).

2.4. Conclusions and outlook

Based on a new global submarine landslide catalogue that comprises 60 case studies, we reviewed the current state of knowledge of weak layers and their controls on submarine landslide formation. We show that the classification into *inherited* and *induced* weak layers (Locat et al., 2014) is not applicable for various case studies (Tab. 2.1), and does not readily enable an identification of weak layers from sediment cores or in-situ measurements of unfailed sediments. We therefore introduce a new classification scheme for weak layers that is based on lithology (Tab. 2.2). Such a classification has the

advantage of enabling weak layer recognition from sediment cores, including those sampling unfailed sediments. In addition, it allows the correlation of different types of weak layers (which are linked to sediment lithology) to specific geographical and physiographic locations. These include contourite or turbidite systems that can create siliciclastic sediment sequences, areas of high productivity where biogenic sediments may dominate, or regions that experience repeated ash deposition from proximal or distal volcanic sources (Fig. 2.8). Successfully identifying weak layers and further relating them to specific failure mechanisms will significantly advance the assessment of submarine landslide hazard and will inform management strategies.

Our data clearly show that the sequencing of specific sediment layers, such as sand-clay, ash-clay or diatom-clay, is key to the formation of weak layers. In total, 21 of our 60 case studies were related to distinct sediment sequences, while three submarine landslides were related to clay weak layers (Fig. 2.7E, F). In addition, failure along lithological contrasts was inferred for another six case studies. These submarine landslides, however, could not be classified properly, because the published data was insufficient. Failure mechanisms were often deduced from geophysical data alone rather than from direct sampling. In total, excess pore pressure was invoked as the main failure mechanism in 19 of the 60 case studies. Another seven case studies linked slope failure to a combination of excess pore pressure and strain softening, while failure due to strain softening alone was referenced in two case studies (Fig. 2.7C, D).

The robust investigation and characterisation of weak layers and their mechanisms in a submarine landslide setting is a function of their accurate identification, their recovery during sediment coring, and careful sampling as well as the choice of analytical methods. It further requires the sampling of weak layers in their undisturbed form, i.e. from the undisturbed adjacent slope. Sediment cores and in-situ measurements that sample relevant sediments, in particular the undisturbed sediment sequence outside the slide area, however, are rare (Fig. 2.7A, B).

In the following, we outline some of the key requirements for future weak layer investigations:

- There is a clear need for research cruises that are tailored towards failure plane and weak layer investigations. The identification and characterisation of failure planes and weak layers are usually not the primary aim of current sampling campaigns; hence, the applied methods (e.g. coring techniques) are often not suitable to sample failure planes and failure plane equivalent samples outside the slide area.
- Instead of targeting large submarine landslides, whose failure planes are buried tens to hundreds of metres below the seafloor (e.g. Haflidason et al., 2004), it may be more prudent to focus efforts on the investigation of smaller landslides. The investigation of smaller submarine

landslides has shown good results (e.g. Strozyk et al., 2010b; Baeten et al., 2014; Gatter et al., 2020), as they allow for the deployment of more cost-effective coring devices, which can be used to obtain a number of cores, inside and outside the slide area. Another alternative is to study landslides in lakes, which are also smaller in size and readily accessible (e.g. Van Daele et al., 2017; Moernaut et al., 2020; Stegmann et al., 2007). It is clearly important, however, to understand how much of the information we can extrapolate from small to larger landslides. Several previous studies suggest that morphometry and other characteristics may be similar between cohesive landslides across many orders of magnitude (e.g. Micallef et al., 2008; Moernaut and De Batist, 2011; Urgeles and Camerlenghi, 2013; Casas et al., 2016; Clare et al., 2017); hence this may be a sensible approach where and until deeper sampling is not viable.

- The successful sampling (and investigation) of weak layers requires new technologies, e.g. further development of seafloor drill rigs. Seafloor drill rigs have the potential to fill the gap between relatively cost-effective, but short, conventional coring devices, such as gravity or piston corer that can sample dense or weakly cemented strata, and the use of drill ships (Freudenthal and Wefer, 2013). They have the clear advantage that once they are deployed on the seafloor, they can collect a number of sediment cores relatively time-effective. Additionally, they allow for further borehole logging and in-situ testing (e.g. Spagnoli et al., 2015; Huhn et al., 2019). Such integrated technologies may fill the gaps from individual datasets.
- It is of critical importance to combine various sampling (e.g. coring and in-situ measurements) and analytical (e.g. sedimentological, geochemical, geotechnical) methods to investigate weak layers. In order to overcome limitations inherent to individual methods, the integration of datasets becomes imperative and should include high-resolution data from grain-scale analyses, such as micro-CT (Computed Tomography) or SEM. Such high-resolution analyses appear necessary in order to capture the processes that underlie and control weak layer formation, and that could not be resolved by other techniques. The combination and integration of various methods enables to compensate for uncertainties and to fill gaps of individual datasets.
- Finally, a systematic approach of weak layer investigation is required. Many current limitations are related to a lack of data, but also inconsistency in data acquisition. There is a clear need for a more complete data collection and uniform workflow for a better comparison between individual studies and consequently weak layer characterisation.

Glossary

Basal surface: Defined, deepest boundary of a submarine landslide.

Case study or **study:** May include only one or several independent published research papers that all deal with the same submarine landslide or slide complex.

Failure mechanism: A physical, chemical or other process that results in failure; the direct cause of a failure mode.

Failure mode: The cause of failure; the direct effect of failure mechanisms.

Failure plane: The surface or sediment horizon within the slope stratigraphy along which failure initiates. If no substantial erosion occurs the failure plane also acts as *glide plane*.

Glide plane: The surface within the slope stratigraphy along which slide movement occurs. This surface can coincide with the *failure plane*, but does not have to be identical, e.g. if substantial erosion occurs during the slide movement, thereby remoulding and removing the failure plane.

Liquefaction: Occurs when a loosely packed sediment loses strength under environmental conditions such as cyclic loading from earthquakes. The sediment particles temporarily lose contact with one another, and the particle weight is temporarily sustained by the pore fluid, causing transient pore pressures and subsequent failure.

Permeability: A measurement of the sediment's capability to let fluids pass through.

Porosity: Measures the void (pore) space of the sediment, and is the fraction of the volume of voids over the total volume.

Pre-conditioning factor: Long-term factors (e.g. sedimentation) that bring submarine slopes closer towards failure.

Sediment horizon: A bedding surface with a marked change in lithology, or a distinct layer or thin bed with a characteristic lithology or geotechnical properties within the stratigraphy.

Sediment sequence: Refers to alternating layers of varying physical and geotechnical properties, e.g. particle size, shear strength or porosity.

Sensitive clay: A clay where the remoulded shear strength shows a clear decrease in comparison to the undisturbed shear strength. The ratio of undisturbed to disturbed strength is termed sensitivity.

Slope failure: Refers to the downward movement of slope material in response to mainly gravitational stresses. Slope failure occurs when the downward driving forces exceed the resisting forces of the slope material.

Strain softening: Decrease in shear strength with increasing strain.

Submarine landslide: Gravity-driven mass movement that occurs in a variety of underwater slope settings worldwide.

Submarine landslide complex: Multi-failure complex, defined by multiple steps.

Triggering mechanism: An external, short-term stimulus that initiates slope failure.

Acknowledgments

S. Kutterolf is gratefully thanked for providing the SEM images of volcanic material from the Integrated Ocean Drilling Program (IODP) Expedition 375. This work was supported by the European Union's Horizon 2020 research and innovation programme under the Marie Skłodowska-Curie grant agreement No. 721403.

Supplementary material

Appendix 2.A: Supplementary data file

Description:

The accompanying Excel spreadsheet summarises the data used in this literature review, including all discussed case studies (sheet 'Case Studies' and 'Case Studies – Summary') and related references (sheet 'References'). 'Case Studies' lists the information available for each case study according to individual references. 'Case Studies - Summary' provides a summary of the gathered information from all references (as listed in 'Case Studies'), which was used as raw data for this literature review.

File name:

Appendix2.A_WeakLayer_CaseStudies.xlsx

References

Ai, F., Strasser, M., Preu, B., Hanebuth, T.J.J., Krastel, S., Kopf, A., 2014. New constraints on oceanographic vs. seismic control on submarine landslide initiation: a geotechnical approach off Uruguay and northern Argentina. Geo-Marine Letters, 34, 399-417. Doi: 10.1007/s00367-014-0373-3

Antobreh, A., Krastel, S., 2007. Mauritania Slide Complex: morphology, seismic characterisation and processes of formation. International Journal of Earth Sciences, 96, 451-472.

Baeten, N.J., Laberg, J.S., Forwick, M., Vorren, T.O., Vanneste, M., Forsberg, C.F., Kvalstad, T.J., Ivanov, M., 2013. Morphology and origin of smaller-scale mass movements on the continental slope off northern Norway. Geomorphology, 187, 122-134, https://doi.org/10.1016/j.geomorph.2013.01.008

Baeten, N.J., Laberg, J.S., Vanneste, M., Forsberg, C.F., Kvalstad, T.J., Forwick, M., Vorren, T.O., Haflidason, H., 2014. Origin of shallow submarine mass movements and their glide planes - Sedimentological and geotechnical analyses from the continental slope off northern Norway. Journal of Geophysical Research: Earth Surface, 119, 2335-2360, https://doi.org/10.1002/2013JF003068

Berg, K., Solheim, A., Bryn, P., 2005. The Pleistocene to recent geological development of the Ormen Lange area. Marine and Petroleum Geology, 22, 45-56, https://doi.org/10.1016/j.marpetgeo.2004.10.009

Berndt, C., Costa, S., Canals, M., Camerlenghi, A., de Mol, B., Saunders, M., 2012. Repeated slope failure linked to fluid migration: The Ana submarine landslide complex, Eivissa Channel, Western Mediterranean Sea. Earth and Planetary Science Letters, 319-320, 65-74, https://doi.org/10.1016/j.epsl.2011.11.045

Bolt, G.H., 1956. Physio-chemical analysis of the compressibility of pure clays. Géotechnique, 6(2), 86-93, https://doi.org/10.1680/geot.1956.6.2.86

Bryn, P., Berg, K., Forsberg, C.F., Solheim, A., Kvalstad, T.J., 2005a. Explaining the Storegga Slide. Marine and Petroleum Geology, 22, 11-19, https://doi.org/10.1016/j.marpetgeo.2004.12.003

Bryn, P., Berg, K., Stoker, M.S., Haflidason, H., Solheim, A., 2005b. Contourites and their relevance for mass wasting along the Mid-Norwegian Margin. Marine and Petroleum Geology, 22, 85-96, https://doi.org/10.1016/j.marpetgeo.2004.10.012

Bugge, T., Belderson, R.H., Kenyon, N.H., 1988. The Storegga Slide. Philosophical Transactions of the Royal Society, 325, 357-388.

Canals, M., Lastras, G., Urgeles, R., Casamor, J.L., Mienert, J., Cattaneo, A., De Batist, M., Haflidason, H., Imbo, Y., Laberg, J.S., Locat, J., Long, D., Longva, O., Masson, D.G., Sultan, N., Trincardi, F., Bryn, P., 2004. Slope failure dynamics and impacts from seafloor and shallow sub-seafloor geophysical data: case studies from the COSTA project. Marine Geology, 213, 9-72, https://doi.org/10.1016/j.margeo.2004.10.001

Carter, L., Gavey, R., Talling, P.J., Liu, J.T., 2014. Insights into submarine geohazards from breaks in subsea telecommunication cables. Oceanography, 27(2), 58–67, http://dx.doi.org/10.5670/oceanog.2014.40

Casas, D., Chiocci, F., Casalbore, D., Ercilla, G., De Urbina, J.O., 2016. Magnitude-frequency distribution of submarine landslides in the Gioia Basin (southern Tyrrhenian Sea). Geo-Marine Letters, 36(6), 405-414.

Casas, D., Ercilla, G., Yenes, M., Estrada, F., Alonso, B., García, M., Somoza, L., 2011. The Baraza Slide: model and dynamics. Marine Geophysical Research, 32, 245-256.

Cauchon-Voyer, G., Locat, J., Leroueil, S., St-Onge, G., Demers, D., 2011. Large-scale subaerial and submarine Holocene and recent mass movements in the Betsiamites area, Quebec, Canada. Engineering Geology, 121, 28-45, https://doi.org/10.1016/j.enggeo.2011.04.011

Cauchon-Voyer, G., Locat, J., St-Onge, G., 2008. Late-Quaternary morpho-sedimentology and submarine mass movements of the Betsiamites area, Lower St. Lawrence Estuary, Quebec, Canada. Marine Geology, 251, 233-252, https://doi.org/10.1016/j.margeo.2008.03.003

Cauchon-Voyer, G., Locat, J., St-Onge, G., Leroueil, S., Lajeunesse, P., 2012. Development and Potential Triggering Mechanisms for a Large Holocene Landslide in the Lower St. Lawrence Estuary. In: Yamada, Y., Kawamura, K., Ikehara, K., Ogawa, Y., Urgeles, R., Mosher, D., Chaytor, J., Strasser, M. (Eds) Submarine Mass Movements and Their Consequences, Advances in Natural and Technological Hazards Research, 31, 67-76. Springer Science+Business Media B.V., Dordrecht.

Chaytor, J.D., Twichell, D.C., ten Brink, U.S., 2012. A Reevaluation of the Munson-Nygren-Retriever Submarine Landslide Complex, Georges Bank Lower Slope, Western North Atlantic. In: Yamada, Y., Kawamura, K., Ikehara, K., Ogawa, Y., Urgeles, R., Mosher, D., Chaytor, J., Strasser, M. (Eds) Submarine Mass Movements and Their Consequences, Advances in Natural and Technological Hazards Research, 31, 135-145. Springer Science+Business Media B.V., Dordrecht.

Clare, M.A., Vardy, M.E., Cartigny, M.J.B., Talling, P.J., Himsworth, M.D., Dix, J.K., Harris, J.M., Whitehouse, R.J.S., Belal, M., 2017. Direct monitoring of active geohazards: emerging geophysical tools for deep-water assessments. Near Surface Geophysics, 15, 427-444, https://doi.org/10.3997/1873-0604.2017033

Clarke, S., Hubble, T., Webster, J., Airey, D., De Carli, E., Ferraz, C., Reimer, P., Boyd, R., Keene, J., Shipboard party SS12/2008, 2016. Sedimentology, structure and age estimate of five continental slope submarine landslides, eastern Australia. Australian Journal of Earth Sciences, 63(5), 631-652, https://doi.org/10.1080/08120099.2016.1225600

Cukur, D., Kim, SP., Kong, GS., Bahk, JJ., Horozal, S., Um, IK., Lee, GS., Chang, TS., Ha, HJ., Völker, D., Kim, JK., 2016. Geophysical evidence and inferred triggering factors of submarine landslides on the western continental margin of the Ulleung Basin, East Sea. Geo-Marine Letters, 36, 425-444. Doi: 10.1007/s00367-016-0463-5

Cukur, D., Um, IK., Chun, JH., Lee, GS., Kim, SR., Bahk, JJ., Urgeles, R., Horozal, S., 2020. Factors leading to slope failure on a sediment-starved margin: The southwestern continental margin of the East Sea, Korea. Marine Geology, 428, 106282, https://doi.org/10.1016/j.margeo.2020.106282

Dalla Valle, G., Gamberi, F., Foglini, F., Trincardi, F., 2015. The Gondola Slide: A mass transport complex controlled by margin topography (South-Western Adriatic Margin, Mediterranean Sea). Marine Geology, 336, 97-113, https://doi.org/10.1016/j.margeo.2015.05.001

Dan, G., Sultan, N., Savoye, B., 2007. The 1979 Nice harbour catastrophe revisited: Trigger mechanism inferred from geotechnical measurements and numerical modelling. Marine Geology, 245(1-4), 40-64, https://doi.org/10.1016/j.margeo.2007.06.011

Díaz-Rodríguez, J.A., 2011. Diatomaceous soils: monotonic behaviour. International Symposium on Deformation Characteristics of Geomaterials, Seoul, Korea, September 1-3, 2011.

Dutkiewicz, A., Müller, R.D., O'Callaghan, S., Jónasson, H., 2015. Census of seafloor sediments in the world's ocean. Geology, 43(9), 795-798, https://doi.org/10.1130/G36883.1

Dziadek, R., 2014. Drained and Undrained Shear Strength Characteristics of Reconstituted Bio-siliceous Sediments, University of Bremen - FB5 Geowissenschaften. University of Bremen, Bremen.

Edwards, B.D., Lee, H.J., Field, M.E., 1995. Mudflow generated by retrogressive slope failure, Santa Barbara Basin, California continental borderland. Journal of Sedimentary Research, A65(1), 57-68, https://doi.org/10.1306/D4268022-2B26-11D7-8648000102C1865D

Elger, J., Berndt, C., Krastel, S., Piper, D.J.W., Gross, F., Geissler, W.H., 2017. Chronology of the Fram Slide Complex offshore NW Svalbard and its implications for local and regional slope stability. Marine Geology, 393, 141-155, https://doi.org/10.1016/j.margeo.2016.11.003

Elger, J., Berndt, C., Krastel, S., Piper, D.J.W., Gross, F., Spielhagen, R.F., Meyer, S., 2015. The Fram Slide off Svalbard: a submarine landslide on a low-sedimentation-rate glacial continental margin. Journal of Geological Society, 172, 153-156, https://doi.org/10.1144/jgs2014-055

Evans, D., Harrison, Z., Shannon, P.M., Laberg, J.S., Nielsen, T., Ayers, S., Holmes, R., Hoult, R.J., Lindberg, B., Haflidason, H., Long, D., Kuijpers, A., Andersen, E.S., Bryn, P., 2005. Palaeoslides and other mass failures of Pliocene to Pleistocene age along the Atlantic continental margin of NW Europe. Marine and Petroleum Geology, 22, 1131-1148, https://doi.org/10.1016/j.marpetgeo.2005.01.010

Fine, I.V., Rabinovich, A.B., Bornhold, B.D., Thomson, R.E., Kulikov, E.A., 2005. The Grand Banks landslide-generated tsunami of November 18, 1929: preliminary analysis and numerical modeling. Marine Geology, 215, 45-57, https://doi.org/10.1016/j.margeo.2004.11.007

Fisher, M.A., Normark, W.R., Greene, H.G., Lee, H.J., Sliter, R.W., 2005. Geology and tsunamigenic potential of submarine landslides in Santa Barbara Channel, Southern California. Marine Geology, 224, 1-22, https://doi.org/10.1016/j.margeo.2005.07.012

Förster, A., Ellis, R.G., Henrich, R., Krastel, S., Kopf, A.J., 2010. Geotechnical characterization and strain analyses of sediment in the Mauritania Slide Complex, NW-Africa. Marine and Petroleum Geology, 27, 1175-1189, https://doi.org/10.1016/j.marpetgeo.2010.02.013

Freudenthal, T., Wefer, G., 2007. Scientific Drilling with the Sea Floor Drill Rig MeBo. Scientific Drilling, 5, 63-66.

Freudenthal, T., Wefer, G., 2013. Drilling cores on the sea floor with the remote-controlled sea floor drilling rig MeBo. Geoscientific Instrumentation Methods and Data Systems, 2, 329-337.

Freire, F., Gyllencreutz, R., Jafri, R.U., Jakobsson, M., 2014. Acoustic evidence of a submarine slide in the deepest part of the Arctic, the Molloy Hole. Geo-Marine Letters, 34, 315-325. Doi: 10.1007/s00367-014-0371-5

Gamberi, F., Dalla Valle, G., Foglini, F., Rovere, M., Trincardi, F., 2019. Submarine Landslides on the Seafloor: Hints on Subaqueous Mass-Transport Processes From the Italian Continental Margins (Adriatic and Thyrrenian Seas, Offshore Italy). In: Ogata, K., Festa, A., Pini, G.A. (Eds) Submarine Landslides: Subaqueous Mass Transport Deposits from Outcrops to Seismic Profiles, Geophysical Monography, 246, 339-356, https://doi.org/10.1002/9781119500513.ch20

Gamberi, F., Rovere, M., Marani, M., 2011. Mass-transport complex evolution in a tectonically active margin (Gioia Basin, Southeastern Tyrrhenian Sea). Marine Geology, 279, 98-110, https://doi.org/10.1016/j.margeo.2010.10.015

Gardner, J.V., Prior, D.B., Field, M.E., 1999. The Humboldt Slide - a large shear-dominated retrogressive slope failure. Marine Geology, 154, 323-338, https://doi.org/10.1016/S0025-3227(98)00121-2

Gatter, R., Clare, M.A., Hunt, J.E., Watts, M., Madhusudhan, B.N., Talling, P.J., Huhn, K., 2020. A multi-disciplinary investigation of the AFEN Slide: The relationship between contourites and submarine landslides. Geological Society, London, Special Publications, 500, 173-193, https://doi.org/10.1144/SP500-2019-184

Gee, M.J.R., Uy, H.S., Warren, J., Morley, C.K., Lambiase, J.J., 2007. The Brunei slide: A giant submarine landslide on the North West Borneo Margin revealed by 3D seismic data. Marine Geology, 246, 9-23, https://doi.org/10.1016/j.margeo.2007.07.009

Georgiopoulou, A., Masson, D.G., Wynn, R.B., Krastel, S., 2010. Sahara Slide: Age, initiation, and processes of a giant submarine slide. Geochemistry, Geophysics, Geosystems, 11(7), Q07014, https://doi.org/10.1029/2010GC003066

Global Volcanism Program, 2013. Volcanoes of the World, v. 4.9.4 (17 Mar 2021). Venzke, E. (Ed) Smithsonian Institution. Downloaded 27 Mar 2021, https://doi.org/10.5479/si.GVP.VOTW4-2013

Greene, H.G., Murai, L.Y., Watts, P., Maher, N.A., Fisher, M.A., Paull, C.E., Eichhubl, P., 2006. Submarine landslides in the Santa Barbara Channel as potential tsunami sources. Natural Hazards and Earth System Sciences, 6, 63-88, https://doi.org/10.5194/nhess-6-63-2006

Haflidason, H., Lien, R., Sejrup, H.P., Forsberg, C.F., Bryn, P., 2005. The dating morphometry of the Storegga Slide. Marine and Petroleum Geology, 22, 123-136, https://doi.org/10.1016/j.marpetgeo.2004.10.008

Haflidason, H., Sejrup, H.P., Berstad, I.M., Nygård, A., Richter, T., Bryn, P., Lien, R., Berg, K., 2003. A Weak Layer Feature on the Northern Storegga Slide Escarpment. In: Mienert, J., Weaver, P. (Eds) European Margin Sediment Dynamics, Side-Scan Sonar and Seismic Images, 55-62. Springer-Verlag, Berlin, Heidelberg.

Haflidason, H., Sejrup, H.P., Nygård, A., Mienert, J., Bryn, P., Lien, R., Forsberg, C.F., Berg, K., Masson, D., 2004. The Storegga Slide: architecture, geometry and slide development. Marine Geology, 213, 201-234, https://doi.org/10.1016/j.margeo.2004.10.007

Hampton, M.A., Lee, H.J., Locat, J., 1996. Submarine Landslides. Reviews of Geophysics, 34, 35-59, https://doi.org/10.1029/95RG03287

Harbitz, C.B., Løvholt, F., Bungum, H., 2014. Submarine landslide tsunamis: how extreme and how likely?. Natural Hazards, 72, 1341-1374.

Harders, R., Kutterolf, S., Hensen, C., Moerz, T., Brueckmann, W., 2010. Tephra layers: A controlling factor on submarine translational sliding?. Geochemistry, Geophysics, Geosystems, 11(5), Q05S23, https://doi.org/10.1029/2009GC002844

Henkel, S., Strasser, M., Schwenk, T., Hanebuth, T.J.J., Hüsener, J., Winkelmann, D., Tomasini, J., Krastel, S., Kasten, S., 2011. An interdisciplinary investigation of a recent submarine mass transport deposit at the continental margin off Uruguay. Geochemistry, Geophysics, Geosystems, 12(8), Q08009, https://doi.org/10.1029/2011GC003669

Henrich, R., Hanebuth, T.J.J., Krastel, S., Neubert, N., Wynn, R.B., 2008. Architecture and sediment dynamics of the Mauritania Slide Complex. Marine and Petroleum Geology, 25, 17-33, https://doi.org/10.1016/j.marpetgeo.2007.05.008

Hill, J.C., Brothers, D.S., Craig, B.K., ten Brink, U.S., Chaytor, J.D., Flores, C.H., 2017. Geologic controls on submarine slope failure along the central U.S. Atlantic margin: Insights from the Currituck Slide Complex. Marine Geology, 385, 114-130, https://doi.org/10.1016/j.margeo.2016.10.007

Horozal, S., Bahk, JJ., Lee, S.H., Cukur, D., Urgeles, R., Kim, G.Y., Kim, SP., Ryu, BJ., Kim, JH., 2019. Mass-wasting processes along the margins of the Ulleung Basin, East Sea: insights from multichannel seismic reflection and multibeam echosounder data. In: Lintern, D.G. et al (Eds.) Subaqueous Mass Movements and their Consequences: Assessing Geohazards, Environmental Implications and Economic Significance of Subaqueous Landslides. Geological Society, London, Special Publications, 477, 107-119, https://doi.org/10.1144/SP477.18

Hubble, T., Yeung, S., Clarke, S., Baxter, A., De Blasio, F., 2019. Submarine landslides offshore Yamba, NSW, Australia: an analysis of their timing, downslope motion and possible causes. In: Lintern, D.G., Mosher, D.C., Moscardelli, L.G., Bobrowsky, P.T., Campbell, C., Chaytor, J., Clague, J., Georgiopoulou, A., Lajeunesse, P., Normandeau, A., Piper, D., Scherwath, M., Stacey, C., Turmel, D. (Eds) Subaqueous Mass Movements and their Consequences: Assessing Geohazards, Environmental Implications and Economic Significance of Subaqueous Landslides. Geological Society, London, Special Publications, 477: 207-222, https://doi.org/10.1144/SP477.11

Huhn, K., Arroyo, M., Cattaneo, A., Clare, M.A., Gràcia, E., Harbitz, C.B., Krastel, S., Kopf, A., Løvholt, F., Rovere, M., Strasser, M., Talling, P.J., Urgeles, R., 2020. Modern Submarine Landslide Complexes. In: Ogata, K., Festa, A., Pini, G.A. (Eds) Submarine Landslides: Subaqueous Mass Transport Deposits from Outcrops to Seismic Profiles. Geophysical Monograph Series, 246, 183-200. American Geophysical Union and John Wiley & Sons, Inc., Washington, https://doi.org/10.1002/9781119500513.ch12

Huhn, K., Freudenthal, T., Gatter, R., Hilgenfeldt, C., Hönekopp, L., Hornbach, M., Kühn, M., Kuhlmann, J., Kutterolf, S., Meyer-Schack, B., Pallapies, K., Rapp, S.K., Sievers, C., Watt, S., Stelzner, M., 2019. FS METEOR M154-2 Cruise Report "Sector collapse kinematics and tsunami implications – SEKT", Point-à-Pitre - Point-à-Pitre, April 29 - May 23 2019, Reports from MARUM and Department of Geosciences, University of Bremen, p. 82.

Hühnerbach, V., Masson, D.G., partners of COAST-Project, 2004. Landslides in the North Atlantic and its adjacent seas: an analysis of their morphology, setting and behaviour. Marine Geology, 213, 343-362, https://doi.org/10.1016/j.margeo.2004.10.013

Hunt, J.E., Wynn, R.B., Masson, D.G., Talling, P.J., Teagle, D.A.H., 2011. Sedimentological and geochemical evidence for multistage failure of volcanic island landslides: A case study from Icod landslide on north Tenerife, Canary Islands. Geochemistry, Geophysics, Geosystems, 12(12), Q12007, https://doi.org/10.1029/2011GC003740

Kämpf, J., Chapman, P., 2016. Upwelling Systems of the World: A Scientific Journey to the Most Productive Marine Ecosystems, p. 47. Springer International Publishing Switzerland.

Kluesner, J.W., Brothers, D.S., Wright, A.L., Johnson, S.Y., 2020. Structural Controls on Slope Failure Within the Western Santa Barbara Channel Based on 2-D and 3-D Seismic Imaging. Geochemistry, Geophysics, Geosystems, 21, e2020GC009055, https://doi.org/10.1029/2020GC009055

Kopf, A.J., Stegmann, S., Garziglia, S., Henry, P., Dennielou, B., Haas, S., Weber, KC., 2016. Soft sediment deformation in the shallow submarine slope off Nice (France) as a result of a variably charged Pliocene aquifer and mass wasting processes. Sedimentary Geology, 344, 290-309, http://dx.doi.org/10.1016/j.sedgeo.2016.05.014

Korup, O., 2012. Earth's portfolio of extreme sediment transport events. Earth-Science Reviews, 112, 115-125, https://doi.org/10.1016/j.earscirev.2012.02.006

Korup, O., Clague, J.J., Hermanns, R.L., Hewitt, K., Strom, A.L., Weidinger, J.T., 2007. Giant landslides, topography, and erosion. Earth and Planetary Science Letters, 261, 578-589, https://doi.org/10.1016/j.epsl.2007.07.025

Krastel, S., Urlaub, M., Georgiopoulou, A., Wynn, R.B., Schwenk, T., Stevenson, C., Feldens, P., 2019. Mass wasting along the NW African continental margin. In: Lintern, D.G., Mosher, D.C., Moscardelli, L.G., Bobrowsky, P.T., Campbell, C., Chaytor, J.D., Clague, J.J., Georgiopoulou, A., Lajeunesse, P., Normandeau, A., Piper, D.J.W., Scherwath, M., Stacey, C., Turmel, D. (Eds) Subaqueous Mass Movements and their Consequences: Assessing Geohazards, Environmental Implications and Economic Significance of Subaqueous Landslides. Geological Society, London, Special Publications, 477, 151-167, https://doi.org/10.1144/SP477.36

Krastel, S., Wefer, G., Hanebuth, T.J.J., Antobreh, A.A., Freudenthal, T., Preu, B., Schwenk, T., Strasser, M., Violante, R., Winkelmann, D., M78/3 shipboard scientific party, 2011. Sediment dynamics and geohazards off Uruguay and the de la Plata River region (northern Argentina and Uruguay). Geo-Marine Letters, 31, 271-283. Doi: 10.1007/s00367-011-0232-4

Krastel, S., Wynn, R.B., Feldens, P., Schürer, A., Böttner, C., Stevenson, C., Cartigny, J.B., Hühnerbach, V., Unverricht, D., 2016. Flow Behaviour of a Giant Landslide and Debris Flow Entering Agadir Canyon, NW Africa. In: Lamarche, G., Mountjoy, J., Bull, S., Hubble, T., Krastel, S., Lane, E., Micallef, A., Moscardelli, L., Mueller, C., Pecher, I., Woelz, S. (Eds) Submarine Mass Movements and Their Consequences, Advances in Natural and Technological Hazards Research, 41, 145-154. Springer International Publishing Switzerland, Cham.

Kuhlmann, J., Asioli, A., Strasser, M., Trincardi, F., Huhn, K., 2014. Integrated Stratigraphic and Morphological Investigation of the Twin Slide Complex Offshore Southern Sicily. In: Krastel, S., Behrmann, JH., Völker, D., Stipp, M., Berndt, C., Urgeles, R., Chaytor, J., Huhn, K., Strasser, M., Harbitz, C.B. (Eds) Submarine Mass Movements and Their Consequences, Advances in Natural and Technological Hazards Research, 37, 583-594, Springer International Publishing Switzerland, Cham.

Kuhlmann, J., Huhn, K., Ikari, M., 2016. Do Embedded Volcanoclastic Layers Serve as Potential Glide Planes: An Integrated Analysis from the Gela Basin Offshore Southern Sicily. In: Lamarche, G., Mountjoy, J., Bull, S., Hubble, T., Krastel, S., Lane, E., Micallef, A., Moscardelli, L., Mueller, C., Pecher, I., Woelz, S. (Eds) Submarine Mass Movements and Their Consequences, Advances in Natural and Technological Hazards Research, 41, 273-280. Springer International Publishing Switzerland, Cham.

Kuhlmann, J., Asioli, A., Trincardi, F., Klügel, A., Huhn, K., 2017. Landslide Frequency and Failure Mechanisms at NE Gela Basin (Strait of Sicily). Journal of Geophysical Research Earth Surface, 122, 2223-2243, https://doi.org/10.1002/2017JF004251

Kuhlmann, J., Orpin, A.R., Mountjoy, J.J., Crutchley, G.J., Henrys, S., Lunenburg, R., Huhn, K., 2019. Seismic and lithofacies characterization of a gravity core transect down the submarine Tuaheni Landslide Complex, NE New Zealand. In: Lintern, D.G., Mosher, D.C., Moscardelli, L.G., Bobrowsky, P.T., Campbell, C., Chaytor, J.D., Clague, J.J., Georgiopoulou, A., Lajeunesse, P., Normandeau, A., Piper, D.J.W., Scherwath, M., Stacey, C., Turmel, D. (Eds) Subaqueous Mass Movements and their Consequences: Assessing Geohazards, Environmental Implications and Economic Significance of Subaqueous Landslides. Geological Society, London, Special Publications, 477, 479-495, https://doi.org/10.1144/SP477.37

Kvalstad, T.J., Andresen, L., Forsberg, C.F., Berg, K., Bryn, P., Wangen, M., 2005. The Storegga slide: evaluation of triggering sources and slide mechanics. Marine and Petroleum Geology, 22, 245-256, https://doi.org/10.1016/j.marpetgeo.2004.10.019

L'Heureux, JS., Glimsdal, S., Longva, O., Hansen, L., Harbitz, C.B., 2011. The 1888 shoreline landslide and tsunami in Trondheimsfjorden, central Norway. Marine Geophysical Research, 32, 313-329. Doi: 10.1007/s11001-010-9103-z.

L'Heureux, JS., Hansen, L., Longva, O., Emdal, A., Grande, L.O., 2010. A multidisciplinary study of submarine landslides at the Nidelva fjord delta, Central Norway - Implications for geohazard assessment. Norwegian Journal of Geology, 90, 1-20.

L'Heureux, JS., Longva, O., Hansen, L., Vanneste, M., 2014. The 1930 Landslide in Orkdalsfjorden: Morphology and Failure Mechanism. In: Krastel, S., Behrmann, JH., Völker, D., Stipp, M., Berndt, C., Urgeles, R., Chaytor, J., Huhn, K., Strasser, M., Harbitz, C.B. (Eds) Submarine Mass Movements and Their Consequences, Advances in Natural and Technological Hazards Research, 37, 239-247. Springer International Publishing Switzerland, Cham.

L'Heureux, JS., Longva, O., Steiner, A., Hansen, L., Vardy, M.E., Vanneste, M., Haflidason, H., Brendryen, J., Kvalstad, T.J., Forsberg, C.F., Chand, S., Kopf, A., 2012. Identification of Weak Layers and Their Role for the Stability of Slopes at Finneidfjord, Northern Norway. In: Yamada, Y., Kawamura, K., Ikehara, K., Ogawa, Y., Urgeles, R., Mosher, D., Chaytor, J., Strasser, M. (Eds.) Submarine Mass Movements and Their Consequences, Advances in Natural and Technological Hazards Research, 31, 321-330. Springer Science+Business Media B.V., Dordrecht.

L'Heureux, J.S., Vanneste, M., Rise, L., Brendryen, J., Forsberg, C.F., Nadim, F., Longva, O., Chand, S., Kvalstad, T.J., Haflidason, H., 2013. Stability, mobility and failure mechanism for landslides at the upper continental slope off Vesterålen, Norway. Marine Geology, 346, 192-207, https://doi.org/10.1016/j.margeo.2013.09.009

Laberg, J.S., Camerlenghi, A., 2008. Chapter 25 The Significance of Contourites for Submarine Slope Stability. Developments in Sedimentology, 60, 537-556, https://doi.org/10.1016/S0070-4571(08)10025-5

Laberg, J.S., Kawamura, K., Amundsen, H., Baeten, N., Forwick, M., Rydningen, T.A., Vorren, T.O., 2014. A submarine landslide complex affecting the Jan Mayen Ridge, Norwegian-Greenland Sea: slide-scar morphology and processes of sediment evacuation. Geo-Marine Letters, 34, 51-58.

Laberg, J.S., Vorren, T.O., 1993. A Late Pleistocene submarine slide on the Bear Island Trough Mouth Fan. Geo-Marine Letters, 13, 227-234.

Laberg, J.S., Vorren, T.O., 2000. The Trænadjupet Slide, offshore Norway - morphology, evacuation and triggering mechanisms. Marine Geology, 171, 95-114, https://doi.org/10.1016/S0025-3227(00)00112-2

Laberg, J.S., Vorren, T.O., Dowdeswell, J.A., Kenyon, N.H., Taylor, J., 2000. The Andøya Slide and the Andøya Canyon, north-eastern Norwegian-Greenland Sea. Marine Geology, 162, 259-275, https://doi.org/10.1016/S0025-3227(99)00087-0

Laberg, J.S., Vorren, T.O., Mienert, J., Evans, D., Lindberg, B., Ottesen, D., Kenyon, N.H., Henriksen, S., 2002. Late Quaternary paleoenvironment and chronology in the Trænadjupet Slide area offshore Norway. Marine Geology, 188, 35-60, https://doi.org/10.1016/S0025-3227(02)00274-8

Laberg, J.S., Vorren, T.O., Mienert, J., Haflidason, H., Bryn, P., Lien, R., 2003. Preconditions leading to the Holocene Trænadjupet Slide offshore Norway. In: Locat, J., Mienert, J. (Eds) Submarine Mass Movements and Their Consequences, Natural and Technological Hazards Research, 19, 247-254. Springer Science+Business Media, Dordrecht.

Lafuerza, S., Sultan, N., Canals, M., Lastras, G., Cattaneo, A., Frigola, J., Costa, S., Berndt, C., 2012. Failure mechanisms of Ana Slide from geotechnical evidence, Eivissa Channel, Western Mediterranean Sea. Marine Geology, 307-310, 1-21, https://doi.org/10.1016/j.margeo.2012.02.010

Lastras, G., Canals, M., Amblas, D., Frigola, J., Urgeles, R., Calafat, A.M., Acosta, J., 2007. Slope instability along the northeastern Iberian and Balearic continental margins. Geologica Acta, 5, 35-47.

Lastras, G., Canals, M., Urgeles, R., De Batist, M., Calafat, A.M., Casamor, J.L., 2004. Characterisation of the recent BIG'95 debris flow deposit on the Ebro margin, Western Mediterranean Sea, after a variety of seismic reflection data. Marine Geology, 213, 235-255, https://doi.org/10.1016/j.margeo.2004.10.008

Lee, H.J., Locat, J., Desgagnés, P., Parsons, J.D., McAdoo, B.G., Orange, D.L., Puig, P., Wong, F.L., Dartnell, P., Boulanger, E., 2007. Submarine mass movements on continental margins. In: Nittrouer, C.A., Austin, J.A., Field, M.E., Kravitz, J.H., Syvitski, J.P.M., Wiberg, P.L. (Eds) Continental Margin Sedimentation: From Sediment Transport to Sequence Stratigraphy, 213-274. Blackwell Publishing Ltd, Oxford, UK, https://doi.org/10.1002/9781444304398.ch5

Le Friant, A., Lebas, E., Brunet, M., Lafuerza, S., Hornbach, M., Coussens, M., Watt, S., Cassidy, M., Talling, P.J., IODP 340 Expedition Ship Party, 2020. Submarine Landslides Around Volcanic Island: A Review of What Can Be Learned From the Lesser Antilles Arc. In: Ogata, K., Festa, A., Pini, G.A. (Eds) Submarine Landslides: Subaqueous Mass Transport Deposits from Outcrops to Seismic Profiles. Geophysical Monograph Series, 246, 277-297. American Geophysical Union and John Wiley & Sons, Inc., Washington, https://doi.org/10.1002/9781119500513.ch17

León, R., Urgeles, R., Pérez-López, R., Payo, E., Vázquez-Izquierdo, A., Giménez-Moreno, C.J., Casas, D., 2020. Geological and tectonic controls on morphometrics of submarine landslides of the Spanish margins. In: Georgiopoulou, A., Amy, L.A., Benetti, S., Chaytor, J.D., Clare, M.A., Gamboa, D., Haughton, P.D.W., Moernaut, J., Mountjoy, J.J. (Eds) Subaqueous Mass Movements and their Consequences: Advances in Process Understanding, Monitoring and Hazards Assessment. Geological Society, London, Special Publication, 500, 495-513, https://doi.org/10.1144/SP500-2019-153

Lewis, K.B., 1971. Slumping on a continental slope inclined at 1°-4°. Sedimentology, 16, 97-110, https://doi.org/10.1111/j.1365-3091.1971.tb00221.x

Leynaud, D., Mienert, J., Vanneste, M., 2009. Submarine mass movements on glaciated and non-glaciated European continental margins: A review of triggering mechanisms and preconditions to failure. Marine and Petroleum Geology, 26, 618-632, https://doi.org/10.1016/j.marpetgeo.2008.02.008

Leynaud, D., Sultan, N., Mienert, J., 2007. The role of sedimentation rate and permeability in the slope stability of the formerly glaciated Norwegian continental margin: the Storegga slide model. Landslides, 4, 297-309.

Li, W., Alves, T.M., Urlaub, M., Georgiopoulou, A., Klaucke, I., Wynn, R.B., Gross, F., Meyer, M., Repschläger,J., Berndt, C., Krastel, S., 2017. Morphology, age and sediment dynamics of the upper headwall of the Sahara Slide Complex, Northwest Africa: Evidence for a large Late Holocene failure. Marine Geology, 393, 109-123, https://doi.org/10.1016/j.margeo.2016.11.013

Li, W., Krastel, S., Alves, T.M., Urlaub, M., Mehringer, L., Schürer, A., Feldens, P., Gross, F., Stevenson, C.J., Wynn, R.B., 2018. The Agadir Slide offshore NW Africa: Morphology, emplacement dynamics, and potential contribution to the Moroccan Turbidite System. Earth and Planetary Science Letters, 498, 436-449, https://doi.org/10.1016/j.epsl.2018.07.005

Li, W., Wu, S., Völker, D., Zhao, F., Mi, L., Kopf, A., 2014a. Morphology, seismic characterization and sediment dynamics of the Baiyun Slide Complex on the northern South China Sea margin. Journal of the Geological Society, London, 171, 865-877, https://doi.org/10.1144/jgs2014-034

Li, W., Wu, S., Wang, X., Zhao, F., Wang, D., Mi, L., Li, Q., 2014b. Baiyun Slide and Its Relation to Fluid Migration in the Northern Slope of Southern China Sea. In: Krastel, S., Behrmann JH., Völker, D., Stipp, M., Berndt, C., Urgeles, R., Chaytor, J., Huhn, K., Strasser, M., Harbitz, C.B. (Eds.) Submarine Mass Movements and Their Consequences, Advances in Natural and Technological Hazards Research, 37, 105-115. Springer International Publishing Switzerland, Cham.

Lindberg, B., Laberg, J.S., Vorren, T.O., 2004. The Nyk Slide - morphology, progression, and age of a partly buried submarine slide offshore northern Norway. Marine Geology, 213, 277-289, https://doi.org/10.1016/j.margeo.2004.10.010

Locat, J., Lee, H.J., 2002. Submarine landslides: advances and challenges. Canadian Geotechnical Journal, 39, 193-212, https://doi.org/10.1139/t01-089

Locat, J., Leroueil, S., Locat, A., Lee, H., 2014. Weak Layers: Their Definition and Classification from a Geotechnical Perspective. In: Krastel, S., Behrmann, JH., Völker, D., Stipp, M., Berndt, C., Urgeles, R., Chaytor, J., Huhn, K., Strasser, M., Harbitz, C.B. (Eds) Submarine Mass Movements and Their Consequences, Advances in Natural and Technological Hazards Research, 37, 3-12. Springer International Publishing Switzerland, Cham.

Luo, M., Torres, M.E., Kasten, S., Mountjoy, J.J., 2020. Constraining the age and evolution of the Tuaheni Landslide Complex, Hikurangi Margin, New Zealand, using pore-water geochemistry and numerical modelling. Geophysical Research Letters, 47, e2020GL087243, https://doi.org/10.1029/2020GL087243

Lykousis, V., Roussakis, G., Alexandri, M., Pavlakis, P., Papoulia, I., 2002. Sliding and regional slope stability in active margins: North Aegean Trough (Mediterranean). Marine Geology, 186, 281-298, https://doi.org/10.1016/S0025-3227(02)00269-4

Madhusudhan, B.N., Clare, M.A., Clayton, C.R.I., Hunt, J.E., 2017. Geotechnical profiling of deep-ocean sediments at the AFEN submarine slide complex. Quarterly Journal of Engineering Geology and Hydrogeology, 50, 148-157, https://doi.org/10.1144/qjegh2016-057

Masson, D.G., Harbitz, C.B., Wynn, R.B., Pedersen, G., Løvholt, F., 2006. Submarine landslides: processes, triggers and hazard prediction. Philosophical Transactions of The Royal Society, 364, 2009-2039, https://doi.org/10.1098/rsta.2006.1810

Masson, D.G., Wynn, R.B., Talling, P.J., 2010. Large Landslides on Passive Continental Margins: Processes, Hypotheses and Outstanding Questions. In: Mosher, D.C., Shipp, R.C., Moscardelli, L., Chaytor, J.D., Baxter, C.D.P., Lee, H.J., Urgeles, R. (Eds) Submarine Mass Movements and Their Consequences, Advances in Natural and Technological Hazards Research, 28, 153-166. Springer Science+Business Media B.V., Dordrecht.

McAdoo, B.G., Pratson, L.F., Orange, D.L., 2000. Submarine landslide geomorphology, US continental slope. Marine Geology, 169, 103-136, https://doi.org/10.1016/S0025-3227(00)00050-5

Meyer, M., Geersen, J., Krastel, S., Schwenk, T., Winkelmann, D., 2012. Dakar slide offshore Senegal, NW-Africa: interaction of stacked giant mass-wasting events and canyon evolution. In: Yamada, Y., Kawamura, K., Ikehara, K., Ogawa, Y., Urgeles, R., Mosher, D., Chaytor, J., Strasser, M. (Eds) Submarine Mass Movements and Their Consequences, Advances in Natural and Technological Hazards Research, 31, 177-188. Springer Science+Business Media B.V., Dordrecht.

Micallef, A., Berndt, C., Masson, D.G., Stow, D.A., 2008. Scale invariant characteristics of the Storegga Slide and implications for large-scale submarine mass movements. Marine Geology, 247(1-2), 46-60, https://doi.org/10.1016/j.margeo.2007.08.003

Micallef, A., Person, M., Berndt, C., Bertoni, C., Cohen, D., Dugan, B., Evans, R., Haroon, A., Hensen, C., Jegen, M., Key, K., Kooi, H., Liebetrau, V., Lofi, J., Mailloux, B.J., Martin-Nagle, R., Michael, H.A., Müller, T., Schmidt, M., Schwalenberg, K., Trembath-Reichert, E., Weymer, B., Zhang, Y., Thomas, A.T., 2021. Offshore Freshened Groundwater in Continental Margins. Reviews of Geophysics, 58, e2020RG000706, https://doi.org/10.1029/2020RG000706

Minisini, D., Trincardi, F., Asioli, A., 2006. Evidence of slope instability in the Southwestern Adriatic Margin. Natural Hazards and Earth System Sciences, 6, 1-20, https://doi.org/10.5194/nhess-6-1-2006

Miramontes, E., Sultan, N., Garziglia, S., Jouet, G., Pelleter, E., Cattaneo, A. (2018). Altered volcanic deposits as basal failure surfaces of submarine landslides. Geology, 46(7), 663-666, https://doi.org/10.1130/G40268.1

Moernaut, J., De Batist, M., 2011. Frontal emplacement and mobility of sublacustrine landslides: Results from morphometric and seismostratigraphic analysis. Marine Geology, 285, 29-45, https://doi.org/10.1016/j.margeo.2011.05.001

Moernaut, J., Wiemer, G., Kopf, A., Strasser, M., 2020. Evaluating the sealing potential of young and thin mass-transport deposits: Lake Villarrica, Chile. In: Georgiopoulou, A., Amy, L.A., Benetti, S., Chaytor, J.D., Clare, M.A., Gamboa, D., Haughton, P.D.W., Moernaut, J., Mountjoy, J.J. (Eds) Subaqueous Mass Movements and their Consequences: Advances in Process Understanding, Monitoring and Hazards Assessment. Geological Society, London, Special Publication, 500, 129-146, https://doi.org/10.1144/SP500-2019-155

Mollison, K.C., Power, H.E., Clarke, S.L., Baxter, A.T., Lane, E.M., Hubble, T.C.T., 2020. The sedimentology and tsunamigenic potential of the Byron submarine landslide off New South Wales, Australia. Geological Society, London, Special Publications, 500, 27-40, https://doi.org/10.1144/SP500-2019-160

Moore, R., 1991. The chemical and mineralogical controls upon the residual strength of pure and natural clays. Géotechnique, 41(1), 35-47, https://doi.org/10.1680/geot.1991.41.1.35

Moore, J.G., Clague, D.A., Holcomb, R.T., Lipman, P.W., Normark, W.R., Torresan, M.E., 1989. Prodigious Submarine Landslides on the Hawaiian Ridge. Journal of Geophysical Research, 94(B12), 17,465-17,484, https://doi.org/10.1029/JB094iB12p17465

Morgenstern, N. R., 1967. Submarine slumping and the initiation of turbidity currents. In: Richards, A. F. (Ed), Marine Geotechnique, 189-220. University of Illinois Press, Urbana, Ill.

Mosher, D.C., Piper, D.J.W., 2007. Analysis of multibeam seafloor imagery of the Laurentian Fan and the 1929 Grand Banks landside area. In: Lykousis, V., Sakellariou, D., Locat, J. (Eds.) Submarine Mass Movements and Their Consequences, Advances in Natural and Technological Hazards Research, 27, 77-88. Springer, Dordrecht.

Mulder, T., Cochonat, P., 1996. Classification of offshore mass movements. Journal of Sedimentary Research, 66, 43-57, https://doi.org/10.1306/D42682AC-2B26-11D7-8648000102C1865D

Mumpton, F.A., 1999. La roca magica: Uses of zeolites in agriculture and industry. Proceedings of the National Academy of Sciences of the United States of America, 96(7), 3463-3470, https://doi.org/10.1073/pnas.96.7.3463

Normark, W. R., 1974. Ranger Submarine Slide, Northern Sebastian Vizcaino Bay, Baja California, Mexico. Geological Society of America Bulletin, 85, 781-784, https://doi.org/10.1130/0016-7606(1974)85<781:RSSNSV>2.0.CO;2

Normark, W. R., 1990. Return to Ranger Submarine Slide, Baja California, Mexico. Geo-Marine Letters, 10, 81-91.

O'Leary, D.W., 1991. Structure and morphology of submarine slab slides: Clues to origin and behaviour. Marine Geotechnology, 10(1-2), 53-69, https://doi.org/10.1080/10641199109379882

Osti, G., Franek, P., Forwick, M., Laberg, J.S., 2017. Controlling factors for slope instability in a seismically active region: The NW-Svalbard continental margin. Marine Geology, 390, 131-146, https://doi.org/10.1016/j.margeo.2017.06.005

Paull, C.K., Buelow, W.J., Ussler III, W., Borowski, W.S., 1996. Increased continental-margin slumping frequency during sea-level lowstands above gas hydrate-bearing sediments. Geology, 24, 143-146, https://doi.org/10.1130/0091-7613(1996)024<0143:ICMSFD>2.3.CO;2

Piper, D.J.W., Cochonat, P., Morrison, M.L., 1999. The sequence of events around the epicentre of the 1929 Grand Banks earthquake: initiation of debris flows and turbidity current inferred from sidescan sonar. Sedimentology, 46, 79-97, https://doi.org/10.1046/j.1365-3091.1999.00204.x

Piper, D.J.W., Shor, A.N., Clarke, J.E.H., 1988. The 1929 "Grand Banks" earthquake, slump, and turbidity current. Geological Society of America, Special Paper 229, 77-92, https://doi.org/10.1130/SPE229-p77

Pope, E.L., Talling, P.J., Carter, L., 2017. Which earthquakes trigger damaging submarine mass movements: Insights from a global record of submarine cable breaks?. Marine Geology, 384(1), 131-146, https://doi.org/10.1016/j.margeo.2016.01.009

Prandle, D., 2009. Estuaries. Dynamics, Mixing, Sedimentation and Morphology. Cambridge University Press, New York, US, pp. 248.

Principaud, M., Mulder, T., Hanquiez, V., Ducassou, E., Eberli, G.P., Chabaud, L., Borgomano, J., 2018. Recent morphology and sedimentary processes along the western slope of Great Bahama Bank (Bahamas). Sedimentology, 65, 2088-2116, https://doi.org/10.1111/sed.12458

Principaud, M., Mulder, T., Gillet, H., Borgomano, J., 2015. Large-scale carbonate submarine mass-wasting along the northwestern slope of the Great Bahama Bank (Bahamas): Morphology, architecture, and mechanisms. Sedimentary Geology, 317, 27-42, https://doi.org/10.1016/j.sedgeo.2014.10.008

Prior, D.B., Doyle, E.H., Neurauter, T., 1986. The Currituck Slide, Mid-Atlantic Continental Slope - Revisited. Marine Geology, 73, 25-45, https://doi.org/10.1016/0025-3227(86)90109-X

Puga-Bernabéu, A., Beaman, R.J., Webster, J.M., Thomas, A.L., Jacobsen, G., 2017. Gloria Knolls Slide: A prominent submarine landslide complex on the Great Barrier Reef margin of north-eastern Australia. Marine Geology, 385, 68-83, https://doi.org/10.1016/j.margeo.2016.12.008

Puga-Bernabéu, A., Webster, J.M., Beaman, R.J., Thran, A., López-Cabrera, J., Hinestrosa, G., Daniell, J., 2019. Submarine Landslide Along the Mixed Siliciclastic-Carbonate Margin of the Great Barrier Reef (Offshore Australia). In: Ogata, K., Festa, A., Pini, G.A. (Eds) Submarine Landslides: Subaqueous Mass Transport Deposits from Outcrops to Seismic Profiles. Geophysical Monograph Series, 246, 313-338, https://doi.org/10.1002/9781119500513.ch19

Rack, F.R., Bryant, W.R., Julson, A.P., 1993. Microfabric and Physical Properties of Deep-Sea High Latitude Carbonate Oozes. In: Rezak, R., Lavoie, D.L. (Eds) Carbonate Microfabrics, 129-147. Springer-Verlag, New York.

Rebesco, M., Hernández-Molina, F.J., Van Rooji, D., Wåhlin, A., 2014. Contourites and associated sediments controlled by deep-water circulation processes: State-of-the-art and future considerations. Marine Geology, 352, 111-154, https://doi.org/10.1016/j.margeo.2014.03.011

Riley, C.M., Rose, W.I., Bluth, G.J.S., 2003. Quantitative shape measurements of distal volcanic ash. Journal of Geophysical Research, 108(B10), 2504, https://doi.org/10.1029/2001JB000818

Rise, L., Chand, S., Hjelstuen, B.O., Haflidason, H., Bøe, R., 2010. Late Cenozoic geological development of the south Vøring margin, mid-Norway. Marine and Petroleum Geology, 27, 1789-1803, https://doi.org/10.1016/j.marpetgeo.2010.09.001

Rise, L., Ottesen, D., Longva, O., Solheim, A., Andersen, E.S., Ayers, S., 2006. The Sklinnadjupet slide and its relation to the Elsterian glaciation on the mid-Norwegian margin. Marine and Petroleum Geology, 23, 569-583, https://doi.org/10.1016/j.marpetgeo.2006.05.005

Rodríguez-Ochoa, R., Nadim, F., Hicks, M.A., 2015. Influence of weak layers on seismic stability of submarine slopes. Marine and Petroleum Geology, 65, 247-268, https://doi.org/10.1016/j.marpetgeo.2015.04.007

Rosenqvist, I.TH., 1966. Norwegian Research into the properties of quick clay – A review. Engineering Geology, 1(6), 445-450, https://doi.org/10.1016/0013-7952(66)90020-2

Rovere, M., Gamberi, F., Mercorella, A., Leidi, E., 2014. Geomorphometry of a submarine mass-transport complex and relationships with active faults in a rapidly uplifting margin (Gioia Basin, NE Sicily margin). Marine Geology, 356, 31-43, https://doi.org/10.1016/j.margeo.2013.06.003

Sammartini, M., Camerlenghi, A., Budillon, F., Insinga, D.D., Zugur, F., Conforti, A., Iori, M., Romeo, R., Tonielli, R., 2019. Open-slope, translational submarine landslide in a tectonically active volcanic continental margin (Licosa submarine landslide, southern Tyrrhenian Sea). In: Lintern, D.G., Mosher, D.C., Moscardelli, L. G., Bobrowsky, P.T., Campbell, C., Chaytor, J.D., Clague, J.J., Georgiopoulou, A., Lajeunesse, P., Normandeau, A., Piper, D.J.W., Scherwath, M., Stacey, C., Turmel, D. (Eds) Subaqueous Mass Movements and their Consequences: Assessing Geohazards, Environmental Implications and Economic Significance of Subaqueous Landslides. Geological Society, London, Special Publication, 477,133-150, https://doi.org/10.1144/SP477.34

Sawyer, D.E., Hodelka, B., 2016. Tiny Fossils, Big Impact: The Role of Foraminifera-Enriched Condensed Section in Arresting the Movement of a Large Retrogressive Submarine Landslide in the Gulf of Mexico. In: Lamarche, G., Mountjoy, J., Bull, S., Hubble, T., Krastel, S., Lane, E., Micallef, A., Moscardelli, L., Mueller, C., Pecher, I., Woelz, S. (Eds) Submarine Mass Movements and their Consequences, Advances in Natural and Technological Hazards Research, 41, 479-486. Springer International Publishing Switzerland, Cham.

Schmuck, E.A., Paull, C.K., 1993. Evidence for gas accumulation associated with diapirism and gas hydrates at the head of the Cape Fear Slide. Geo-Marine Letters, 13, 145-152.

Schulten, I., Mosher, D.C., Krastel, S., Piper, D.J.W., Kienast, M., 2019a. Surficial sediment failures due to the 1929 Grand Banks Earthquake, St Pierre Slope. In: Lintern, D.G., Mosher, D.C., Moscardelli, L.G., Bobrowsky, P.T., Campbell, C., Chaytor, J.D., Clague, J.J., Georgiopoulou, A., Lajeunesse, P., Normandeau, A., Piper, D.J.W., Scherwath, M., Stacey, C., Turmel, D. (Eds) Submarine Mass Movements and their Consequences: Assessing Geohazards, Environmental Implications and Economic Significance of Subaqueous Landslide. Geological Society, London, Special Publications, 477, 583-596, https://doi.org/10.1144/SP477.25

Schulten, I., Mosher, D.C., Piper, D.J.W., Krastel, S., 2019b. A Massive Slump on the St. Pierre Slope, A New Perspective on the 1929 Grand Banks Submarine Landslide. Journal of Geophysical Research: Solid Earth, 124, 7538-7561, https://doi.org/10.1029/2018JB017066

Shiwakoti, D.R., Tanaka, H., Tanaka, M., Locat, J., 2002. Influences of diatom microfossils on engineering properties of soils. Soils and Foundations, 42(3), 1-17, https://doi.org/10.3208/sandf.42.3_1

Silver, E., Day, S., Ward, S., Hoffmann, G., Llanes, P., Driscoll, N., Appelgate, B., Saunders, S., 2009. Volcano collapse and tsunami generation in the Bismarck Volcanic Arc, Papua New Guinea. Journal of Volcanology and Geothermal Research, 186, 210-222, https://doi.org/10.1016/j.jvolgeores.2009.06.013

Solheim, A., Berg, K., Forsberg, C.F., Bryn, P., 2005. The Storegga Slide complex: repetitive large scale sliding with similar cause and development. Marine and Petroleum Geology, 22, 97-107, https://doi.org/10.1016/j.marpetgeo.2004.10.013

Spagnoli, G., Finkenzeller, S., Freudenthal, T., Hoekstra, T., Woollard, W., Storteboom, O., van den Berg, A.P., Weixler, L., 2015. First Deployment of the Underwater Drill Rig MeBo200 in the North Sea and its Application for the Geotechnical Exploration. Proceedings of the SPE Offshore Europe Conference & Exhibition in Aberdeen, Scotland, UK, 8-11 May 2015.

Stacey, C.D., Lintern, D.G., Enkin, R.J., 2018. Multifaceted re-analysis of the enigmatic Kitimat slide complex, Canada. Sedimentary Geology, 369: 46-59, https://doi.org/10.1016/j.sedgeo.2018.01.006

Stegmann, S., Kopf, A., 2007. Marine deep-water free-fall CPT measurements for landslide characterisation off Crete, Greece (eastern Mediterranean Sea), Part 1: A new 4000m cone penetrometer. In: Lykouses, V., Sakellariou, D., Locat, J. (Eds) Submarine Mass Movements and Their Consequences, Advances and Natural and Technological Hazards Research, 27, 171-177. Springer, Dordrecht, The Netherlands.

Stegmann, S., Kreiter, S., L'Heureux, JS., Vanneste, M., Völker, D., Baeten, N.J., Knudsen, S., Rise, L., Longva, O., Brendryen, J., Haflidason, H., Chand, S., Mörz, T., Kopf, A., 2016. First Results of the Geotechnical In Situ Investigation for Soil Characterization Along the Upper Slope Off Vesterålen: Northern Norway. In: Lamarche, G., Mountjoy, J., Bull, S., Hubble, T., Krastel, S., Lane, E., Micallef, A., Moscardelli, L., Mueller, C., Pecher, I., Woelz, S (Eds) Submarine Mass Movements and Their Consequences, Advances in Natural and Technological Hazards Research, 41, 211-219. Springer International Publishing Switzerland, Cham.

Stegmann, S., Sultan, N., Kopf, A., Apprioual R., Pelleau, P., 2011. Hydrogeology and its effects on slope stability along the coastal aquifer of Nice, France. Marine Geology, 280, 168-181, https://doi.org/10.1016/j.margeo.2010.12.009

Steiner, A., L'Heureux, JS., Kopf, A., Vanneste, M., Longva, O., Lange, M., Haflidason, H., 2012. An In-Situ Free-Fall Piezocone Penetrometer for Characterizing Soft and Sensitive Clays at Finneidfjord (Northern Norway). In: Yamada, Y., Kawamura, K., Ikehara, K., Ogawa, Y., Urgeles, R., Mosher, D., Chaytor, J., Strasser, M. (Eds.) Submarine Mass Movements and Their Consequences, Advances in Natural and Technological Hazards Research, 31, 99-109. Springer Science+Business Media B.V., Dordrecht.

Strozyk, F., Strasser, M., Förster, A., Kopf, A., Huhn, K., 2010a. Slope failure repetition in active margin environments: Constraints from submarine landslides in the Hellenic fore arc, eastern Mediterranean. Journal of Geophysical Research, 115, B08103, https://doi.org/10.1029/2009JB006841

Strozyk, F., Strasser, M., Krastel, S., Meyer, M., Huhn, K., 2010b. Reconstruction of retreating mass wasting in response to progressive slope steepening of the northeastern Cretan margin, eastern Mediterranean. Marine Geology, 271, 44-54, https://doi.org/10.1016/j.margeo.2010.01.008

Sultan, N., Cochonat, P., Canals, M., Cattaneo, A., Dennielou, B., Haflidason, H., Laberg, J.S., Long, D., Mienert, J., Trincardi, F., Urgeles, R., Vorren, T.O., Wilson, C., 2004. Triggering mechanisms of slope instability processes and sediment failures on continental margins: a geotechnical approach. Marine Geology, 213, 291-321, https://doi.org/10.1016/j.margeo.2004.10.011

Sun, Q., Cartwright, J., Xie, X., Lu, X., Yuan, S., Chen, C., 2018. Reconstruction of repeated Quaternary slope failures in the northern South China Sea. Marine Geology, 401, 17-35, https://doi.org/10.1016/j.margeo.2018.04.009

Sun, Q., Xie, X., Piper, D.J.W., Wu, J., Wu, S., 2017. Three dimensional seismic anatomy of multi-stage mass transport deposits in the Pearl River Mouth Basin, northern China Sae: Their ages and kinematics. Marine Geology, 393, 93-108, https://doi.org/10.1016/j.margeo.2017.05.005

Syvitski, J.P.M., Burrell, D.C., Skei, J.M., 1987. Fjords. Springer-Verlag, New York, US. pp. 215.

Talling, P.J., 2014. On the triggers, resulting flow types and frequencies of subaqueous sediment density flows in different settings. Marine Geology, 352, 155-182, https://doi.org/10.1016/j.margeo.2014.02.006

Talling, P.J., Clare, M., Urlaub, M., Pope, E., Hunt, J.E., Watt, S.F.L., 2014. Large submarine landslides on continental slopes: Geohazards, methane release, and climate change. Oceanography, 27(2), 32-45, http://dx.doi.org/10.5670/oceanog.2014.38

Talling, P.J., Wynn, R.B., Masson, D.G., Frenz, M., Cronin, B.T., Schiebel, R., Akhmetzhanov, A.M., Dallmeier-Tiessen, S., Benetti, S., Weaver, P.P.E., Georgiopoulou, A., Zühlsdorff, C., Amy, L.A., 2007. Onset of submarine debris flow deposition far from original giant landslide. Nature, 450, 541-544.

Tanaka, H., Locat, J., 1999. A microstructural investigation of Osaka Bay clay: the impact of microfossils on its mechanical behaviour. Canadian Geotechnical Journal, 36, 493-508, https://doi.org/10.1139/t99-009

Tanaka, M., Tanaka, H., Kamei, T., Hayashi, S., 2003. Effects of Diatom Microfossil Contents on Engineering Properties of Soils. Proceedings of the Thirteenth International Offshore and Polar Engineering Conference, Honolulu, Hawaii, USA, May 25-30, 2003.

Tappin, D.R., Watts, P., McMurtry, G.M., Lafoy, Y., Matsumoto, T., 2001. The Sissano, Papua New Guinea tsunami of July 1998 – offshore evidence on the source mechanism. Marine Geology, 175(1-4), 1-23, https://doi.org/10.1016/S0025-3227(01)00131-1

ten Brink, U.S., Lee, H.J., Geist, E.L., Twitchell, D., 2009. Assessment of tsunami hazard to the U.S. East Coast using relationships between submarine landslides and earthquakes. Marine Geology, 264(1-2), 65-73, https://doi.org/10.1016/j.margeo.2008.05.011

Thomas, S., Hooper, J., Clare, M., 2010. Constraining Geohazards to the Past: Impact Assessment of Submarine Mass Movements on Seabed Developments. In: Mosher, D.C., Shipp, C., Moscardelli, L., Chaytor, J., Baxter, C., Lee, H., Urgeles, R. (Eds) Submarine Mass Movements and Their Consequences, Advances in Natural and Technological Hazards Research, 28, 387-398. Springer Science+Business Media B.V., Dordrecht.

Thran, A.C., Dutkiewicz, A., Spence, P., Müller, R.D., 2018. Controls on the global distribution of contourite drifts: Insights from an eddy-resolving ocean model. Earth and Planetary Science Letters, 489, 228-240, https://doi.org/10.1016/j.epsl.2018.02.044

Torrance, J.K., 1974. A laboratory investigation of the effect of leaching on the compressibility and shear strength of Norwegian marine clays. Géotechnique, 24(2), 155-173, https://doi.org/10.1680/geot.1974.24.2.155

Torrance, J.K., 1983. Towards a general model of quick clay development. Sedimentology, 30, 547-555, https://doi.org/10.1111/j.1365-3091.1983.tb00692.x

Tournadour, E., Mulder, T, Borgomano, J., Hanquiez, V., Ducassou, E., Gillet, H., 2015. Origin and architecture of a Mass Transport Complex on the northwest slope of Little Bahama Bank (Bahamas): Relations between off-bank transport, bottom current sedimentation and submarine landslides. Sedimentary Geology, 317, 9-26, https://doi.org/10.1016/j.sedgeo.2014.10.003

Trincardi, F., Cattaneo, A., Correggiari, A., Mongardi, S., Breda, A., Asioli, A., 2003. Submarine Slides During Relative Sea Level Rise: Two Examples from the Eastern Tyrrhenian Margin. In: Locat, L., Mienert, J. (Eds) Submarine Mass Movements and Their Consequences, Advances in Natural and Technological Hazards Research, 19, 469-478. Springer Science+Business Media, Dordrecht.

Urgeles, R., Camerlenghi, A., 2013. Submarine landslides of the Mediterranean Sea: Trigger mechanisms, dynamics, and frequency-magnitude distribution. Journal of Geophysical Research: Earth Surface, 118(4), 2600-2618, https://doi.org/10.1002/2013JF002720

Urgeles, R., Lastras, G., Canals, M., Willmott, V., Moreno, A., Casas, D., Baraza, J., Berné, S., 2003. The BIG'95 debris flow and adjacent unfailed sediments in the NW Mediterranean Sea: Geotechnical-sedimentological properties, and dating. In: Locat, J., Mienert, J. (Eds) Submarine Mass Movements and Their Consequences, Advances in Natural and Technological Hazards Research, 19, 479-487. Springer Science+Business Media, Dordrecht.

Urgeles, R., Laynaud, D., Lastras, G., Canals, M., Mienert, J., 2006. Back-analysis and failure mechanisms of a large submarine slide on the ebro slope, NW Mediterranean. Marine Geology, 226, 185-206, https://doi.org/10.1016/j.margeo.2005.10.004

Urlaub, M., Geersen, J., Krastel., S., Schwenk, T., 2018. Diatom ooze: Crucial for the generation of submarine mega-slides?. Geology, 46(4), 331-334, https://doi.org/10.1130/G39892.1

Urlaub, M., Krastel, S., Schwenk, T., 2020. Submarine Landslides in an Upwelling System: Climatically Controlled Preconditioning of the Cap Blanc Slide Complex (Offshore NW Africa). In: Ogata, K., Festa, A., Pini, G.A. (Eds) Submarine Landslides: Subaqueous Mass Transport Deposits from Outcrops to Seismic Profiles, Geophysical Monograph, 246, 299-311, https://doi.org/10.1002/9781119500513.ch18

Urlaub, M., Talling, P.J., Zervos, A., Masson, D., 2015. What causes large submarine landslides on low gradient (<2°) continental slopes with slow (~0.15 m/kyr) sediment accumulation?. Journal of Geophysical Research: Solid Earth, 120, 6722-6739, https://doi.org/10.1002/2015JB012347

Van Daele, M., Meyer, I., Moernaut, J., De Decker, S., Verschuren, D., De Batist, M., 2017. A revised classification and terminology for stacked and amalgamated turbidites in environments dominated by (hemi)pelagic sedimentation. Sedimentary Geology, 357, 72-82, https://doi.org/10.1016/j.sedgeo.2017.06.007

Vanneste, M., Forsberg, C.F., Knudsen, S., Kvalstad, T.J., L'Heureux, JS., Lunee, T., Vardy, M.E., Chand, S., Longva, O., Morgan, E., Kopf, A., Mörz, T., Steiner, A., Brendryen, J., Haflidason, H., 2015. Integration of very-high-resolution seismic and CPTU data from a coastal area affected by shallow landsliding - the Finneidfjord natural laboratory. Frontiers in Offshore Geotechnics III, Chapter 137, International Symposium on Frontiers in Offshore Geotechnics, Oslo, Norway.

Vanneste, M., L'Heureux, JS., Baeten, N., Brendryen, J., Vardy, M.E., Steiner, A., Forsberg, C.F., Kvalstad, T.J., Laberg, J.S., Chand, S., Longva, O., Rise, L., Haflidason, H., Hjelstuen, B.O., Forwick, M., Morgan, E., Lecomte, I., Kopf, A., Vorren, T.O., Reichel, T., 2012. Shallow Landslides and Their Dynamics in Coastal and Deepwater Environments, Norway. In: Yamada, Y., Kawamura, K., Ikehara, K., Ogawa, Y., Urgeles, R., Mosher, D., Chaytor, J., Strasser, M. (Eds) Submarine Mass Movements and Their Consequences, Advances in Natural and Technological Hazards Research, 31, 29-41. Springer Science+Business Media B.V., Dordrecht.

Vanneste, M., Longva, O., L'Heureux, JS., Vardy, M.E., Morgan, E., Forsberg, C.F., Kvalstad, T.J., Strout, J.M., Brendryen, J., Haflidason, H., Lecomte, I., Steiner, A., Kopf, A., Mörz, T., Kreiter, S., 2013. Finneidfjord, a Field Laboratory for Integrated Submarine Slope Stability Assessments and Characterization of Landslide-Prone Sediments: A Review. Offshore Technology Conference, OTC 13OTC-P-686-OTC, Huston, Texas, USA.

Vanneste, M., Mienert, J., Bünz, S., 2006. The Hinlopen Slide: A giant, submarine slope failure on the northern Svalbard margin, Arctic Ocean. Earth and Planetary Science Letters, 245, 373-388, https://doi.org/10.1016/j.epsl.2006.02.045

Vanneste, M., Sultan, N., Garziglia, S., Forsberg, C.F., L'Heureux, JS., 2014. Seafloor instabilities and sediment deformation processes: The need for integrated, multi-disciplinary investigations. Marine Geology, 352, 183-214, https://doi.org/10.1016/j.margeo.2014.01.005

Vardy, M.E, L'Heureux, JS., Vanneste, M., Longva, O., Steiner, A., Forsberg, C.F., Haflidason, H., Brendryen, J., 2012. Multidisciplinary investigation of a shallow near-shore landslide, Finneidfjord, Norway. Near Surface Geophysics, 10, 267-277, https://doi.org/10.3997/1873-2012022

Verdicchio, G., Trincards, F., 2008. Mediterranean shelf-edge muddy contourites: examples from the Gela and South Adriatic basin. Geo-Marine Letters, 28, 137-151.

Volpi, V., Camerlenghi, A., Hillenbrand, CD., Rebesco, M., Ivaldi, R., 2003. Effects of biogenic silica on sediment compaction and slope stability on the Pacific margin of the Antarctic Peninsula. Basin Research, 15, 339-363, https://doi.org/10.1046/j.1365-2117.2003.00210.x

Watt, S.F.L., Talling, P.J., Vardy, M.E., Heller, V., Hühnerbach, V., Urlaub, M., Sarkar, S., Masson, D.G., Henstock, T.J., Minshull, T.A., Paulatto, M., Le Friant, A., Berndt, C., Crutchley, G.J., Karstens, J., Stinton, A.J., Maeno, F., 2012. Combinations of volcanic-flank and seafloor-sediment failure offshore Montserrat, and their implications for tsunami generation. Earth and Planetary Science Letters, 319-320, 228-240, https://doi.org/10.1016/j.epsl.2011.11.032

Watts, A.B., Masson, D.G., 1995. A giant landslide on the north flank of Tenerife, Canary Islands. Journal of Geophysical Research, 100(B12), 21,487-24,498, https://doi.org/10.1029/95JB02630

Webster, J.M., George, N.P.J., Beaman, R.J., Hill, J., Puga-Bernabéu, Á., Hinestrosa, G., Abbey, E.A., Daniell, J.J., 2016. Submarine landslides on the Great Barrier Reef shelf edge and upper slope: A mechanism for generating tsunamis on the north-east Australian coast?. Marine Geology, 371, 120-129, https://doi.org/10.1016/j.margeo.2015.11.008

Wiemer, G., Kopf, A., 2015. Altered marine tephra deposits as potential slope failure planes?. Geo-Marine Letters, 35, 305-314.

Wiemer, G., Kopf, A., 2017a. Influence of diatom microfossils on sediment shear strength and slope stability. Geochemistry, Geophysics, Geosystems, 18, 333-345, https://doi.org/10.1002/2016GC006568

Wiemer, G., Kopf, A., 2017b. On the role of volcanic ash deposits as preferential submarine slope failure planes. Landslides, 14, 223-232.

Wilson, C.K., Long, D., Bulat, J., 2003. The Afen Slide - A Multistaged Slope Failure in the Faroe-Shetland Channel. In: Locat, J., Mienert, J. (Eds) Submarine Mass Movements and Their Consequences, Advances in Natural and Technological Hazards Research, 19, 317-324. Springer Science+Business Media, Dordrecht.

Wilson, C.K., Long, D., Bulat, J., 2004. The morphology, setting and processes of the Afen Slide. Marine Geology, 213, 149-167, https://doi.org/10.1016/j.margeo.2004.10.005

Winkelmann, D., Geissler, W., Schneider, J., Stein, R., 2008. Dynamics and timing of the Hinlopen/Yermak Megaslide north of Spitsbergen, Arctic Ocean. Marine Geology, 250, 34-50, https://doi.org/10.1016/j.margeo.2007.11.013

Winkelmann, D., Jokat, W., Niessen, F., Stein, R., Winkler, A., 2006. Age and extent of the Yermak Slide north of Spitsbergen, Arctic Ocean. Geochemistry, Geophysics, Geosystems, 7(6), Q06007, https://doi.org/10.1029/2005GC001130

Winkelmann, D., Stein, R., 2007. Triggering of the Hinlopen/Yermak Megaslide in relation to paleoceanography and climate history of the continental margin north of Spitsbergen. Geochemistry, Geophysics, Geosystems, 8(6), Q06018, https://doi.org/10.1029/2006GC001485

3. Manuscript II

A multi-disciplinary investigation of the AFEN Slide: The relationship between contourites and submarine landslides

R. Gatter, M.A. Clare, J.E. Hunt, M. Watts, B.N. Madhusudhan, P.J. Talling, K. Huhn

Published as:

Gatter, R., Clare, M.A., Hunt, J.E., Watts, M., Madhusudhan, B.N., Talling, P.J., Huhn, K., 2020. A multi-disciplinary investigation of the AFEN Slide: The relationship between contourites and submarine landslides. *Geological Society, London, Special Publications*, 500, 173-193, https://doi.org/10.1144/SP500-2019-184

Abstract

Contourite drifts are sediment deposits formed by ocean bottom currents on continental slopes worldwide. Although it has become increasingly apparent that contourites are often prone to slope failure, the physical controls on slope instability remain unclear. This study presents high-resolution sedimentological, geochemical and geotechnical analyses of sediments to better understand the physical controls on slope failure that occurred within a sheeted contourite drift within the Faroe-Shetland Channel. We aim to identify and characterise the failure plane of the late Quaternary landslide (the AFEN Slide), and explain its location within the sheeted drift stratigraphy. The analyses reveal abrupt lithological contrasts characterised by distinct changes in physical, geochemical and geotechnical properties. Our findings indicate that the AFEN Slide likely initiated along a distinct lithological interface, between overlying sandy contouritic sediments and softer underlying mud-rich sediments. These lithological contrasts are interpreted to relate to climatically-controlled variations in sediment input and bottom current intensity. Similar lithological contrasts are likely to be common within contourite drifts at many other oceanic gateways worldwide; hence our findings are likely to apply more widely. As we demonstrate here, recognition of such contrasts requires multi-disciplinary data over the depth range of stratigraphy that is potentially prone to slope failure.

3.1. Introduction

Thermohaline-driven ocean bottom currents create sedimentary accumulations called contourites that are found along the world's continental margins (e.g. McCave and Tucholke, 1986; Rebesco and Stow 2001; Stow et al., 2002). Contourites can cover extremely large areas (from <100 km^2 to >100,000 km^2), forming a variety of depositional geometries that include elongated, mounded, sheeted, channelized and mixed drift systems (Faugères et al., 1999; Rebesco and Stow, 2001; Stow et al., 2002; Faugères and Stow, 2008). It has become increasingly apparent that contourite drifts are prone to slope instability (Laberg and Camerlenghi, 2008), with submarine landslides recognised in a wide range of locations affected by bottom currents (Tab. 3.1).

Table 3.1 Examples of submarine landslides in contourites. Slide volume, seabed gradient and sediment accumulation rate are given where available. Main controls of slope failure are listed where they are known or discussed in the literature.

Slide name	Location	Setting	Slide volume (km^3)	Seabed gradient (°)	Sediment accumulation rate (cm/ka)	Drift type	Main control	References
Hinlopen-Yermak Slide	Northern Svalbard margin, Arctic Ocean	Northern high-latitudes	1200 to 1350	<0.5		?	Lithological and geotechnical contrasts	Vanneste et al. (2006); Winkelmann et al. (2008)
Fram Slide Complex	Offshore northwest Svalbard, Arctic Ocean	Northern high-latitudes	~1470 (17 failures)	~1.5 to 4.5	3 to 19	Plastered drift	Toe erosion, morphology	Mattingsdal et al. (2014); Elger et al. (2017)
-	Lofoten Islands, offshore Norway, Norwegian Sea	Northern high-latitudes	<1 to 8.7 (individual landslides)	4 to 1	Up to 4	Mounded, elongated drift (Lofoten drift)	Under-cutting	Laberg et al. (2001); Baeten et al. (2013, 2014)
Trænadjupet Slide	Offshore Norway, Norwegian Sea	Northern high-latitudes	~900	2.3 to 0.6	Up to 65	Mounded, elongated drift (Nyk drift)	Weak layer	Laberg and Vorren (2000); Laberg et al. (2001, 2002, 2003)
Nyk Slide	Offshore Norway, Norwegian Sea	Northern high-latitudes			Up to 1.2	Mounded, elongated drift (Nyk drift)	Weak layer	Laberg et al. (2001, 2002); Lindberg et al. (2004)
Sklinnadjuped Slide	Offshore Norway, Norwegian Sea	Northern high-latitudes			Up to 0.5	Infilling drift (Sklinnadjuped drift)	Weak layer (?)	Laberg et al. (2001); Dahlgren et al. (2002)
Storegga Slide	Offshore Norway, Norwegian Sea	Northern high-latitudes	2400 to 3200	0.5 to 1.0		Mounded, elongated drift	Sensitive clay layer	Bryn et al. (2005a, b); Haflidason et al. (2005); Kvalstad et al. (2005)

Tampen Slide	Offshore Norway, Norwegian Sea	Northern high-latitudes				Mounded elongated drift (?)		Evans et al. (2005); Solheim et al. (2005)
Northern Faroe Slide Complex	Faroe Islands, offshore UK, Norwegian Sea	Northern high-latitudes			14 to 30	Mounded, elongated drift (Faroe drift)		Rasmussen et al. (1996, 1998); Van Weering et al. (1998); Kuijpers et al. (2001); Long et al. (2004)
AFEN Slide	Offshore UK, Faroe-Shetland Channel	Northern high-latitudes	~0.153 (all phases)	1 to 3	Up to 10	Sheeted to mounded drift (West Shetland drift)	Sandy layer (?)	Knutz and Cartwright (2004); Wilson et al. (2004)
Rockall Bank Slide Complex	Offshore Ireland, Rockall Trough	Northern high-latitudes	265 to 765	5 to 10	5 to 17.1	Elongated, mounded drift (Feni drift)	Weak layers	Van Weering and Rijk (1991); Faugères et al. (1999); Georgiopoulou et al. (2013, 2019)
-	Offshore eastern Canada, North Atlantic	Northern mid-latitudes				Plastered drift (?)		Piper (2005)
-	Grand Banks, offshore eastern Canada, North Atlantic	Northern mid-latitudes		2	Up to 50	Plastered drift	Lithological and geotechnical contrasts	Rashid et al. (2017)
-	Pianosa Ridge, Mediterranean Sea	Northern mid-latitudes		3 to 10 (locally 20)	13	Plastered drift	Over-steepening	Miramontes et al. (2016, 2018)
-	Gela and south Adriatic Basin, Mediterranean Sea	Northern mid-latitudes	0.1 to 0.2 (individual mass transport deposits)	~3	22.5	Elongated and separated drifts	Mechanical boundary, clay layer	Minisini et al. (2007); Verdicchio and Trincardi (2008)

-	SW Mallorca Island, Mediterranean Sea	Northern mid-latitudes		1.3 to 2.9	5.8 (?)	Mounded, elongated drifts		Lüdmann et al. (2008)
-	Alboran Sea, Mediterranean Sea	Northern mid-latitudes				Contourite dispositional system		Ercilla et al. (2016)
-	Levant Basin, Mediterranean Sea	Northern mid-latitudes	Generally <1 (individual landslides)	>4	25 to 130	Plastered drift	Over-steepening	Katz et al. (2015); Hübscher et al. (2016)
-	Bahamas Bank	Norther low-latitudes	2 to 20 (individual landslides)	~3		Plastered drift	Stratigraphic control (?)	Mulder et al. (2011); Principaud et al. (2015); Tournadour et al. (2015)
-	Offshore Uruguay	Southern mid-latitudes	<2 (individual landslides)	1-3	8 to 18	Contourite depositional system	Lithological control	Henkel et al. (2011); Krastel et al. (2011); Ai et al. (2014); Hernández-Molina et al. (2016)
-	Offshore Argentina	Southern mid-latitudes		3 to 7	Up to 1.6	Contourite depositional system	Lithological control; over-steepening	Hernández-Molina et al. (2009); Ai et al. (2014); Krastel et al. (2011); Preu et al. (2013)
-	Offshore Antarctic Peninsula, Pacific Ocean	Southern low-latitudes		2 to 3	Decrease from 18 to ~8	Mounded drifts	Under-cutting; weak layer	Iwai et al. (2002); Volpi et al. (2003, 2011)

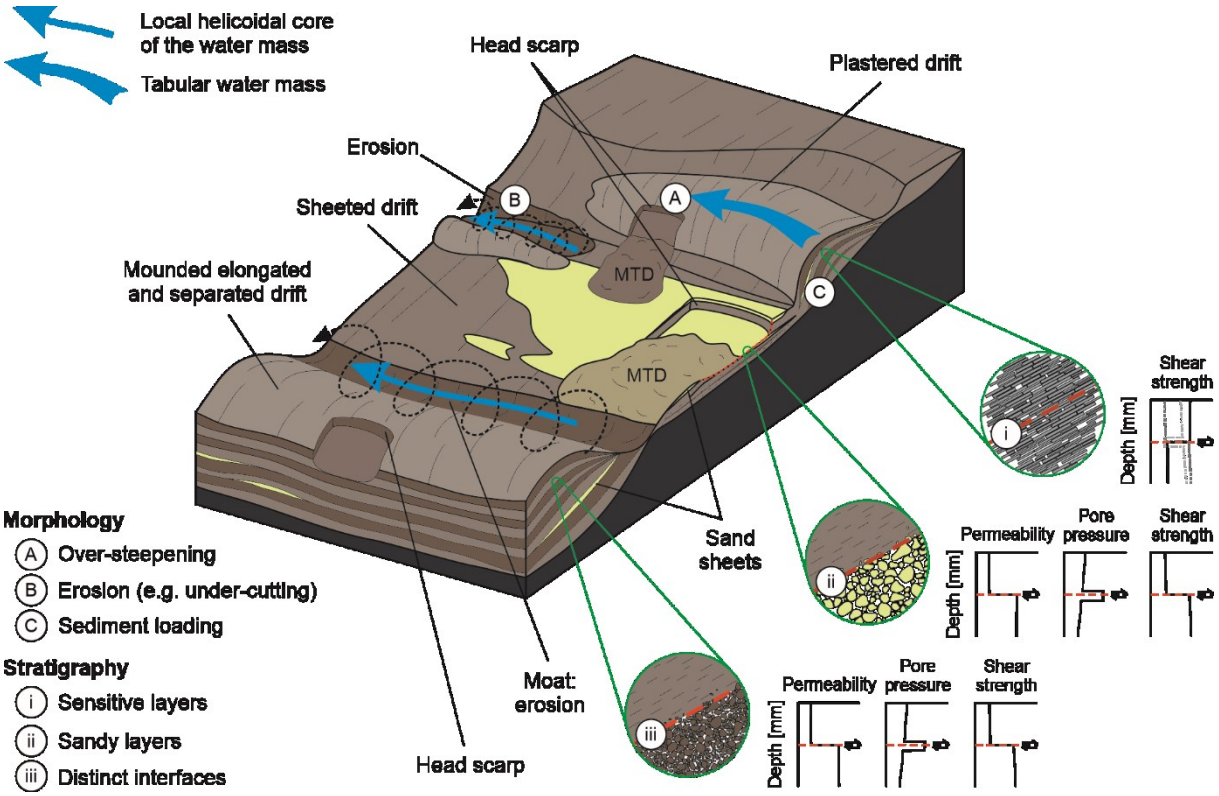

Figure 3.1. Key characteristics of contourites that favour the formation of submarine landslides. Morphological controls: A – over-steepening, B – erosion, C – sediment loading; stratigraphic controls: i – laterally extensive sensitive clay layers that are prone to sudden strength loss, possible shear strength depth profiles are shown as black; dark grey, dashed and light grey, dotted lines; ii – thick accumulation of sandy layers which can accommodate excess pore pressure due to high sedimentation rates; iii – distinct lithological and/or geotechnical interfaces. Contourite depositional system adopted from Hernández-Molina et al. (2008).

The affinity of contourite drifts for slope failure can be linked in part to deposit morphology (Fig. 3.1, Tab. 3.1). In some locations, contour-parallel currents modify the continental slope profile, creating mounded accumulations of sediment which are thicker and steeper than those on slopes unaffected by bottom currents (Laberg and Camerlenghi, 2008; Rebesco et al., 2014). Factors such as sediment supply, intensity and location of currents, and sea level and climatic changes control the presence or absence, location, growth and morphology of contourites (Faugères and Stow, 2008; Rebesco et al., 2014). A number of compound morphological effects have been implicated as pre-conditioning and/or triggering mechanisms for slope instability, which include: slope over-steepening due to rapid sediment accumulation (A, Fig. 3.1) or due to erosion by vigorous along-slope currents (B, Fig. 3.1), and loading resulting from differential sediment accumulation (C, Fig. 3.1). These effects occur particularly where contourites form as mounded accumulations (Laberg and Camerlenghi, 2008; Prieto et al., 2016;

Miramontes et al., 2018). However, submarine landslides, some of which include the largest on our planet (e.g. Storegga; Bryn et al., 2005a), often occur within contourite drifts with very low angle (<2°) slopes (e.g. Hühnerbach et al., 2004). Another explanation for slope instability in contourite drifts, therefore, relates to specific compositional and geotechnical properties of contourites (Fig. 3.1, Tab. 3.1; Lindberg et al., 2004; Kvalstad et al., 2005). Plausible controls include prominent layers within the slope stratigraphy (Fig. 3.1) which may feature a lower peak or post-peak shear strength than over- and underlying strata, such as i) laterally extensive (sometimes centimetre-thin) homogeneous layers of weaker, sensitive material which is prone to sudden strength loss (e.g. sensitive clay in the Storegga Slide, Norway – Kvalstad et al., 2005; sensitive zeolite layer in the N Tyrrhenian Sea – Miramontes et al., 2018), or ii) thick accumulations of sandy material which is characterised by high sedimentation rates, promoting excess pore pressure (Laberg and Camerlenghi, 2008; Ai et al., 2014). Another plausible control relates to lithological and/or geotechnical contrasts within a depositional sequence that may result from rapid changes in current regime, sediment input or type (e.g. Rashid et al., 2017; iii, Fig. 3.1).

Detailed sedimentological and geotechnical studies of landslides within contourites are scarce (Baeten et al., 2013; Miramontes et al., 2018), and there is still much uncertainty as to which specific aspects act as the dominant control on slope instability. Many studies rely solely upon remote geophysical data for landslide characterisation, and if sediment cores are acquired, they typically do not penetrate to the failure plane (which may be tens to hundreds of metres below the seafloor; Talling et al., 2014). Such cores also tend to focus on characterisation of the failed landslide mass, rather than targeting sediments from adjacent undisturbed slopes. Targeting the undisturbed sediments of the adjacent slopes, including those stratigraphically equivalent to the failure plane of the landslide, however, is necessary in order to identify and characterise the material along which the landslide initiated, as these are usually removed or remoulded during failure. It is of critical importance to be able to identify sediments, which are prone to failure in order to perform reliable slope stability assessments (L'Heureux et al., 2012; Vardy et al., 2012).

3.1.1. Aims

Here, we present a detailed characterisation of a bedding-parallel, cohesive submarine landslide (called the AFEN Slide) that occurred within a low angle (<2.5°) laterally extensive sheeted contourite drift, based on physical, geochemical, sedimentological and geotechnical analyses. We focus on a core targeted to sample the pre-landslide sedimentary sequence, including sediments that correlate stratigraphically with the failure plane located further upslope. Based on centimetre-resolution characterisation of these deposits we address the following questions. First, what is the nature of the

undisturbed sediment and do material heterogeneities explain the location of the failure plane? As many aspects of cohesive landslides appear to be scale invariant, this study of a relatively small landslide may provide key insights into our understanding of much larger ones (Micallef et al., 2008; Chaytor et al., 2009; Baeten et al., 2013; Casas et al., 2016; Clare et al., 2018). Second, what causes the observed heterogeneities within the stratigraphy? We explore how climatic changes and ocean circulation may play a key role in governing not just the failure plane depth, but also influence the timing of slope failure. Finally, we discuss the implications of climatically-controlled sediment supply and deep ocean circulation for pre-conditioning slope instability in contourite depositional systems in oceanic gateways, which are narrow, deep passages connecting two adjacent basins, elsewhere in the world.

3.2. Background

3.2.1. Regional setting

3.2.1.1. Geological and morphological setting

The study area lies on the eastern flank of the Faroe-Shetland Channel, which is located north of Scotland, extending over 400 km between the Wyville-Thomson Ridge and the Norwegian Basin (Fig. 3.2). The Faroe-Shetland Channel is a narrow basin, measuring 250 km at its widest in the northeast and less than 130 km in the southwest. The channel closely follows the trend of the regional NE-SW structural lineaments, and one of the NW-SE transfer zones (Victory Transfer Zone) passes close to the study area (Rumph et al., 1993; Wilson et al., 2004). The Faroe-Shetland channel is the present-day expression of the Faroe-Shetland Basin that can be dated back to the Late Palaeozoic (e.g. Rumph et al., 1993). Basin formation was probably initiated during the Devonian, while the main rift phase occurred during Cretaceous times (Dean et al., 1999; Roberts et al., 1999). Although extension is thought to have continued in places until the early to mid-Palaeocene (Smallwood and Gill, 2002), more or less continuous post-rift subsidence predominated throughout the Cenozoic (Turner and Scrutton, 1993). This subsidence was interrupted at various stages by contractional deformation (Ritchie et al., 2003; Johnson et al., 2005; Stoker et al., 2005; Ritchie et al., 2008) and regional uplift and tilting (Andersen et al, 2000; Smallwood and Gill, 2002; Stoker et al, 2002; Stoker et al., 2005). Following Late Palaeocene uplift, the Faroe-Shetland Channel has subsided about 2000 m, with present-day water depths of 1700 m in the north-east and 1000 m in the south-west, and slope angles between 1° and 3° flanking the eastern channel margin (Stoker et al., 1998; Andersen et al., 2000; Smallwood and Gill, 2002). The channel forms an important oceanic gateway, exchanging water masses between the North Atlantic and the Norwegian Sea (Broecker and Denton, 1990; Rahmstorf, 2002) since at least the Early Oligocene (Davies et al., 2001).

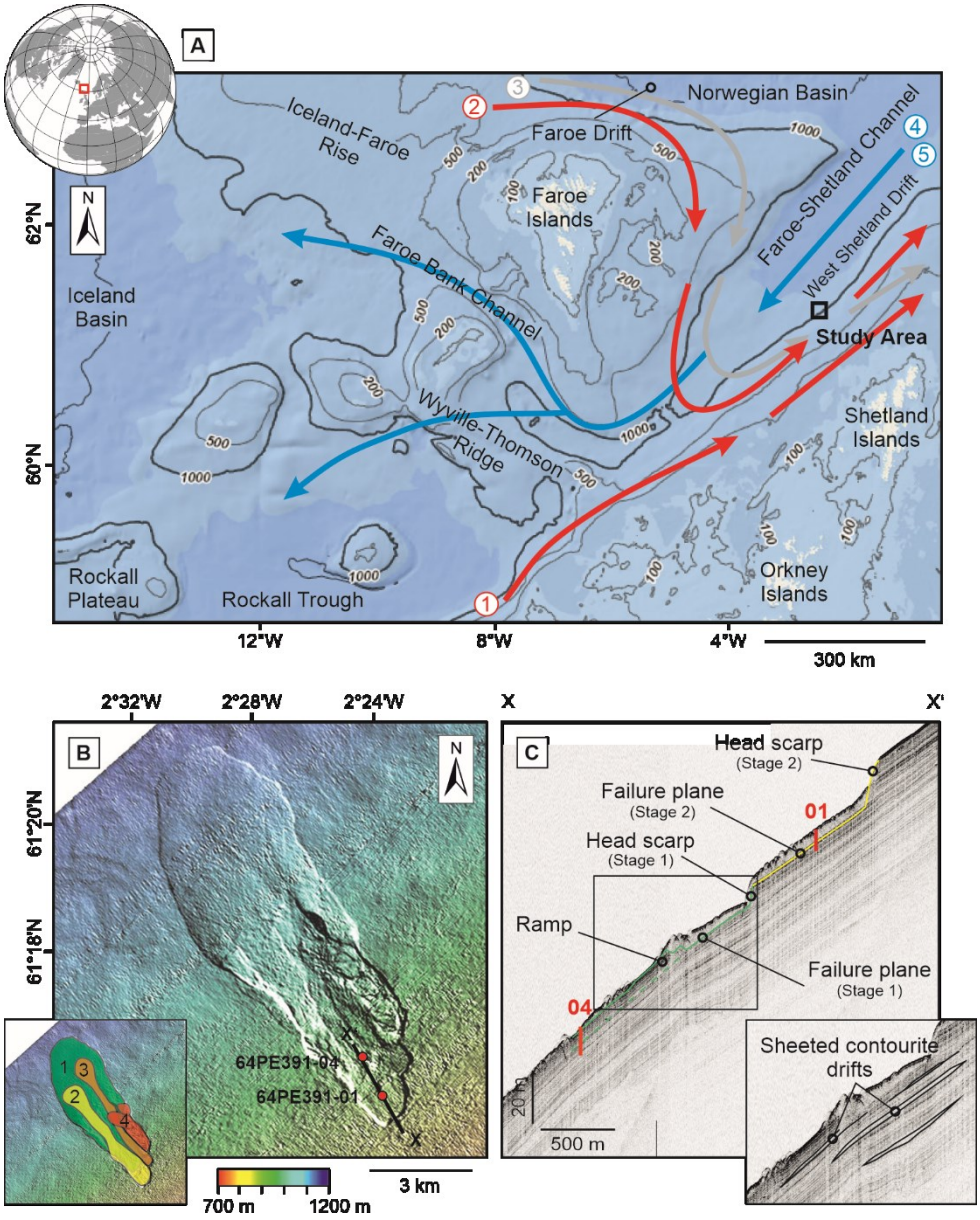

Figure 3.2. (**A**) Schematic diagram of current regime in and around the Faroe-Shetland Channel. Arrows indicate the five main water masses: red 1 – North Atlantic Water; red 2 – Modified North Atlantic Water; grey 3 – Arctic Intermediate Water; blue 4 – Norwegian Sea Arctic Intermediate Water; blue 5 – Faroe-Shetland Channel Bottom Water (after Turrell et al., 1999). Study area is outlined with a black rectangle. (**B**) Outline of the AFEN Slide, showing piston core 64PE391-01 (61°15'40.679"N, 02°23'42.899"W; Madhusudhan et al., 2017) and Core 64PE391-04 (61°16'17.651"N, 02°24'21.959"W) as red circles. Black line illustrates the seismic line shown in C. Inset image shows the four stages of the failure as interpreted by Wilson et al. (2004). Modified from Madhusudhan et al. (2017) (**C**) Seismic line across the AFEN Slide showing piston core 01 and 04. Insert image illustrates the distribution of sheeted contourite drifts in the area (after Wilson et al., 2004).

3.2.1.2. Oceanography and palaeoceanography

In general, the present-day oceanography in the Faroe-Shetland Channel consists of warm surface water moving towards the northeast, and cold bottom water, generating relatively strong, erosive bottom currents (with velocities in the range between <0.3 and >1.0 m/s; Masson et al., 2004), moving towards the southwest (Fig. 3.2A; Saunders, 1990; Turrell et al., 1999; Rasmussen et al., 2002). Five distinct water masses can be recognised based on their salinity and temperature characteristics (Turrell et al., 1999). Two distinct, surface water masses transport warm water from the North Atlantic into the channel. North Atlantic Water (NAW) flows northward from the Rockall Trough (Turrell et al., 1999), while Modified North Atlantic Water (MNAW) flows clockwise around the Faroe Islands before turning northward in the Faroe-Shetland Channel (Saunders, 1990). These surface waters typically occupy the upper 200-400 m of the water column (Turrell et al., 1999). Arctic Intermediate Water (AIW) flows anticlockwise along the southern edge of the Norwegian Basin and around the Faroe-Shetland Channel, typically between 400 m and 600 m water depth (Blindheim, 1990). At the base of the channel (usually below 600 m water depth), the Norwegian Sea Arctic Intermediate Water (NSAIW) and the Faroe-Shetland Channel Bottom Water (FSCBW) are funnelled along the Faroe-Shetland Channel towards the south (Turrell et al., 1999) and flow along the Faroe Bank Channel into the Atlantic (Saunders, 1990). A small portion of the cold bottom water flows across the western end of the Wyville-Thomson Ridge south into the Rockall Trough (Stow and Holbrook, 1984). The velocity of these water masses is variable, both across the channel and over time. Average along slope velocities, mainly directed northeast of around 0.2 to 0.25 m/s were measured at around 500 to 700 m water depth (Van Raaphorst et al., 2001; Bonnin et al., 2002) and velocities over >1.0 m/s associated with southwest-directed bottom currents were inferred from observed bedforms (Masson et al., 2004). Periodical changes in salinity and temperature cause shifts of the boundaries between water masses on timescales from decades to hours (Turrell et al., 1999). Since the Last Glacial Maximum (LGM), when bottom and surface currents were weak, eight distinct changes in surface and bottom current regime were identified, which are related to the changes in climatic conditions (Rasmussen et al., 2002). Climatic and palaeoceanographic changes also reportedly caused strong cyclical variation in sediment accumulation (with up to 30 cm/ka along the Faroe Drift and up to 10 cm/ka along the West Shetland Drift; Rasmussen et al., 1996, 1998; Knutz and Cartwright, 2004; Nielsen et al., 2007).

3.2.1.3. Contourite deposits in the Faroe-Shetland Channel

The regional oceanography has controlled the depositional architecture of the slope sediments, creating elongated mounded contourite drifts at the base of the slope (to the northeast of the AFEN Slide) and sheeted contourite drifts in the slide area (Long et al., 2004; Hohbein and Cartwright, 2006). These

sheeted drifts are characterised by parallel, laterally continuous reflectors on seismic profiles (Masson, 2001). These reflectors can be traced over more than 50 km below the sea floor of the Faroe-Shetland Channel, which emphasises the regional scale of bottom current activity and sheeted contourite drift accumulation (Stoker et al, 1998).

3.2.2. The AFEN Slide

The AFEN Slide was first identified in 1996, during an environmental survey for the Atlantic Frontiers Environmental Network in the region (Wilson et al., 2004). The slide is interpreted as a four-stage retrogressive landslide that occurred northwest of the Shetland Islands (UK) at water depths of 830 m to 1120 m on a slope varying from approximately 0.7° to about 2.5° (Wilson et al., 2004; Fig. 3.2B). The total length from the head scarp to the toe of the lobe is over 12 km, and the maximum width is around 4.5 km. The slide involved ~200 x 10^6 m^3 of sediment and the slide debris has a maximum thickness of 20 m, averaging between 5 m to 10 m (Wilson et al., 2004). Radiocarbon dating and biostratigraphy from the slide suggest that the first stage took place around 16 to 13 ka BP and the later retrogressive phases after 5.8 ka BP and prior to 2.8 ka BP (Wilson et al., 2004). Initial studies, based on high-resolution seismic data and cores, which did not penetrate the base of the slide, inferred that the failure plane comprised well-sorted contourite sands, which may liquefy during an earthquake (e.g. 10 000-year return period earthquake; Jackson et al., 2004). This hypothesis was supported by the presence of a buried slide, which appears to have occurred under similar physiographic conditions (Masson, 2001; Wilson et al., 2004). Such well-sorted contourite sands were not found by Madhusudhan et al. (2017), who analysed a new sediment core (64PE391-01) that penetrated through the full extent of the deposits from the second stage of the landslide (Fig. 3.2C). Instead, they proposed progressive failure of geotechnically-sensitive clays or liquefaction of silt layers. None of these previous cores sampled undisturbed material that corresponds stratigraphically with the failure plane.

3.3. Data and methods

Core 64PE391-04, which is the focus of this present study, was obtained during the RV Pelagia cruise 64PE391 in 2014 using a piston corer. The core was sampled within the AFEN Slide area, at a water depth of 945 m. It was targeted to sample undisturbed sediments, i.e. those characterised on seismic data by continuous reflectors and avoiding acoustically transparent, chaotic or disrupted seismic units and areas of hummocky seafloor texture likely indicative of slope failure (Shipp et al., 2011; Fig. 3.2). Fig. 3.2 shows the location of core 64PE391-04 on the deep tow boomer seismic profile, which has a maximum theoretical vertical resolution of 0.5 m, with a penetration of 100 ms, and was obtained from the BGS 00/02 survey (Wilson et al., 2005). The core recovered 11.49 m of sediment in a 15 m core

barrel and was stored in the refrigerated storage at the British Ocean Sediment Core Facility (BOSCORF), UK, prior to study.

3.3.1. Physical properties analysis

A Geotek MSCL-S (Standard) multi-sensor core logger, based at BOSCORF, was used to measure P-wave velocity, gamma-ray bulk density, electrical resistivity, magnetic susceptibility, and fractional porosity which is derived from the measured sediment density at 1 cm intervals on split cores. MSCL is a commonly used, non-destructive tool that allows the recognition of subtle changes in sediment physical properties. The data is commonly used for correlation between cores, and calibration of seismic data using P-wave velocity. Density serves as an effective proxy for changes in sediment lithology and is used for the calculation of fractional porosity (Gunn and Best, 1998). Core images were obtained using the BOSCORF Geotek MSCL-CIS (Core Imaging System), which enables the acquisition of precise depth-registered images that can be correlated with the other datasets.

3.3.2. Geochemical analysis

XRF (X-ray fluorescence) core scanning was used to determine the geochemical composition of the sediment (ITRAX™ COX Ltd. at BOSCORF; Croudace et al., 2006) at a spatial resolution of 1 cm. ITRAX scanning is a useful, rapid, non-destructive, high-resolution scanning technique which is widely used in earth and environmental sciences (Croudace and Rothwell, 2015). This method enables the measurement of element intensities, such as Ca and Sr, which correlate well with the carbonate content, or Fe, Ti and K which are related to the siliciclastic components, and vary directly with the terrigenous sediment input (e.g. Röhl and Abrams, 2000; Hepp et al., 2006). ITRAX data represents a semi-quantitative analysis of the relative element abundances downcore. Data is expressed as counts per second (cps), and are presented as log ratios which are accepted as a more accurate estimation of element concentrations. In addition, all XRF data is shown as log ratios of two elements, in order to show element concentrations more accurately and minimise matrix effects inherent to XRF (Weltje and Tjallingii, 2008). Ca/Sr, Ca/Fe and Fe/K have been selected, as these element ratios have been shown to reflect changes in sea level and temperature, sediment supply, and have been applied in climate studies (see Croudace and Rothwell, 2015). In addition to geochemical composition, the ITRAX instrument provided X-radiographs. X-radiographs are digital images of the internal structure and physical property changes within a split core section that are obtained using optical and radiographic line cameras.

3.3.3. Particle size distribution

Particle size analysis was carried out at 10 cm depth intervals for sediments of Unit 2, 3 and 4 (see results for definition), following the procedures in Rothwell et al. (2006). The sediment was sieved to remove particles larger than 2 mm before the sample was dispersed in a 1 litre mixing chamber by shaking it for 24 hours. The dispersed sediment was circulated through a Malvern Mastersizer 3000 for 120 seconds over which time 12 measurements are taken and then averaged to obtain the particle size distribution.

3.3.4. Geotechnical analyses

Water content and fall cone measurements were carried out at 10 cm intervals (BSI, 1990; BSI, 2004). Measurements of water content could be used as a first order approximation of the sediment's shear strength and compressibility (i.e. higher water content is related to poor shear strength and compressibility). An 80 g 30° fall cone was used on the split cores, regardless of the particle size and whether the tested material was considered to be saturated or not. The undrained shear strength was calculated from the fall cone measurements assuming all tests were carried out on saturated clays. Subsamples were taken for subsequent direct shear and oedometric tests.

3.3.4.1. Static, drained shear test

Direct shear experiments were carried out to compare the drained shear strength of prominent layers, identified from down-core logging, particle size distribution and standard geotechnical data. Cylindrical, undisturbed samples (~5 cm^2, 2.5 cm height) of intact samples were placed in the shear apparatus and consolidated via a vertical ram to in-situ normal stress (σ_n). The sample was consolidated until the sample height was constant (or min. 24 hours), so that the sample is assumed to be fully drained and the applied σ_n is approximately equal to the effective normal stress (σ'_n). The effective normal stress is the difference between the normal stress and the pore water pressure ($\sigma'_n = \sigma_n - u$; Terzaghi, 1925). Shearing occurs on a predefined plane, perpendicular to the vertical ram that exerts the normal stress. The shear displacement for each experiment was 9.5 mm at a shear rate of 0.008 mm/min. This shear rate is slow enough to allow constant drainage during shearing (Deutsches Institut für Normung, 2002). Samples were taken from around 7 m core depth, which corresponds to around 18 m below sea floor (assuming around 10 m of sediment was removed during the failure). The samples were sheared at a normal stress 170 kPa, simulating the effective hydrostatic vertical overburden stress (σ'_{v0}) acting at around 18 m below sea floor (m b.s.f.) assuming an average sediment effective unit weight (γ') of 9.5 kN/m^3.

3.3.4.2. Oedometer test

One-dimension consolidation tests were performed on selected undisturbed core samples (~20 cm^2, 1.9 cm height) in order to measure and compare their permeability and consolidation parameters. The measured initial porosity, coefficient of compression (c_v) and permeability (k) can be used to make assumptions regarding the sediments' potential to build excess pore pressure. Incremental loading and unloading of 1 kPa to 7100 kPa stress were applied onto the sediment and the resulting displacement (change in volume) was measured. Each load was applied gradually and left until the displacement stabilised or primary consolidation was completed. Consolidation and permeability parameters were calculated from the settlement characteristics of the sediment using standard equations (Powrie, 2013).

3.3.5. Data analysis

Physical and geochemical properties were compared using non-parametric tests that compare two unpaired groups of data and compute p values testing the null hypothesis of two groups having the same distribution. The data was analysed for the discrepancy between the mean ranks of two groups (Mann-Whitney test) and for their varying cumulative distribution (Kolmogorov-Smirnov test) (Sheskin, 2011). The significance level for both tests was set to 0.05 (Fisher, 1926).

3.4. Results

Piston core 64PE391-04 was obtained about 750 m down-slope from where the sediment ramped up the failure plane onto the seabed (failure Stage 1, Wilson et al, 2004; Fig. 3.2C). The deep-tow boomer reflection seismic data indicate that the core penetrated pre-landslide sediments, including those stratigraphically equivalent to the failure plane of the slide. Based on the newly obtained data, we identify five main lithological units within the sediment core, which we now characterise using results from visual sediment core logging, particle size distribution, X-ray scanning, and continuous physical properties (MSCL) and geochemical (XRF) measurements (see summary in Fig. 3.3 and 3.4). In addition, we present a geotechnical characterisation of the recovered sediment based on water content and fall cone analyses, as well as direct shear (DS) and oedometer tests.

Visual sedimentary logging and particle size analysis indicate that the general lithology is bioturbated silty clay to clayey silt with a number of sandy silt and silty sand layers; consistent with previous analysis of sediment cores from the area (Madhusudhan et al., 2017). Sandy layers are only found in the upper part of the core (above 7.3 m depth). The lithology in the lower part of the core is generally homogenous with an absence of sand.

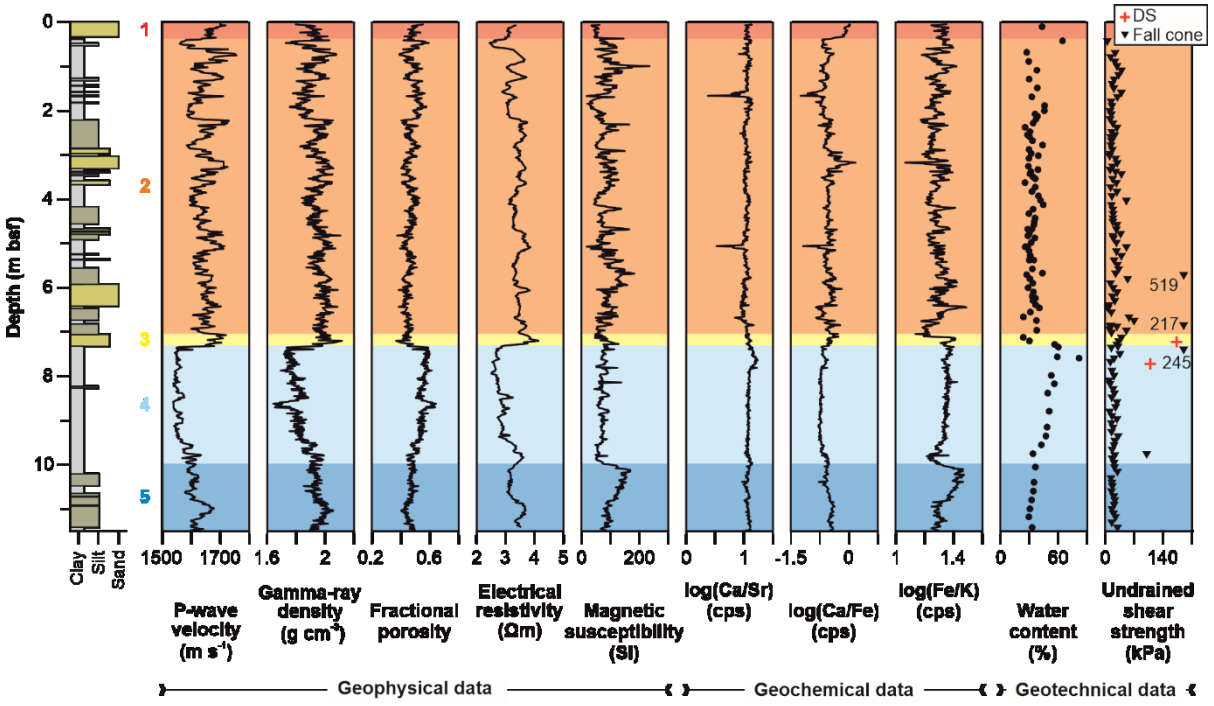

Figure 3.3. Summary of sediment core analyses (64PE391-04), including visual sedimentary, physical properties (multi-sensor core logging) and geochemical (ITRAX XRF) core log data, and geotechnical data (water content, drained and undrained shear strength). Unit 1 to 5 are outlined.

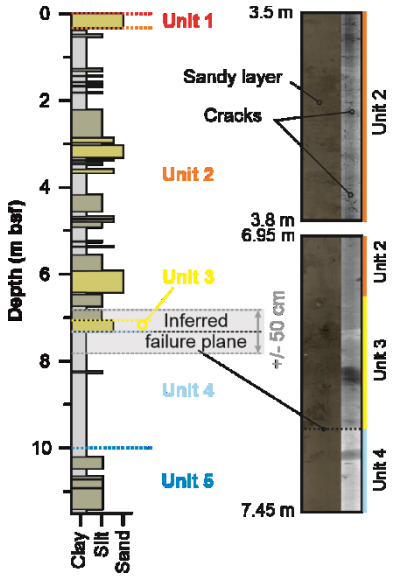

Figure 3.4. Inferred location of the main failure plane based on down-core logging and deep-tow boomer reflection seismic data. Unit 1 to 5 are outlined. Vertical error in failure plane delineation, resulting from the vertical resolution of the seismic data is indicated by grey lines (+/- 50 cm from the inferred failure plane). Core images and x-radiographs from the inferred failure plane, and cracks in Unit 2 are also shown.

3.4.1. Multi-Sensor Core Logger (MSCL) data

Down-core logging data show an abrupt and distinct change in physical properties at around 7.3 m depth, as well as more subtle variations that enabled demarcation of the five sediment units (Fig. 3.3; Tab. 3.2). Unit 1 is largely indiscernible from Unit 2 based on physical properties, but does have much lower magnetic susceptibility. The sediments above the abrupt contact at 7.3 m (Unit 2 and 3) are generally characterised by high relative P-wave velocities, gamma-ray densities, electrical resistivity, and low relative values of fractional porosity (on average under 0.5). Unit 3 shows the highest electrical resistivity and gamma-ray densities in the core; hence is demarcated as an individual unit, rather than being subsumed within Unit 2. In the sediments immediately below 7.3 m (Unit 4), the most marked step in physical properties is observed, including a reduction in gamma-ray density from 2.0 to 1.7 g/cm^3, and an increase in fractional porosity from approximately 0.45 to >0.55. Such a marked change was not observed in the magnetic susceptibility either side of this contact; however, the signal is generally more erratic above and less variable below (Fig. 3.3). Below the contact at 7.3 m, P-wave velocity, gamma-ray density, and electrical resistivity gradually increase down-core (inversely mirroring a steady decrease in fractional porosity) until the start of Unit 5, which is marked by a sharp increase in magnetic susceptibility (from <70 to >165 m^3/kg), and subtle increase in average P-wave velocity and gamma-ray density (Fig. 3.3).

3.4.2. X-ray Fluorescence (XRF) data

Distinct changes in geochemistry are also observed from the XRF analysis between the sediment units (Fig. 3.3 and 3.5), which correspond to very similar depths (±0.3 m) where physical property changes are noted. The first order observations are of: i) a step in Fe/K, Ca/Fe and Ca/Sr elemental ratios between 7.1 and 7.3 m (i.e. straddling Unit 2/3/4 contacts); ii) a switch from more variable (noisy) elemental ratios above 7.1 to 7.3 m (Units 2 and 3), with centimetre-scale variations in geochemical composition, to less noisy ratios below (Unit 4). Below Unit 4, variations in elemental ratios are also observed, supporting the demarcation of Unit 5. Cross plotting of the elemental ratios (Fig. 3.6) supports the demarcation of the five identified sediment units, as well as illustrating the range in variability between each unit (e.g. large spread of values in Unit 2, compared to Unit 4).

Table 3.2. Summary of sediment core's sedimentological, and geophysical and geochemical characteristics.

Unit and depth range	General sedimentological description	MSCL characterisation	XRF characterisation	Possible deposit interpretation
Unit 1 (0 – 0.33 m)	Muddy sand	Lower magnetic susceptibility no distinct trends in other geophysical properties	>Ca/Fe; No distinct Ca/Sr or Fe/K trend	Recent current reworked deposits
Unit 2 (0.33 – 7.11 m)	Stratified unit, consisting of bioturbated clayey silt to silty clay and sandy silt to silty sand layers; drop stones in the upper part of the unit	Strong variations in P-wave velocity, gamma-ray density, fractional porosity and magnetic susceptibility; down-core increase in p-wave velocity and gamma-ray density, and decrease in fractional porosity	Strong variations especially in Ca/Fe	Post-glacial deposits, with variable pulses of sediment flux including melt-water plumes
Unit 3 (7.11– 7.32 m)	Sandy silt layer; mud clasts	High P-wave velocity and electrical resistivity	Increase in Ca/Sr; decrease in Ca/Fe; distinct increase in Fe/K	Sandy contourite, reworked from immediate post-glacial meltwater-derived sediments
Unit 4 (7.32 – 10.00 m)	Relatively homogeneous bioturbated silty clay to clayey silt; drop stones throughout the unit	Distinct and abrupt decrease in P-wave velocity, gamma-ray density and electrical resistivity, and increase in fractional porosity at contact with Unit 3; less variation in magnetic susceptibility	Relatively constant element ratios; higher average Ca/Sr (and peak); lower average Ca/Fe; higher average Fe/K	Steady glaciomarine deposition
Unit 5 (10.00 m – end)	Clayey silt to sandy silt	Distinct and abrupt increase in magnetic susceptibility at contact with Unit 4; slight increase in P-wave velocity and gamma-ray density	Slightly variations in Ca/Sr; increasing Ca/Fe; distinct increase in Fe/K;	Steady interstadial deposition

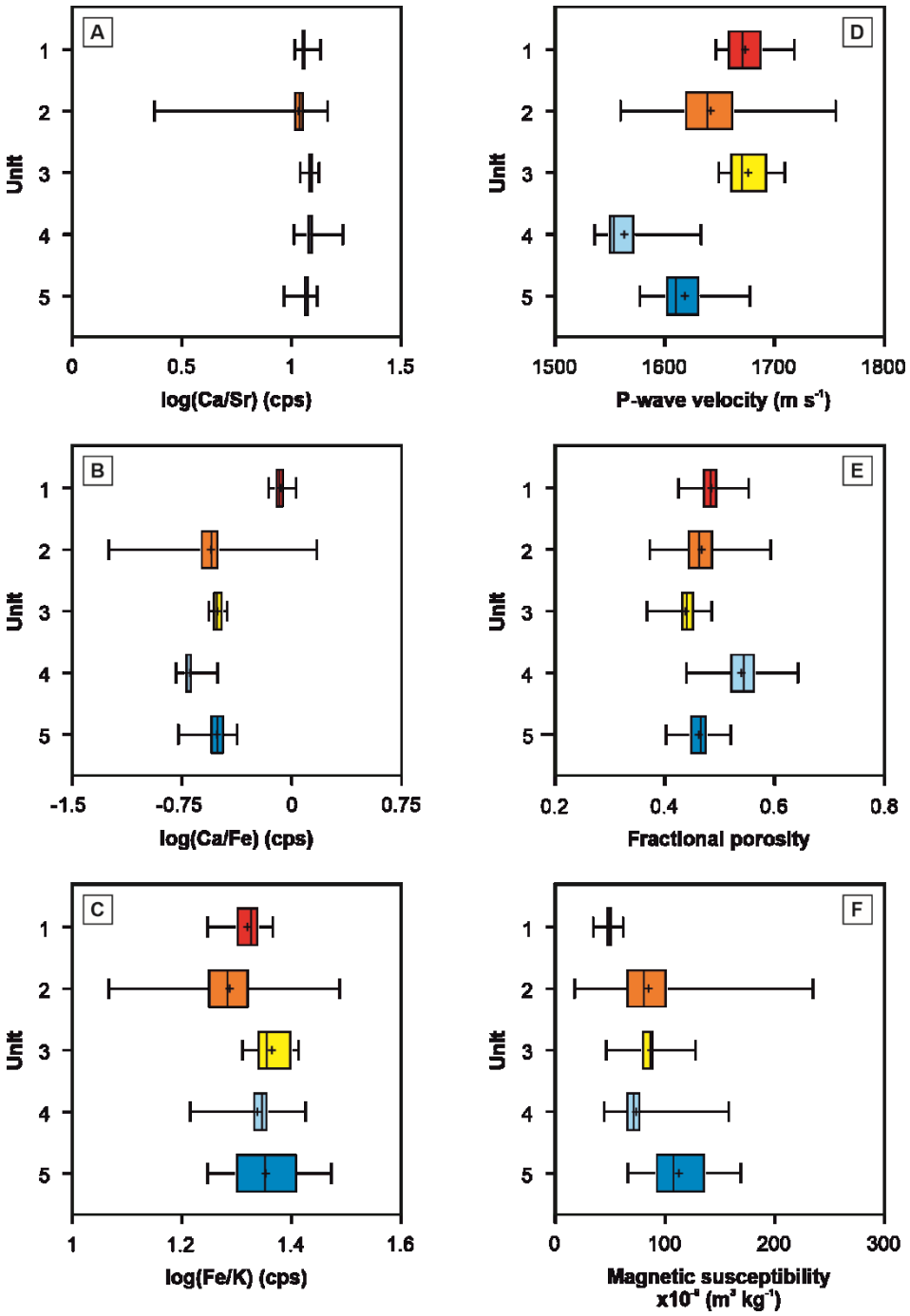

Figure 3.5. Box-Whisker plots showing the variation in element ratios Ca/Sr (**A**), Ca/Fe (**B**) and Fe/K (**C**), and physical properties (**D** to **F**) between Units 1 to 5. The lines of the box indicate the upper and lower quartiles and the median, lines extending parallel form the boxes indicate the maximum and minimum values, and the cross illustrates the mean value.

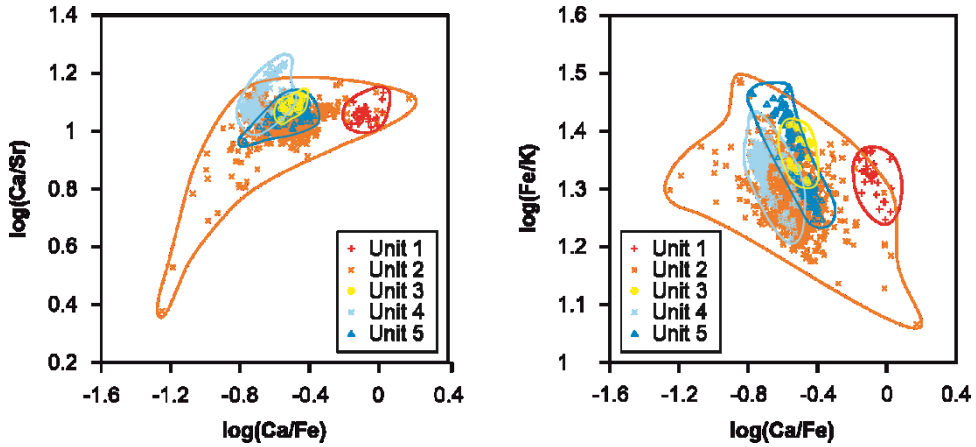

Figure 3.6. ITRAX XRF composition of individual subunits: red crosses – Unit 1, orange crosses – Unit 2, yellow circles – Unit 3, light blue stars – Unit 4, dark blue triangles – Unit 5.

3.4.3. Particle size distribution

Fig. 3.7 summarises particle size distribution data for core section 64PE391-04-D (6.5 to 7.7 m depth), which include sediments from Unit 2, 3 and 4. The data illustrate the change in composition at around 7.3 m depth. Unit 4 (below 7.3 m depth) is characterised by a higher silt content, in comparison to overlying sediments. Unit 3 is recognised as a sandy silt layer, and the sampled sediments of Unit 2 show a switch from sandy silt to clayey silt, which support the distinct changes in lithology seen in the visual core log.

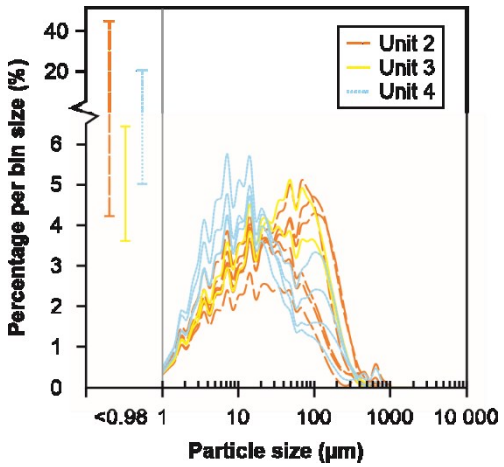

Figure 3.7. Particle size distribution data illustrated as percentage per bin.

3.4.4. Geotechnical data

A distinct change in water content can be observed, which increases from around 30 % to over 60 % at 7.3 m depth (i.e. at the contact between Unit 3 and 4; Fig. 3.3). Unit 1 has a slightly higher water content than Unit 3 (more or less constant 30 %). Unit 4 and 5 are characterised by decreasing water content. A distinct change in undrained shear strength is not observed, although the scatter is greater in the upper part of the core (Unit 2 and 3). Individual outliers (>100 kPa) are related to drop stones or mud clasts.

A summary of the key sample parameters and test results of the direct shear and oedometer tests are given in Tab. 3.3. The peak drained shear strength of Unit 3 and 4 are shown in Fig. 3.3 (indicated by red crosses). It can be seen that Unit 3 encompasses a higher peak shear strength (173 kPa) than Unit 4 (109 kPa). Typical porosity (n) versus applied normal stress (σ_n) is shown in Fig. 3.8. It is apparent that porosity decreases with increasing normal stress and increases slightly during the rebound phase. Unit 3 has a lower initial porosity, and higher permeability (k) and compressibility (c_v) than Unit 4.

Table 3.3. Key sample parameters and results from direct shear and oedometer tests.

Sample	Unit 3	Unit 4
LL (%)	26.5	56.1
PL (%)	-	25
γ' (kN/m^3)	9.5	9.5
σ'_n (kPa)	170	170
τ_{max} (kPa)	173	109
n	0.43	0.55
c_v (m^2/s)	5.2 x 10^{-4}	7.6 x 10^{-5}
k (m/s)	4.3 x 10^{-7}	7.8 x 10^{-8}

LL is the Liquid Limit, PL is the Plastic Limit, γ' is the effective unit weight, σ'_n is the effective normal stress, τ_{max} is the maximum shear strength, n is the porosity, c_v is the compressibility, and k is the permeability.

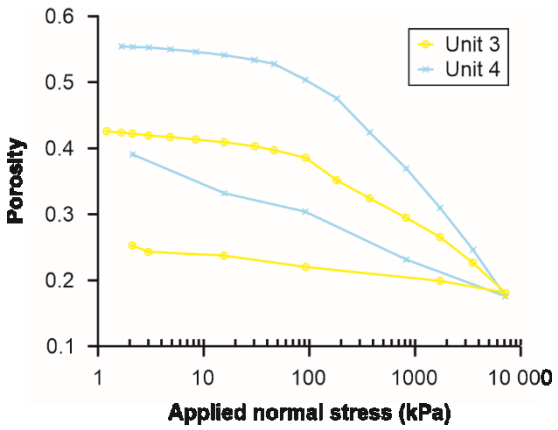

Figure 3.8. Porosity versus applied normal stress curves from one-dimensional consolidation tests.

3.5. Discussion

The recovered slope sediment obtained from core 64PE391-04 is characterised by a distinct step change in both physical and geochemical properties between around 7.1 and 7.3 m depth, as well as a distinct high-density contrast at that depth which was recorded by X-Ray imaging (Fig. 3.3 and 3.4). These transitions are related to an abrupt change in lithology from a thick relatively homogeneous clayey silt, silty clay unit (Unit 4; Fig. 3.3 and 3.5) to an overlying 25 cm-thick sandy silt layer (Unit 3; Fig. 3.3 and 3.5). The depth of this distinct change matches well with the seismostratigraphic horizon that is equivalent to the main failure plane outlined in the deep-tow boomer reflection seismic data (assuming a seismic velocity of 1600 m/s; Wilson et al., 2004), which is supported by the available MSCL data.

The sediment above this distinct interface is characterised by slightly higher P-wave velocities and gamma-ray densities, as well as a lower fractional porosity than would be expected for continental slope sediments (Fig. 3.3; Hamilton, 1970). Small cracks were recorded by X-Ray imaging, but are limited to parts of Unit 2 (Fig. 3.4). These observations could be related to a slight compaction of the sediment, e.g. due to compression by the partially confined landslide debris above the sediment ramp (Fig. 3.2C; e.g. Frey-Martínez et al., 2006; Principaud et al., 2015; Brooks et al., 2018), or to the around 10 m missing sediment sequence at the 64PE391-04 core location (Fig 3.2), whose removal could have disturbed the slope sediments. The potential deformation, however, is not resolved in the seismic data, and the distinct change at around 7.1 to 7.3 m depth is not limited to the physical properties, but is also noted in the geochemical properties. We therefore infer that although the sediment might have been slightly deformed, it probably did not move (no sliding motion) and the stratigraphy was not altered.

3.5.1. Lithological contrasts appear to play a key role in dictating the location of the failure plane

Wilson et al. (2004) previously suggested that the AFEN Slide could have initiated along a sandy contouritic layer embedded within the slope stratigraphy, but were unable to sample deep enough to prove its occurrence. Our deeper core now shows that this hypothesis may be plausible, given the presence of Unit 3. Although this unit was not identified as a contourite in the seismic data (Fig. 3.2C, Wilson et al., 2004), we interpret it as a sheeted sandy contourite drift. This assumption is considered reasonable as the vertical resolution of the seismic data (0.5 m; Wilson et al., 2005) might be too low to register this 25 cm-thick layer. Furthermore, we also show that there is much greater lithological heterogeneity (based on physical properties and geochemistry) within these sheeted drifts than has been previously documented, aside from simply variations in particle size. Without detailed geochemical and physical properties data, this abrupt lithological change would not have been identified.

Abrupt lithological changes (such as between Unit 3 and 4) may instead play a key role in defining the location of the failure plane. Unfortunately, the vertical resolution of the existing seismic data does not enable us to categorically determine whether the failure plane should correspond to the Unit 3/4 or Unit 2/3 contact. Although varying the assumed seismic velocity within reasonable ranges for sediments only results in a vertical offset of 0.5 m, the failure plane falls within the depth window that includes the interfaces between Units 2/3 and Unit 3/4 (Fig. 3.4). Wilson et al. (2004) implicated sandy contouritic sediments as potential "weak layers" (i.e. Unit 2/3 scenario), because of their potential to host excess pore pressures, when bound by an overlying lower permeability unit. This is a reasonable suggestion; however, the fractional porosity data indicate that the sand-rich Unit 3 instead features slightly lower porosity than the overlying sediments, while the underlying mud-rich sediments (Unit 4) have an even higher porosity. This observation is supported by water content data, which show the highest values in the mud-rich Unit 4 and abruptly decreases at the interface to Unit 3. Oedometer tests carried out on undisturbed samples from Unit 3 and 4 reveal a higher initial porosity and lower compressibility of Unit 4. This relationship is in contrast to an established empirical relationship between coarser particle size and greater porosity (or larger pore size; Ren and Santamarina, 2018). This apparent contradiction is explained by the presence of detrital clay that fills in pore spaces between sand grains (Unit 3); whereas the relatively open structure of the underlying muddier deposits (Unit 4) explains their higher relative porosity (Marion et al., 1992; Revil and Cathles III, 1999). In contrast to porosity, however, permeability is found to be higher in the sand-rich sediments (Unit 3; Tab. 3.3). Considering the higher permeability and compressibility of Unit 3, it is possible for excess pore pressure to accumulate within the sandy contouritic sediments (e.g. during an earthquake). Although this observation would support the 'weak layer' hypothesis, it has to be noted that the water content is actually higher in Unit 4 and abruptly drops at the interface to Unit 3, instead of increasing within the layer.

Another noticeable observation is the difference in shear strength between Unit 3 and 4. Both drained and undrained shear strength are lower in the mud-rich Unit 4, which can be related to the higher water content and to the lack of sandy material within the unit. Taking all these observations into account, we suggest that it is possible that a failure plane could generate at an interface where sand overlies finer grained cohesive sediments. The high water content and lower shear strength of the fine-grained material could allow the overlying sediment to slide on top of it. We are unable to be more absolute on the failure depth, but we have demonstrated that variability in sheeted drifts can also include abrupt whole-scale changes in sediment properties, as well as the presence of thin coarser units, which have traditionally been invoked to explain bedding parallel failures in contourite sheeted drifts (Laberg and Camerlenghi, 2008). Such variability may not necessarily be expected based on the available seismic data.

3.5.2. Climate change is a likely control on creating failure-prone lithological contrasts

Down-core changes in Ca/Sr ratios have been successfully related to variations in sea level and water temperature (through integration with oxygen isotope curves and biostratigraphy), wherein high Ca/Sr ratios are indicative of ice-rafted debris and changes from colder to warmer conditions (e.g. Smith et al., 1979; Thomson et al., 2004; Hodell et al., 2008). High Fe/K ratios and low Ca/Fe on the other hand have been related to colder periods (Kuijpers et al., 2003; Perez et al., 2016). The increased Ca/Sr ratio above 7.6 m depth could therefore indicate a stronger meltwater flux, carrying ice-rafted debris into the channel, while the changes in Fe/K and Ca/Fe ratios at 7.1 to 7.3 m are also interpreted to indicate a switch from cold conditions (Unit 4) to warmer conditions (Unit 2/3). This switch was coincident with a transition from finer grained, stable sedimentation to a more variable regime with pulsed influxes of coarser material. Given the existing knowledge about the timing of the AFEN slides (Unit 1 should postdate 2.8 to 5.8 ka BP, while the pre-failure sediments must be older than 16 ka BP; Wilson et al., 2004) this transition fits within a time window that includes the switch from the Last Glacial Maximum (18 ka BP) to post-glacial conditions. Glacial conditions would have seen sediment largely locked up in ice sheets, while the melt-out during the immediate postglacial window involved pulses of fine and coarser-grained sediment. The nearby Faroe-Shetland Channel is the main oceanic gateway between the North Atlantic and the Norwegian Sea (Broecker and Denton, 1990; Rahmstorf, 2002); where a direct relation exists between ocean circulation and climate. Rapid changes in the exchange of water masses between the northeast Atlantic and the Norwegian Sea occurred following the last glacial maximum at 18 ka BP (Rasmussen et al., 2002), which would have compounded the abruptness of a switch in sediment transfer. We therefore suggest that the abrupt change in physical properties and geochemistry may relate to this climatic transition.

Previous studies have investigated the role of climate change on submarine landslides, primarily focusing on their timing. A number of early studies suggested that submarine landslides, particularly in higher latitudes, may be more likely during sea level low-stands. Recent work, however, has suggested that there is no clear statistical relationship or at least that there are too few observations to be confident (e.g. Maslin et al., 2004; Brothers et al., 2013; Urlaub et al., 2013, 2014; Pope et al., 2015). Indeed, recent work has shown that such margins may feature many more late Holocene submarine landslides than previously thought (Normandeau et al., 2019). Proving a clear link between submarine landslides and sea level or climate change is most likely complicated by a range of factors, including time lags in offshore sediment transport, residence times of excess pore pressures following periods of rapid sediment accumulation, local sea level changes (e.g. isostatic rebound following glaciations) and other factors (Masson et al., 2006; Urgeles and Camerlenghi, 2013; Talling et al., 2014). Whether climate

change has played any role in the timing of the slope failures at AFEN remains unclear; however, it may have played a key role in one aspect: the location of the failure plane. Our data indicate that the slope failure most likely initiated along a distinct lithological interface that is interpreted to relate to a switch in depositional regime: from cold and uniform to warm and variable depositional conditions. The close connection between thermohaline circulation, sea level and temperature, and sediment supply in this region may explain why the switch in deposition was so rapid.

3.5.3. Broader implications for slope instability in contourites at climatically-influenced ocean gateway

The origin of distinct lithological interfaces may result in a variety of ways, and may be very common in contouritic sediments near ocean gateways where climatic changes may affect bottom current intensity (and thus controls the particle size that is transported; Faugères and Mulder et al., 2011), as well as the type of sediment that is distributed by the bottom currents (e.g. terrestrial and biogenic fluxes may vary during different climatic windows; Faugères et al., 1993; Maldonado et al., 2005). Such effects can be felt at a variety of latitudes, ranging from tropical to polar settings (e.g. Kuijpers et al., 2001; Principaud et al., 2015; Elger et al., 2017). In such settings climate may play a key role in dictating the location of potential failure planes. While many previous studies have invoked dominantly geometric controls on slope failure in contourite drifts, our study contributes to a growing literature base that indicates that lithological interfaces may explain the strong affinity of contourite deposits to slope instability. We posit that in low-angle, sheeted contourite drifts, such as AFEN, it is such material interfaces that are most important for preconditioning slopes to failure.

3.6. Conclusions

The integration of physical properties and geochemical core-log data, particle size distribution, and geotechnical data indicates that the AFEN Slide initiated along a distinct lithological interface within the slope stratigraphy, which matches the depth of the failure plane obtained from seismic data. This lithological interface correlates with the base of a 25 cm sandy contourite layer, overlying a thick, relatively homogeneous silty clay unit. Based on this high-resolution multi-proxy analysis, it was possible to resolve small-scale material changes within the slope stratigraphy, which cannot be distinguished from seismic data alone (owing to its the limited vertical resolution of 0.5 m). Integrating the core analyses with our knowledge about the current regime prevailing in the Faroe-Shetland Channel for the last 18 ka, it seems that climate change might pre-condition the location of failure initiation. This highlights the fact that in order to understand submarine landslide hazard, it is necessary to include

information from all different scales, ranging from the small-scale high-resolution analysis of core material to the understanding of the regional oceanographic setting.

Acknowledgements

The authors thank the British Geological Survey for the supply of the deep-tow boomer reflection seismic data and previous contributions (in particular David Tapping and David Long). Thanks, are also given to the crew of the R.V. Pelagia for their efforts during data collection. We thank BOSCORF and its staff (S. MacLachan, M. Edwards and M. Charidemou) for their services in maintaining the cores and assisting with some of the analytical techniques, and Achim Kopf for letting us use his geotechnical laboratory to carry out the shear tests. We acknowledge the constructive reviews by A. Cattaneo and U. Nicholson, and editor J. Mountjoy. Credits for the bathymetric metadata is given to ESRI, Garmin, GEBCO, NOAA NGDC, and other contributors.

Funding

This project has received funding from the European Union's Horizon 2020 research and innovation programme under the Marie Skłodowska-Curie grant agreement No 721403. We acknowledge research funding from the UK National Environmental Research Council (NE/K0008X/1) for core collection.

References

Ai, F., Strasser, M., Preu, B., Hanebuth, T.J.J., Krastel, S., Kopf, A., 2014. New constraints on oceanographic vs. seismic control on submarine landslides initiation: a geotechnical approach off Uruguay and northern Argentina. Geo-Marine Letters, 34, 399-417, https://doi.org/10.1007/s00367-014-0373-3

Andersen, M.S., Nielsen, T., Sørensen, A.B., Boldreel, L.O., Kuijpers, A., 2000. Cenozoic sediment distribution and tectonic movements in the Faroe region. Global and Planetary Change, 24, 239-259, https://doi.org/10.1016/S0921-8181(00)00011-4

Baeten, N.J., Laberg, J.S., Forwick, M., Vorren, T.O., Vanneste, M., Forsberg, C.F., Kvalstad, T.J., Ivanov, M., 2013. Morphology and origin of smaller-scale mass movements on the continental slope off northern Norway. Geomorphology, 187, 122-134, https://doi.org/10.1016/j.geomorph.2013.01.008

Baeten, N.J., Laberg, J.S., Vanneste, M., Forsberg, C.F., Kvalstad, T.J., Forwick, M., Vorren, T.O., Haflidason, H., 2014. Origin of shallow submarine mass movements and their glide planes - Sedimentological and geotechnical analyses from the continental slope off northern Norway. Journal of Geophysical Research: Earth Surface, 119, 2335-2360, https://doi.org/10.1002/2013JF003068

Blindheim, J., 1990. Arctic Intermediate Water in the Norwegian Sea. Deep-Sea Research, 37, 1475-1489.

Broecker, W.S., Denton, G.H., 1990. The role of ocean-atmosphere reorganizations in glacial cycles. Quaternary Science Reviews, 9, 305-341.

Bonnin, J., van Raaphorst, W., Brummer, GJ., van Haren, H., Malschaert, H., 2002. Intense mid-slope resuspension of particulate matter in the Faeroe-Shetland Channel: short-term deployment of near-bottom sediment traps. Deep-Sea Research I, 49, 1485-1505.

Brooks, H.L., Hodgson, D.M., Brunt, R.L., Peakall, J., Flint, S.S., 2018. Exhumed lateral margins and increasing flow confinement of a submarine landslide complex. Sedimentology, 65, 1067-1069, https://doi.org/10.1111/sed.12415

Brothers, D.S., Luttrell, K.M., Chaytor, J.D., 2013. Sea-level–induced seismicity and submarine landslide occurrence. Geology, 41, 979-982, https://doi.org/10.1130/G34410.1

Bryn, P., Berg, K., Forsberg, C.F., Solheim, A., Kvalstad, T.J., 2005a. Explaining the Storegga Slide. Marine and Petroleum Geology, 22, 11-19, https://doi.org/10.1016/j.marpetgeo.2004.12.003

Bryn, P., Berg, K., Stoker, M.S., Haflidason, H., Solheim, A., 2005b. Contourites and their relevance for mass wasting along the Mid-Norwegian Margin. Marine and Petroleum Geology, 22, 85-96, https://doi.org/10.1016/j.marpetgeo.2004.10.012

BSI, 1990. Methods of test for soils for civil engineering purposes – Part 2: Classification tests, In: British Standard BS 1377-2. British Standards Institution, London.

BSI, 2004. Geotechnical investigation and testing – laboratory testing of soils. Part 6: Fall cone tests, In: DD CEN ISO/TS 17892-6. British Standards Institution, London.

Casas, D., Chiocci, F., Casalbore, D., Ercilla, G., De Urbina, J.O., 2016. Magnitude-frequency distribution of submarine landslides in the Gioia Basin (southern Tyrrhenian Sea). Geo-Marine Letters, 36, 405-414, https://doi.org/10.1007/s00367-016-0458-2

Chaytor, J.D., Uri, S., Solow, A.R., Andrews, B.D., 2009. Size distribution of submarine landslides along the US Atlantic margin. Marine Geology, 264, 16-27, https://doi.org/10.1016/mj.margeo.2008.08.007

Clare, M.A., Chaytor, J., Dabson, O., Gamboa, D., Georgiopoulou, A., Eady, H., Hunt, J., Jackson, C., Katz, O., Krastel, S., León, R., Micallef, A., Moernaut, J., Moriconi, R., Moscardelli, L., Mueller, C., Normandeau, A., Patacci, M., Steventon, M., Urlaub, M., Völker, D., Wood, L., Jobe, Z., 2018. A consistent global approach for the morphometric characterization of subaqueous landslides. In: Lintern, D.G., Mosher, D.C, Moscardelli, L.G., Bobrowsky, P.T., Campbell, C., Chaytor, J.D., Clague, J.J., Georgiopoulou, A., Lajeunesse, P., Normandeau, A., Piper, D.J.W., Scherwath, M., Stacey, C., Turmel, D. (Eds) Subaqueous Mass Movements. Geological Society, London, Special Publications, 477, 455-477, https://doi.org/10.1144/SP477.15

Croudace, I.W., Rindby, A., Rothwell, R.G., 2006. ITRAX: description and evaluation of a new multi-function X-ray core scanner. In: Rothwell, R.G. (Ed) New Techniques in Sediment Core Analysis. Geological Society, London, Special Publications, 267, 51-63.

Croudace, I.W., Rothwell, R.G. (Eds) 2015. Micro-XRF Studies of Sediment Cores. Applications of a non-destructive tool for the environmental sciences. Springer, Dordrecht. pp. 656

Dahlgren, K.I.T., Vorren, T.O., Laberg, J.S., 2002. Late Quaternary glacial development of the mid-Norwegian margin – 65 to 68°N. Marine and Petroleum Geology, 19, 1089-1113, https://doi.org/10.1016/S0264-8172(03)00004-7

Davies, R.J., Cartwright, J.A., Pike, J., Line, C., 2001. Early Oligocene initiation of North Atlantic deep water formation. Nature, 410, 917-920.

Dean, K., McLachlan, K., Chambers, A., 1999. Rifting and the development of the Faeroe-Shetland Basin. In: Fleet, A.J., Boldy, S.A.R. (Eds) Petroleum Geology of Northwest Europe Proceedings of the 5th Conference. Geological Society, London, Petroleum Geology Conference series, 5, 533-544, https://doi.org/10.1144/0050533

Deutsches Institut für Normung, 2002. Baugrund, Untersuchung von Bodenproben —Bestimmung der Scherfestigkeit, In: DIN-Norm 18137- 3, Beuth, Berlin.

Elger, J., Berndt, C., Krastel, S., Piper, D.J.W., Gross, F., Geissler, W.H., 2017. Chronology of the Fram Slide Complex offshore NW Svalbard and its implications for local and regional slope stability. Marine Geology, 393, 141-155, https://doi.org/10.1016/j.margeo.2016.11.003

Ercilla, G., Juan, C., Hernández-Molina, F.J., Bruno, M., Estrada, F., Alonso, B., Casas, D., Farran, M., Llave, E., García, M., Vázquez, J.T., D'Acremont, E., Gorini, C., Palomino, D., Valencia, J., El Moumni, B., Ammar, A., 2016. Significance of bottom currents in deep-sea morphodynamics: An example from the Alboran Sea. Marine Geology, 378, 157-170, https://doi.org/10.1016/j.margeo.2015.09.007

Evans, D., Harrison, Z., Shannon, P.M., Laberg, J.S., Nielsen, T., Ayers, S., Holmes, R., Hoult, R.J., Lindberg, B., Haflidason, H., Long, D., Kuijpers, A., Andersen, E.S., Bryn, P., 2005. Palaeoslides and other mass failures of Pliocene to Pleistocene age along the Atlantic continental margin of NW Europe. Marine and Petroleum Geology, 22, 1131-1148, https://doi.org/10.1016/j.marpetgeo.2005.01.010

Faugères, JC., Stow, D.A.V., Imbert, P., Viana, A., 1999. Seismic features diagnostic of contourite drifts. Marine Geology, 162, 1-38, https://doi.org/10.1016/S0025-3227(99)00068-7

Faugères, JC., Mulder, T., 2011. Contour Currents and Contourite Drifts. Developments in Sedimentology, 63, 149-214, https://doi.org/10.1016/B978-0-444-53000-4.00003-2

Faugères, JC., Mézerais, M.L., Stow, D.A.V., 1993. Contourite drift types and their distribution in the North and South Atlantic Ocean basins. Sedimentary Geology, 82, 189-203.

Faugères, JC., Stow, D.A.V., 2008. Contourite Drifts: Nature, Evolution and Controls. Developments in Sedimentology, 60, 259-288, https://doi.org/10.1016/S0070-4571(08)10014-0

Faugères, JC., Stow, D.A.V., Imbert, P., Viana, A., 1999. Seismic features diagnostic of contourite drifts. Marine Geology, 162, 1-38.

Fisher, R.A., 1926. The arrangement of field experiments. Journal of the Ministry of Agriculture of Great Britain, 33, 503-513.

Frey-Martínez, J., Cartwright, J., James, D., 2006. Frontally confined versus frontally emergent submarine landslides: A 3D seismic characterisation. Marine and Petroleum Geology, 23, 585-604, https://doi.org/10.1016/j.marpetgeo.2006.04.002

Georgiopoulou, A., Krastel, S., Finch, N., Zehn, K., McCarron, S., Huvenne, V.A.I., Haughton, P.D.W., Shannon, P.M., 2019. On the Timing and Nature of the Multiple Phase of Slope Instability on Eastern Rockall Bank, Northeast Atlantic. Geochemistry, Geophysics, Geosystems, 20, 594-613, https://doi.org/10.1029/2018GC007674

Georgiopoulou, A., Shannon, P.M., Sacchetti, F., Haughton, P.D.W., Benetti, S., 2013. Basement-controlled multiple slope collapses, Rockall Bank Slide Complex, NE Atlantic. Marine Geology, 336, 198-214, https://doi.org/10.1016/j.margeo.2012.12.003

Gunn, D.E., Best, A.I. 1998. A new automated non- destructive system for high resolution multi-sensor core logging of open sediment cores. Geo-Marine Letters, 18, 70-77.

Haflidason, H., Lien, R., Sejrup, H.P., Forsberg, C.F., Bryn, P., 2005. The dating and morphometry of the Storegga Slide. Marine and Petroleum Geology, 22, 123-136, https://doi.org/10.1016/j.marpetgeo.2004.10.008

Hamilton, E.L., 1970. Sound Velocity and Related Properties of Marine Sediments, North Pacific. Journal of Geophysical Research, 75, 4423-4446.

Henkel, S., Strasser, M., Schwenk, T., Hanebuth, T.J.J., Hüsener, J., Winkelmann, D., Tomasini, J., Krastel, S., Kasten, S., 2011. An interdisciplinary investigation of a recent submarine mass transport deposit at the continental margin off Uruguay. Geochemistry, Geophysics, Geosystems, 12(8), Q08009, https://doi.org/10.1029/2011GC003669

Hepp, D.A., Mörz, T., Grützner, J., 2006. Pliocene glacial cyclicity in a deep-sea sediment drift (Antarctic Peninsula Pacific Margin). Paleogeography, Paleoclimatology, Paleoecology, 231, 181-198, https://doi.org/10.1016/j.palaeo.2005.07.030

Hernández-Molina, F.J., Paterlini, M., Violante, R., Marshall, P., de Isasi, M., Somoza, L., Rebesco, M., 2009. Contourite depositional system on the Argentine Slope: An exceptional record of the influence of Antarctic water masses. Geology, 37, 507-510, https://doi.org/10.1130/G25578A.1

Hernández-Molina, F.J., Soto, M., Piola, A.R., Tomasini, J., Preu, B., Thompson, P., Badalini, G., Creaser, A., Violante, R.A., Morales, E., Paterlini, M., De Sanata Ana, H., 2016. A contourite depositional system along the Uruguayan continental margin: Sedimentary, oceanographic and paleoceanographic implications. Marine Geology, 378, 333-349, https://doi.org/10.1016/j.margeo.2015.10.008

Hodell, D.A., Channell, J.E.T., Curtis, J.H., Romero, O.E., Röhl, U., 2008. Onset of "Hudson Strait" Heinrich events in the eastern North Atlantic at the end of the middle Pleistocene transition (~640 ka)?. Paleoceanography, 23, PA4218, https://doi.org/10.1029/2008PA001591

Hohbein, M., Cartwright, J., 2006. 3D seismic analysis of the West Shetland Drift system: Implications for Late Neogene paleoceanography of the NE Atlantic. Marine Geology, 230, 1-20, https://doi.org/10.1016/j.margeo.2006.03.009

Hübscher, C., Betzler, C., Reiche, S., 2016. Seismo-stratigraphic evidences of deep base level control on middle to late Pleistocene drift evolution and mass wasting along southern Levant continental slope (Eastern Mediterranean). Marine and Petroleum Geology, 77, 526-534, https://doi.org/10.1016/j.marpetgeo.2016.07.008

Iwai, M., Acton, G.D., Lazarus, D., Osterman, L.E., Williams, T., 2002. Magnetobiochronologic synthesis of ODP Leg 178 rise sediments from the Pacific sector of the Southern Ocean: Sites 1095, 1096, and 1101. In: Barker, P.F., Camerlenghi, A., Acton, G.D., Ramsay, A.T.S. (Eds) Proceedings of Ocean Drilling Program, Scientific Results, 178, 1–40.

Johnson, H., Ritchie, J.D., Hitchen, K., Mcinroy, D.B., Kimbell, G.S., 2005. Aspects of the Cenozoic deformational history of the Northeast Faroe-Shetland Basin, Wyville-Thomson Ridge and Hatton Bank areas. In: Doré, A.G., Vining, B.A. (Eds) Petroleum Geology: North-West Europe and Global Perspectives – Proceedings of the 6th Petroleum Geology Conference, Geological Society, London, Petroleum Geology Conference series, 6, 993-1007, https://doi.org/10.1144/0060993

Katz, O., Reuven, E., Aharonov, E., 2015. Submarine landslides and fault scarps along the eastern Mediterranean Israeli continental-slope. Marine Geology, 369, 100-115, https://doi.org/10.1016/j.margeo.2015.08.006

Knutz, P.C., Cartwright, J.A., 2004. 3D anatomy of late Neogene contourite drifts and associated mass flows in the Faroe-Shetland Basin. In: Davies, R.J., Cartwright, J.A., Stewart, S.A., Lappin, M., Underhill, J.R. (Eds) 3D Seismic Technology: Application to the Exploration of Sedimentary Basins. Geological Society, London, Memoirs, 29, 63-71, https://doi.org/10.1144/GSL.MEM.2004.029.01.07

Krastel, S., Wefer, G., Hanebuth, T.J.J., Antobreh, A.A., Freudenthal, T., Preu, B., Schwenk, T., Strasser, M., Violante, R., Winkelmann, D., M78/3 shipboard scientific party, 2011. Sediment dynamics and geohazards off Uruguay and the de la Plata River region (northern Argentina and Uruguay). Geo-Marine Letters, 31, 271-283. Doi: 10.1007/s00367-011-0232-4

Kuijpers, A., Nielsen, T., Akhmetzhanov, A., de Haas, H., Kenyon, N.H., van Weering, T.C.E., 2001. Late Quaternary slope instability on the Faeroe margin: mass flow features and timing of events. Geo-Marine Letters, 20, 149-159, https://doi.org/10.1007/s003670000053

Kuijpers, A., Troelstra, S.R., Prins, M.A., Linthout, K., Akhmetzhanov, A., Bouryak, S., Bachmann, M.F., Lassen, S., Rasmussen, S., Jensen, J.B., 2003. Late Quaternary sedimentary processes and ocean circulation changes at the Southeast Greenland margin. Marine Geology, 195, 109-129, https://doi.org/10.1016/S0025-3227(02)00684-9

Kvalstad, T.J., Andresen, L., Forsberg, C.F., Berg, K., Bryn, P., Wangen, M., 2005. The Storegga slide: evolution of triggering sources and slide mechanics. Marine and Petroleum Geology, 22, 245-256, https://doi.org/10.1016/j.marpetgeo.2004.10.019

L'Heureux, JS., Longva, O., Steiner, A., Hansen, L., Vardy, M.E., Vanneste, M., Haflidason, H., Brendryen, J., Kvalstad, T.J., Forsberg, C.F., Chand, S., Kopf, A., 2012. Identification of Weak Layers and Their Role for the Stability of Slopes at Finneidfjord, Northern Norway. In: Yamada, Y., Kawamura, K., Ikehara, K., Ogawa, Y., Urgeles, R., Mosher, D., Chaytor, J., Strasser, M. (Eds) Submarine Mass Movements and Their Consequences, Advances in Natural and Technological Hazards Research, 31, 321-330. Springer Science+Business Media B.V., Dordrecht.

Laberg, J.S., Camerlenghi, A., 2008. The Significance of Contourites for Submarine Slope Stability. Developments in Sedimentology, 60, 537-556. https://doi.org/10.1016/S0070-4571(08)10025-5

Laberg, J.S., Dahlgren, T., Vorren, T.O., Haflidason, H., Bryn, P., 2001. Seismic analyses of Cenozoic contourite drift development in the Northern Norwegian Sea. Marine Geophysical Researches, 22, 401-416, https://doi.org/10.1023/A:1016347632294

Laberg, J.S., Vorren, T.O., 2000. The Trænadjuped Slide, offshore Norway – morphology, evacuation and triggering mechanisms. Marine Geology, 171, 95-114, https://doi.org/10.1016/S0025-3227(00)00112-2

Laberg, J.S., Vorren, T.O., Mienert, J., 2003. Preconditions leading to the Holocene Trænadjuped Slide offshore Norway. In: Locat, J., Mienert, J. (Eds) Submarine Mass Movements and Their Consequences, Advances in Natural and Technological Hazards Research., 19, 247-254. Springer, Dordrecht.

Laberg, J.S., Vorren, T.O., Mienert, J., Evans, D., Lindberg, B., Ottesen, D., Kenyon, N.H., Henriksen, S., 2002. Late Quaternary paleoenvironment and chronology in the Trænadjuped Slide area offshore Norway. Marine Geology, 188, 35-60, https://doi.org/10.1016/S0025-3227(02)00274-8

Lindberg, B., Laberg, J.S., Vorren, T.O., 2004. The Nyk Slide – morphology, progression, and age of a partly buried submarine slide offshore northern Norway. Marine Geology, 213, 277-289, https://doi.org/10.1016/j.margeo.2004.10.010

Long, D., Bulat, J., Stoker, M.S., 2004. Sea bed morphology of the Faroe-Shetland Channel derived from 3D seismic datasets. In: Davies, R.J., Cartwright, J.A., Stewart, S.A., Lapping, M. & Underhill, J.R. (eds) 3D Seismic Technology: Application to the Exploration of Sedimentary Basins. Geological Society, London, Memoirs, 29, 53-61, https://doi.org/10.1144/GSL.MEM.2004.029.01.06

Lüdmann, T., Wiggershaus, S., Betzler, C., Hübscher, C., 2012. Southwest Mallorca Island: A cool-water carbonate margin dominated by drift deposition associated with giant mass wasting. Marine Geology, 307-310, 73-87, https://doi.org/10.1016/j.margeo.2011.09.008

Madhusudhan, B.N., Clare, M.A., Clayton, C.R.I., Hunt, J.E., 2017. Geotechnical profiling of deep-ocean sediments at the AFEN submarine slide complex. Quarterly Journal of Engineering Geology and Hydrology, 50, 148-157, https://doi.org/10.1144/qjegh2016-057

Maldonado, A., Barnolas, A., Bohoyo, F., Escutia, C., Galindo-Zaldívar, J., Hernández-Molina, J., Jabaloy, A., Lobo, F.J., Nelson, C.H., Rodríguez-Fernández, J., Somoza, L., Vázquez, JT., 2005. Miocene to Recent contourite drifts development in the northern Weddell Sea (Antarctica). Global and Planetary Change, 45, 99-129, https://doi.org/10.1016/j.gloplacha.2004.09.013

Marion, D., Nur, A., Yin, H., Han, D., 1992. Compressional velocity and porosity in sand-clay mixtures. Geophysics, 57, 554-563.

Maslin, M., Owen, M., Day, S., Long, D., 2004. Linking continental-slope failures and climate change: Testing the clathrate gun hypothesis. Geology, 32, 53-56, https://doi.org/10.1130/G20114.1

Masson, D.G., 2001. Sedimentary processes shaping the eastern slope of the Faeroe-Shetland Channel. Continental Shelf Research, 21, 825-857, https://doi.org/10.1016/S0278-4343(00)00115-1

Masson, D.G., Harbitz, C.B., Wynn, R.B., Pedersen, G., Løvholt, F., 2006. Submarine Landslides: Processes, Triggers and Hazard Prediction. Philosophical Transactions: Mathematical, Physical and Engineering Sciences, 354, 2009-2039, https://doi.org/10.1098/rsta.2006.1810

Masson, D.G., Wynn, R.B., Bett, B.J., 2004. Sedimentary environment of the Faroe-Shetland and Faroe Bank Channels, north-east Atlantic, and the use of bedforms as indicators of bottom current velocity in the deep ocean. Sedimentology, 51, 1207-1241, https://doi.org/10.1111/j.1365-3091.2004.00668.x

Mattingsdal, R., Knies, J., Andreassen, K., Fabian, K., Husum, K., Grøsfjeld, K., De Schepper, S., 2014. A new 6 Myr stratigraphic framework for the Atlantic-Arctic Gateway. Quaternary Science Reviews, 92, 170-178, https://doi.org/10.1016/j.quascirev.2013.08.022

McCave, I.N., Tucholke, B.E., 1986. Deep current controlled sedimentation in the western North Atlantic. In: Vogt, P.R., Tucholke, B.E. (Eds) The Western North Atlantic Region. Geology of North America, Volume M, 451-468.

Micallef, A., Berndt, C., Masson, D.G., Stow, D.A., 2008. Scale invariant characteristics of the Storegga Slide and implications for large-scale submarine mass movements. Marine Geology, 247, 46-60, https://doi.org/10.1016/j.margeo.2007.08.003

Minisini, D., Trincardi, F., Asioli, A., Canu, M., Foglini, F., 2007. Morphologic variability of exposed mass-transport deposits on the eastern slope of Gela Basin (Sicily channel). Basin Research, 19, 217-240, https://doi.org/10.1111/j.1365-2117.2007.00324.x

Miramontes, E., Cattaneo, A., Jouet, G., Thomas, Y., Rovere, M., Cauquil, E., Trincardi, F., 2016. The Pianosa Contourite Depositional System (Northern Tyrrhenian Sea): Drift morphology and Plio-Quaternary stratigraphic evolution. Marine Geology, 378, 20-42, https://doi.org/10.1016/j.margeo.2015.11.004

Miramontes, E., Garziglia, S., Sultan, N., Jouet, G., Cattaneo, A., 2018. Morphological control of slope instability in contourites: a geotechnical approach. Landslides, 15, 1085-1095, https://doi.org/10.1007/s10346-018-0956-6

Mulder, T., Ducassou, E., Eberli, G.P., Hanquiez, V., Gonthier, E., Kindler, P., Principaud, M., Fournier, F., Léonide, P., Billeaud, I., Marsset, B., Reijmer, J.J.G., Bondu, C., Joussiaume, R., Pakiades, M., 2012. New insights into the morphology and sedimentary processes along the western slope of Great Bahama Bank. Geology, 40, 603-606, https://doi.org/10.1130/G32972.1

Nielsen, T., Rasmussen, T.L., Ceramicola, S., Kuijpers, A., 2007. Quaternary sedimentation, margin architecture and ocean circulation variability around the Faroe Islands, North Atlantic. Quaternary Science Reviews, 26, 1016-1036, https://doi.org/10.1016/j.quascirev.2006.12.005

Normandeau, A., Campbell, D.C., Piper, D.J., Jenner, K.A., 2019. Are submarine landslides an underestimated hazard on the western North Atlantic passive margin?. Geology, 47, 848-852, https://doi.org/10.1130/G46201.1

Perez, L., Garcá-Rodríguez, F., Hanebuth, T.J.J., 2016. Variability in terrigenous sediment supply offshore of the Río de la Plata (Uruguay) recording the continental climatic history over the past 1200 years. Climate of the Past, 12, 623-634, https://doi.org/10.5194/cp-12-623-2016

Piper, D.J.W., 2005. Late Cenozoic evolution of the continental margin of eastern Canada. Norwegian Journal of Geology, 85, 305-318.

Pope, E.L., Talling, P.J., Urlaub, M., Hunt, J.E., Clare, M.A., Challenor, P., 2015. Are large submarine landslides temporally random or do uncertainties in available age constraints make it impossible to tell?. Marine Geology, 369, 19-33, https://doi.org/10.1016/j.margeo.2015.07.002

Powrie, W., 2013. Soil Mechanics: Concepts and Applications. 3rd Edition, CRC Press, Taylor & Francis, 682.

Preu, B., Hernández-Molina, F.J., Violante, R., Piola, A.R., Paterlini, C.M., Schwenk, T., Voigt, I., Krastel, S., Spiess, V., 2013. Morphosedimentary and hydrographic features of the northern Argentine margin: The interplay between erosive, depositional and gravitational processes and its conceptual implications. Deep-Sea Research I, 75, 157-174, https://doi.org/10.1016/j.dsr.2012.12.013

Prieto, M.I., Moscardelli, L., Wood, L.J., 2016. Exploring the influence of deepwater currents as potential triggers for slope instability. In: Lamarche, G., Mountjoy, J., Bull, S., Hubble, T., Krastel, S., Lane, E., Micallef, A., Moscardelli, L., Mueller, C., Pecher, I., Woelz, S. (Eds) Submarine Mass Movements and Their Consequences, Advances in Natural and Technological Hazards Research, 41, 331-338. Springer, Cham.

Principaud, M., Mulder, T., Gillet, H., Borgomano, J., 2015. Large-scale carbonate submarine mass-wasting along the northwestern slope of the Great Bank (Bahamas): Morphology, architecture, and mechanisms. Sedimentary Geology, 317, 27-42, https://doi.org/10.1016/j.sedgeo.2014.10.008

Rahmstorf, S., 2002. Ocean circulation and climate during the last 120,000 years. Nature, 419, 207–214.

Rashid, H., MacKillop, K., Sherwin, J., Piper, D.J.W., Marche, B., Vermooten, M., 2017. Slope instability on a shallow contourite-dominated continental margin, southeastern Grand Banks, eastern Canada. Marine Geology, 393, 203-215, https://doi.org/10.1016/j.margeo.2017.01.001

Rasmussen, T.L., Bäckström, D., Heinemeier, J., Klitgaard-Kristensen, D., Knutz, P.C., Kuijpers, A., Lassen, S., Thomsen, E., Troelstra, S.R., van Weering, T.C.E., 2002. The Faroe-Shetland Gateway: Late Quaternary water mass exchange between the Nordic seas and the northeastern Atlantic. Marine Geology, 188, 165-192, https://doi.org/10.1016/S0025-3227(02)00280-3

Rasmussen, T.L., Thomsen, E., van Weering, T.C.E., 1998. Cyclic sedimentation of the Faeroe Drift 53-10 ka BP related to climatic variations. In: Stoker, M.S., Evans, D., Cramp, A. (Eds) Geological Processes on Continental Margins: Sedimentation, Mass-Wasting and Stability. Geological Society, London, Special Publications, 129, 255-267.

Rasmussen, T.L., Thomsen, E., van Weering, T.C.E., Labeyrie, L., 1996. Rapid changes in surface and deep water conditions at the Faeroe Margin during the last 58,000 years. Paleoceanography, 11, 757-771.

Rebesco, M., Hernández-Molina, F.J., Van Rooij, D., Wåhlin, A., 2014. Contourites and associated sediments controlled by deep-water circulation processes: State-of-the-art and future considerations. Marine Geology, 352, 111-154, https://doi.org/10.1016/j.margeo.2014.03.011

Rebesco, M., Stow, D., 2001. Seismic expression of contourites and related deposits: a preface. Marine Geophysical Researches, 22, 303-308, https://doi.org/10.1023/A:1016316913639

Ren, X.W., Santamarina, J.C., 2018. The hydraulic conductivity of sediments: A pore size perspective. Engineering Geology, 233, 48-54, https://doi.org/10.1016/j.enggeo.2017.11.022

Revil, A., Cathles III, L.M., 1999. Permeability of shaly sands. Water Resource Research, 35, 651-662, https://doi.org/10.1029/98WR02700

Ritchie, J.D., Johnson, H., Kimbell, G.S., 2003. The nature and age of Cenozoic contractional deformation within the NE Faroe-Shetland Basin. Marine and Petroleum Geology, 20, 399-409, https://doi.org/10.1016/S0264-8172(03)00075-8

Ritchie, J.D., Johnson, H., Quinn, M.F., Gatliff, R.W., 2008. The effects of Cenozoic compression within the Faroe-Shetland Basin and adjacent areas. In: Johnson, H., Doré, A.G., Gatliff, R.W., Holdsworth, R., Lundin, E.R., Richie, J.D. (Eds) The Nature and Origin of Compression in Passive Margin. Geological Society, London, Special Publications, 306, 121-136, https://doi.org/10.1144/SP306.5

Roberts, D.G., Thompson, M., Mitchener, B., Hossack, J., Carmichael, S., Bjørnseth, H.-M., 1999. Palaeozoic to Tertiary rift and basin dynamics: mid-Norway to the Bay of Biscay – a new context for hydrocarbon prospectivtiy in the deep water frontier. In: Fleet, A.J., Boldy, S.A.R. (Eds) Petroleum Geology of Northwest Europe: Proceedings of the 5th Conference. Geological Society, London, Petroleum Geology Conference Series, 5, 7-40, https://doi.org/10.1144/0050007

Röhl, U., Abrams, L.J., 2000. High-resolution, downhole and non-destructive core measurements from Sites 999 and 1001 in the Caribbean Sea: application to the Late Paleocene Thermal Maximum. In: Leckie, R.M., Sigurdsson, H., Acton, G.D., Draper, G. (Eds) Proceedings of the Ocean Drilling Program, Scientific Results, 165,191–203.

Rothwell, R.G., Rack, F.R., 2006. New techniques in sediment core analysis: an introduction. In: Rothwell, R.G. (Ed), New Techniques in Sediment Core Analysis. Geological Society, London, Special Publications, 267, 1–29, https://doi.org/10.1144/GSL.SP.2006.267.01.01

Rumph, B., Reaves, C.M., Orange, V.G., Robinson, D.L., 1993. Structuring and transfer zones in the Faeroe Basin in a regional tectonic context. In: Parker, J.R. (Ed) Petroleum Geology of Northwest Europe: Proceedings of the 4th Conference. Geological Society, London, Petroleum Geology Conference series, 4, 999-1009, https://doi.org/10.1144/0040999

Saunders, P.M., 1990. Cold outflow from the Faroe Bank Channel. Journal of Physical Oceanography, 20, 29-43.

Sheskin, D.J., 2011. Handbook of parametric and nonparametric statistical procedures. 5th Edition, CRC Press, Taylor & Francis, 1886.

Shipp, R.C., Weimer, P., Posamentier, H.W. (Eds) 2011. Mass-transport deposits in deepwater settings. SEPM Special Publication 96, SEPM Society for Sedimentary Geology, https://doi.org/10.2110/sepmsp.096.

Smith, S.V., Buddemeier, R.W., Redalje, R.C., Houck, J.E., 1979. Strontium-Calcium Thermometry in Coral Skeletons. Science, 207, 404-407.

Smallwood, J.R., Gill, C.E., 2002. The rise and fall of the Faroe-Shetland Basin: evidence from seismic mapping of the Balder Formation. Journal of the Geological Society, London, 159, 627-630.

Solheim, A., Berg, K., Forsberg, C.F., Bryn, P., 2005. The Storegga Slide complex: repetitive large scale sliding with similar cause and development. Marine and Petroleum Geology, 22, 97-107, https://doi.org/10.1016/j.marpetgeo.2004.10.013

Stoker, M.S., Akhurst, M.C., Howe, J.A., Stow, D.A.V., 1998. Sediment drifts and contourites on the continental margin off northwest Britain. Sedimentary Geology, 15, 33-51.

Stoker, M.S., Hoult, R.J., Nielsen, T., Hjelstuen, B.O., Laberg, J.S., Shannon, P.M., Praeg, D., Mathiesen, A., van Weering T.C.E., McDonnell, 2005. Sedimentary and oceanographic responses to early Neogene compression on the NW European margin. Marine and Petroleum Geology, 22, 1031-1044, https://doi.org/10.1016/j.marpetgeo.2005.01.009

Stoker, M.S., Nielsen, T., van Weering, T.C.E., Kuijpers, A., 2002. Towards an understanding of the Neogene tectonostratigraphic framework of the NE Atlantic margin between Ireland and the Faroe Islands. Marine Geology, 188, 233-248, https://doi.org/10.1016/S0025-3227(02)00282-7

Stow, D.A.V., Faugères, J.C., Howe, J.A., Pudsey, C.J., Viana, A.R., 2002. Bottom currents, contourites and deep-sea sediment drifts: current state-of-the-art. In: Stow, D.A.V., Pudsey, C.J., Howe, J.A., Faugères, J.C., Viana, A.R. (Eds) Deep-Water Contourite Systems: Modern Drifts and Ancient Series, Seismic and Sedimentary Characteristics. Geological Society, London, Memoirs, 22, 7–20, https://doi.org/10.1144/GSL.MEM.2002.022.01.02

Stow, D.A.V., Holbrook, J.A., 1984. Hatton Drift contourites, northeast Atlantic, Deep Sea Drilling Project Leg 81. Initial Reports Deep-Sea Drilling Project, 81, 695-699, doi:10.2973/dsdp.proc.81.125.1984

Talling, P.J., Clare, M.L., Urlaub, M., Pope, E., Hunt, J.E., Watt, S.F., 2014. Large submarine landslides on continental slopes: geohazards, methane release, and climate change. Oceanography, 27, 32-45.

Terzaghi, K., 1925. Erdbaumechanik auf Bodenphysikalischer Grundlage, F. Deuticke, Leipzig u. Wien

Thomson, J., Crudeli, D., De Lange, G., Slomp, C.P., Erba, E., Corselli, C., Calvert, S.E., 2004. Florisphaera profunda and the origin and diagenesis of carbonate phases in eastern Mediterranean sapropel units. Paleoceanography, 19, PA3003, https://doi.org/10.1029/2003PA000976

Tournadour, E., Mulder, T., Borgomano, J., Hanquiez, V., Ducassou, E., Gillet, H., 2015. Origin and architecture of a Mass Transport Complex on the northwest slope of Little Bahama Bank (Bahamas): Relations between off-bank transport, bottom current sedimentation and submarine landslides. Sedimentary Geology, 317, 9-26, https://doi.org/10.1016/j.sedgeo.2014.10.003

Turner, J.D., Scrutton, R.A., 1993. Subsidence patterns in western margin basins: evidence from the Faeroe-Shetland Basin. In: Parker, J.R. (Ed) Petroleum Geology of Northwest Europe: Proceedings of the 4th Conference. Geological Society, London, Petroleum Geology Conference series, 4, 975-983, https://doi.org/10.1144/0040975

Turrell, W.R., Slesser, G., Adams, R.D., Payne, R., Gillibrand, P.A., 1999. Decadal variability in the composition of Faroe Shetland Channel bottom water. Deep-Sea Research I, 46, 1-25.

Urgeles, R., Camerlenghi, A., 2013. Submarine landslides of the Mediterranean Sea: Trigger mechanisms, dynamics, and frequency-magnitude distribution. Journal of Geophysical Research: Earth Surface, 118, 2600-2618, https://doi.org/10.1002/2013JF002720

Urlaub, M., Talling, P.J., Masson, D.G., 2013. Timing and frequency of large submarine landslides: implications for understanding triggers and future geohazard. Quaternary Science Reviews, 72, 63-82, https://doi.org/10.1016/j.quascirev.2013.04.020

Urlaub, M., Talling, P., Clare, M., 2014. Sea-level-induced seismicity and submarine landslide occurrence: Comment. Geology, 42, 337.

Van Raaphorst, W., Malschaert, H., van Haren, H., Boer, W., Brummer, GJ., 2001. Cross-slope zonation of erosion and deposition in the Faerow-Shetland Channel, North Atlantic Ocean. Deep-Sea Research I, 48, 567-591, https://doi.org/10.1016/S0967-0637(00)00052-2

Van Weering, T.C.E., Nielsen, T., Kenyon, N.H., Akentieva, K., Kuijpers, A.H., 1998. Sediments and sedimentation at the NE Faeroe continental margin; contourites and large-scale sliding. Marine Geology, 152, 159-176, https://doi.org/10.1016/S0025-3227(98)00069-3

Van Weering, Tj.C.E., de Rijk, S., 1991. Sedimentation and climate-induced sediments on Feni Ridge, Northeast Atlantic Ocean. Marine Geology, 101, 49-69.

Vanneste, M., Mienert, J., Bünz, S., 2006. The Hinlopen Slide: A giant, submarine slope failure on the northern Svalbard margin, Arctic Ocean. Earth and Planetary Science Letters, 245, 373-388, https://doi.org/10.1016/j.epsl.2006.02.045

Vardy, M.E., L'Heureux, JS., Vanneste, M., Longva, O., Steiner, A., Forsberg, C.F., Haflidason, H., Brendryen, J., 2012. Multidisciplinary investigation of a shallow near-shore landslides, Finneidfjord, Norway. Near Surface Geophysics, 10, 267-277, https://doi.org/10.3997/1873-2012022

Verdicchio, G., Trincardi, F., 2008. Mediterranean shelf-edge muddy contourites: examples from the Gela and South Adriatic basins. Geo-Marine Letters, 28, 137-151, https://doi.org/10.1007/s00367-007-0096-9

Volpi, V., Amblas, D., Camerlenghi, A., Canals, M., Rebesco, M., Urgeles, R., 2011. Late Neogene to recent seafloor instability on the deep pacific margin of the Antarctic Peninsula. In: Shipp, R.C., Weimer, P. & Posamentier, H.W. (eds) Mass-Transport Deposits in Deepwater Settings. SEPM Special Publication 96, SEPM Society of Sedimentary Geology, 161-177, https://doi.org/10.2110/sepmsp.096.161

Volpi, V., Camerlenghi, A., Hillenbrand, C.D., Rebesco, M., Ivaldi, R., 2003. Effects of biogenic silica on sediment compaction and slope stability on the Pacific margin of the Antarctic Peninsula. Basin Research, 15, 339-363, https://doi.org/10.1046/j.1365-2117.2003.00210.x

Weltje, G.J., Tjallingii, R., 2008. Calibration of XRF core scanners for quantitative geochemical logging of sediment cores: Theory and application. Earth and Planetary Science Letters, 274, 423-438, https://doi.org/10.1016/j.epsl.2008.07.054

Wilson, C.K., Long, D., Bulat, J., 2003. The Afen Slide – A multistage slope failure in the Faroe-Shetland Channel. In: Locat, J., Mienert, J. (Eds) Submarine Mass Movements and Their Consequences, Advances in Natural and Technological Hazards Research. Springer, Dordrecht, 317-324.

Wilson, C.K., Long, D., Bulat, J., 2004. The morphology, setting and processes of the Afen Slide. Marine Geology, 213, 149-167, https://doi.org/10.1016/j.margeo.2004.10.005

Wilson, C.K. Bulat, J., Long, D., 2005. The Afen Slide. British Geological Survey Commissioned Report, CR/05/003, 96.

Winkelmann, D., Geissler, W., Schneider, J., Stein, R., 2008. Dynamics and timing of the Hinlopen/Yermak Megaslide north of Spitsbergen, Arctic Ocean. Marine Geology, 250, 34-50, https://doi.org/10.1016/j.margeo.2007.11.013

4. Manuscript III

Pore structure of weak layers: Micro-CT imaging of the Finneidfjord Slide

R. Gatter, M. Clare, B.N. Madhusudhan, M.E. Vardy, K. Huhn

Manuscript in preparation for *Frontiers in Earth Sciences*

Abstract

Many studies have suggested that weak layers within the slope stratigraphy control the formation of submarine landslides; however, very little is known about their structure and composition. Although weak layers seem to be an essential pre-conditioning factor for slope failure, many questions remain unanswered, such as where with respect to weak layers do failure planes form: within the weak layer, above or below it? Many studies have relied on sedimentological and/or geotechnical sediment core and in-situ analyses to investigate weak layers; however, such techniques usually do not provide the information needed to qualitatively and quantitatively investigate weak layers. Here, we present a new approach towards weak layer investigation that is based on high-resolution micro-Computed Tomography (CT) imaging. This method allows the visualisation of the internal structure (e.g. pore space) of weak layers in 3D. Our results show a clear dependency of pore structure on the type of sediment, i.e. larger pores are typically found in coarser-grained sediments, but also a dependency on the sedimentation regime. Moreover, we show a high spatial variability of pore space on a sub-millimetre-scale. Such small-scale changes are not measurable with standard bulk geotechnical tests, which require larger sediment samples, and only give information averaged over the entire sample. The identification of such small-scale changes, however, may be crucial for the formation of weak layers, as they appear to dictate the location of the failure plane. We demonstrate the huge potential of micro-CT to investigate the weak layer structure, getting information that is not resolved and/or lost with other analytical methods.

4.1. Introduction

Submarine landslides occur in a variety of underwater slope settings worldwide (e.g. Lee et al., 2007). They are gravity-driven mass movements that range from giant landslides which involve thousands of cubic kilometres of sediment (e.g. Bugge et al., 1988; Piper et al., 1999; Vanneste et al., 2006; Georgiopoulou et al., 2010; Sun et al., 2018; Krastel et al., 2019) to smaller-scale failures of a few hundred cubic metres of sediment (e.g. Lastras et al., 2004; L'Heureux et al., 2012; Beaten et al., 2014; Kuhlmann et al., 2017; Cukur et al., 2020; Gatter et al., 2020). The socio-economic consequences of submarine landslides can be severe, especially if occurring in near coastal environments. A notable example is found offshore Finneidfjord, Norway where a submarine landslide retrogressed onshore, destroying parts of the highway and causing fatalities (Longva et al., 2003). In addition, submarine landslides are known to have caused damage to important offshore infrastructure such as equipment for the hydrocarbon industry or seafloor telecommunication cables (e.g. Fine et al., 2005; Thomas et al., 2010; Carter et al., 2014; Pope et al., 2017), they may even generate devastating and deadly tsunamis (e.g. Tappin et al., 2001; ten Brink et al., 2009; Harbitz et al., 2014).

Numerous studies have concluded that weak layers within the slope stratigraphy (in particular the sequencing of different lithologies; see Chapter 3) play an important role in the formation of submarine landslides of all scales (e.g. O'Leary, 1991; Laberg et al., 2003; Kvalstad et al., 2005; Harders et al., 2010; L'Heureux et al., 2012; Locat et al., 2014; Li et al., 2017; Urlaub et al., 2018). Stratigraphically-controlled permeability contrasts between layers (e.g. sand and clay sequencing) has been proposed as one of the key aspects to explain the formation of weak layers (e.g. L'Heureux et al., 2012; Locat et al., 2014). Excess pore pressure generation (i.e. above hydrostatic pressure) is often associated with such permeability contrasts, as the sealing capacity of low-permeability sediments may hinder the vertical dissipation of pore fluids trapped within underlying high-permeability sediments (e.g. Dugan and Sheahan, 2012). Although key to understand the ultimate failure mechanism, many aspects of weak layers remain unclear. Even in the case of one of the best studied submarine landslides, the 1996 Finneidfjord Slide, questions remain regarding the structural and compositional characteristics and the role of the weak layer in dictating failure plane location (e.g. Vardy et al., 2012; Vanneste et al., 2014).

Bulk sediment properties can be characterised using laboratory-based methods, such as oedometer, direct shear and triaxial tests. Such geotechnical tests usually require large amounts (several tens of cubic centimetres) of undisturbed sediment from sediment cores, which are often not readily available, and are expensive and challenging to acquire. Moreover, such methods primarily give information averaged over the entire sample depth, i.e. up to 10 cm. A complementary approach is therefore to visualise the pore space with emerging imaging techniques, such as high-resolution micro-CT (Computed Tomography) imaging. Micro-CT is a type of radiographic imaging technique that has been proven to be a useful tool in geosciences (Cnudde and Boone, 2013), enabling the visualisation of the pore structure of a target material in three-dimensions (3D) down to sub-micrometre resolution. In comparison to geotechnical measurements, it adds the benefit of showing individual pores, displaying their size, shape, spatial distribution and connectivity with other pores (e.g. Al-Raoush and Willson, 2005; Wildenschild and Sheppard, 2012; Bultreys et al., 2015; Shah et al., 2016; Chandrappa and Biligiri, 2018; Chung et al., 2019).

Porosity, pore size distribution and pore geometry are some of the most important material properties for the investigation of weak layers, since they influence the permeability of fluid transport through the sediment. Precisely how porosity and permeability vary across and within weak layers, however, remains unclear. In this study, we aim to address this issue and investigate whether micro-structural properties, in particular pore structure, play a role in weak layer and failure plane formation. We do this using high-resolution micro-CT imaging of undisturbed sediments that correlate stratigraphically with the previously identified weak layer of the 1996 Finneidfjord Slide, offshore Norway (e.g. L'Heureux et al., 2012; Vardy et al., 2012). We visualise and analyse pore structure of selected samples at a sub-

millimetre resolution, in order to identify, and qualitatively and quantitatively investigate pore structure changes throughout the weak layer and the background sediment. We further evaluate potential factors that may control pore structure and how changes in pore structure may influence failure plane formation. Finally, we discuss the potential and outstanding challenges in the application of micro-CT imaging for weak layer research.

4.2. The Finneidfjord Slide

The Finneidfjord Slide, which occurred in 1996, is one of several Holocene submarine landslides that have been identified along the steep slopes of Sørfjorden, Northern Norway (Fig. 4.1; Longva et al., 2003; Vardy et al., 2012; Vanneste et al., 2013). This near-shore landslide initiated along a regional weak layer before retrogressing 100 – 150 m onshore, mobilising a total volume of about 0.001 km^3 (Longva et al., 2003). The 1996 Finneidfjord Slide is one of the best studied submarine landslides, having been the focus of several previous high-resolution geological, geophysical and geotechnical investigations (e.g. Vanneste et al., 2011, 2013; 2014; L'Heureux et al., 2012; Steiner et al., 2012; Vardy et al., 2012).

As indicated by these prior studies the landslide initiated along a well-defined regional event bed that is characterised by a thin sand layer sandwiched between two clay layers that originated from a terrestrial quick clay slide (e.g. Vardy et al., 2012). The initial quick clay slide was suggested to be responsible for the lower clay, while also triggering a turbidity current that deposited the fining upwards sand (turbidite). The capping clay was interpreted as fall-out of fine-grained suspended sediments following the turbidity current (Vanneste et al., 2011).

Several factors were suggested to have contributed towards slope failure, which included the generation of excess pore pressure as a result of climatic and anthropogenic factors (e.g. Longva et al., 2003), the increase in overburden stress due to alongshore dumping of material (e.g. Vanneste et al., 2011), or the accumulation of free gas (Best et al., 2003; Morgan et al., 2012). More recent studies proposed that regional weak layers characterised by low-permeability event beds combined with periods of heavy rainfall prior to the landslide may have enabled the formation of artesian groundwater pressure, thus promoting failure (e.g. L'Heureux et al. 2012; Vardy et al., 2012).

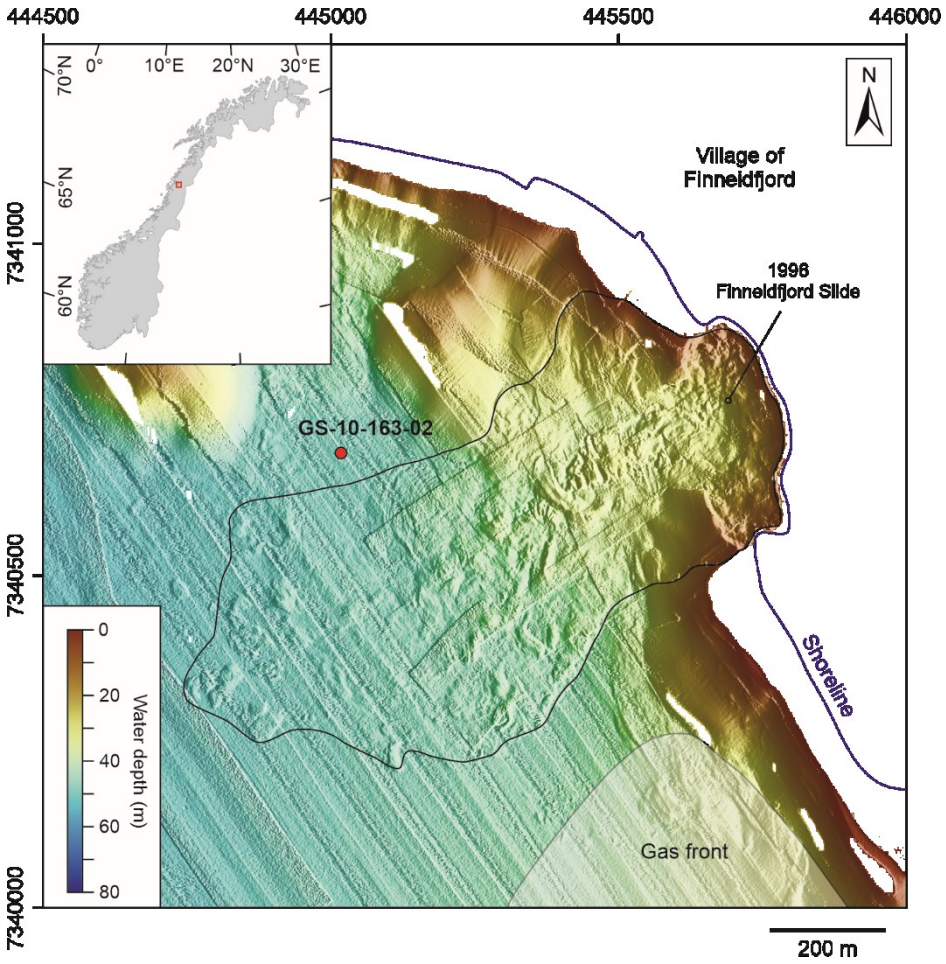

Figure 4.1. Location of the study area (red rectangle in inset image) with the 1996 Finneidfjord Slide outlined (projection in UTM Zone 33N coordinate system). Location of the Calypso piston core GS-10-163-02 is indicated by a red dot (after Vardy et al., 2012).

4.3. Materials and methods

This study focuses on the Kullenberg-Calypso piston core GS-10-163-02PC, which was collected during the 2010 R/V G.O. Sars, UiB (University of Bergen) cruise No. GS-10-163, IMR cruise No. 2010109 offshore Finneidfjord, Norway (Vanneste et al., 2011). The core targeted the undisturbed sediment sequence outside the slide area (Fig. 4.1), including those sediments that correlate stratigraphically with the regional event bed that acted as weak layer for the 1996 Finneidfjord Slide (e.g. L'Heureux et al., 2012). In order to address the previously stated research questions, five sediment sub-samples were taken from the core (see Fig. 4.2 for location) and analysed by means of high-resolution X-ray micro-Computed Tomography (micro-CT) imaging. In the following section, we outline the workflow of our study from data acquisition (Section 4.3.1) to data analysis, which includes phase segmentation (Section 4.3.2.1) and phase characterisation (Section 4.3.2.2).

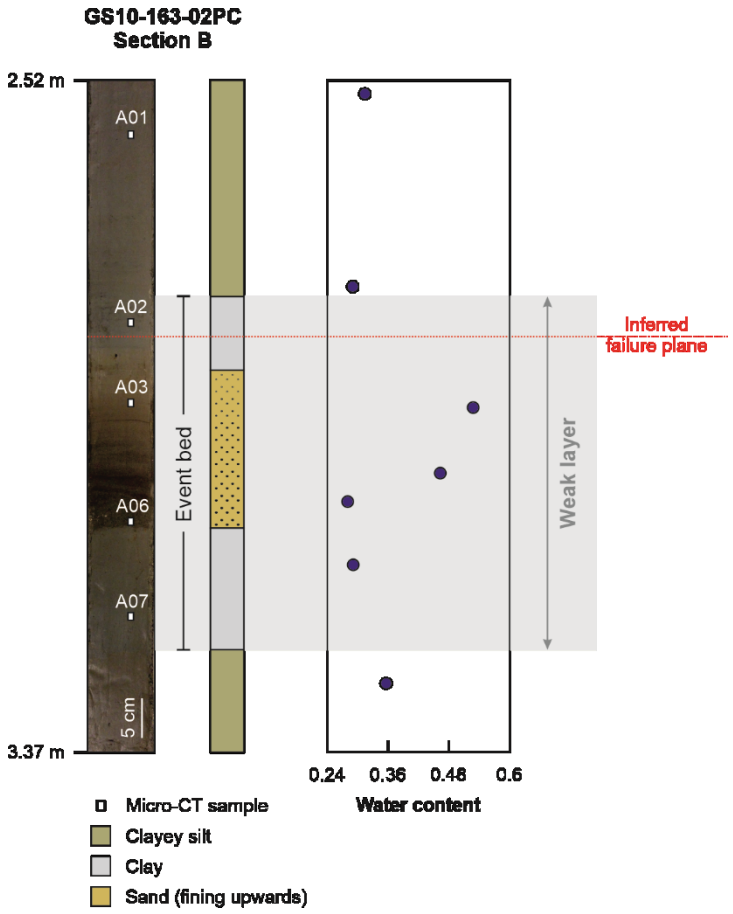

Figure 4.2. Core image and stratigraphy (as described by L'Heureux et al., 2012) of the Kullenberg-Calypso piston core GS10-163-02PC, Section B with locations of micro-CT samples indicated by white rectangles, and water content measurements (Vanneste et al., 2011) for the section. Weak layer and failure plane are outlined according to L'Heureux et al. (2012) and Vardy et al. (2012).

4.3.1. Data acquisition

4.3.1.1. Sample preparation

In total, five cylindrical samples of undisturbed sediment were taken from the piston core (Fig. 4.2). Four samples were taken from the three sub-units of the event bed, one of them from the lower clay layer, two from the fining upwards sand layer (sampling the lower coarse-grained and upper finer-grained part of the layer), and the forth from the upper clay layer. The fifth sample was taken from the background sediment, characterised as clayey silt, overlying the event bed.

The samples were taken using carbon fibre tubes (internal diameter 3 mm, height 7 mm, wall thickness 1 mm) with a cutting edge. Carbon fibre was chosen because of the material's low density, allowing X-rays to pass through without or with minimal attenuation, which makes it suitable for micro-CT imaging (i.e. transparent in scans).

4.3.1.2. Synchrotron X-ray Computed Tomography (CT)

Micro-CT imaging was performed, using monochromatic X-rays from a synchrotron source, at the TOMCAT Beamline of the Swiss Light Source (SLS), Paul Scherrer Institute, Switzerland. The technique enables discrimination between materials with different X-ray attenuation, which is a function of the material's composition (effective atomic number) and density (e.g. Cnudde and Boone, 2013). X-ray attenuation is described by the Lambert-Beer law (e.g. Phillips and Lannutti, 1997; Cnudde and Boone, 2013) that states that X-rays are attenuated as a function of the material they are propagating through, and can be used to visualise subtle changes in sediment composition (e.g. Goldfinger et al., 2012; van Daele et al., 2014; van der Bilt et al., 2021). Micro-CT is unique in the sense that it enables the 3D visualisation of the internal structure of the scanned material at a sub-micrometre resolution. This allows not only the recognition of subtle compositional changes, but also changes in sediment (pore) structure (e.g. Cnudde and Boone, 2013).

For this study, a beam energy of 21 keV and a propagation distance of 81 mm were used to scan the samples. Per sample, 1501 projections (over 180° sample rotation) were recorded with an exposure time of 200 ms. The total duration of an individual scan was 6 minutes. X-rays were converted to visible light using a Lutetium Aluminium Garnet (LuAG:Ce) scintillator, and magnified and recorded by sensitive CCD cameras (2560 x 2560 pixel, 10x objective). The projections were post-processed to generate light and dark corrected sinograms. These were in turn converted into 16-bit greyscale micro-CT volumes at a final 3D voxel resolution of 0.325 µm, using the reconstruction algorithm described by Paganin et al. (2002). Each individual 3D volume consists of 2160 individual 2D cross-sections (2560 x 2560 pixel), which are stacked together. These 2D sections are further termed cross-sectional 'images'. The procedure of data acquisition is illustrated in Fig. 4.3.

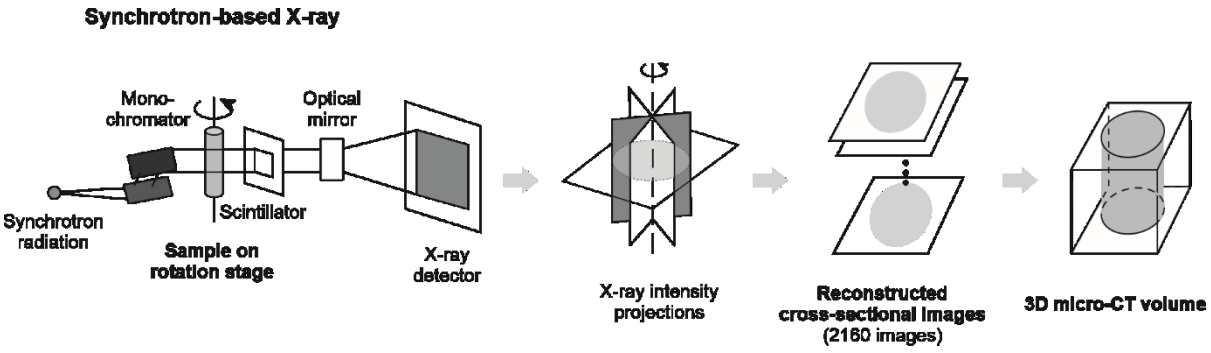

Figure 4.3. Synchrotron X-ray (micro-) CT setup (after Chung et al., 2019).

4.3.2. Data analysis

The reconstructed micro-CT data were processed with the Amira ZIB edition software, version 2021.08 (Stalling et al., 2005; http://amira.zib.de). The greyscale images of all five scanned samples were first cropped to 1730 x 1730 pixel, in order to only accommodate the window of interest, i.e. the cylindrical sample in the reconstructed, rectangular 3D micro-CT volume (Supplementary Fig. 4.A). In addition, the five 3D micro-CT volumes were resampled with the *Resample* module to 1 µm voxel resolution. This was done, because the obtained 3D volumes were too large in size for further analysis.

4.3.2.1. Phase segmentation

To differentiate pores from particles, an image segmentation was performed. This operation was used to classify the greyscale images into three different phases (termed 'labels' in Amira): the *pore* phase, i.e. apparently 'empty' pores, the *solid* phase consisting of particles, and a *mixed* phase comprising water-filled pores and small-(clay-)sized particles without distinctive particle boundaries. For the segmentation, a marker-based watershed algorithm (*Watershed* module) segmentation, was used. Markers were set with the *SegmentationEditor* by threshold segmentation (threshold values: Supplementary Tab. 4.A). To further investigate the pore structure of the samples, a segmentation of the *pore* and *matrix* labels was performed with the *RandomWalkDistanceTransformation* (threshold: 10^{-6}) and *ContourTreeSegmentation* (persistence value: 0.4 – 1) modules. For the *ContourTreeSegmentation*, a persistence value of 1 was used to analyse the connectivity of the labels of interest. Persistence values of 0.4 – 0.8 were used for an automatic segmentation of the selected labels with a separation of neighbouring pores.

4.3.2.2. Phase characterisation

The labels of interest were subsequently parameterised with the *ShapeAnalysis* and *VoxelCounter* modules (Fiji plugin for ImageJ fiji; Schindelin et al., 2012), and visualised with the *GenerateSurface* and *SurfaceView* modules. Finally, quantitative analyses were performed on the *pore* and *matrix* labels: The volume fraction of each segmented label per 3D volume was calculated for information regarding the total phase distribution of these labels. Depth-dependent changes in phase distribution were detected with porosity profiles, i.e. the area fraction of each segmented label in each 2D image. Phase size distributions were based on the count of individual phase voxel cluster (e.g. number of pores) per 3D volume. Phase connectivity was computed from the size distribution of these individual phase voxel cluster (Renard and Allard, 2013):

$$\text{Connectivity} = \frac{1}{N_v^2} \sum_{i=1}^{N_c} n_i^2 \tag{4.1}$$

where N_v is the number of voxel per phase, N_c is the number of individual cluster per phase, and n_i is the number of voxel per phase cluster i. If connectivity equals 1, all pores are connected.

4.4. Results

Five samples were taken from the sub-units of the weak layer underlying the Finneidfjord Slide and the background sediment, and analysed by means of micro-CT imaging. Sample segmentation resulted in images consisting of three phases (or labels): the *pore* phase, i.e. apparently 'empty' pores, the *mixed* phase, which consists of water-filled pores and small-(clay-)sized particles without distinctive particle boundaries, and a *solid* phase consisting of distinctive particles. 'Empty' pores and silt (larger than about 3 µm) and sand particles were clearly visible, but the discrimination between water-filled pores and fine particles (i.e. clay and fine silt, <3 µm) was difficult due to overlapping grey-values (Fig. 4.4). To avoid errors induced by subjective user interpretation, only clearly visible 'empty' pores and particles were segmented into *pore* and *solid* phase, respectively. Especially in fine-grained sediments, this may result in an overestimation of the volume fraction of water-filled pores, which could not be clearly discriminated from small-(clay)-sized particles and were combined in the *mixed* phase. When analysing the total pore structure, i.e. *pore* + *mixed* phase, this error needs to be considered (see discussion below).

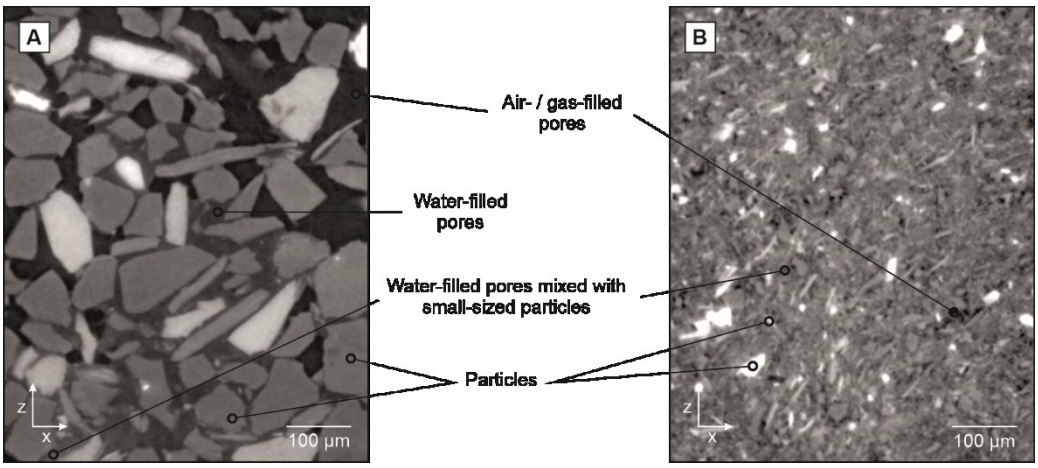

Figure 4.4. Greyscale images of **(A)** coarse-grained (sample A06) and **(B)** fine-grained (sample A07) sediments. Empty (air- or gas-filled) and water-filled pores, water-filled pores mixed with small-sized particles, and larger particles are outlined.

Representative examples of the unprocessed 3D volume and the three segmented phases for fine- and coarse-grained sediments are shown in Fig. 4.5. The *pore* and *pore* + *mixed* phases of all samples were further analysed to qualitatively and quantitatively investigate the effect of pore structure on weak layer and failure plane formation.

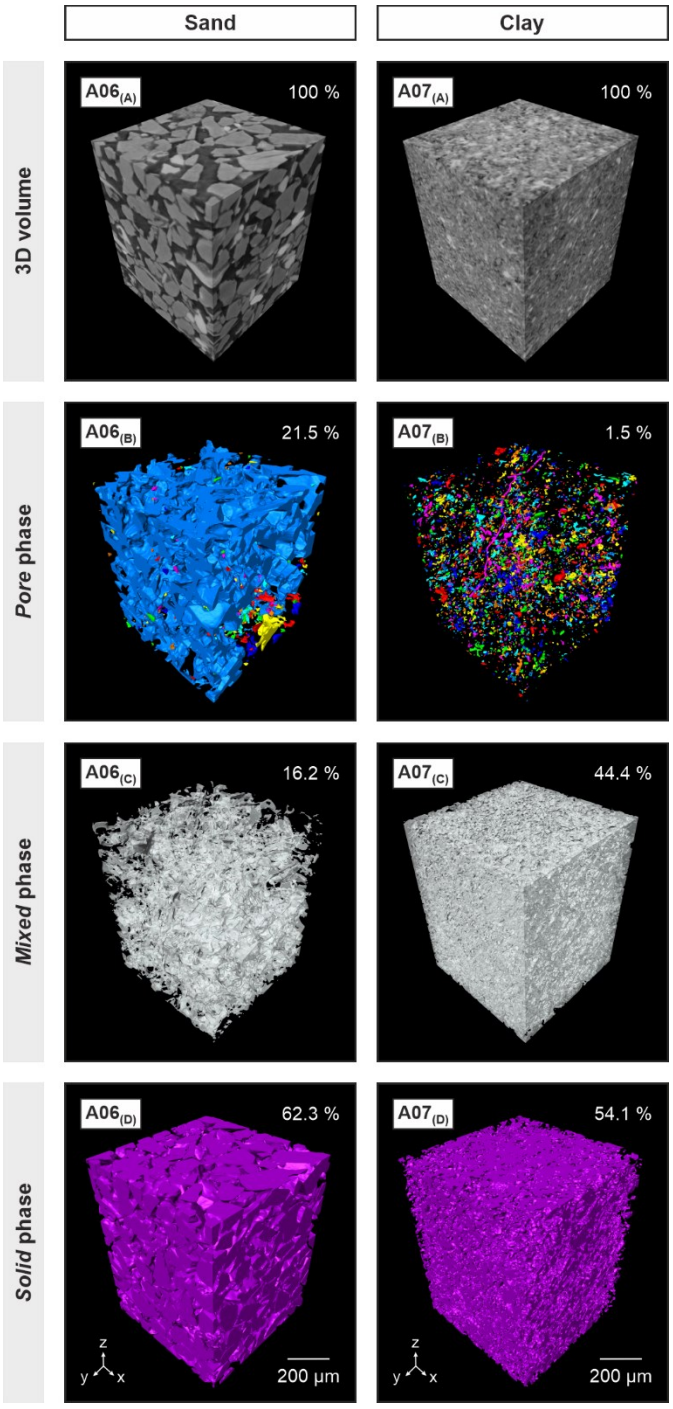

Figure 4.5. Examples of the segmented phases of sample A06, sand and sample A07, clay. **(A)** 3D micro-CT volume, **(B)** segmented *pore* phase, **(C)** segmented *mixed* phase, and **(D)** segmented *solid* phase. Volume fractions (i.e. phase distribution) of each phase are given.

4.4.1. Phase distribution

Pore phase distribution shows great variability between individual samples (Fig. 4.6). In general, volume fractions of the *pore* phase are higher in the event bed (sample A02 – A07), accounting for 1.5 % to 21.5 % of the sediment samples. The highest volume fraction of *pore* phase is found in the fining upwards sand layer of the event bed, accounting for 21.5 % and 11.6 % of sample A06 (sand) and sample A03 (here identified as clayey silt), respectively. Lower volume fractions are found in the upper and lower clays of the event bed, accounting for 2.1 % of sample A02 and 1.5 % of sample A07. The background sediment (sample A01), on the other hand, has almost no *pore* phase (0.6 %).

A similar trend is observed for the *pore* + *matrix* phase distribution. Volume fractions of the *pore* + *matrix* phase are higher within the event bed (A02 – A07) than the background sediment (A01). Sample A01 has a *pore* + *matrix* phase accounting for 20.1 %. The *pore* + *matrix* phase of the sample A03 and A06 accounts for 39.4 % and 37.7 %, respectively. Sample A02 has only a slightly lower volume fraction of 35.3 %. The highest volume fraction of *pore* + *matrix* phase is found in sample A07 and accounts for 45.9 %.

4.4.1.1. Pore size distribution

In Fig. 4.7, pore size distribution curves for the *pore* phase of all samples are shown. Larger individual pores are found in the samples taken from the fining upwards sand, A03 and A06. Overall smaller pores dominate the other three samples. Note that the smallest pore size, i.e. 1 μm^3, is governed by the resolution (1 µm voxel resolution) of the micro-CT data.

Figure 4.6. (*next page*) Phase distributions of event bed (A02, A03, A06, A07) and background (A01) sediment samples with respective volume fractions indicated. **(A)** Segmented *pore* phase, different colours represent individual pores. **(B)** Segmented *pore* + *matrix* phase, individual pores in colour, *mixed* phase in grey. **(C)** The segmented *mixed* phase is shown in grey.

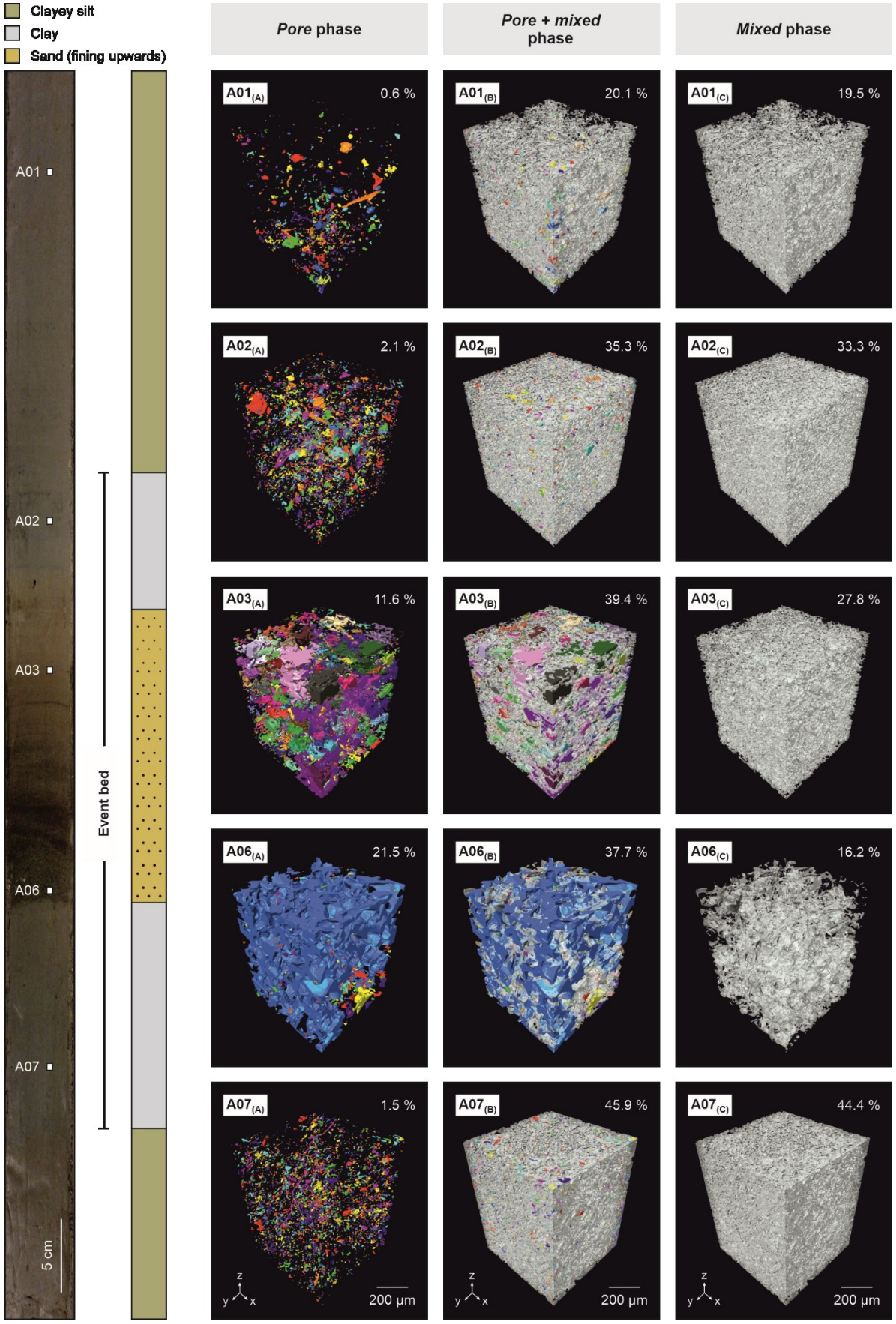
Clayey silt
Clay
Sand (fining upwards)
Pore phase
Pore + mixed phase
Mixed phase
A01
A02
A03
A06
A07
Event bed
5 cm
A01(A) 0.6 %
A01(B) 20.1 %
A01(C) 19.5 %
A02(A) 2.1 %
A02(B) 35.3 %
A02(C) 33.3 %
A03(A) 11.6 %
A03(B) 39.4 %
A03(C) 27.8 %
A06(A) 21.5 %
A06(B) 37.7 %
A06(C) 16.2 %
A07(A) 1.5 %
A07(B) 45.9 %
A07(C) 44.4 %
z
y x
200 µm

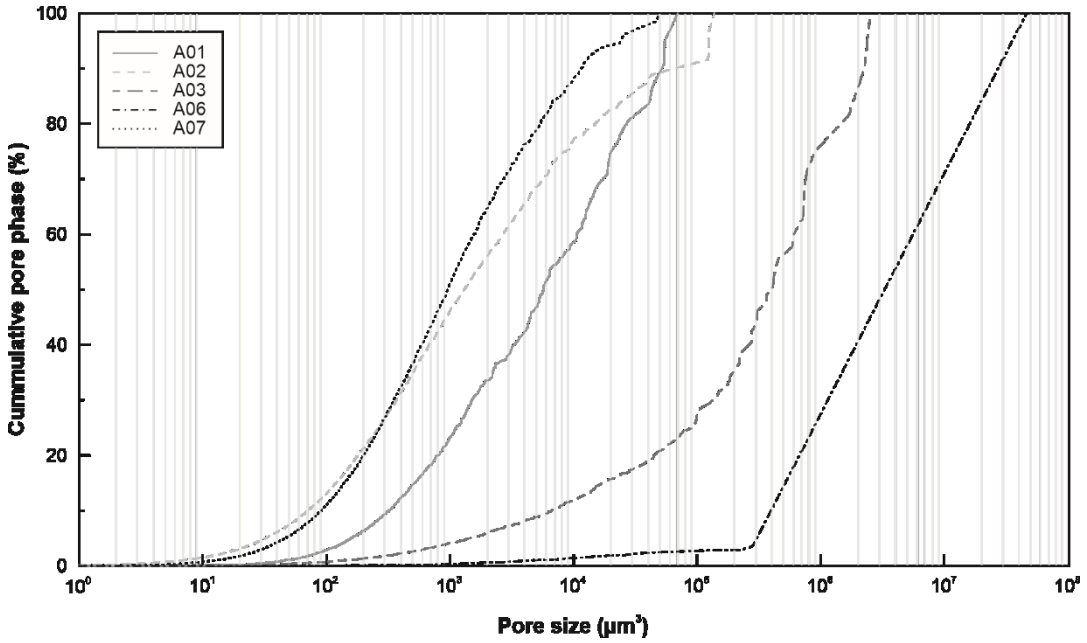

Figure 4.7. Pore size distribution curves for the *pore* phase of all samples.

4.4.1.2. Porosity

Bulk-porosity of the entire pore structure can be approximated through the *pore* + *matrix* phase distribution (see Section 4.4.1). Bulk-porosity ranges between 35.3 % and 45.9 % in the event bed and is considerably lower in the background sediment, 20.1 % (Fig. 4.6). Note that due to uncertainties in the estimates of volume fractions of the total pore space, which arise from the previously mentioned overestimation of the *mixed* phase, porosity itself could only be approximated.

In addition to differences in bulk-porosity, considerable depth-dependent changes in pore structure can be observed within all samples (Fig. 4.8A-E). These changes in pore structure are most pronounced in the background sediment (sample A01) that varies between 13 % and 33.5 % depth-dependent porosity. Sample A02 and A06 show similar depth-dependent porosity variability, ranging between about 32 % and 43 %. Porosity of A03 varies between 32.3 % and 48.6 %. The lowest variability is found in the lower clay (sample A07) with a porosity between 42.1 % and 50 %. Note that boundary artefacts seem to appear in the upper and lower part of some samples that may slightly overestimate the maximum phase volume fractions; however, to keep consistency in our workflow, we did not exclude these values.

Figure 4.8. (*next page*) Phase connectivity considering the *pore* phase (empty circles) or *pore* + *mixed* phase (filled circles) of each sample, and depth-dependent phase distribution (i.e. *pore*, *matrix* and *solid* phase) for each sample (A01-A07).

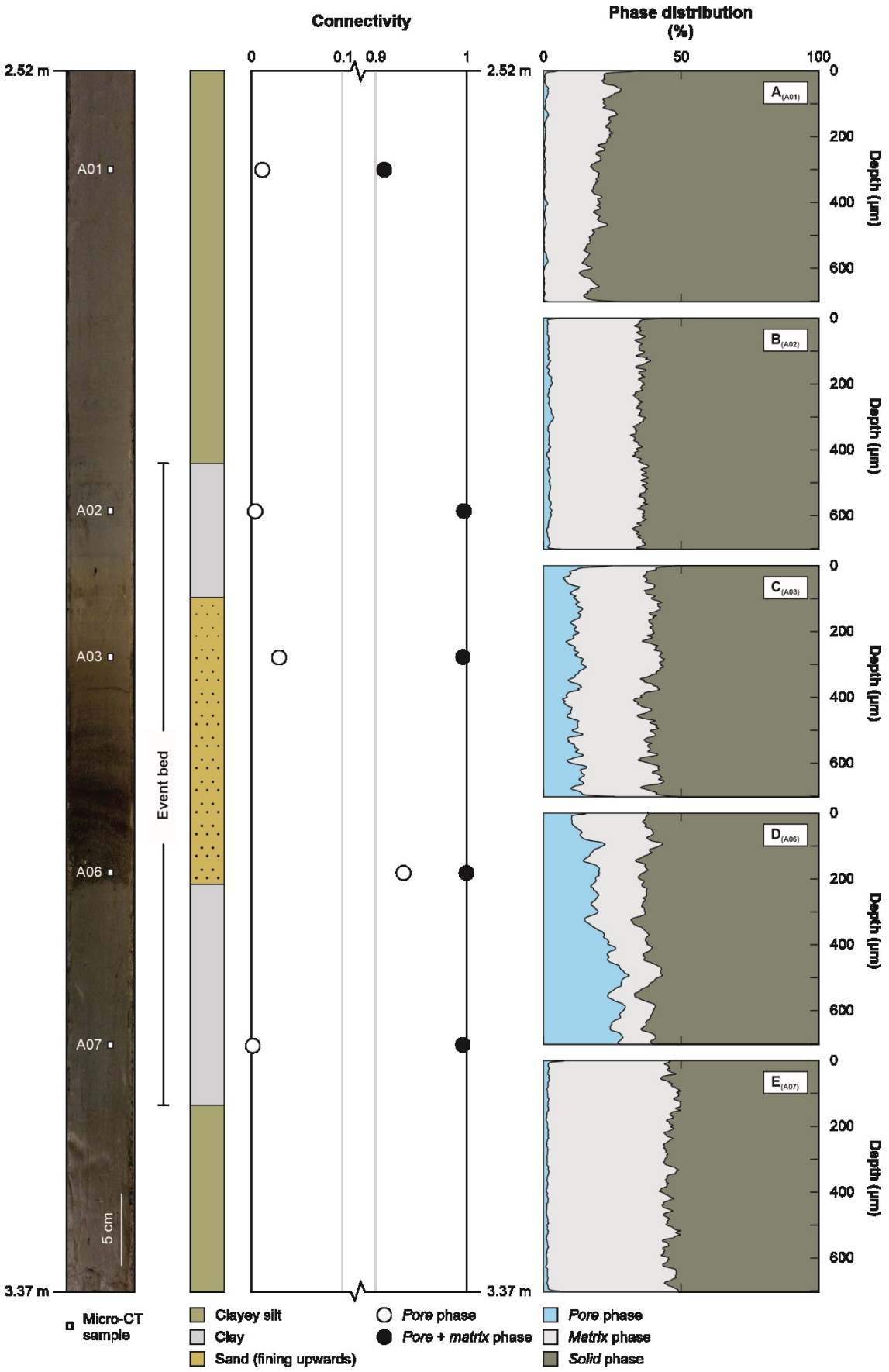
Connectivity
0
0.1
0.9
1
Phase distribution
(%)
0
50
100
2.52 m
2.52 m
3.37 m
3.37 m
A01
A02
A03
A06
A07
5 cm
Event bed
A(A01)
B(A02)
C(A03)
D(A06)
E(A07)
Depth (µm)
0
200
400
600
Micro-CT sample
Clayey silt
Clay
Sand (fining upwards)
Pore phase
Pore + matrix phase
Pore phase
Matrix phase
Solid phase

4.4.1.3. Connectivity

To approximate permeability of each sample, connectivity of the *pore* and *pore* + *matrix* phases were estimated. Connectivity is closely related to the total phase distribution (Fig. 4.6) and shows clear changes throughout the event bed and background sediment samples (Fig. 4.8). *Pore* phase connectivity exhibits the highest value of 0.93 in the sand layer (A06) and very low values of 0.004 and 0.001 in the upper and lower clay layers (A02 and A07), respectively. Connectivity of the *pore* + *matrix* phase reaches a value of almost 1 in all event bed samples (A02 – A07), but is slightly lower (0.91) in the background sediment.

4.5. Discussion

4.5.1. Pore structure changes

The micro-CT data shows clear differences in pore structure between the event bed and the background sediment. Bulk-porosity estimates of the event bed are more than 10 % higher compared to the background sediment, accounting for 35 – 46 % of the samples (Fig.4.6). Although these estimates are in good agreement with water content measurements (Fig. 4.2, e.g. Vanneste et al., 2011; L'Heureux et al., 2012), it appears that we considerably overestimate bulk-porosity of the lower clay layer. Such strong deviation between bulk-porosity and water content may result from various factors. The main error is likely related to uncertainties in the bulk-porosity estimate, which heavily relies on accurate phase segmentation. This was especially challenging for sample A07 (lower clay) and resulted in a large volume fraction of the *mixed* phase (44.4 %). In addition, although the micro-CT sample (A07) and water content measurement were taken from the same sub-unit of the event bed, they were not taken from the exact same depth in the core, but rather lie 5 cm apart (Fig. 4.2). Such deviation in sampling/measuring depth is the case for all micro-CT and water content measurements. When analysing micro-CT, which works on a sub-millimetre resolution, such differences in depth may greatly affect the reliability of the data comparison. Apart from bulk-porosity, the pore space of the weak layer also exhibits a higher degree of connectivity than the background sediment (Fig. 4.8).

Variations in pore space are not limited to the contrast between event bed and background sediments, but are also observed within the sub-units of the event bed. The main differences are related to the *pore* phase and can be largely attributed to variations in particle size, i.e. larger pores with a higher degree of connectivity are found in the sand layer of the event bed, while the clay layers are generally characterised by smaller pores that are less connected (Fig. 4.7 and 4.8). The data also highlights a considerable contrast between the two samples (A03 and A06) that were taken from the sand layer of the event bed. Our results indicate that the two samples have different lithologies, i.e. sand (A06) and clayey silt (A03), which may explain the contrasting pore structure (Fig. 4.6).

In addition, we observe considerable spatial variability in pore space within individual samples. The greatest depth-dependent changes (Fig. 4.8A-E) are observed in sample A01. The pore space has a total volume fraction of 20 %, but varies locally between 13 % and 33.5 %. Slightly smaller changes in pore space are observed in all samples, usually ranging in the order of about 10% to 15 % difference throughout the samples' depth range. Such small-scale, sub-millimetre, changes in pore structure could not be observed with other analytical methods, which require larger amounts of sediments (usually in the order of several tens of cubic-centimetres), and give an averaged value over the entire tested sample (e.g. L'Heureux et al., 2012; Steiner et al., 2012; Vanneste et al., 2013).

Another interesting observation is found in the segmented *pore* phase, which illustrates apparently 'empty' pores. That is to say that these pores are either air- or gas-filled. For coarse-grained sediments it appears reasonable to assume that pore water may have been lost during the sampling process; however, this should not have been the case for the finer-grained samples. In fine-grained samples the pores are surrounded by a dense matrix of fine-grained particles, which should hinder the loss of water during sampling. Therefore, another mechanism may be needed to explain the 'empty' pore space. One possibility is the occurrence of free gas. Seismic data indicates a shallow gas front to the southeast of the slide area (e.g. Best et al., 2003), and previous studies have suggested up to 0.05 % to 0.1 % of free gas in the pore volume (e.g. Morgan et al., 2012). Although no (macroscopic) evidence of free gas, i.e. gas bubbles, were found in the Calypso core from previous studies (e.g. L'Heureux et al., 2012), our new data suggests that small amounts of gas may be present in the sand layer of the event bed and potentially to less degree in the clay layers (Fig. 4.6 A02 – $A07_{(A)}$). Another interesting observation is the shape of individual pores. These appear to be ellipsoid-shaped pores and horizontally-aligned within the sediment samples. This may be a feature characteristic of tubridites, i.e. a result of deposition, however, to our knowledge such features have not been observed before. We are also not clear whether these structures were formed syn- or post-depositional.

4.5.2. Implications of changes in pore structure on the formation of weak layers

Our new micro-CT data show clear variations in pore space on various scales, ranging from differences in bulk-porosity between the event bed and background sediments, varying pore space in the sub-units of the event bed, to considerable spatial variability within individual samples. All of these variations may be of importance, but it appears that especially the differences and changes in pore structure found within the event bed and individual samples, may have allowed the formation of the weak layer. Vardy et al. (2012) found that failure likely initiated within the upper clay layer of the event bed, and that failure is likely related to 'weakness' within this layer, rather than a result of contrasts between the weak layer (i.e. event bed) and the background sediment. Our data support this conclusion, as we observe

noticable changes in pore structure between sample A03 (upper par of the fining upwards sand) to sample A02 (upper clay). Although we are unsure about the exact failure mechanism, it appears that local changes in pore structure may have promoted failure within the upper clay layer of the event bed. In addition, failure may have been facilitated by the horizontally-aligned pores in sample A03 and A02. Such alignment may have enabled the formation of a local permeability contrast, further promoting failure. It stands to reason that the identification of such small-scale changes may be crucial, as previous studies have suggested that even small changes may be enough to initiate failure (e.g. shear band propagation; Puzrin and Germanovich, 2005; Puzrin et al., 2016).

4.6. Conclusions

The Finneidfjord Slide offshore Norway is one of the best studied submarine landslides to date. Several studies have suggested that a regional stratified event bed acted as weak layer and pre-conditioned the slope to failure. New high-resolution synchrotron micro-CT data show that pore structure, including pore size distribution, porosity and connectivity of the pores, differs considerably between the weak layer and the background sediment. In addition, the sub-units of the event bed, which together comprise the weak layer, show great variability in pore space. This variability can be largely associated with changes in particle size, e.g. larger, more connected pores are found in the sand layer, while smaller, disconnected pores dominate the clay layers. Even more astounding, however, is the large spatial variability of the pore space within individual samples. Our findings suggest a depth-dependent variability in porosity of up to more than 20 %, over a sample that is less than a centimetre in height. To our knowledge, this is the first time such small-scale, sub-millimetre, changes in pore space have been observed in sediments that range in particle size from clay to sand. In order to overcome current limitations in the application of micro-CT, more research will be needed in terms of image processing (e.g. optimising phase segmentation). Another important aspect is data integration. In order to reliably compare micro-CT data with other datasets, measurements need to target the sediment of interest at the same depth, as we have demonstrated the great variability even within one sediment unit. Nevertheless, our results demonstrate the potential of micro-CT to both qualitatively and quantitatively investigate the micro-pore structure of weak layers. Such small-scale changes in pore structure appear to be crucial for weak layer formation, as they appear to dictate the failure plane location.

Acknowledgments

The authors thank the Paul Scherrer Institut, Villigen, Switzerland for providing synchrotron radiation beamtime at the TOMCAT Beamline of the Swiss Light Source (SLS), and all researchers and technical staff who assisted with the beam experiments that have contributed to this manuscript. We extend our appreciation to J. Titschack for providing access to his CT-Workstation and Amira, and his assistance during the micro-CT analysis. We thank the SEABED project with the Norwegian Deepwater Program for the supply of the bathymetry and water content data, as well as previous contributions. This work received funding from the European Union's Horizon 2020 research and innovation programme under the Marie Skłodowska-Curie grant agreement No. 721403.

Supplementary material

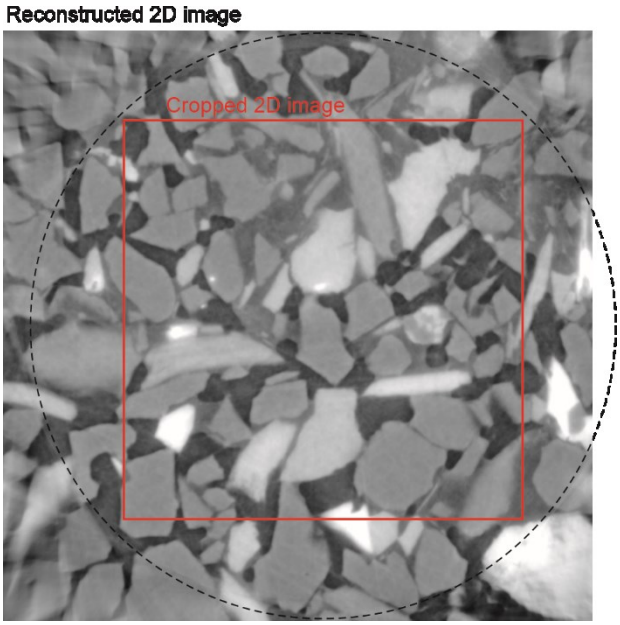

Figure 4.A. Reconstructed 2D image (2560 x 2560 px) versus cropped image (1730 x 1730 px) outlined in red. Dashed line shows the location of cylindrical sediment sample in the 2D cross-sectional image.

Table 4.A. Watershed seed thresholds

Sample ID	*Pore* phase	*Mixed* phase	*Solid* phase
A01	<11 000	15 000 – 20 000	>22 000
A02	<14 500	17 000 – 22 000	>25 500
A03	<19 000	20 000 – 23 500	>24 500
A06	<14 000	17 000 – 21 000	>27 000
A07	<16 000	20 000 – 30 000	>32 500

References

Al-Raoush, R.I., Willson, C.S., 2005. Extraction of physically realistic pore network properties from three-dimensional synchrotron X-ray microtomography images of unconsolidated porous media systems. Journal of Hydrology, 300, 44-64, https://doi.org/10.1016/j.jhydrol.2004.05.005

Baeten, N.J., Laberg, J.S., Vanneste, M., Forsberg, C.F., Kvalstad, T.J., Forwick, M., Vorren, T.O., Haflidason, H., 2014. Origin of shallow submarine mass movements and their glide planes - Sedimentological and geotechnical analyses from the continental slope off northern Norway. Journal of Geophysical Research: Earth Surface, 119: 2335-2360. Doi: 10.1002/2013JF003068.

Best, A.I., Clayton, C.R.I., Longva, O., Szuman, M., 2003. The role of free gas in the activation of submarine slides in Finneidfjord. In: Locat, J., Mienert, J. (Eds) Submarine Mass Movements and Their Consequences, Advances in Natural and Technological Hazards Research, 19, 491–498. Springer, Dordrecht.

Bugge, T., Belderson, R.H., Kenyon, N.H., 1988. The Storegga Slide. Philosophical Transactions of the Royal Society, 325: 357-388.

Bultreys, T., Van Hoorebeke, L., Cnudde, V., 2015. Multi-scale, micro-computed tomography-based pore network models to simulate drainage in heterogeneous rocks. Advances in Water Resources, 78, 36-49, https://doi.org/10.1016/j.advwatres.2015.02.003

Carter, L., Gavey, R., Talling, P.J., Liu, J.T., 2014. Insights into submarine geohazards from breaks in subsea telecommunication cables. Oceanography 27(2):58–67, http://dx.doi.org/10.5670/oceanog.2014.40

Chandrappa, A.K., Biligiri, K.P., 2018. Pore Structure Characterization of Pervious Concrete Using X-Ray Microcomputed Tomography. Journal of Materials in Civil Engineering, 30(6), 04018108, https://doi.org/10.1061/(ASCE)MT.1943-5533.0002285

Chung, SY., Kim, JS., Stephan, D., Han, TS., 2019. Overview of the use of micro-computed tomography (micro-CT) to investigate the relation between the material characteristics and properties of cement-based materials. Construction and Building Materials, 229, 116843, https://doi.org/10.1016/j.conbuildmat.2019.116843

Cnudde, V., Boone, M.N., 2013. High-resolution X-ray computed tomography in geosciences: A review of the current technology and applications. Earth-Science Reviews, 123, 1-17, https://doi.org/10.1016/j.earscirev.2013.04.003

Cukur, D., Um, IK., Chun, JH., Lee, GS., Kim, SR., Bahk, JJ., Urgeles, R., Horozal, S., 2020. Factors leading to slope failure on a sediment-starved margin: The southwestern continental margin of the East Sea, Korea. Marine Geology, 428: 106282, https://doi.org/10.1016/j.margeo.2020.106282

Dugan, B., Sheahan, T.C., 2012. Offshore sediment overpressures of passive margins: mechanisms, measurement, and models. Review in Geophysics, 50: RG3001, https://doi.org/10.1029/2011RG000379

Fine, I.V., Rabinovich, A.B., Bornhold, B.D., Thomson, R.E., Kulikov, E.A., 2005. The Grand Banks landslide-generated tsunami of November 18, 1929: preliminary analysis and numerical modeling. Marine Geology, 215: 45-57, https://doi.org/10.1016/j.margeo.2004.11.007

Gatter, R., Clare, M.A., Hunt, J.E., Watts, M., Madhusudhan, B.N., Talling, P.J., Huhn, K., 2020. A multi-disciplinary investigation of the AFEN Slide: The relationship between contourites and submarine landslides. Geological Society, London, Special Publications, 500: 173-193, https://doi.org/10.1144/SP500-2019-184

Georgiopoulou, A., Masson, D.G., Wynn, R.B., Krastel, S., 2010. Sahara Slide: Age, initiation, and processes of a giant submarine slide. Geochemistry, Geophysics, Geosystems, 11(7): Q07014, https://doi.org/10.1029/2010GC003066

Goldfinger, C., Nelson, C.H., Morey, A.E., Johnson, J.R., Patton, J., Karabanov, E., Gutierrez-Pastor, J., Eriksson, A.T., Gracia, E., Dunhill, G., Enkin, R.J., Dallimore, A., Vallier, T., 2012. Turbidite event history–methods and implications for Holocene paleoseismicity of the Cascadia subduction zone.U.S. Geological Survey Professional Paper, 1661–F, pp. 170, http://pubs.usgs.gov/pp/pp1661/f.

Harbitz, C.B., Løvholt, F., Bungum, H., 2014. Submarine landslide tsunamis: how extreme and how likely?. Natural Hazards, 72: 1341-1374.

Harders, R., Kutterolf, S., Hensen, C., Moerz, T., Brueckmann, W., 2010. Tephra layers: A controlling factor on submarine translational sliding?. Geochemistry, Geophysics, Geosystems, 11(5): Q05S23, https://doi.org/10.1029/2009GC002844

Krastel, S., Urlaub, M., Georgiopoulou, A., Wynn, R.B., Schwenk, T., Stevenson, C., Feldens, P., 2019. Mass wasting along the NW African continental margin. In: Lintern, D.G., Mosher, D.C., Moscardelli, L.G., Bobrowsky, P.T., Campbell, C., Chaytor, J.D., Clague, J.J., Georgiopoulou, A., Lajeunesse, P., Normandeau, A., Piper, D.J.W., Scherwath, M., Stacey, C., Turmel, D. (Eds) Subaqueous Mass Movements. Geological Society, London, Special Publications, 477: 151-167, https://doi.org/10.1144/SP477.36

Kuhlmann, J., Asioli, A., Trincardi, F., Klügel, A., Huhn, K., 2017. Landslide Frequency and Failure Mechanisms at NE Gela Basin (Strait of Sicily). Journal of Geophysical Research: Earth Surface, 122: 2223-2243, https://doi.org/10.1002/2017JF004251

Kvalstad, T.J., Andresen, L., Forsberg, C.F., Berg, K., Bryn, P., Wangen, M., 2005. The Storegga slide: evaluation of triggering sources and slide mechanics. Marine and Petroleum Geology, 22: 245-256, https://doi.org/10.1016/j.marpetgeo.2004.10.019

L'Heureux, JS., Longva, O., Steiner, A., Hansen, L., Vardy, M.E., Vanneste, M., Haflidason, H., Brendryen, J., Kvalstad, T.J., Forsberg, C.F., Chand, S., Kopf, A., 2012. Identification of Weak Layers and Their Role for the Stability of Slopes at Finneidfjord, Northern Norway. In: Yamada, Y., Kawamura, K., Ikehara, K., Ogawa, Y., Urgeles, R., Mosher, D., Chaytor, J., Strasser, M. (Eds.) Submarine Mass Movements and Their Consequences, Advances in Natural and Technological Hazards Research, 5th International Symposium, 321-330. Springer Netherlands.

Laberg, J.S., Vorren, T.O., Mienert, J., Haflidason, H., Bryn, P., Lien, R., 2003. Preconditions leading to the Holocene Trænadjupet Slide offshore Norway. In: Locat, J., Mienert, J. (Eds) Submarine Mass Movements and Their Consequences, Natural and Technological Hazards Research, 1st International Symposium, 247-254, Springer Netherlands, Dordrecht.

Lastras, G., Canals, M., Urgeles, R., De Batist, M., Calafat, A.M., Casamor, J.L., 2004. Characterisation of the recent BIG'95 debris flow deposit on the Ebro margin, Western Mediterranean Sea, after a variety of seismic reflection data. Marine Geology, 213: 235-255, https://doi.org/10.1016/j.margeo.2004.10.008

Lee, H.J., Locat, J., Desgagnés, P., Parsons, J.D., McAdoo, B.G., Orange, D.L., Puig, P., Wong, F.L., Dartnell, P., Boulanger, E., 2007. Submarine mass movements on continental margins. In: Nittouer, C.A., Austin, J.A., Field, M.E., Kravitz, J.H., Syvitski, J.P.M., Wiberg, P.L. (Eds) Continental Margin Sedimentation: From Sediment Transport to Sequence Stratigraphy, 213-274. Blackwell Publishing Ltd, Oxford, UK, https://doi.org/10.1002/9781444304398.ch5

Li, W., Alves, T.M., Urlaub, M., Georgiopoulou, A., Klaucke, I., Wynn, R.B., Gross, F., Meyer, M., Repschläger,J., Berndt, C., Krastel, S., 2017. Morphology, age and sediment dynamics of the upper headwall of the Sahara Slide Complex, Northwest Africa: Evidence for a large Late Holocene failure. Marine Geology, 393: 109-123.

Locat, J., Leroueil, S., Locat, A., Lee, H., 2014. Weak Layers: Their Definition and Classification from a Geotechnical Perspective. In: Krastel, S., Behrmann, JH., Völker, D., Stipp, M., Berndt, C., Urgeles, R., Chaytor, J., Huhn, K., Strasser, M., Harbitz, C.B. (Eds) Submarine Mass Movements and Their Consequences, Advances in Natural and Technological Hazards Research, 37:3-12, Springer International Publishing Switzerland.

Longva, O., Janbu, N., Blikra, L.H., Bøe, R., 2003. The 1996 Finneidfjord Slide; Seafloor Failure and Slide Dynamics. In: Locat, J., Mienert, J. (Eds) Submarine Mass Movements and Their Consequences, Advances in Natural and Technological Hazards Research, 19, 531-538. Springer, Dordrecht.

Morgan, E.C., Vanneste, M., Lecomte, I., Baise, L.G., Longva, O., McAdoo, B., 2012. Estimation of free gas saturation from seismic reflection surveys by the genetic algorithm inversion of a P-wave attenuation model. Geophysics, 77(4), R175-R187, https://doi.org/10.1190/geo2011-0291.1

O'Leary, D.W., 1991. Structure and morphology of submarine slab slides: Clues to origin and behaviour. Marine Geotechnology, 10(1-2): 53-69, https://doi.org/10.1080/10641199109379882

Paganin, D., Mayo, S.C., Gureyev, T.E., Miller, P.R., Wilkins, S.W., 2002. Simultaneous phase and amplitude extraction from a single defocused image of a homogeneous object. Journal of Microscopy, 203, 33-40, https://doi.org/10.1046/j.1365-2818.2002.01010.x

Phillips, D.H., Lannutti, J.J., 1997. Measuring physical density with X-ray computed tomography. NDT&E International, 30(6), 339-350, https://doi.org/10.1016/S0963-8695(97)00020-0

Piper, D.J.W., Cochonat, P., Morrison, M.L., 1999. The sequence of events around the epicentre of the 1929 Grand Banks earthquake: initiation of debris flows and turbidity current inferred from sidescan sonar. Sedimentology, 46: 79-97, https://doi.org/10.1046/j.1365-3091.1999.00204.x

Pope, E.L., Talling, P.J., Carter, L., 2017. Which earthquakes trigger damaging submarine mass movements: Insights from a global record of submarine cable breaks?. Marine Geology, 384(1): 131-146, https://doi.org/10.1016/j.margeo.2016.01.009

Puzrin, A.M., Germanovich, L.N., 2005. The growth of shear bands in the catastrophic failure of soils. Proceedings of The Royal Society, 461, 1199-1228, https://doi.org/10.1098/rspa.2004.1378

Puzrin, A.M., Germanovich, L.N., Friedli, B., 2016. Shear band propagation analysis of submarine slope stability. Géotechnique, 66(3), 188-201, https://doi.org/10.1680/jgeot.15.LM.002

Renard, P., Allard, D., 2013. Connectivity metrics for subsurface flow and transport. Advances in Water Resources, 51, 168-196, https://doi.org/10.1016/j.advwatres.2011.12.001

Schindelin, J., Arganda-Carreras, I., Frise, E., Kaynig, V., Longair, M., Pietzsch, T., Preibisch, S., Rueden, C., Saalfeld, S., Schmid, B., Tinevez, JY., White, D.J., Hartenstein, V., Eliceiri, K., Tomancak, P., Cardona, A., 2012. Fiji: an open-source platform for biological-image analysis. Nature Methods, 9, 676-682, https://doi.org/10.1038/nmeth.2019

Shah, S.M., Gray, F., Crawshaw, J.P., Boek, E.S., 2016. Micro-computed tomography pore-scale study of flow in porous media: Effect of voxel resolution. Advances in Water Resources, 95, 276-287, https://doi.org/10.1016/j.advwatres.2015.07.012

Stalling, D., Westerhoff, M., Hege, HC., 2005. 38 – Amira: A Highly Interactive System for Visual Data Analysis. In: Hansen, C.D., Johnson, C.R. (Eds) Visualization Handbook, 749-767. Butterworth-Heinemann, Burlington.

Steiner, A., L'Heureux, JS., Kopf, A., Vanneste, M., Longva, O., Lange, M., Haflidason, H., 2012. An In-Situ Free-Fall Piezocone Penetrometer for Characterizing Soft and Sensitive Clays at Finneidfjord (Northern Norway). In: Yamada, Y., Kawamura, K., Ikehara, K., Ogawa, Y., Urgeles, R., Mosher, D., Chaytor, J., Strasser, M. (Eds.) Submarine Mass Movements and Their Consequences, Advances in Natural and Technological Hazards Research, 5th International Symposium, 99-109. Springer Netherlands.

Sun, Q., Cartwright, J., Xie, X., Lu, X., Yuan, S., Chen, C., 2018. Reconstruction of repeated Quaternary slope failures in the northern South China Sea. Marine Geology, 401: 17-35.

Tappin, D.R., Watts, P., McMurtry, G.M., Lafoy, Y., Matsumoto, T., 2001. The Sissano, Papua New Guinea tsunami of July 1998 – offshore evidence on the source mechanism. Marine Geology, 175(1-4):1-23, https://doi.org/10.1016/S0025-3227(01)00131-1

ten Brink, U.S., Lee, H.J., Geist, E.L., Twitchell, D., 2009. Assessment of tsunami hazard to the U.S. East Coast using relationships between submarine landslides and earthquakes. Marine Geology, 264(1-2): 65-73, https://doi.org/10.1016/j.margeo.2008.05.011

Thomas, S., Hooper, J., Clare, M., 2010. Constraining Geohazards to the Past: Impact Assessment of Submarine Mass Movements on Seabed Developments. In: Mosher, D.C., Shipp, C., Moscardelli, L., Chaytor, J., Baxter, C., Lee, H., Urgeles, R. (Eds) Submarine Mass Movements and Their Consequences, Advances in Natural and Technological Hazards Research, 28: 387-398. Springer Netherlands.

Urlaub, M., Geersen, J., Krastel., S., Schwenk, T., 2018. Diatom ooze: Crucial for the generation of submarine mega-slides?. Geology, 46(4): 331-334. Doi: 10.1130/G39892.1, https://doi.org/10.1130/G39892.1

Van Daele, M., Cnudde, V., Duyck, P., Pino, M., Urrutia, R., De Batist, M., 2014. Multidirectional, synchronously-triggered seismo-turbidites and debrites revealed by X-ray computed tomography (CT). Sedimentology, 61, 861-880, https://doi.org/10.1111/sed.12070

Van der Bilt, W.G.M., Cederstrøm, J.M., Støren, E.W.N., Berben, S.M.P., Rutledal, S., 2021. Rapid Tephra Identification in Geological Archives With Computed Tomography: Experimental Results and Natural Applications. Frontiers in Earth Science, 8, 622386, https://doi.org/10.3389/feart.2020.622386

Vanneste, M., Forsberg, C.F., Kvalstad, T.J., L'Heureux, JS., Longva, O., Chand, S., Rise, L., Vardy, M.E., Brendryen, J., Haflidason, H., Lecomte, I., 2011. C-Dog: Coastal and Deepwater Offshore Geohazards. Report to NDP/SEABED, 20100125-1, 66.

Vanneste, M., Longva, O., L'Heureux, JS., Vardy, M.E., Morgan, E., Forsberg, C.F., Kvalstad, T.J., Strout, J.M., Brendryen, J., Haflidason, H., Lecomte, I., Steiner, A., Kopf, A., Mörz, T., Kreiter, S., 2013. Finneidfjord, a Field Laboratory for Integrated Submarine Slope Stability Assessments and Characterization of Landslide-Prone Sediments: A Review. Offshore Technology Conference, OTC 13OTC-P-686-OTC, Huston, Texas, USA.

Vanneste, M., Mienert, J., Bünz, S., 2006. The Hinlopen Slide: A giant, submarine slope failure on the northern Svalbard margin, Arctic Ocean. Earth and Planetary Science Letters, 245: 373-388. Doi: 10.1016/j.epsl.2006.02.045

Vanneste, M., Sultan, N., Garziglia, S., Forsberg, C.F., L'Heureux, JS., 2014. Seafloor instabilities and sediment deformation processes: The need for integrated, multi-disciplinary investigations. Marine Geology, 352: 183-214, https://doi.org/10.1016/j.margeo.2014.01.005

Vardy, M.E, L'Heureux, JS., Vanneste, M., Longva, O., Steiner, A., Forsberg, C.F., Haflidason, H., Brendryen, J., 2012. Multidisciplinary investigation of a shallow near-shore landslide, Finneidfjord, Norway. Near Surface Geophysics, 10, 267-277, https://doi.org/10.3997/1873-2012022

Wildenschild, D., Sheppard, A.P., 2012. X-ray imaging and analysis techniques forquantifying pore-scale structure and processes in subsurface porous mediumsystems. Advances in Water Resources 51, 217–246.

5. Conclusions and future work

5.1. Main conclusions

Submarine landslides have been identified to pose a significant hazard to coastal communities as they can generate powerful tsunamis and threaten critical seafloor infrastructure. Even though understanding of submarine landslides is critical for successful risk assessments and the implementation of risk mitigation strategies, their often-remote location makes their investigation difficult. Weak layers play a key role in dictating where failure occurs; however, their structure and composition, as well as the processes that control and form weak layers are still poorly understood.

This doctoral thesis aims to qualitatively and quantitatively assess the role of sediment structure and composition on the formation of weak layers, and their control on failure plane localisation. A thorough literature review (Chapter 2) summarises the current state of knowledge regarding weak layers and their effect on submarine landslide formation. The review sets out to identify the types of sediment that are capable of forming weak layers and further investigates their global variability, linking different types of weak layers to specific environmental settings. Two case studies, the AFEN and Finneidfjord Slides, were selected to examine the environmental effect (e.g. different sedimentation regimes) on the properties of weak layers and how they may influence the failure mechanism. These case studies were chosen, because sediment cores are available and failure planes can be or are well constrained. In the first case study (AFEN Slide; Chapter 3), physical properties and geochemical core-log, particle size distribution, and geotechnical data were integrated to identify and investigate the failure plane and potential weak layer of the landslide. The weak layer of the second case study (Finneidfjord Slide; Chapter 4) was investigated by means of high-resolution micro-CT imaging. The different scales and resolution of the datasets provide a diverse view on weak layers, and allow to address the main research hypotheses (as outlined in Chapter 1.2):

(1) Weak layers coincide with prominent sediment horizons within the slope stratigraphy, but distinct lithological contrasts control the formation of weak layers and dictate where failure planes form.

Understanding why some areas fail while adjacent areas do not is crucial for submarine landslide risk assessment and mitigation strategies. Nowadays, the concept of weak layers playing a key role in dictating the location and depth of submarine landslides is widely accepted. Although most conceptual models of submarine landslides assume that slope failure initiates along weak layers, the compositional characteristics of weak layers, as well as the processes that control and form them remain poorly understood.

In Chapter 2, we present a new global submarine landslide catalogue that comprises 60 case studies in order to assess which types of sediment are capable of forming weak layers and to investigate their global distribution. Our results show that failure planes usually form in the vicinity of an interface between distinct lithologies (i.e. sediment sequences). The sedimentology of these sequences can be diverse and ranges from siliciclastic (sand-clay or clay-clay) to volcaniclastic (e.g. ash-clay) and fossiliferous (e.g. diatom-clay) sediments. Such sediment sequences appear to be prone to failure due to their capability of forming permeability contrasts, which in turn enable the generation of transient pore pressures, and their often-contrasting strength properties allow focused shearing and failure plane formation.

A classification of weak layers based on their lithology has two main advantages. First, it is reasonable to assume that different types of lithologies will show an affinity to specific environmental settings. Therefore, we can infer likely locations of different types of weak layers, e.g. distinct permeability interfaces related to siliciclastic sediment sequences are typically found in contourite or turbidite systems, fossiliferous sediments dominate areas of high productivity or upwelling regions, and regions that experience repeated ash deposition will favour the formation of volcaniclastic weak layers. Second, potential weak layer lithologies may be recognised from sediment cores. In combination with information regarding the environmental setting (e.g. current regime, sedimentation pattern, tectonic activity, etc.) and further characterisation of the sediments based on Locat et al. (2014)'s geotechnical classification may allow the identification of potential weak layers pre-failure.

Our new global submarine landslide catalogue provides much needed information regarding the different types of weak layers and their global variability; however, it also highlights the current scarcity of adequate data for weak layer research. Many studies focus on large-scale geophysical data alone as sediment cores, especially those sampling the undisturbed sediment sequence, are rare (see discussion Chapter 5.2). Future advances in the field of weak layer research will, therefore, depend on the collection of additional sediment cores, and detailed sedimentological, geochemical and geotechnical analyses of these cores.

(2) Weak layers are formed as a result of various processes, but the type and distribution of weak layers is controlled by the environmental setting.

Knowing the location of (future) submarine landslides is important, but in order to mitigate submarine landslide hazard successfully, we also need to know the ultimate cause of slope failure. Most of the time, it appears that a combination of various pre-conditioning factors and failure mechanisms is needed to cause slope failure; however, the recognition of these factors, pre-failure, and the relative contribution of individual factors towards slope failure are still subject to debate. We discussed how different types

of weak layers that are linked to lithology, show an affinity to different geographic and physiographic regions. In addition, it is reasonable to assume that different types of weak layers will fail under different conditions (i.e. failure mechanisms). Failure mechanisms depend on the type of sediment, especially its geotechnical properties, as well as the acting triggering mechanism, e.g. seismic shaking may cause liquefaction, while slope under-cutting is often linked to progressive failure by strain softening. Triggering mechanisms in turn also vary in different environmental settings. For example, regions known for high tectonic activity will be more prone to earthquake shaking, while in other areas, virtually all possible triggering mechanisms may occur. Therefore, knowledge about the type of weak layer is crucial, as it may be used in combination with information regarding the regional setting to identify potential triggering and ultimately, failure mechanisms.

To investigate this relationship, two case studies, the AFEN Slide (Chapter 3) and the Finneidfjord Slide (Chapter 4), were analysed. The 1996 coastal Finneidfjord Slide offshore Norway is one of the best studied submarine landslides to date. One of the main factors that contributed to slope failure is the occurrence of a regional, turbidite event bed (i.e. weak layer) that contains alterations of clays and sand (clay-sand-clay sequence; e.g. L'Heureux et al., 2012). Several potential failure mechanisms have been discussed, including excess pore pressure generation due to fluid flow, accumulation of free gas or liquefaction, as well as strain softening of the sensitive upper clay unit (e.g. Best et al., 2003; Longva et al., 2003; L'Heureux et al., 2012, Vardy et al., 2012; Morgan et al., 2012). Most recent studies have concluded that the permeability contrast between the upper clay and sand layer within the event bed caused failure due to artesian groundwater pressure and strain softening of the overlying clay (L'Heureux et al., 2012; Vardy et al., 2012). The AFEN Slide, on the other hand, was suggested to have failed due to liquefaction of well-sorted contourite sands or silt layer, or due to progressive failure of geotechnical sensitive clays (Wilson et al., 2004; Madhusudhan et al., 2017). These hypotheses, however, could not be confirmed as none of the previously analysed sediment cores sampled the undisturbed sediments. In Chapter 3, we present data from a new sediment core that sampled the undisturbed sediments that correlate stratigraphically with the inferred failure plane of the slide. In contrast to previous studies, we found that the AFEN Slide initiated along a distinct, climatically-induced, lithological interface within the slope stratigraphy. This interface correlates with the base of a sandy (contourite) layer, overlying a relatively homogeneous silty clay unit. Although our results do not allow a final conclusion regarding the failure mechanism, we demonstrate a clear difference between the two case studies. While slope failure offshore Finneidfjord appears to be governed by distinct permeability contrasts within a sand-clay sequence, failure of the AFEN Slide may rather be caused by distinct strength contrasts between the softer clay and the overlying sandy layer. In addition, we highlight the importance of integrating information from all different scales, ranging from small-scale

high-resolution core analyses to the understanding of the regional oceanographic setting, in order to understand submarine landslide hazard. Integrating core analyses of the AFEN Slide with our knowledge about the current regime prevailing in the Faroe–Shetland Channel for the last 18 ka, we demonstrate that climate change may have preconditioned the location of failure initiation.

(3) For the identification and characterisation of failure planes and weak layers integration of various datasets is critical, but especially high-resolution (sub-millimetre-scale) datasets are needed to assess their structure.

The robust investigation and characterisation of weak layers and their controlling factors heavily depend on the availability of sediment cores and in-situ measurements that sample relevant sediments, i.e. the undisturbed sediments that correlate stratigraphically with the failure plane. Such data, however, are usually rare (Chapter 2). In addition, it is of critical importance to combine various sampling (i.e. coring and in-situ measurements) and analytical (e.g. sedimentological, geochemical and geotechnical) methods to identify failure planes and investigate weak layers. Nevertheless, even if such integrated datasets are available, they usually do not provide the information necessary to characterise weak layers in terms of their structure and it remains unclear precisely where failure planes form in relation to such weak layers and why (Chapter 3). High-resolution imaging techniques, such as micro-Computed Tomography, may allow to answer such questions, as they enable the visualisation of structures (and processes) that cannot be resolved with conventional sedimentological or geotechnical analyses.

In Chapter 4, micro-CT is used to investigate the weak layer of the Finneidfjord Slide. We find that pore space distribution is highly spatially variable and that such high variability is usually masked by bulk porosity measurements. Recognition of such small-scale (sub-millimetre) local changes in sediment structure, however, appears to play a key role in dictating where failure planes form. It is, therefore, of critical importance to be able to resolve such small-scale changes.

Although important for the characterisation of the micro-structure of weak layers, we also need to be aware of the method's limitations. Micro-CT cannot be used as a stand-alone method. It heavily relies on supplementary data from other analytical methods (e.g. porosity and water content measurements, or geochemical characterisation of the scanned sediment samples) for proper validation of the results. Another prerequisite for the application of micro-CT is the knowledge about the location of the weak layer in order to sample layers of interest. Nevertheless, it is a method with great potential that should be integrated in submarine landslide, and especially weak layer research.

5.2. Implications for future weak layer research

This section aims to use the lessons learned from Chapters 2 – 4 to summarise current limitations and challenges in, as well as outline directions for, future weak layer research.

5.2.1. Current limitations and challenges in weak layer research

A reliable investigation and characterisation of weak layers in a submarine landslide setting depends on their accurate identification, their recovery during sediment coring and careful sampling, as well as the choice of analytical methods. In addition to inherent uncertainties of applied methods and acquired data, this task faces a multitude of challenges related to issues such as spatial resolution, data correlation, and sampling bias, as well as sampling quality and quantity. In the following sub-sections, I outline the main challenges and limitations encountered when attempting to identify failure planes and characterise weak layers, and discuss some of the main reasons for these limitations.

5.2.1.1. Identification of weak layers: The importance of spatial resolution and data migration

Where is the failure plane located? The answer to this seemingly simple question is a requisite for successful sampling and analysis of weak layers – and involves many challenges. The accuracy in the positional delineation of failure planes strongly depends on the resolution, precision and integration of datasets of different scales, namely acoustic imaging and geophysical borehole or core logging data.

A major problem in this context is one of resolution: Weak layers often act on decimetre- to sub-decimetre-scales (e.g. L'Heureux et al., 2012; Sammartini et al., 2018; Gatter et al., 2020), but can be buried beneath tens to hundreds of metres of sediment and water. In order to identify and trace the spatial extent of failure planes and weak layers, we rely heavily on acoustic methods that have to compromise between penetration depth and vertical resolution. Both are inversely correlated and strongly depend on the deployed tools (Tab. 5.1), as well as the type of sediment imaged. Sub-bottom profilers (e.g. Chirp-type systems), for example, may reach a vertical resolution of <0.05 m, but have a very limited penetration depth (<tens of metres), especially in thicker, sandy or over-consolidated sediments (e.g. Penrose et al., 2005). Such very-high-resolution datasets are therefore generally not suitable for investigating the failure planes and weak layers of large submarine landslides, as they fail to image the deeper sediment strata. Seismic reflection profiles, on the other hand, routinely reach penetration depths of hundreds of metres, but have a much lower vertical resolution (e.g. Judd and Hovland, 1992). Most of these datasets work on a metre-scale, a magnitude below that of weak layers, and thus may fail to accurately image thin weak layers, causing errors in their depth estimates or entirely failing to image them (e.g. Widess, 1982). In addition, the presence of gaseous sediments may mask the reflection from underlying layers as they scatter acoustic energy, effectively limiting the penetration depth (e.g. Judd and Hovland, 1992; Fleischer et al., 2001). This may result in a significant vertical error in the failure plane delineation when using acoustic imaging alone.

Another challenge is that of data integration: Since acoustic imaging is a function of the travel-time of the emitted signal, we need to convert this time-based measurement to depth in order to enable integration with recovered core material or in-situ measurement methods. This time-depth conversion requires additional information on the velocity of acoustic signals within both the water and sedimentary strata. Ideally, this information is derived from in-situ borehole logging, which provides the means of precisely relating lithological layers in the recovered core material to the acoustic record. Its near-continuous records have been found to considerably enhance the accuracy of time-depth conversions (e.g. Riedel et al., 2020). In-situ logs of chemical and physical properties may also be used to extrapolate lithological information in sections of poor core recovery (e.g. Brewer et al., 1998; Major et al., 1998). Where borehole logging data is absent, we have to rely on geophysical measurements of recovered core material, which introduces several sources of potential inaccuracies (e.g. Weaver and Schultheiss, 1990; Jutzeler et al., 2014):

- Positional uncertainties: Coring devices without a dedicated positioning system may introduce positional uncertainties, as they rely on information provided by research vessels. This is especially true in deep water and strong current settings. Such uncertainties manifest in a spatial offset between the acoustically imaged strata and recovered material. In the case of horizontally heterogeneous sediment distributions (e.g. steep slopes, numerous faults), this spatial offset may severely impair core-acoustic correlation.
- Deviations in coring axis: Ideally, coring devices recover sedimentary strata in the direction of the gravitational centre (i.e. vertically). Deviations from this desired axis can introduce depth offsets in the core-acoustic correlation, which increase proportionally with core depth (e.g. a 5° deviation from the vertical axis may result in a depth offset of 38 centimetres in a 100 m long core, but would increase to an offset of 3.8 metres in a 1000 m long core).
- Poor core recovery: A major challenge in core-acoustic correlations is related to poor core recovery. Not only does the lack of material lead to discontinuous core logging data, it also introduces uncertainties (often on a metre-scale) relating to the vertical position of recovered sediments.
- Seafloor uncertainties: As core devices often disturb the uppermost, soft sediment sedimentary layers, core tops may not always represent in-situ surficial sediments as imaged with acoustic methods (see below as well).
- Sediment compression/expansion: Sediment compression (i.e. under-sampling) disturbs the vertical structure of the sediment and may falsify the relative depth of individual stratigraphic horizons, and is an important consideration for sediment cores. Gravity cores,

in particular, are prone to such under-sampling. Piston cores, on the other hand, have a tendency for sediment expansion (i.e. over-sampling. It has been suggested that cable rebound may cause double penetration and, thus, that heavier piston corers are prone to greater over-sampling (e.g. Skinner and McCave, 2003); even reaching oversampling rates of 30 to 37 % in the top 10 to 15 cm (Széréméta et al., 2004). Another common cause for sediment expansion is the reduction of confining pressure during core recovery and subsequent core handling (i.e. cutting).

- Core logging: Geophysical core logging can introduce systematic errors and produce data that differs greatly from in-situ measurements. Poor quality core log measurements often relate to disturbances of the cored sediments, which include compaction, but also frictional distortion and micro-cracks. Such disturbances are especially prominent in smaller diameter and drilled cores. Additionally, opened or not properly sealed core sections and extended storage in core repositories can reduce the water content of the sediment, and prohibit measurements of the acoustic velocity due to signal loss.

In summary, core-acoustic integration can only provide an estimate of where to find the failure plane. The limited vertical resolution of most datasets and uncertainties in core-acoustic correlation mean that it is usually difficult to determine the exact location of the failure plane and weak layers.

Higher resolution acoustic data (e.g. 2D deep-towed multi-channel or Autonomous Underwater Vessel (AUV)-deployed very high-resolution seismic data; Ker et al., 2010; Marsset et al., 2014; Brothers et al., 2015; Campbell et al., 2015; Kassarie et al., 2017), as well as routine borehole measurements are required to overcome these uncertainties. Such measurements could be integrated relatively easily into IODP or seafloor drill rig (e.g. MeBo; Freudenthal and Wefer, 2007, 2013) campaigns by deploying logging tools after core recovery into the newly-drilled boreholes. If borehole measurements are not available, quick core logging upon recovery or at least quick referential measurements for a correction of logs taken on land are crucial. Positional accuracy in both acoustic imaging and coring to limit spatial offsets is also of high importance. This can be achieved, for example by deploying a positional navigation tool placed on the wire above the coring device. Tiltmeters can be deployed to ensure vertical coring and to enable subsequent corrections in positional accuracy.

Table 5.1. Overview of the most commonly deployed surveying and sampling tools for weak layer investigation.

Hydroacoustic and geophysical surveys			
Application	Seafloor mapping and sub-seafloor profiling, identification of morphological features		
Limitations	No sediment samples for further analyses, no information about sedimentological, geochemical or geotechnical properties of sediments		
Tool	**Description**	**Advantages and disadvantages**	**Examples**
Multi-beam sonar	Seafloor imaging: Multiple sound signals that are reflected by the seafloor are used to detect and map the seafloor	+ Bathymetry (depth information) - Variable resolution - No sub-seafloor information	Operation at different frequencies, higher (>100 kHz) frequencies for shallow and low (<30 kHz) frequencies for deep water, resolution can be as high as <10 m or several hundred of metres (e.g. GEBCO)
Side-scan sonar	Seafloor imaging: High-frequency sound signals that are reflected by the seafloor are used to create an image of the seafloor	+ Relatively cost-effective + Relatively easy usage + High-to very high-resolution + Information about seafloor texture and sediment types - Little depth information - No sub-seafloor information	Frequencies typically 100 – 500 kHz, higher frequencies achieve a higher resolution, but also reduce the swath range; e.g. at 500 kHz the maximum resolution can be a few cm with a maximum swath range of 75 m, at 100 kHz the maximum resolution is 0.15 m with a maximum swath range of 200 – 300 m
Sub-bottom profilers	Sub-seafloor imaging: A sub-bottom profiler uses sound signals that penetrate the shallow sub-seafloor and are reflected by different sediment layers depending on their acoustic impedance (hardness) to map these different layers	+ Fast data collection + High- to very high-resolution + Determination of physical properties of the seafloor - Low penetration depth	Various types of energy sources and frequencies are used, *Parametric* (~100 kHz) and *Chirper* (1 – 10 kHz) for a penetration depth of <100 m and a vertical resolution of <0.05 m; *Boomer* (300 Hz – 3 kHz) system for a penetration depth of 30 – 100 m and a vertical resolution of 0.3 – 1 m; *Sparker* (50 Hz – 4 kHz) system for a penetration depth up to 1000 m (under ideal conditions) and a vertical resolution of >2 m

2D single- or multi-channel seismic reflection	Sub-seafloor imaging: Seismic reflection uses the principal of sound wave transmission and reception to image the sub-seafloor and obtain 2D seismic profiles	+ High penetration depth + Information about sub-seafloor structure - Lower resolution - Data processing	Various types of energy sources and frequencies are used, *Air-Gun* (and *GI-Gun* which consists of two airgun chambers in a single housing) are the most commonly used energy sources, typical penetration of hundreds of metres to a few kilometres
3D seismic reflection	Sub-seafloor imaging: As with 2D seismic reflection, 3D seismic reflection uses the principal of sound wave transmission and reception to image the sub-seafloor. Multiple, parallel, hydrophone-containing streamers spaced a short distance apart from each other enable a 3D view of the sub-seafloor structure.	+ Information about sub-surface structure + High-resolution - Expensive - Data processing	GEOMAR *P-Cable system* with *GI-Gun* as energy source operates at a frequency of 50 – 250 Hz with a vertical resolution of 1 – 2 m and a horizontal resolution of 3 – 6 m; 3D Chirp system operates at a frequency of 1.5 – 13 kHz, with a maximum penetration of 10 – 30 m and vertical and horizontal resolutions at the decimetre-scale
In-situ measurements			
Application	Short- or long-term in-situ measurements of sub-seafloor temperature, pore pressure and geotechnical properties of sediments		
Limitations	Usually limited penetration depth, uncertainty in short-term measurements, no sediment samples for further analyses		
Tool	**Description**	**Advantages and disadvantages**	**Examples**
Piezometer	Piezometer instrument is installed into a borehole in a semi-permanent structure or attached to a gravity-driven piercing lance	+ Long-term pore pressure monitoring and measurement - Cost - Installation requires infrastructure	Gravity-driven IFREMER piezometer for a maximum operation depth of 6000 m and a maximum penetration of 12 m
Dynamic cone penetration testing with pore pressure measurement (CPTu)	Dynamic CPTU probes consisting of a piezocone, strain gauges, a pore pressure port and an inclinometer are gravity- (and winch speed) driven devices to measure in-situ pore pressure and geotechnical properties of sub-seafloor sediments	+ Cost-effective + Fast, continuous profiling + Portable + In-situ pore pressure measurements - Low penetration depth (max. 15 m) - Short-term pore pressure estimates (uncertainty from drilling and installation influences) - unsuitable for gravely sediments	MARUM *Free-Fall Cone Penetrometer with Pore pressure* (FF-CPTu) for shallow water (≤500 m) with a maximum penetration of 8.5 m, or for deep water (≤4000 m) with a maximum penetration of 4.5 m

Static cone penetration testing with pore pressure measurement (CPTu)	Static CPTU systems use a remotely-controlled seafloor rig to push a piezocone into the sediments for the measurement of in-situ pore pressure and geotechnical properties of sub-seafloor sediments	+ Higher penetration depth (max. 100 m) + In-situ pore pressure measurements - Larger vessel needed for deployment - Weather conditions dependent	IFREMER *Penfeld* seabed rig for a maximum operation depth of 6000 m and a maximum penetration of 30 m; MARUM *Geotechnical Offshore Seabed Tool* (GOST) for a maximum operation depth of 4000 m and a maximum penetration of 40 m
Coring devices			
Application	Sampling of sub-seafloor sediments for further analyses (including sedimentological, geochemical and geotechnical analyses)		
Limitations	Limited material, may be disturbed, not under initial pressure/temperature conditions		
Tool	**Description**	**Advantages and disadvantages**	**Examples**
Gravity corer (GC)	Gravity-driven steel pipe for the recovery of short gravity cores	+ Cost-effective + Fast recovery + Portable + Large core diameter (≥10 cm) + Shallow to large water depths - Very low penetration depth (usually 5 – 10 m, max. 20 m) - Prone to sediment under-sampling - Unsuitable for thick layers of coarse-grained or hard sediments (e.g. sandy or ash layers)	Many
Conventional and giant piston corer (PC)	Gravity-driven steel pipe with a tight-fitting piston inside for the recovery of relatively short to medium length piston cores	+ Cost-effective + Portable + Large core diameter (8 - 12 cm) + Giant piston corer: higher penetration depth (usually 30 – 40 m, max. 75 m) - Conventional piston corer: relatively low penetration depth (usually 5 – 15 m) - Prone to over-sampling - Unsuitable for thick layers of coarse sediments (e.g. ash layers) - Giant piston corer: not deployable from all vessels	*Kullenberg* conventional piston corer with a maximum penetration of about 24 m; IFREMER *Calypso* giant piston corer with a maximum penetration of 75 m

Robotic drill rig	Robotic drill rig which is lowered to the seafloor and operated remotely from a vessel for the recovery of sediment cores	+ Relatively high penetration depth + Portable + Operation from a stable platform on the seafloor + In-situ borehole measurements (gammy ray, magnetic susceptibility) + In-situ static cone penetration testing - Slow recovery (sandy to gravely sediments) - Low recovery rate in non-cohesive sediments - Small core diameter (5.7 – 6.3 cm) - Operation only on nearly flat ground (≤5°) to guarantee vertical alignment of drilling axis	MARUM *Meeresboden Bohrgerät* (MeBo70 and MeBo200) for an operation depth of 10 – 2000 m (optional up to 4000 m) and a maximum penetration of 80 m and 200 m
Scientific drill vessels – International Ocean Discovery Program (IODP)	Use of multiple drilling platforms to drill and core sub-seafloor sediments (e.g. JOIDES Resolution, Chikyu)	+ Very high penetration depth + Dynamic positioning system for stable positioning + In-situ borehole measurements - Expensive - Small core diameter (5.87 – 6.2 cm) - High degree of sample disturbance	JOIDES Resolution (IODP) *Advanced Piston Corer* (APC) for a maximum penetration of >300 m; IODP *Extended Core Barrel* (XCB) for a maximum penetration of >700 m

5.2.1.2. Sampling of weak layers: Accessibility and recovery challenges

Many studies rely solely upon remote geophysical data for submarine landslide investigation (Fig. 2.3, 2.7) and, if sediment cores are acquired, they typically do not sample relevant sediment horizons, which may lie tens to hundreds of metres below the seafloor (e.g. Talling et al. 2014; Fig. 2.3). Such cores tend to focus on the characterisation of the landslide deposits or excavated glide planes within the slide area, rather than targeting sediments from adjacent undisturbed slopes. Targeting the undisturbed sediments of the adjacent slopes, including those stratigraphically equivalent to the failure planes, however, is necessary in order to identify and characterise the material along which the landslide initiated.

Sediment cores

There are many coring devices, each with advantages and disadvantages (e.g. Georgiopoulou et al., 2018; Tab. 5.1). Although long cores are usually desirable, not all research vessels can support long and heavy coring devices whose operation is costly, both financially and time-wise. Sample material from such cores is often scarce for any given stratigraphic horizon within a sampled profile. Due to costly operations, the number of cores is limited (often not exceeding one) for each coring site and core diameters are relatively small (Tab. 5.1). These problems can be overcome with shorter gravity or piston cores. Such cores have the main advantage of being relatively cost-effective, and are relatively easy to handle, allowing for multiple deployments at the same site. They also allow the recovery of large diameter (≥10 cm) sediment cores, which are favourable for further laboratory analyses. These cores, however, have very limited penetration depths (Tab. 5.1) and relevant sediment horizons are seldom sampled. Furthermore, in the case of gas-bearing sediments, other coring devices, such as a pressure corer, are required in order to prevent substantial sediment disruption due to gas expansion upon core recovery (e.g. Paull and Ussler III, 2001; Holland et al., 2019). It is, therefore, critical to choose the right coring technique for individual study sites (e.g. Weaver and Schultheiss, 1990; Georgiopoulou et al., 2018).

Another problem is that of sediment recovery (e.g. Jutzeler et al., 2014). Thick, under-consolidated sandy layers are especially difficult to sample, because the loose material is easily washed out of the core barrels during recovery (e.g. Tuaheni Slide offshore New Zealand; Huhn et al. 2016; Pecher et al., 2018). In contrast, even very thin ash layers may be extremely hard to penetrate with conventional coring techniques because their particles interlock if pushed together during coring, thereby increasing the layer's strength exceedingly (e.g. offshore Montserrat; Huhn et al., 2019).

In-situ measurements

Although our capacity to obtain in-situ measurements has greatly improved over the last couple of decades, the devices are still seldomly deployed for weak layer investigation (Fig. 2.3, Tab. 2.1). Similar to coring devices, in-situ measurement tools have to compromise between penetration depth and cost-effectiveness. Cone penetration testing with pore pressure measurement (CPTu) is the primary geotechnical tool to acquire continuous in-situ geotechnical data (Tab. 5.1). Dynamic CPTu (e.g. MARUM *Free-Fall Cone Penetrometer with Pore pressure*; Stegmann et al., 2006) is relatively cost-effective and can be easily deployed, but usually has a limited penetration depth. Higher penetration depths can be achieved with static CPTu (e.g. IFREMER *Penfeld* seabed rig or MARUM *Geotechnical Offshore Seabed Tool* (GOST); Meunier et al., 2004; Sultan et al., 2010; Jorat et al., 2014; Steiner et al., 2014). Static CPTu systems differ from dynamic CPTu instruments,

in that they are pushed at constant penetration rates into the sediment (e.g. Steiner et al., 2014), which allows them to achieve greater penetration depths and also penetrate resistant sediments, such as ash layers. These systems, however, require larger research vessels for deployment, and depending on the sediments encountered may be very time-consuming.

Sediment cores and in-situ measurements that sample relevant sediments, in particular the undisturbed sediment sequence outside the slide area, are rare (Fig. 2.3, Tab. 2.1). Despite continuously emerging tools in marine technology, sampling techniques and in-situ monitoring still generally lag behind the technological advances in geophysical data acquisition (e.g. Clare et al., 2017). The lack of adequate sampling devices constrains our efforts to effectively sample weak layers of submarine landslides. Direct measurement of parameters such as in-situ pore pressure, are time consuming, and are not always feasible due to weather constraints on offshore operations and the expense of ship time. Monitoring of pore pressure variations is also possible, but has been performed in only a limited manner due to logistical complications (Strout and Tjelta, 2005; Flemings et al., 2008; Dugan and Sheahan, 2012). Such monitoring typically requires connection to power and data transfer (e.g. via a seafloor cabled observatory network) which limits the sites that can be studied in detail.

The successful sampling (and investigation) of weak layers requires new technologies, e.g. further development of seafloor drill rigs. Seafloor drill rigs are lowered onto the seafloor from multi-purpose research vessels and retrieve sediment cores by remote control from the ship. They have the potential to bridge the gap between relatively cost-effective, but short, conventional coring devices, such as gravity, piston, or vibra-corer that can sample dense or weakly cemented strata, and the use of expensive drill ships (Freudenthal and Wefer, 2013). They have the advantage that once they are deployed on the seafloor, they can collect a number of sediment cores in a relatively time-effective way, and also enable further borehole logging and in-situ testing (e.g. Spagnoli et al., 2015; Huhn et al., 2019). Such integrated technologies may fill gaps from individual datasets.

Due to difficulties in sampling the failure planes of large submarine landslides that may be buried hundreds of metres below the seafloor (e.g. Haflidason et al., 2004; Georgiopoulou et al., 2010), targeting smaller landslides may prove to be more successful. The investigation of smaller submarine landslides has shown good results (e.g. Strozyk et al., 2010; Berndt et al., 2012; Lafuerza et al., 2012; Baeten et al., 2014; Gatter et al., 2020), as they allow for the deployment of more cost-effective coring devices, which can be used to obtain a number of cores from the slide area and the undisturbed sedimentary sequence. Another alternative is to focus our efforts on landslides in lakes, which are also smaller in size and more readily accessible (e.g. Stegmann et al., 2007; Van Daele et al., 2017; Moernaut et al., 2020; Stegmann et al., 2007). Several previous studies suggest that morphometry and other

characteristics may be similar between cohesive landslides across many orders of magnitude (e.g. Micallef et al., 2008; Moernaut and De Batist, 2011; Urgeles and Camerlenghi, 2013; Casas et al., 2016; Clare et al., 2017), allowing the extrapolation of information from small to larger landslides. Hence, it may be sensible to focus on smaller-scale landslides until deeper sampling is viable.

5.2.1.3. Characterisation of weak layers: A problem of sample quality and quantity

To understand weak layers, it is not enough to know where within the slope's stratigraphy they are located, we also need to characterise them in terms of their sedimentological and geochemical composition, as well as their physical and geotechnical properties. This requires the sampling of weak layers in their undisturbed form, i.e. from the undisturbed adjacent slope.

Visual, descriptive sedimentological and non-destructive MSCL logging data are usually available for sediment cores, but further geotechnical characterisation is often scarce (Fig. 2.4). Advanced geotechnical tests usually require a large amount of undisturbed sediment. Apart from the limited availability of sample material, obtaining high-quality samples is also challenging (i.e. with little deformation due to the recovery and sampling procedures) for such testing (Clayton et al., 1998). Despite the enormous value of deep ocean drilling programmes such as IODP for geological purposes, the samples collected within these programmes are often highly disturbed and, therefore, cannot be used for high-quality geotechnical tests (Vanneste et al., 2014). Although geotechnical properties, such as shear strength and pore pressure estimates, can also be obtained from in-situ measurements, such instruments are not often deployed (Fig. 2.3, Tab. 2.1) and usually have a limited penetration depth (Tab. 5.1). In addition, CPTu-based investigation of sediments does not allow for a compositional classification of the tested sediments, which requires sediment cores or borehole records (e.g. Yin et al., 2021).

Some weak layers, e.g. volcaniclastic, may require additional geochemical analyses. Such sediments can be difficult to identify visually, but have characteristic geochemical signals in XRF-core logging data (e.g. Cassidy et al., 2014). Fossiliferous sediment on the other hand, may require high-resolution visual analyses (e.g. SEM images).

While geophysical data have become more readily available, there is a general scarcity of sedimentological and geotechnical data. Nevertheless, high-quality laboratory tests (e.g. shear strength or permeability) and in-situ geotechnical data are crucial for recognising and evaluating weak layers. In order to overcome limitations inherent to the individual analysis methods (Tab 5.1), the integration of datasets is imperative. The combination of various methods (e.g. geotechnical characterisation from in-situ measurements and from core samples) enables uncertainties to be compensated for, and gaps in individual datasets to be filled.

5.2.2. Suggestions for future weak layer investigation

Despite our increase in knowledge regarding submarine landslides over the past few decades (Fig. 2.2), our understanding of their failure planes and weak layers is still very limited. The main limitations are related to a lack of data and also inconsistency in data acquisition (see Chapter 5.2.1). Some of the most important aspects that should be considered for future weak layer investigations are outlined below:

- Targeted surveys: Maybe the most critical point is the need for research cruises and sampling campaigns tailored towards failure plane and weak layer investigations. The characterisation of weak layers is usually not the primary aim of current cruises; hence, the applied methods (e.g. coring techniques) are often not suitable for sampling relevant sediments outside the slide area.
- Pre-site surveys: A key criterion for successful weak layer investigations are sound pre-site surveys. The data is used to identify and locate the failure plane of submarine landslides and are also essential to identify suitable coring locations. Taking into consideration the limitations of individual surveying techniques, a good approach is the combination of deeply penetrating and high-resolution geophysical tools.
- Sample collection: One of the main limitations in weak layer characterisation is the limited amount of suitable material obtained from sediment cores for further geotechnical analyses (Chapter 2). To ensure enough material is available, we suggest a number of cores (at least two) are taken from each coring site, dedicating one entire core to further geotechnical (and geochemical) testing.
- Consistent workflow: Following a consistent workflow will enable a more complete data collection and a better comparison between individual studies, and consequently weak layer characterisation (Fig. 5.1)
- Micro-CT: High-resolution imaging techniques, such as micro-CT, are crucial for the characterisation of the internal weak layer structure; however, they cannot be used as stand-alone methods (Chapter 4), but need to be validated by means of additional information from other analytical methods. To ensure a reliable validation processes, i.e. information from the same depth, micro-CT samples have to be integrated into a sampling plan from the very beginning.

Finally, integrating offshore investigations with onshore outcrop studies, and implementing our results into numerical models can help to (1) further fill knowledge gaps regarding weak layer composition and structure and (2) allow to futher investigate potential failure mechansims.

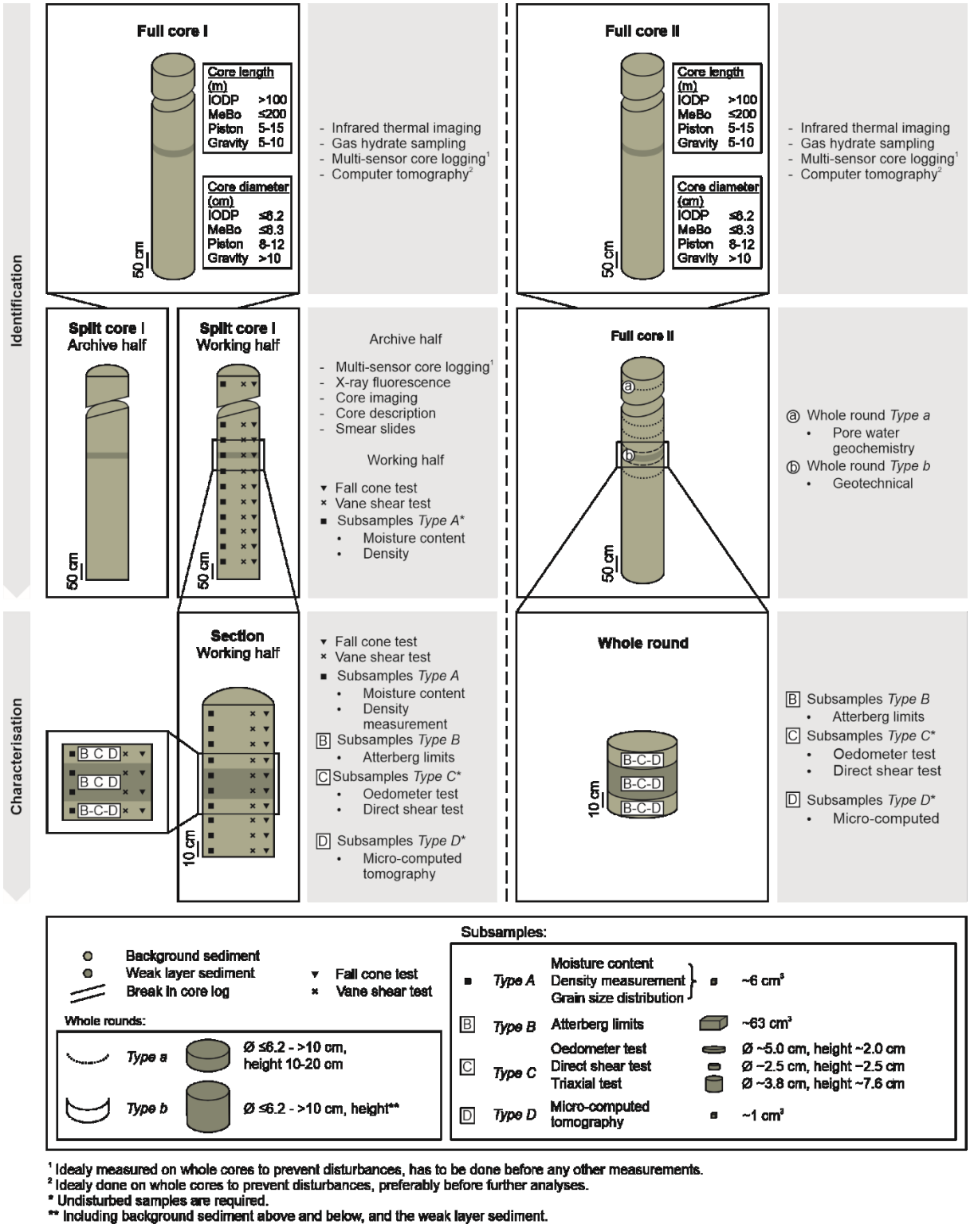

Figure 5.1. Potential workflow for the analysis of sediment cores tailored towards weak layer recognition and characterisation.

References

Baeten, N.J., Laberg, J.S., Vanneste, M., Forsberg, C.F., Kvalstad, T.J., Forwick, M., Vorren, T.O., Haflidason, H., 2014. Origin of shallow submarine mass movements and their glide planes - Sedimentological and geotechnical analyses from the continental slope off northern Norway. Journal of Geophysical Research: Earth Surface, 119, 2335-2360, https://doi.org/10.1002/2013JF003068

Berndt, C., Costa, S., Canals, M., Camerlenghi, A., de Mol, B., Saunders, M., 2012. Repeated slope failure linked to fluid migration: The Ana submarine landslide complex, Eivissa Channel, Western Mediterranean Sea. Earth and Planetary Science Letters, 319-320, 65-74, https://doi.org/10.1016/j.epsl.2011.11.045

Best, A.I., Clayton, C.R.I., Longva, O., Szuman, M., 2003. The role of free gas in the activation of submarine slides in Finneidfjord. In: Locat, J., Mienert, J. (Eds) Submarine Mass Movements and Their Consequences, Advances in Natural and Technological Hazards Research, 19, 491–498. Springer, Dordrecht.

Brewer, T.S., Harvey, P.K., Lovell, M.A., Haggas, S., Williamson, G., Pezard, P., 1998. Ocean floor volcanism: constraints from the integration of core and downhole logging measurements. In: Harvey, P.K., Lovell, M.A. (Eds.) Core-Log Integration. Geological Society, London, Special Publications, 136, 341-362, https://doi.org/10.1144/GSL.SP.1998.136.01.28

Brothers, D.S., Conrad, J.E., Maier, K.L., Paull, C.K., McGann, M., Caress, D.W., 2015. The Palos Verdes Fault offshore Southern California: Late Pleistocene to present tectonic geomorphology, seascape evolution, and slope rate estimate based on AUV and ROV surveys. Journal of Geophysical Research: Solid Earth, 120: 4734-4758, https://doi.org/10.1002/2015JB011938

Campbell, K.J., Kinnear, S., Thame, A., 2015. AUV technology for seabed characterization and geohazards assessment. The Leading Edge, 34(2), 170-178, https://doi.org/10.1190/tle34020170.1

Casas, D., Chiocci, F., Casalbore, D., Ercilla, G., De Urbina, J.O., 2016. Magnitude-frequency distribution of submarine landslides in the Gioia Basin (southern Tyrrhenian Sea). Geo-Marine Letters, 36(6), 405-414.

Cassidy, M., Watt, S.F., Palmer, M.R., Trofimovs, J., Symons, W., Maclachlan, S.E., Stinton, A.J., 2014. Construction of volcanic records from marine sediment cores: A review and case study (Montserrat, West Indies). Earth-Science Reviews, 138, 137-155, https://doi.org/10.1016/j.earscirev.2014.08.008

Clare, M.A., Vardy, M.E., Cartigny, M.J.B., Talling, P.J., Himsworth, M.D., Dix, J.K., Harris, J.M., Whitehouse, R.J.S., Belal, M., 2017. Direct monitoring of active geohazards: emerging geophysical tools for deep-water assessments. Near Surface Geophysics, 15, 427-444, https://doi.org/10.3997/1873-0604.2017033

Clayton, C.R.I., Siddique, A., Hopper, R.J., 1998. Effects of sampler design on tube sampling disturbance—numerical and analytical investigations. Géotechnique, 48(6), 847-867, https://doi.org/10.1680/geot.1998.48.6.847

Dugan, B., Sheahan, T.C., 2012. Offshore sediment overpressures of passive margins: mechanisms, measurement, and models. Review in Geophysics, 50, RG3001, https://doi.org/10.1029/2011RG000379

Fleischer, P., Orsi, T.H., Richardson, M.D., Anderson, A.L., 2001. Distribution of free gas in marine sediments: a global overview. Geo-Marine Letters, 21, 103-122, https://doi.org/10.1007/s00367-002-0114-x

Flemings, P.B., Long, H., Dugan, B., Germaine, J., John, C.M., Behrmann, J.H., Sawyer, D., IODP Expedition 308 Scientists, 2008. Pore pressure penetrometers document high overpressure near the seafloor where multiple submarine landslides have occurred on the continental slope, offshore Louisiana, Gulf of Mexico. Earth and Planetary Science Letters, 269, 309-325, https://doi.org/10.1016/j.epsl.2007.12.005

Freudenthal, T., Wefer, G., 2007. Scientific Drilling with the Sea Floor Drill Rig MeBo. Scientific Drilling, 5, 63-66.

Freudenthal, T., Wefer, G., 2013. Drilling cores on the sea floor with the remote-controlled sea floor drilling rig MeBo. Geoscientific Instrumentation Methods and Data Systems, 2, 329-337.

Gatter, R., Clare, M.A., Hunt, J.E., Watts, M., Madhusudhan, B.N., Talling, P.J., Huhn, K., 2020. A multi-disciplinary investigation of the AFEN Slide: The relationship between contourites and submarine landslides. Geological Society, London, Special Publications, 500, 173-193, https://doi.org/10.1144/SP500-2019-184

Georgiopoulou, A., 2018. Seafloor Sediment and Rock Sampling. In: Micallef, A., Krastel, S., Savini, A. (Eds) Submarine Geomorphology, 75-92. Springer Nature, Cham Switzerland.

Georgiopoulou, A., Masson, D.G., Wynn, R.B., Krastel, S., 2010. Sahara Slide: Age, initiation, and processes of a giant submarine slide. Geochemistry, Geophysics, Geosystems, 11(7), Q07014, https://doi.org/10.1029/2010GC003066

Haflidason, H., Sejrup, H.P., Nygård, A., Mienert, J., Bryn, P., Lien, R., Forsberg, C.F., Berg, K., Masson, D., 2004. The Storegga Slide: architecture, geometry and slide development. Marine Geology, 213, 201-234, https://doi.org/10.1016/j.margeo.2004.10.007

Holland, M.E., Schultheiss, P.J., Roberts, J.A., 2019. Gas hydrate saturation and morphology from analysis of pressure cores acquired in the Bay of Bengal during expedition NGHP-02, offshore India. Marine and Petroleum Geology, 108, 407-423, https://doi.org/10.1016/j.marpetgeo.2018.07.018

Huhn, K., 2016. Cruise Report/Fahrtbericht SO247 – SlamZ: Slide activity on the Hikurangi margin, New Zealand, Wellington (NZ): 27.03.2016–Auckland (NZ): 27.04.2016. MARUM, Center for Marine Environmental Sciences, Bremen, Germany, https://doi.org/10.2312/cr_so247

Huhn, K., Freudenthal, T., Gatter, R., Hilgenfeldt, C., Hönekopp, L., Hornbach, M., Kühn, M., Kuhlmann, J., Kutterolf, S., Meyer-Schack, B., Pallapies, K., Rapp, S.K., Sievers, C., Watt, S., Stelzner, M., 2019. FS METEOR M154-2 Cruise Report "Sector collapse kinematics and tsunami implications – SEKT", Point-à-Pitre - Point-à-Pitre, April 29 - May 23 2019, Reports from MARUM and Department of Geosciences, University of Bremen, pp. 82.

Jorat, M.E., Mörz, T., Schunn, W., Kreiter, S., 2014. Geotechnical Offshore Seabed Tool (GOST): A new cone penetrometer. Third International Symposium on Cone Penetration Testing, Las Vegas, Nevada, USA, 12-14 May 2014.

Judd, A.G., Hovland, M., 1992. The evidence of shallow gas in marine sediments. Continental Shelf Research, 12(10), 1081-1095, https://doi.org/10.1016/0278-4343(92)90070-Z

Jutzeler, M., White, J.D.L., Talling, P. J., McCanta, M., Morgan, S., Le Friant, A., Ishizuka, O., 2014. Coring disturbances in IODP piston cores with implications for offshore record of volcanic events and the Missoula megafloods. Geochemistry, Geophysics, Geosystems, 15, 3572-3590, https://doi.org/10.1002/2014GC005447

Kassarie, K., Mitchell, S., Albertin, M., Hill, A., Carney, R., 2017. Identifying and mitigating against potential seafloor and shallow drilling hazards at a complex Gulf of Mexico Deepwater site using HR3D seismic and AUV data. Near Surface Geophysics, 15, 415-426, https://doi.org/10.3997/1873-0604.2017026

Ker, S., Marsset, B., Garziglia, S., Le Gonidec, Y., Gibert, D., Voisset, M., Adamy, J., 2010. High-resolution seismic imaging in deep sea from a joint deep-towed/OBH reflection experiment: application to a Mass Transport Complex offshore Nigeria. Geophysical Journal International, 182, 1524-1542, https://doi.org/10.1111/j.1365-246X.2010.04700.x

L'Heureux, JS., Longva, O., Steiner, A., Hansen, L., Vardy, M.E., Vanneste, M., Haflidason, H., Brendryen, J., Kvalstad, T.J., Forsberg, C.F., Chand, S., Kopf, A., 2012. Identification of Weak Layers and Their Role for the Stability of Slopes at Finneidfjord, Northern Norway. In: Yamada, Y., Kawamura, K., Ikehara, K., Ogawa, Y., Urgeles, R., Mosher, D., Chaytor, J., Strasser, M. (Eds) Submarine Mass Movements and Their Consequences, Advances in Natural and Technological Hazards Research, 31, 321-330. Springer, Dordrecht.

Lafuerza, S., Sultan, N., Canals, M., Lastras, G., Cattaneo, A., Frigola, J., Costa, S., Berndt, C., 2012. Failure mechanisms of Ana Slide from geotechnical evidence, Eivissa Channel, Western Mediterranean Sea. Marine Geology, 307-310, 1-21, 10.1016/j.margeo.2012.02.010.

Locat, J., Leroueil, S., Locat, A., Lee, H., 2014. Weak Layers: Their Definition and Classification from a Geotechnical Perspective. In: Krastel, S., Behrmann, JH., Völker, D., Stipp, M., Berndt, C., Urgeles, R., Chaytor, J., Huhn, K., Strasser, M., Harbitz, C.B. (Eds) Submarine Mass Movements and Their Consequences, Advances in Natural and Technological Hazards Research, 37, 3-12. Springer, Cham.

Longva, O., Janbu, N., Blikra, L.H., Bøe, R., 2003. The 1996 Finneidfjord Slide; Seafloor Failure and Slide Dynamics. In: Locat, J., Mienert, J. (Eds) Submarine Mass Movements and Their Consequences, Advances in Natural and Technological Hazards Research, 19, 531-538. Springer, Dordrecht.

Madhusudhan, B.N., Clare, M.A., Clayton, C.R.I., Hunt, J.E., 2017. Geotechnical profiling of deep-ocean sediments at the AFEN submarine slide complex. Quarterly Journal of Engineering Geology and Hydrogeology, 50, 148-157, https://doi.org/10.1144/qjegh2016-057

Major, C.O., Pirmez, C., Goldberg, D., LEG 166 Scientific Party, 1998. High-resolution core-log integration techniques: examples from the Ocean Drilling Program. In: Harvey, P.K., Lovell, M.A. (Eds.) Core-Log Integration. Geological Society, London, Special Publications, 136, 285-295, https://doi.org/10.1144/GSL.SP.1998.136.01.24

Marsset, B., Menut, E., Ker, S., Thomas, Y., Regnault, J-P., Leon, P., Martinossi, H., Artzner, I., Chenot, D., Dentrecolas, S., Spychalski, B., Mellier, G., Sultan, N., 2014. Deep-towed High Resolution multichannel seismic imaging. Deep-Sea Research I, 93, 83-90, https://doi.org/10.1016/j.dsr.2014.07.013

Meunier, J., Sultan, N., Jegou, P., Harmegnies, F., 2004. First tests of Penfeld: a new seabed penetrometer. Proceedings of Fourteenth International Society of Offshore and Polar Engineering Conference, Toulon, France, 23-28 May 2004.

Micallef, A., Berndt, C., Masson, D.G., Stow, D.A., 2008. Scale invariant characteristics of the Storegga Slide and implications for large-scale submarine mass movements. Marine Geology, 247(1-2), 46-60, https://doi.org/10.1016/j.margeo.2007.08.003

Moernaut, J., De Batist, M., 2011. Frontal emplacement and mobility of sublacustrine landslides: Results from morphometric and seismostratigraphic analysis. Marine Geology, 285, 29-45, https://doi.org/10.1016/j.margeo.2011.05.001

Moernaut, J., Wiemer, G., Kopf, A., Strasser, M., 2020. Evaluating the sealing potential of young and thin mass-transport deposits: Lake Villarrica, Chile. In: Georgiopoulou, A.A.L.A. et al. (Eds.) Subaqueous Mass Movements and their Consequences: Advances in Process Understanding, Monitoring and Hazard Assessments. Geological Society, London, Special Publications, 500, 129-146, https://doi.org/10.1144/SP500-2019-155

Morgan, E.C., Vanneste, M., Lecomte, I., Baise, L.G., Longva, O., McAdoo, B., 2012. Estimation of free gas saturation from seismic reflection surveys by the genetic algorithm inversion of a P-wave attenuation model. Geophysics, 77(4), R175-R187, https://doi.org/10.1190/geo2011-0291.1

Paull, C.K., Ussler III, W., 2001. History and Significance of Gas Sampling During DSDP and ODP Drilling Associated with Gas Hydrates. In: Paull, C.K., Dillon, W.P. (Eds.) Natural Gas Hydrates: Occurrence, Distribution, and Detection. Geophysical Monograph 124, 53-65. American Geophysical Union, Washington DC, USA.

Pecher, I.A., Barnes, P.M., Levay, L.J., Expedition 372 Scientists, 2018. Expedition 372 Preliminary Report: Creeping Gas Hydrate Slides and Hikurangi LWD, 26.11.2017-04.01.2018, https://doi.org/10.14379/iodp.pr.372.2018

Penrose, J.D., Siwabessy, P.J.W., Gavrilov, A., Parnum, I., Hamilton, L.J., Bickers, A., Brooke, B., Ryan, D.A., Kennedy, P., 2005. Acoustic Techniques for Seabed Classification. Cooperative Research Centre for Coastal Zone Estuary and Waterway Management, Technical Report 32, pp. 142.

Riedel, M., Freudenthal, T., Bergenthal, M., Haeckel, M., Wallmann, K., Spangenberg, E., Bialas, J., Bohrmann, G., 2020. Physical properties and core-log seismic integration from drilling at the Danube deep-sea fan, Black Sea. Marine and Petroleum Geology, 114, 104192, https://doi.org/10.1016/j.marpetgeo.2019.104192

Sammartini, M., Camerlenghi, A., Budillon, F., Insinga, D.D., Zugur, F., Conforti, A., Iori, M., Romeo, R., Tonielli, R., 2018. Open-slope, translational submarine landslide in a tectonically active volcanic continental margin (Licosa submarine landslide, southern Tyrrhenian Sea). In: Lintern, D.G., Mosher, D.C., Moscardelli, L. G., Bobrowsky, P.T., Campbell, C., Chaytor, J.D., Clague, J.J., Georgiopoulou, A., Lajeunesse, P., Normandeau, A., Piper, D.J.W., Scherwath, M., Stacey, C., Turmel, D. (Eds.) Subaqueous Mass Movements. Geological Society, London, Special Publication, 477, https://doi.org/10.1144/SP477.34

Skinner, L.C., McCave, I.N., 2003. Analysis and modelling of gravity- and piston coring based on soil mechanics. Marine Geology, 199, 181-204, https://doi.org/10.1016/S0025-3227(03)00127-0

Spagnoli, G., Finkenzeller, S., Freudenthal, T., Hoekstra, T., Woollard, W., Storteboom, O., van den Berg, A.P., Weixler, L., 2015. First Deployment of the Underwater Drill Rig MeBo200 in the North Sea and its Application for the Geotechnical Exploration. Proceedings of the SPE Offshore Europe Conference & Exhibition in Aberdeen, Scotland, UK, 8-11 May 2015.

Stegmann, S., Mörz, T., Kopf, A., 2006. Initial Results of a new Free Fall-Cone Penetrometer (FF-CPT) for geotechnical in situ characterisation of soft marine sediments. Norwegian Journal of Geology, 86, 199-208

Stegmann, S., Strasser, M., Anselmetti, F., Kopf, A., 2007. Geotechnical in situ characterization of subaquatic slopes: The role of pore pressure transients versus frictional strength in landslide initiation. Geophysical Research Letters, 34, L07607, https://doi.org/10.1029/2006GL029122

Steiner, A., Kopf, A., L'Heureux, JS., Kreiter, S., Stegmann, S., Haflidason, H., Moerz, T., 2014. In situ dynamic piezocone penetrometer tests in natural clayey soils – a reappraisal of strain-rate corrections. Canadian Geotechnical Journal, 51, 272-288.

Strout, J.M., Tjelta, T.I., 2005. In situ pore pressures: What is their significance and how can they be reliably measured?. Marine and Petroleum Geology, 22, 275-285, https://doi.org/10.1016/j.marpetgeo.2004.10.024

Strozyk, F., Strasser, M., Krastel, S., Meyer, M., Huhn, K., 2010. Reconstruction of retreating mass wasting in response to progressive slope steepening of the northeastern Cretan margin, eastern Mediterranean. Marine Geology, 271, 44-54, https://doi.org/10.1016/j.margeo.2010.01.008

Sultan, N., Savoye, B., Jouet, G., Leynaud, D., Cochonat, P., Henry, P., Stegmann, S., Kopf, A., 2010. Investigation of a possible submarine landslide at the Var delta front (Nice continental slope, southeast France). Canadian Geotechnical Journal, 47, 486-496.

Széréméta, N., Bassinot, F., Balut, Y., Labeyrie, L., Pagel, M., 2004. Oversampling of sedimentary series collected by giant piston corer: Evidence and corrections based on 3.5-kHz chirp profiles. Paleoceanography, 19, PA1005, https://doi.org/10.1029/2002PA000795

Talling, P.J., 2014. On the triggers, resulting flow types and frequencies of subaqueous sediment density flows in different settings. Marine Geology, 352, 155-182, https://doi.org/10.1016/j.margeo.2014.02.006

Urgeles, R., Camerlenghi, A., 2013. Submarine landslides of the Mediterranean Sea: Trigger mechanisms, dynamics, and frequency-magnitude distribution. Journal of Geophysical Research: Earth Surface, 118(4), 2600-2618, https://doi.org/10.1002/2013JF002720

Van Daele, M., Meyer, I., Moernaut, J., De Decker, S., Verschuren, D., De Batist, M., 2017. A revised classification and terminology for stacked and amalgamated turbidites in environments dominated by (hemi)pelagic sedimentation. Sedimentary Geology, 357, 72-82, https://doi.org/10.1016/j.sedgeo.2017.06.007

Vanneste, M., Sultan, N., Garziglia, S., Forsberg, C.F., L'Heureux, JS., 2014. Seafloor instabilities and sediment deformation processes: The need for integrated, multi-disciplinary investigations. Marine Geology, 352, 183-214, https://doi.org/10.1016/j.margeo.2014.01.005

Vardy, M.E, L'Heureux, JS., Vanneste, M., Longva, O., Steiner, A., Forsberg, C.F., Haflidason, H., Brendryen, J., 2012. Multidisciplinary investigation of a shallow near-shore landslide, Finneidfjord, Norway. Near Surface Geophysics, 10, 267-277, https://doi.org/10.3997/1873-2012022

Weaver, P.P.E., Schultheiss, P.J., 1990. Current Methods for Obtaining, Logging and Splitting Marine Sediment Cores. Marine Geophysical Researches, 12, 85-100.

Widess, M.B., 1982. Quantifying the resolving power of seismic systems. Geophysics 47(8), 1160–1173, https://doi.org/10.1190/1.1441379

Wilson, C.K., Long, D., Bulat, J., 2004. The morphology, setting and processes of the Afen Slide. Marine Geology, 213, 149-167, https://doi.org/10.1016/j.margeo.2004.10.005

Yin, K.S., Zhang, L.M., Wang, H.J., Zou, H.F., Li, J.H., 2021. Marine soil behaviour classification using piezocone penetration tests (CPTu) and borehole records. Canadian Geotechnical Journal, 58, 190-199, https://doi.org/10.1139/cgj-2019-0571

Acknowledgments

First, I would like to thank my main supervisor Katrin Huhn for providing the funding and giving me the opportunity to work on this project in her working group. I greatly appreciate all the opportunities I was given during the last three-and-a-half years. Not many people have the chance to go on several secondments to collaborating institutes, have yearly workshops and watch the sunset behind Montserrat from a research vessel as part of their PhD. Thank you for your kind support and the freedom to build my own science, guiding me on the way.

I would also like to thank all the people I was fortunate enough to meet and work with during my secondments in Southampton; especially Mike Clare who kindly took the position as my second supervisor. I benefitted greatly from each and every discussion and am very thankful for your support throughout my PhD. Thank you for allowing me to spend several months of secondment in Southampton, working at NOCS and the University of Southampton. A big thanks to the people from BOSCORF for taking their time to show me several of their cores (over and over again) and teaching me about different core-logging methods. Thanks also to Madhu for hosting me at the University of Southampton, guiding me in geotechnical lab work and micro-CT analysis.

This work would not have been possible without ITN SLATE and its great community. I would like to thank everyone in SLATE for the great experiences shared and still to come. Massive thanks to Kate, Madda and Rachel. I would not have completed this PhD without your support. Thank you for all the scientific and non-scientific chats, and always positive vibes during workshops, conferences, holidays and skype :)

To my working group, thank you for all the support during the last years. A special thanks to Mona for walking the first confusing months together with me – everything is easier together, even walking up the stairs! Hadar and Marine, I miss our coffee breaks and brunch dates. Nothing was better to forget about all the PhD troubles than a nice food-coma. Thanks to Gerry for scientific, but especially non-scientific chats. They always help to bring everything back into perspective. Jannis, thank you for always having an open door and for your relentless support during my time in Bremen; SLATIES all over Europe would not be without you.

Thanks to all my friends in Bremen, for helping me and giving me support. A special thanks to Leonie. Thanks for your continuous support, with coffee breaks, puzzle evenings, spontaneous walks, chats and laughs. I enjoyed every minute of it.

My final thanks are to my family and friends abroad. Thank you for sticking with me, for helping as much as you could, whenever needed. Walter, thank you for working your way through this work of

mine. I am so very grateful for all the time and effort you, have once again, put into this. And finally, sorry mum and dad for making you worry these last couple of weeks; but it is okay, now it is over :) Thank you all for always being with me, no matter if from afar or close by.